EXPERIMENTAL INVESTIGATION OF CAI COMBUSTION IN A TWO-STROKE POPPET VALVE DI ENGINE

A thesis submitted for the degree of Doctor of Philosophy

By

Yan Zhang

College of Engineering, Design and Physical Sciences
Brunel University London
United Kingdom

October 2014

Brunel University London
College of Engineering, Design and Physical Sciences
United Kingdom

Yan Zhang

Experimental investigation of CAI combustion in a two-stroke poppet valve DI engine

October 2014

Abstract

Due to their ability to simultaneously reduce fuel consumption and NOx emissions, Controlled Auto Ignition (CAI) and HCCI combustion processes have been extensively researched over the last decade and adopted on prototype gasoline engines. These combustion processes were initially achieved on conventional two-stroke ported gasoline engines, but there have been significantly fewer studies carried out on the CAI combustion in two-stroke engines. This is primarily due to the inherent problems associated with conventional two-stroke engine intake and exhaust ports.

Meanwhile, engine downsizing has been actively researched and developed as an effective means to improve the vehicle's fuel economy. This is achieved by operating the engine at higher load regions of lower fuel consumption and by reducing the number of cylinders. However, aggressive downsizing of the current 4-stroke gasoline engine is limited by the knocking combustion and high peak cylinder pressure. As an alternative approach to engine downsizing, boosted two-stroke operation is being researched. In this thesis, it has been shown that the CAI combustion in the two-stroke cycle could be readily achieved at part-load conditions with significant reductions in CO and uHC emissions when compared to typical SI combustion in a single cylinder gasoline direct injection camless engine. In addition, extensive engine experiments have been performed to determine the optimum boosting for minimum fuel consumption during the two-stroke operation. In order to minimise the air short-circuiting rate, the intake and exhaust valve timings were varied and optimised. It is shown that the lean operation under boosted condition can extend the range of CAI combustion and increase combustion and thermal efficiencies as well as producing much lower CO and HC emissions. By means of the cycle-resolved in-cylinder measurements and heat release

analysis, the improvement in combustion and thermal efficiencies were attributed to the improved in-cylinder mixture, optimised autoignition, and combustion phases. Finally, in view of the increased use of ethanol in gasoline engines, E15 and E85 were used and their effect on engine performance, fuel economy and exhaust emissions were investigated.

Acknowledgements

If life is a journey, PhD study must be a part of my journey. I would like to thank everyone who helped me through this part of my journey.

I would like to express, first and foremost, my deep gratitude to Professor Hua Zhao for all his help and support during the course of this project. I owe to him all the knowledge and experience acquired during the past 3 years.

I would like to acknowledge Ricardo UK, Cambustion Ltd., and Prof. Nick Colling's group for all the support to engine control, the fast CO_2 and O_2 measurements during this research.

I would like to express my gratitude to the continual assistance from various technicians for their expertise and assistance for commissioning and maintaining the test cell. Special thanks go to Clive Barrett, Andy Selway and Ken Anstiss.

I would like to thank my colleagues and friends Mohammed Ojapah and Macklini Dolla Nora for their continuous help and support in solving the problems that happened during this period and for their friendship that always helped to keep me motivated during difficult moments.

I would also like to thank all my other colleagues and friends for their company, friendship and moral support that made this a joyful time.

Finally, my most sincere gratitude goes to my family for their endless love, who has helped me to keep my faith and motivation high, giving me the strength and support to overcome the difficulties and to make the most of this experience.

Nomenclature

General Abbreviations

AC	Alternating Current
ACEA	European Automobile Manufacturers' Association
AFR	Air/Fuel Ratio
AFRS	Stoichiometric Air/Fuel Ratio
ARC	Active Radical Combustion
ATAC	Active Thermal Atmosphere Combustion
ATDC	After Top Dead Centre
BDC	Bottom Dead Centre
BMEP	Brake Mean Effective Pressure
BSCO	Brake Specific Carbon Monoxide
BSFC	Brake Specific Fuel Consumption
BSHC	Brake Specific Hydro-Carbons
BSNO	Brake Specific Nitrogen Oxides
BTDC	Before Top Dead Centre
CA	Crank Angle
CA	Crank Angle
CAAA	Clean Air Act Amendments
CAI	Controlled Auto-Ignition
CARB	Californian Air Resource Board
CI	Compression Ignition
CR	Compression Ratio
DAQ	Data Acquisition Board
DI	Direct Injection
ECU	Electronic Control Unit
EGR	Exhaust Gas Re-circulation
EPA	Environmental Protection Agency-USA
EVC	Exhaust Valve Closing
EVO	Exhaust Valve Opening
FID	Flame Ionization Detection
FTP	Federal Test Procedure
GDI	Gasoline Direct Injection
HCCI	Homogeneous Charge Compression Ignition

HEV	Hybrid Electric Vehicle
IC	Internal Combustion
IMEP	Indicated Mean Effective Pressure
ISCO	Indicated Specific Carbon Monoxide
ISFC	Indicated Specific Fuel Consumption
ISHC	Indicated Specific Hydro-carbons
ISNO	Indicated Specific Nitrogen Oxides
IVC	Intake Valve Closing
IVO	Intake Valve Opening
JAMA	Japan Automobile Manufacturers' Association
KAMA	Korean Automobile Manufacturers' Association
LEV	Low Emission Vehicle
MBT	Minimum Spark Advance for Best Torque
MFB	Mass Fraction Burn
MHI	Mitsubishi Heavy Industries
MPD	Magneto-Pneumatic Detection
NDIR	Non-Dispersive Infrared
NIMEP	Net Indicated Mean Effective Pressure
NOx	Nitrogen Oxides
NVO	Negative Valve Overlap
NVO	Negative Valve Overlap
PC	Personal Computer
PM	Particulate Matter
PMEP	Pumping Mean Effective Pressure
ppm	Parts per Million
PRF	Primary Reference Fuel
PZEV	Partial Zero Emissions Vehicle
RESS	Rechargeable Energy Storage System
RON	Research Octane Number
rpm	Revolutions per Minute
SAE	Society of Automotive Engineers
SCR	Selective Catalyst Reduction
SI	Spark Ignition
SULEV	Super Low Emissions Vehicle
TDC	Top Dead Centre

TLEV	Transitional Low Emissions Vehicle
TPS	Throttle Position Sensor
uHC	Unburned Hydrocarbons
ULEV	Ultra Low Emissions Vehicle
VBA	Visual Basic for Applications
VCT	Variable Compression Ratio
VCT	Variable Cam Timing
VGT	Variable Geometry Turbocharger
VOC	Variable Organic Compounds
VR	Variable Reluctance
VVA	Variable Valve Actuation
WOT	Wide Open Throttle
ZEV	Zero Emission Vehicle

Contents **Page Number**

List of Figures

List of Tables

Chapter 1

Introduction

Chapter 1 Introduction

1.1 Introduction

Transportation is a necessary part of daily human life. From ancient times to present day, in every place where human beings exist in the world, people have been always trying to find ways to transport themselves and goods robustly and efficiently over long distances. The advent of the automobile has significantly changed the world and the lifestyle of human beings. Although it is actually hard to imagine the world without automobile today, no doubt it would have been impossible to make the first vehicle without the contribution of internal combustion engine, this engine is attributed to the effort of an engineer called Nikolaus Otto who gave his name to the 'Otto' cycle which has been utilised in hundreds of millions of IC engines all over the world.

After the IC engine was applied to the motor vehicle, revolution of the transportation industry took place. As important as the steam engine which brought up the early stage train and railway, the IC engine solved the problem with moving heavy goods on the road without the use of rails. This invention injected infinite vigour and vitality into the modern consumer culture.

The IC engine is a machine that converts the thermal energy from a chemical reaction of air and fuel into mechanical power. Initially, it had very low fuel conversion efficiency and produced relatively high emissions. Over the last century, with the development of innovative engine technologies, the IC engine has been developed into a high power density powerplant of high fuel conversion efficiency and low emissions.

In order to further improve the fuel economy and reduce emissions of the IC engine, alternative combustion systems have been proposed and investigated. In particular, a new generation of combustion methodology known as Controlled Auto Ignition (CAI) or Homogeneous Charge Compression Ignition (HCCI). These are researched due to their potential to achieve simultaneous reductions in fuel consumption and NOx and Particulate Matter (PM) emissions by combining the advantage of homogenous charge in gasoline engines and compression ignition in diesel engines. This combustion system

provides a way to alleviate the pressure on the requirement of expensive, complex and inefficient after-treatment systems under the increasingly strict emissions legislations.

Another engine technology for better fuel economy is engine downsizing which involves the replacement of a bigger engine with a smaller engine of reduced displacement volume and the number of cylinders. A lot of research and development efforts have been made in engine downsizing in the last decade, which has led to the introduction of turbocharged direct injection gasoline engines of higher power density and greater BMEP.

To date, passenger cars in series production have been powered almost exclusively by four-stroke reciprocating piston engines. However, due to their part-load pumping losses and lower compression ratio, conventional four-stroke spark ignition (SI) gasoline combustion engines are much less efficient than the high speed direct injection (HSDI) diesel engines. Gasoline Direct Injection (GDI) engines are regarded as the most promising technology to minimise fuel consumption. In the meanwhile, two-stroke cycles, because of its higher specific output, are particularly attractive for automotive applications. A four-stroke engine can be 50% downsized by halving the number of cylinders but running in two-stroke operation.

In this work, two-stroke CAI combustion was achieved and investigated in a 2/4stroke switchable DI gasoline engine equipped with poppet valves and a fully flexible variable valve actuation system. The two-stroke CAI operational range from idle to part-load was investigated. The combustion system, injection strategy, and boosting strategy were optimized for best fuel economy and emissions. The results were compared to different operating modes, such as 4-stroke throttled SI, Intake valve throttled SI, Positive valve overlap SI, Negative valve overlap CAI, Exhaust rebreathing CAI and two-stroke SI. The effect of ethanol content on the two-stroke engine's performance, fuel economy and emissions were also studied.

1.2 Project objectives

The aim of the project is to evaluate the potential of two-stroke CAI operations in a direct injection gasoline engine with poppet valves and the effect of ethanol on such operations. The specific objectives are:

1. To explore and research CAI combustion for stable, fuel efficient and low emission part-load operations in a boosted DI gasoline engine with poppet valves operated in two-stroke mode.
2. To study the effect of scavenging during gas exchange process on composition of in-cylinder mixture and subsequent combustion process in two-stroke CAI and SI modes.
3. To investigate the performance, combustion and emission characteristics of two-stroke CAI combustion and the effect of fuel injection strategy and valve timings.
4. To investigate the effect of blended ethanol and gasoline fuels on combustion, engine efficiency and emissions from such an engine.

1.3 Thesis outline

Following this introduction, Chapter 2 gives a review of literature related to this work. In Chapter 3, the experimental setup and test facilities are described in detail. This includes the engine, dynamometer, supercharger and data acquisition system developed by the author. The phenomenon of 'air short-circuiting' is introduced and an innovative method of measuring it on the engine is also presented in Chapter 4. The results of two-stroke CAI operating range, performance and emissions with exhaust lambda=1 are discussed in Chapter 5. Further analysis, including injection timing effects and comparison between two-stroke, four-stroke, SI, CAI operation, is presented in Chapter 6. Ethanol content effect on two-stroke CAI is discussed in Chapter 7. In order to minimise air short-circuiting, lean boost operation was investigated and their results are presented in Chapter 8. Chapter 9 includes the conclusion and recommendation for future work.

Chapter 2

Literature Review

Chapter 2 Literature Review

2.1 Introduction

Since the 1960s, people have started paying more attention to the impact of the gaseous and particulate emissions from vehicles and engines on environmental pollution. Over the last 30 years, many countries have introduced more stringent legislations to limit emissions from vehicles. The concern with limited fossil fuel reserves and recent climate change caused by CO2 emissions led to the increasing rise in the road tax and fuel tax, and more recently the introduction of CO2 and fuel economy limits. As a result, automobile manufacturers are forced to research, develop and manufacture more efficient and cleaner vehicles. Newly implemented technologies, such as battery electric vehicles and fuel cell vehicles, have shown the potential to replace IC engines with minimal pollution at the point of use. However, none of them can be utilised as a direct replacement of the internal combustion engine so far due to the issues of their practicality, cost, range, the source of electricity/hydrogen and the charging facilities. Due to these drawbacks, the IC engine will still be the primary powertrain for vehicles.

In terms of energy consumption, IC engines are the main consumer of fossil fuels. Statistical data from the Organization of the Petroleum Exporting Countries (OPEC) showed in 2009 57% of global fossil fuels were consumed in vehicular traffic areas and it is predicted that the percentage will increase to over 60% by 2035. This is due to an increase in vehicle ownership in the developing countries [1].

The scientific community generally believes that burning fossil fuels is one of the main causes of increased greenhouse gas concentrations in the atmosphere, contributing to global warming in the last decades of the 20th century [2]. With the increase of car ownership, the car has become one of the major sources of CO2 emissions. The most effective way to reduce engine CO2 emissions is to improve fuel efficiency of the engine. In addition, CO2 emissions can be reduced by the use of renewable fuels, such as ethanol and bio-diesel.

In response to concerns with global warming and limited petroleum, a number of countries have introduced fuel economy or CO_2 emission legislations [3-7]. As shown in Figure 2.1, Europe, US, Japan, and Canada have started CO2 legislation in 2000. In the

EU and Japan, CO2 legislation is more stringent than the US and Canada due to the popularity of small vehicles. China, South Korea, and Australia began their CO2 legislation and their limit value is between that of the US and EU. The limit of CO2 emissions in each country is decreasing every year, but the rate at which it's reducing is getting smaller after 2010. Currently, the limit is about 130g/km in Europe while 167 g/km in China and 180 g/km in US. It is expected that the rate of reduction of the CO2 emission limit will be higher in the next 5 years due to the development of new advanced engine technologies. By 2020, the CO2 regulations in Europe will be the most stringent in the world, where 95g/km is nearly a half of that in 2000. The US is expected to reduce CO2 emissions by more than 50% in a 25 year timeframe from 2000 to 2025. The situation remains critical, as vehicle ownership in the world has increased by more than 10 times in the past 15 years.

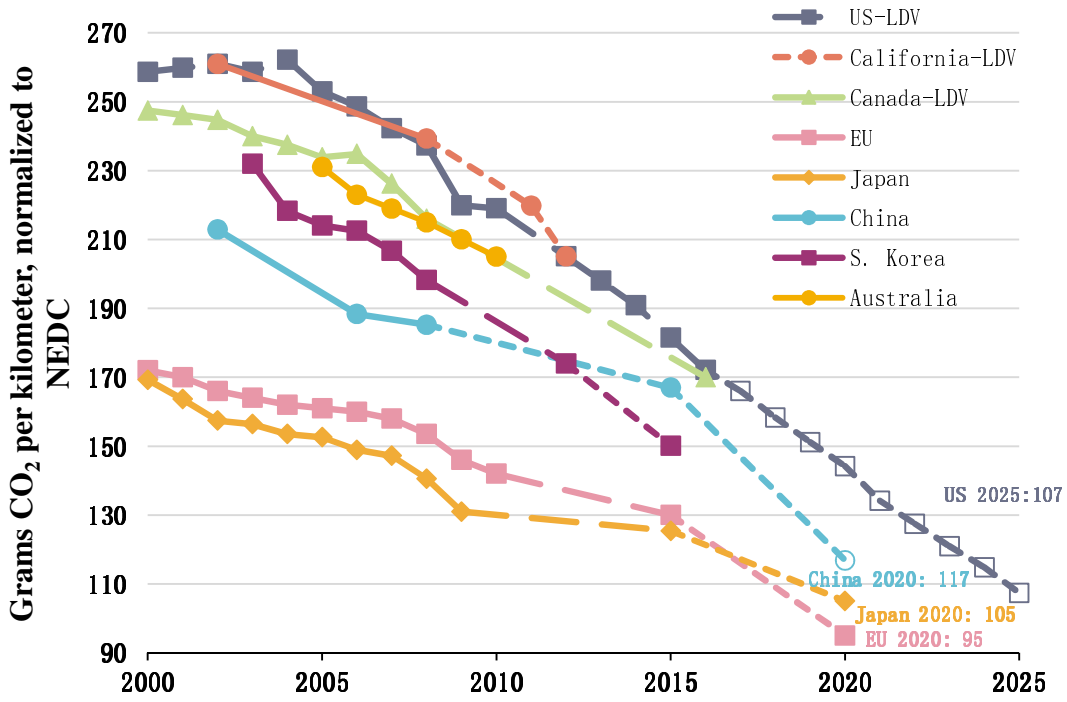

Figure 2.1 CO_2 Emission Standards [3]

Burning fossil fuels also produces harmful emissions such as carbon monoxide (CO), unburnt hydrocarbons (uHC), nitrogen oxides (NOx) and particulate matter (PM). Over the past 40 years many countries have implemented increasingly stringent emission legislations to limit the output of harmful emissions from vehicles. The EU and California emissions legislation for passenger cars are shown in Table 2.1 and 2.2 respectively [8, 9]. Other countries and regions have developed their own emission regulations corresponding to their specific situations. Currently, the California emission

standards are the most stringent in the world. The United States and European emission regulations were different in detection mode, but after normalization of LEV II and Euro IV standard requirements, HC emissions are almost identical.[10] However, the limits of NOx emissions in LEV II is only half of Euro IV. This led to the high speed diesel engine and gasoline direct injection engine not being able to appear in the market before their corresponding after treatment system development.

Table 2.1 EU Emission Standards for Passenger Cars [8]

Stage	**Date**	**CO**	**HC**	**HC+NOx**	**NOx**	**PM**	**PN**
		g/km					*#/km*
Compression Ignition (Diesel)							
Euro 1†	1992.07	2.72 (3.16)	-	0.97 (1.13)	-	0.14 (0.18)	-
Euro2, IDI	1996.01	1.0	-	0.7	-	0.08	-
Euro 2, DI	1996.01[a]	1.0	-	0.9	-	0.10	-
Euro 3	2000.01	0.64	-	0.56	0.50	0.05	-
Euro 4	2005.01	0.50	-	0.30	0.25	0.025	-
Euro 5a	2009.09[b]	0.50	-	0.23	0.18	0.005[f]	-
Euro 5b	2011.09[c]	0.50	-	0.23	0.18	0.005[f]	6.0×10^{11}
Euro 6	2014.09	0.50	-	0.17	0.08	0.005[f]	6.0×10^{11}
Positive Ignition (Gasoline)							
Euro 1†	1992.07	2.72 (3.16)	-	0.97 (1.13)	-	-	-
Euro 2	1996.01	2.2	-	0.5	-	-	-
Euro 3	2000.01	2.30	0.20	-	0.15	-	-
Euro 4	2005.01	1.0	0.10	-	0.08	-	-
Euro 5	2009.09[b]	1.0	0.10[d]	-	0.06	0.005[e,f]	-
Euro 6	2014.09	1.0	0.10[d]	-	0.06	0.005[e,f]	6.0×10^{11} [e,g]
* At the Euro 1..4 stages, passenger vehicles > 2,500 kg were type approved as Category N_1 vehicles							

Stage	Date	CO	HC	HC+NOx	NOx	PM	PN
		g/km					*#/km*

† Values in brackets are conformity of production (COP) limits

a. until 1999.09.30 (after that date DI engines must meet the IDI limits)

b. 2011.01 for all models

c. 2013.01 for all models

d. and NMHC = 0.068 g/km

e. applicable only to vehicles using DI engines

f. 0.0045 g/km using the PMP measurement procedure

g. 6.0×10^{12} /km within first three years from Euro 6 effective dates

Table 2.2 CARB Emission Legislations for Passenger Cars [9]

Standard	Year of Approval	Durability Vehicle Basis	Engine type	CO (g/km)	NMOG (g/km)	NOx (g/km)	HCHO (g/km)	PM (g/km)
Tier I (LEV I)	2001-03	100,000 mi						
TLEV			Any	2.61	0.097	0.37	0.0112	0.05
LEV			Any	2.61	0.056	0.19	0.0112	0.05
ULEV			Any	1.30	0.034	0.19	0.0068	0.02
LEV II	2004-10	120,000 mi						
LEV			Any	2.61	0.056	0.04	0.0112	0.01
ULEV			Any	1.30	0.034	0.04	0.0068	0.01
SULEV			Any	0.06	0.006	0.01	0.0025	0.01
LEV III	2015-25	150,000 mi			NMOG+NOx (g/km)			
LEV160			Any	2.61	0.099	-	0.0025	0.0062
ULEV125			Any	1.30	0.0776	-	0.0025	0.0062
SULEV30			Any	0.621	0.0186	-	0.0025	0.0062

Achieving high efficiency, low fuel consumption, and emissions in the internal combustion engine has been a common challenge faced by engine researchers and the engine manufacturers of the world.

2.2 Internal Combustion Engine Technology

2.2.1 Two-Stroke Cycle

Two-stroke cycle operation is not a new concept and was used in engines even earlier than the four-stroke engine. Modern two-stroke engines are refined and have high performance are compact and lightweight power devices. The largest and smallest reciprocating piston engines are in two-stroke cycles. [11]

As shown in Figure 2.2, a typical two-stroke engine completes one working cycle within one revolution of the crankshaft. As the firing rate is doubled compared to the four-stroke cycle engines, two-stroke cycle engines produce high power density.

The most significant difference between two-stroke and four-stroke cycles is the gas exchange processes. Different from the gas exchange process in four-stroke engines where the exhaust gases are expelled first by the high cylinder charge pressure and followed by the movement of the piston in the exhaust stroke, the exhaust gases are scavenged in the two-stroke cycle by the pressurised intake air during the intake and exhaust valve overlap period, known as the scavenging process. The gas exchange and scavenging process strongly affects the two-stroke engine performance, fuel economy and emissions [12-14].

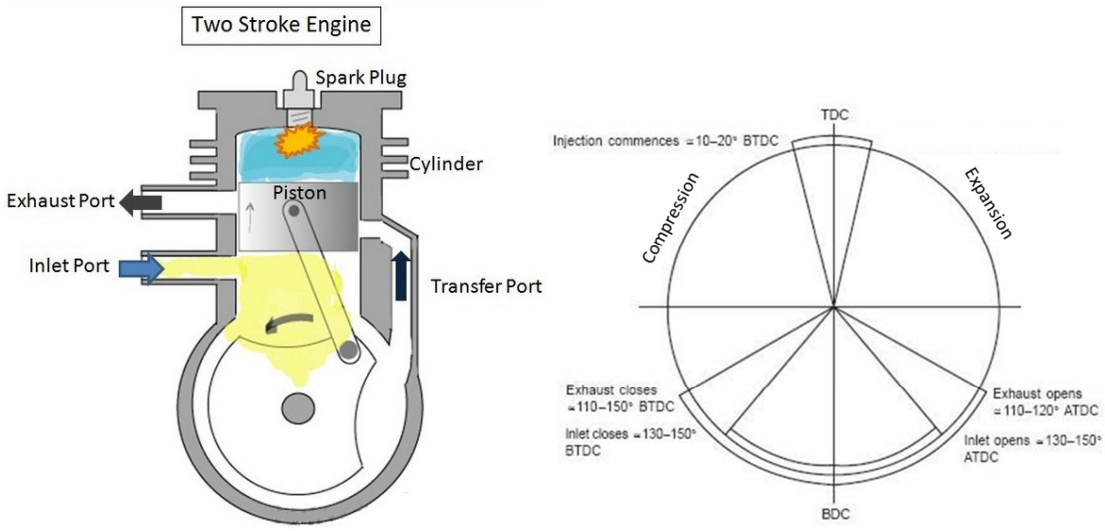

Figure 2.2 A Typical Two-stroke Cycle Engine and Its Sequence of Two-stroke Cycle Events[15]

2.2.2 Four-Stroke Cycle

Conventional two-stroke gasoline engines have been gradually replaced by four-stroke engines in automotive applications because of inherent problems with emissions. Two-strokes have high CO and HC emissions due to burning of mixed fuel and oil and fuel short-circuiting, cylinder liner and piston deformation due to uneven thermal stress of hot exhaust and cold intake ports, poor scavenging and low trapping efficiency with fixed symmetrical port timings. In addition, conventional spark ignition combustion in the two-stroke cycle suffers from high cyclic variation and sometimes misfire due to the presence of significant amount of residual gases, ultimately resulting in high HC and CO emissions and poor fuel economy.

In recognition of the drawbacks of two-stroke engines, the four-stroke engine was invented. This was mainly aimed to improve the gas exchange process of two-stroke engines. Firstly, as shown in Figure 2.3, compared to two-stroke cycle, the intake and exhaust strokes are split out in the four-stroke engine. There are 2 independent cycles for intake and exhaust process. Secondarily, the intake and exhaust ports in two-stroke engines are replaced with poppet valves. In this case, there is no need for fresh air to go through crankcase, where lubricant oil can mix with fresh air.

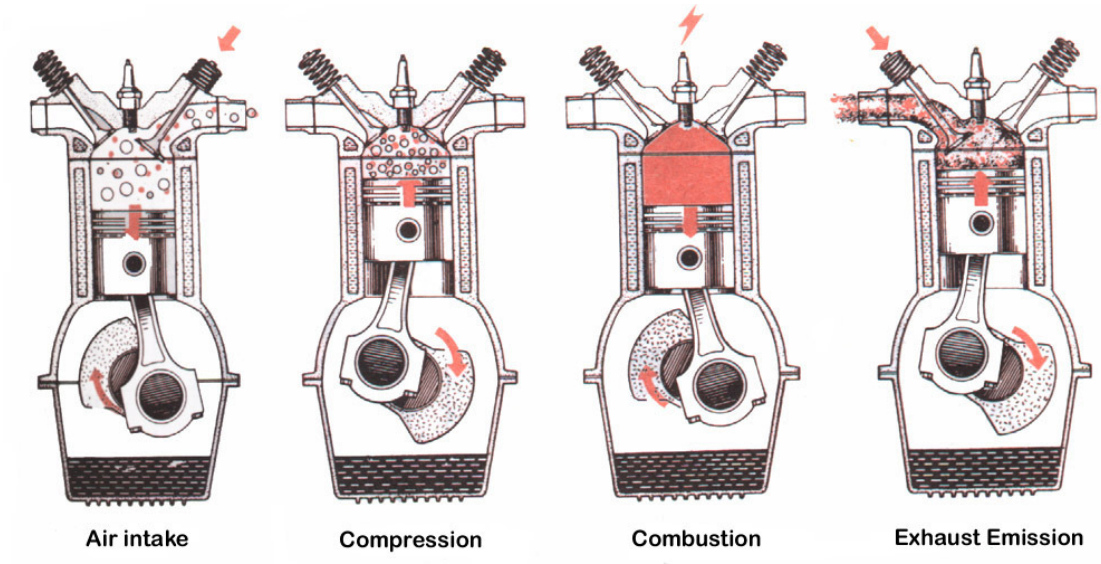

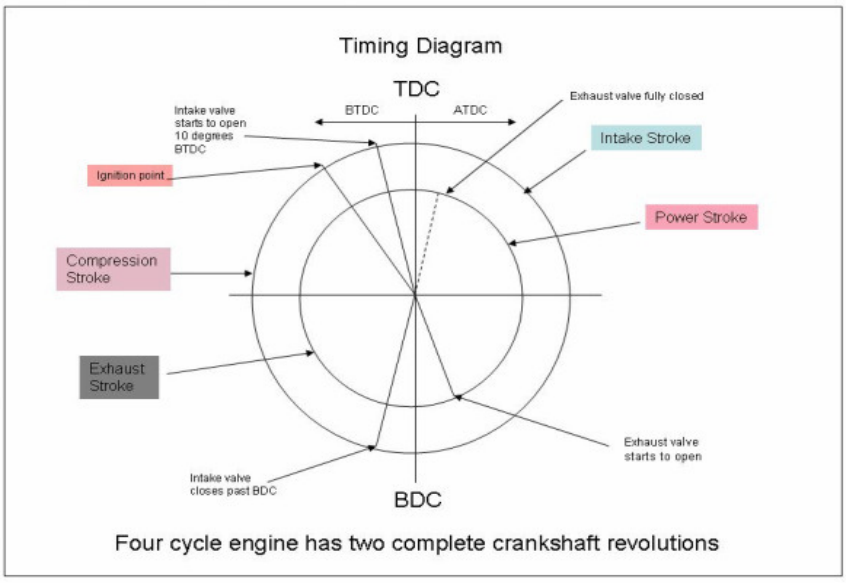

Figure 2.3 A Typical Four-stroke Cycle Engine and Its Sequence of Four-stroke Cycle Events [16]

Nowadays all the vehicles are driven by four-stroke engines equipped with poppet valves because of their lower emissions and better fuel economy than the conventional ported two-stroke engines.

2.2.3 Variable Valve Actuation

The gas exchange process has a significant effect on engine performance and emissions of modern engines. Apart from gas flow direction control, the amount of gas going in and out of the engine cylinder is mainly controlled by intake and exhaust valve timings. The study on the valve timing control technology started in 1880s. However, the progress initially was very slow. The primary outcome was only achieved after 1985[17] and its developing trend is shown in Figure 2.4.

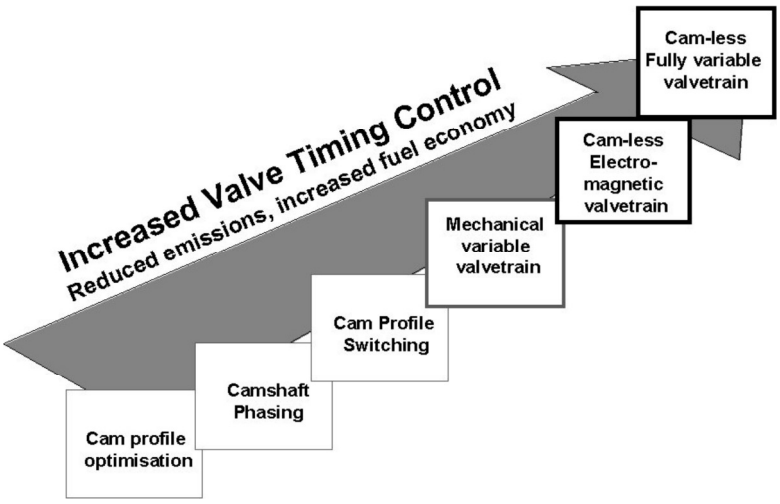

Figure 2.4 Trend towards Increased Valve Timing Control [17]

The typical production valvetrain comprises of camshafts, valve springs, tappets and poppet valves and is driven by a crankshaft through a transmission such as a belt, chain, or gears. This design makes the intake and exhaust valve timings and opening durations fixed to the crankshaft. Large amounts of work have been done to optimise cam profile and valve opening and closing timings. It is also found that the fixed valve timings are no longer adequate to deliver the improved engine performance and combustion efficiency required over such a wide engine speed and load operating conditions. Thus, a range of variable valve technologies has begun to appear in the market place. Variable Cam Timing (VCT) has been considered as the most effective valve timing control technology and has been widely implemented on a large number of modern gasoline engines.

With the engine VVA development, various innovative designs were invented. When compared with conventional valves driven by cam, the camless electromagnetic or electro-hydraulic valvetrains have more advantages in terms of valve timing flexibility. However, the complexity and cost of their auxiliary control system and accessories is the main obstacle in mass production. Mechanical VVA driven by cam is relatively small and costly.

2.2.4 Direct Injection

Another thread of engine development is the advance in fuelling control technology. As shown in Figure 2.5, in the gasoline engine development history, the revolution from simple carburettors to electronically controlled port fuel injection started from the 1970s.

The second revolution was the invention of gasoline direct injection (GDI) and its contribution was never less than the first in terms of the flexibly control of the fuel supplied into the engine, although every step increased more complex control. GDI engines can be operated in both stratified charge and homogeneous mixtures. In particular, GDI is typically combined with turbocharging in the downsized engine to take advantage of the charge cooling effects of direct fuel injection.

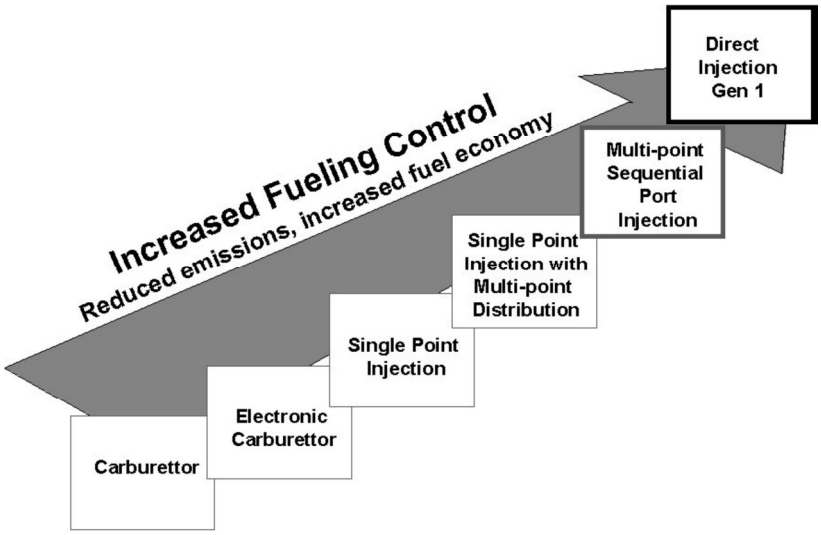

Figure 2.5 Trend towards Increased Fuelling Control [17]

In order to deliver finer fuel droplets and faster evaporation, the DI injector has evolved from the single/double slit and swirl injectors to the multi-hole solenoid injector. In order to improve the response of the injector, the piezo actuator is used in the pintle type outward opening injector. Both side mounted and centrally mounted DI injectors are used in production GDI engines. The latter arrangement is preferred for the stratified charge operation [18]. In the case of two-stroke engines, GDI is necessary to avoid the fuel short-circuiting [19].

GDI engines appeared on the market since 1990s and most of them operated with stoichiometric combustion systems, which raised the cost of injection and control system but did not provide satisfied fuel savings because their DI systems were wall-guided and air-guided. [18] In late 2000s, the spray-guided stratified charge combustion systems were introduced to the market by BMW and Mercedes-Benz. The fuel saving was achieved by operating in globally lean conditions, while their after-treatment had to be

replace by lean NOx catalyst system to lower the high NOx emissions produced by the lean combustion in the cylinder.

2.2.5 Engine Downsizing

In the last several years, engine downsizing has been actively researched and developed as an effective means to improve the vehicle's fuel economy. This is achieved by operating the engine at higher load and more efficient regions and by reducing the number of cylinders. However, aggressive engine downsizing of the current four-stroke gasoline engine is limited by the knocking combustion and high peak cylinder pressure. On the other hand, the two-stroke engine, due to its doubled firing frequency of four-stroke engines, is capable of producing significantly greater torque and power output at the same engine speed without the need for increased complexity of valvetrain. By means of direct fuel injection and optimised combustion system, it is possible to realise the two-stroke cycle operation in the poppet valved engine without the shortcomings of the conventional ported two-stroke engines [20, 21]. Furthermore, with the development and availability of Variable Valve Timing (VVT) and high efficiency boosting devices as well as more flexible fuel injection equipment (FIE), a poppet valve two-stroke engine can be boosted to produce superior low speed torque than the turbocharged 4-stroke engine as demonstrated in a previous study [22]. However, to avoid the unstable SI combustion and hence poor fuel economy at part-load of the two-stroke cycle operation, 4-stroke spark ignition combustion was retained and a sophisticated two/four stroke switching system and control had to be included in the engine. As an alternative approach to engine downsizing, boosted two-stroke operation in a poppet valve engine was proposed and investigated in the current research.

2.2.6 Boosting Technologies

In order to maintain the full load torque and power performance, engine downsizing requires engine boosting through a turbocharger or/and a supercharger [23]. The supercharger is usually driven off of the engine crank shaft and it provides excellent transient response [24-27]. The turbocharger comprises an exhaust gas turbine and a compressor and is driven by the exhaust energy. Compared with supercharging,

turbocharging is more efficient but suffers from low speed lag. The Variable Geometry Turbocharger (VGT) has the ability to improve the engine's low speed response and is widely used in high-speed diesel engine but its application to gasoline engines is constrained by the engine's higher exhaust gas temperature. Two-stage turbocharging or compound supercharging and turbocharging can be used for further downsized four-stroke gasoline engines [28].

In two-stroke operation, the intake pressure must always be higher than exhaust pressure to realise the scavenging process. In this case, on the poppet valve two-stroke engine (different from the ported two-stroke engines), the intake must be boosted. A single turbocharger is inadequate for two-stroke engines as it cannot provide the intake air at elevated pressure during the engine start-up and very low load operations when there is little exhaust energy to drive the turbocharger. Therefore, an engine driven or preferably electric supercharging or a combination of electric supercharging and turbocharging will be needed.

An electric turbo compound or electrically assisted turbocharger [29, 30] could be a good solution for two-stroke poppet valve engines. Base on the design of a turbocharger, an electric motor is mounted in the middle of the shaft connecting the compressor and turbine, as shown in Figure 2.6. With the electric turbo compound, the compressor can be driven by the motor during the engine starting process. At some low load conditions where the turbine energy is insufficient, the motor can supply extra energy and speed up the compressor. At some high load conditions, where the turbine produces surplus energy, the motor can work as a generator to absorb it.

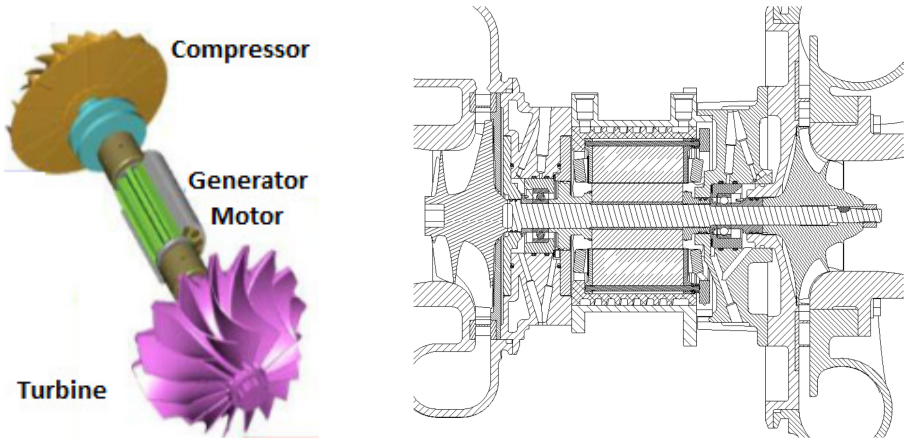

Figure 2.6 Electric Turbo Compound [29, 30]

2.3 Controlled Auto-Ignition (CAI) Combustion

2.3.1 Principle of CAI and Previous Studies on Gasoline CAI Combustion

A more advanced combustion process, referred as Homogeneous Charge Compression Ignition (HCCI) or Controlled Auto-Ignition (CAI), different from conventional gasoline spark ignition and diesel compression ignition has been widely studied in four-stroke gasoline engines in the last 15 years because of its ability to simultaneously reduce engine fuel consumption and NOx emissions [31].

CAI combustion is a process where a premixed mixture of fuel, air and recirculated gases auto-ignites at multi points around the piston top dead centre when the charge temperature reaches auto-ignition temperature. It typically features homogeneous charge, auto ignition and low temperature combustion.

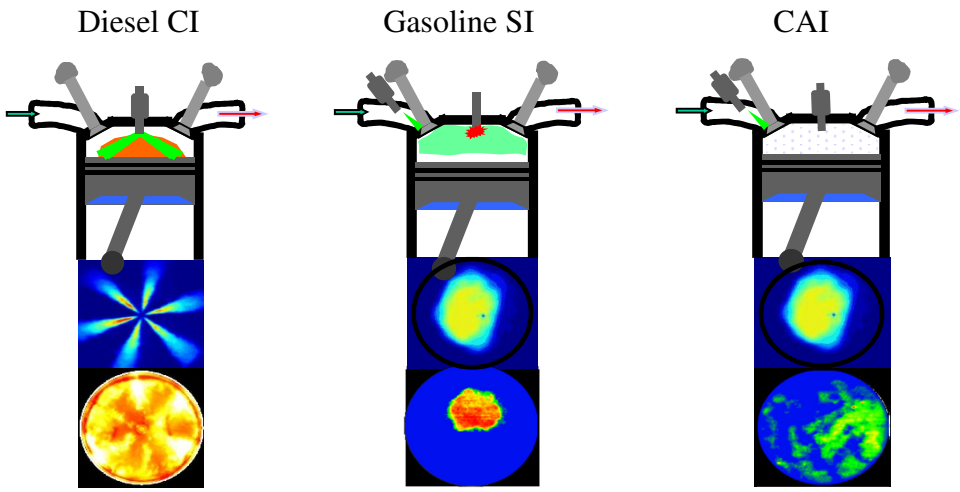

	Diesel CI	Gasoline SI	CAI
Mixture:	Non-premixed	Premixed, homogeneous	Premixed, homogeneous
Combustion:	Diffusion	Flame propagation	Ignition at multi points
Emissions:	High NOx and soot	High NOx	Low soot and NOx

Figure 2.7 Comparison of CI, SI and CAI Combustion Modes

As shown in Figure 2.7, in terms of mixture preparation, CAI is similar to gasoline SI mode in which the premixed air and fuel mixture is formed in the intake port (PFI) or in the cylinder (GDI) during the compression stroke. In comparison, the high pressure

diesel is injected into the combustion chamber just before the desired start of diesel CI combustion.

From a combustion standpoint, diesel CI operation is dominated by diffusion combustion and gasoline SI combustion is characterised by flame propagation from the spark to the cylinder wall. However, CAI starts at the end of compression stroke and at some spots where the mixture temperature has reached the auto-ignition temperature. Therefore, the combustion takes place at multiple points in the cylinder and more ignition cores are generated because of the rise in unburnt gas temperature caused by the compression from the burnt gas to the unburnt gas. Compared to SI and CI, CAI combustion is more uniform and faster.

The origin of CAI/HCCI combustion may be traced back to 1930s, when Russian scientist Nikolai Semenov and his colleagues started studying a chemical-kinetic controlled combustion process for IC engines, in order to overcome the limitations imposed by the physical-dominating processes of SI and CI engines. In 1975, Semenov and Gussak found that when the thermodynamic and chemical conditions of the entire cylinder charge are similar to those of cool flames of hydrocarbon air mixtures, a more uniform heat release process should be reached. This led to the first 'Controlled Combustion', also named as 'Avalanche Activated Combustion' at that time [32]. In 1979, Onishi and Noguchi carried out systematic study on this combustion process in a two-stroke engine. Onishi proposed to improve HC and CO emissions and fuel economy at part loads by utilizing CAI combustion (at that time referred as ATAC－Active Thermo-Atmosphere Combustion) in the two-stroke engine [33]. Experimental results showed very low cycle to cycle variations when engine running in ATAC mode. Through optical study, it was seen there was no visible flame front throughout the combustion chamber. Then, Onishi summarized ATAC as: (1) Heating effect by hot residuals; (2) homogeneous mixing of residuals and fresh charge; (3) Limited operating conditions of ATAC mode. Noguchi analysed the middle product of CAI combustion in a two-stroke engine [34]. Results showed there were massive CH_2O, HO_2 and O species produced before auto-ignition process taking place. These intermediate products were recognized as low temperature combustion products of hydrocarbons. After auto-ignition, there were a lot of CH, H and OH produced, which indicates the intensive heat release process of high temperature. This phenomenon is totally different from conventional gasoline SI combustion process.

In 1983 Najt and Foster studied the autoignition combustion mechanism in a four-stroke single cylinder engine using heating [35]. In 1979, Thring carried out the premixed compression ignition combustion of diesel and introduce the definition of HCCI [36].

In 1990s, the strength and depth of research on CAI were greatly enhanced. In 1992, Stockinger et al. showed for the first time that a four-cylinder gasoline engine could be operated with auto-ignition by means of higher compression ratio and intake heating. Although its speed and load range was very limited, the part load brake efficiency was increased by 14~34%. [37] In the late 1990s, Olsson *et al* demonstrated CAI combustion on a modified 12-litre six-cylinder diesel engine over a much wider speed and load range by combined use of isooctane and heptane, closed loop control, turbocharging, higher compression ratio and intake heating.[38]

The approaches to achieve CAI on gasoline engines can be summarised as follows:

1) Direct intake heating

Direct intake heating is the most obvious approach to achieve auto-ignition in gasoline engines. Through heating the intake charge the initial temperature of the charge is increased and thus the in-cylinder temperature history is varied without significant change in cylinder pressure. Najt and Thring are the earliest researchers adopting intake heating to achieve CAI combustion. In their work, the intake charge was heated up to 300℃. [35, 36] Oakley et al. [39, 40] also carried out CAI study on a four-stroke gasoline engine with throttle removed and 320℃ intake temperature. Results showed the mixture could reach auto-ignition temperature at the end of compression stroke with the aid of the heat from external EGR. Figure 2.8 is the CAI operating range over the lambda and EGR rate map. Knocking, misfiring and partially burning boundary were obtained as well. Through this approach, NOx emissions were reduced by 97% at most of the operating conditions and fuel consumption was reduced by 20% at maximum load condition. However, the drawback is the high power consumption and large intake heating system, which brought high heat inertia and reduced the engine response. Therefore, this approach is not applicable for the production engine.

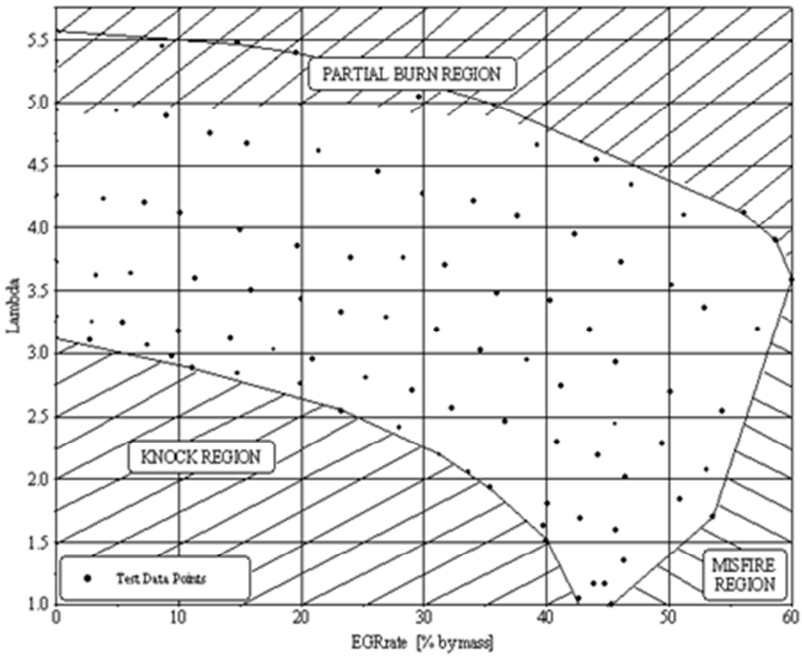

Figure 2.8 Gasoline CAI Operating Range [39, 40]

2) Higher compression ratio

Similar to the intake heating approach, a higher compression ratio increases the cylinder temperature at the end of compression stroke and then lead to the fuel auto-ignition. With increased compression rate, the ignition timing advances and the heat release rate significantly increases. Although this approach can apparently improve CAI stability at medium-low load operations, it will also lead to the violent combustion process and unacceptable combustion noise at high load operations. Najt and Foster tried different compression ratios with PRF fuel. [35] Thring found it was necessary to dilute the combustible mixture in order to reduce the combustion rate when compression ratio was relatively high, which also led to the fact that the CAI engine maximum load reduced [36].

In order to overcome the limitation of fixed higher compression ratio, Haraldsson et al. investigated CAI combustion in a Saab prototype VCR engine and found that the compression ratio needed to be adjusted for different intake temperatures[41].

3) Variation in fuel blends

It is also a good solution to achieve CAI combustion through varying fuel properties to suit CAI combustion at different load conditions. Research results [38, 42-44] have shown the composition and properties of the fuel have strong effects on the CAI combustion process, and thus can improve the operating range, emissions and combustion noise of CAI engines. However, this method requires some unconventional fuel, such as ethanol or DME, to be blended with gasoline in the cylinder. Therefore, in practice, it is limited by the current lack of infrastructure to supply the required fuels as well as the complexity and cost of a dual fuel system.

4) Exhaust gas recirculation (EGR)

From the path of the recirculated exhaust gas, EGR can be classified as External EGR (eEGR) and Internal EGR (iEGR).

External EGR is an approach to recirculate exhaust gases on the engine by introducing it from exhaust pipe into intake pipe to have it re-enter the cylinder while mixing with fresh air. Compared to iEGR, eEGR temperature is much lower as the exhaust gas has flown through a long pipe out of engine, plus the effect of inter-cooling. As a result, low temperature exhaust gasses mixed with fresh charge is introduced into the cylinder. It is hard for the fresh charge to reach auto-ignition temperature simply by the compression from piston. Therefore, on the CAI engine, eEGR has to be used with other approaches, such as intake heating [39, 40] and iEGR [45].

Internal EGR is the approach of recirculating exhaust gases by retaining it in the cylinder instead of displacing it out of the engine. It is necessary to work with Variable Valve Actuation (VVA), which is capable of flexibly adjusting the amount of recirculated exhaust gas and intake air by varying the valve opening timing and duration. Generally speaking, iEGR can be classified as exhaust gas trapping and exhaust gas rebreathing according to the valve control strategy and the way to retain exhaust gas internally.

1. Exhaust gas rebreathing:

   The exhaust gas is recirculated by the means of drawing the exhaust gas back into the cylinder. Usually it is accomplished by the following two methods.

- Opening the intake valve in the exhaust stroke to allow a portion of exhaust gas flow into intake port so it can be sucked back into cylinder in the following intake stroke. (It is rarely used because of the plastic intake manifold and port fuel injection (PFI) on the gasoline engine.)
- Opening the exhaust valve in the intake stroke to suck a porting of exhaust gas back into cylinder.[46-48]

This strategy requires the valvetrain system to provide much more complex valve lift profiles, typically either the intake or exhaust valve needs to open twice with one engine cycle or remain open within the gas-exchange period. Firstly this strategy led to the increase in the difficulty of the engine control. Secondly, for double-open valve case, the requirement of valvetrain response is doubled. For the extended valve opening case, there is a risk of valve-piston contact. Furthermore, the cylinder-to-cylinder variation of air and rebreathed exhaust gas increases in the multi-cylinder engine.

2. Exhaust gas trapping:

Trapping exhaust gas in the cylinder by earlier closing of the exhaust valve is also a way to internally recirculate exhaust gas. In this case, the intake valve open timing should be retarded in order to minimize the pumping loss during the gas exchange process. By this way, instead of normal positive valve overlap, a negative valve overlap (NVO) is formed to retain the hot burnt gas in the cylinder, which is used as hot source to heat the fresh charge in next cycle. With the aid of heat from residual gas, the air fuel mixture could auto-ignite around the end of compression stroke. Hence, this approach is also known as NVO or residual gas trapping strategy. It can be realised by the conventional cam driven valvetrain with a modified cam profile, where the maximum lift is lower and opening duration is shorter than that of original valve profiles, as shown in Figure 2.9.

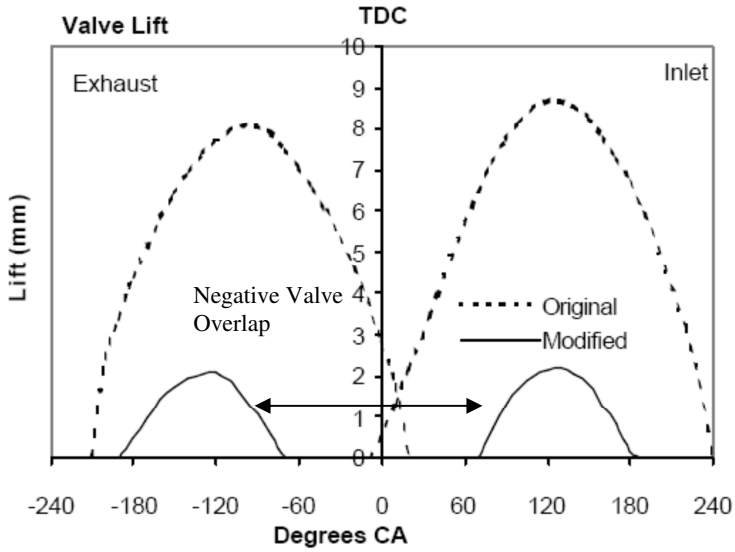

Figure 2.9 Valve Lift Profiles for CAI Operation [49]

It was the first time that CAI was achieved by means of exhaust gas trapping via NVO by Willand [49]. By reducing the valve opening duration, the exhaust gas that was trapped in the cylinder in the exhaust stroke was increased to 40%, which initiated CAI combustion in the next cycle. Later on, Kontarakis demonstrated stable CAI combustion on a single cylinder four-stroke unthrottled gasoline engine in the speed range from 1300 rpm to 2000rpm, IMEP range from 2.5bar to 3.6bar and lambda range from 0.95 to 1.1. [50] It was found that fuel consumption can be improved but lambda range for stable CAI combustion was relatively narrow.

Systematic research of CAI combustion with exhaust gas trapping strategy has been carried out at Brunel since the late 1990s. The effect of residual gas on CAI combustion and engine emissions was analysed and summarised as heating, dilution, heat capacity and chemical effects [51]. The results showed that the heating effect of residual gas had the largest effect in promoting CAI which was slightly delayed by the increased heat capacity. The combustion duration also increased under the combined effect of increased heat capacity and dilution. The dilution effect reduced the peak pressure rising rate, particularly when residual gas fraction was over 40%. In 2001, Li, *et al* demonstrated the CAI operation on Ford 1.7L Zetec-SE 16V 4-cylinder engine through the NVO method using the variable cam timing (VCT) and lower lift camshafts. The maximum BMEP achieved with CAI operation was 4bar. At part load, BSFC was reduced by up to 30% and NOx reduced up to 99%, compared to that with SI operation [52]. However, the CAI range was limited.

Apart from what was previously mentioned, there were a few other approaches to achieve CAI combustion, such as pulsed flame jet [53] and laser induction [54]. However, these can be demonstrated only in a laboratory setting and is not feasible in production at this stage.

In summary, exhaust gas trapping has been considered as the most feasible approach to product gasoline CAI engine. [55] In the meantime, this approach can be used under stoichiometric conditions so that it is compatible with a 3-way catalyst which is a mature, highly efficient catalytic after-treatment widely used on modern gasoline vehicles. Nevertheless, internal EGR achieved via VVA is a relatively simple and more practical approach to CAI in gasoline engines, as it can be adapted for not only steady operating conditions but also transient operating conditions.

2.3.2 Advantages and Challenges of CAI combustion in four-stroke gasoline engines

When compared with SI combustion operation, the CAI combustion mode in a gasoline engine has following advantages [56]:

1) <u>High thermodynamic efficiency:</u>

   As CAI takes place at multiple points in the combustion chamber, the heat release rate is higher, which is closer to an ideal constant volume heat release process. Secondly, the CAI combustion temperature is lower as the combustion takes place without significant flame propagation. Therefore, the thermodynamic efficiency of CAI engines can be as similar to that of diesel engines.

2) <u>Low fuel consumption:</u>

   As the load of CAI engines are no longer controlled by throttle, it minimises the pumping losses at part load conditions and is capable of decreasing fuel consumption by 15% to 20%, compared to a conventional gasoline engine.

3) <u>Low cyclic variation:</u>

The ignition process of SI combustion is more sensitive to air flow and fuel distribution in the combustion chamber. Cycle to cycle flow variation is known to cause SI combustion to vary from cycle to cycle. When the thermal conditions are homogeneous during CAI combustion, the ignition starts at multiple sites and leads to rapid heat release process that is less prone to flow structure or local turbulence.

4) Low emissions:

The NOx emission in CAI combustion is typically more than 90% lower than the SI combustion, due to low temperature heat release reactions of diluted mixture.

The main challenges facing gasoline CAI combustion include [57-60]:

1) Ignition timing and combustion phase control

On the conventional gasoline engine, ignition timing is controlled by spark timing and on diesel engine ignition timing is controlled by fuel injection timing. However, on CAI engine, it is much more difficult to control the ignition timing as cylinder temperature, pressure, and composition of the mixture all indirectly control auto-ignition timing and combustion process. So ignition timing control is one of the biggest challenges of CAI engines. Also, the change of engine load output requires altering fuel injection quantity and fuel concentration in the cylinder correspondingly. In order to keep the proper ignition timing, the adjustment of cylinder temperature history is necessary. On the other hand, the variation in engine speed changes the chemical reaction accumulated time for the mixture to auto-ignite, resulting in the change in ignition phase corresponding to crank angle. This also must be compensated by changing cylinder temperature history. Christensen [58] also pointed out that it was necessary to take many effects into account for CAI ignition timing control, such as compression ratio, intake temperature, intake manifold pressure, fuel property, air fuel ratio, EGR rate, engine speed, and coolant temperature. In case of GDI engine, injection timing should also be considered for ignition timing control. In case of CAI engine equipped with VVA system, it is also necessary to have more precise valve events collaborative adjustment [61-64].

2) CAI operating range extension

As stated previously, CAI combustion is a premixed mixture compression ignition process and combustion takes place simultaneously throughout combustion chamber, which leads to a more rapid combustion rate compared to that of SI and CI combustion. Knock is more likely to occur at high load operating conditions due to the increased CAI combustion rate. The higher cylinder pressure rise rate can lead to higher mechanical load and heat load, which can cause engine damage in the worst cases. Meanwhile, the engine noise and NOx emissions reach unacceptable levels. On the other hand, as CAI achieved by internal EGR requires trapping a large amount of exhaust gas in the cylinder, the engine high load output is limited. As a result, to extend the high load output of CAI engines is another challenge. [36, 42, 65]

When burning high octane fuel at low load and speed, lower combustion reaction rates occur because of the presence of a high concentration of residual gasses. This leads to low charge temperature and unstable ignition conditions. This is the cause of insufficient combustion in the cylinder and the formation of unburnt hydrocarbon. Therefore, misfire often occurs at low load and idle operations in CAI engines. The excessively rich mixture or high EGR rates form the misfire limit of CAI. [36]

Li J. [52] found the upper load boundary of CAI engine operating range could be split into knock limit and gas-exchange limit, which is caused by the use of low lift cam to trap residual gas in the cylinder. At high speeds and high loads, there was insufficient fresh charge going into the cylinder during gas-exchange process. Furthermore, at low loads, too high of residual gas fraction and too low of residual temperature led to the fact that mixture cannot reach auto-ignition conditions and caused misfire at low load CAI operating boundary.

In summary, gasoline CAI engines suffer from too narrow of an operating range and cannot meet the demand of whole vehicle driving cycles. This is another key issue facing mass production of CAI technology.

3) Cold start

In the internal EGR approach to CAI combustion, the combustible mixture needs to be heated by the exhaust gas from previous cycles. At engine cold start, without heating from exhaust gas, the mixture temperature is too low during the compression stroke to initiate auto-ignition. It is very difficult to start engine, especially when the combustion chamber surface is cold.

Due to the presence of the above issues, CAI technology has not been implemented on production engines. Therefore, in order to advance the process of CAI technology mass production, CAI researchers must raise practical solutions to these challenges.

2.3.3 Two-stroke CAI

Running CAI in two-stroke cycles is not a new idea, although most research on CAI combustion has been carried out on the four-stroke engine in the last decade [31, 56] due to the dominance of four-stroke engines.

In order to overcome the partial burn and misfire of spark ignited mixture at part load in the conventional two-stroke engine [11], CAI combustion was first achieved and applied to some two-stroke engines in the late 1970s [33]. In the port scavenging two-stroke engine, its poor scavenging was utilised to obtain CAI combustion by means of a large quantity of hot residual gases [34]. Later on, Durret tried to apply CAI combustion to a DI two-stroke engine while the residual gas was trapped using a butterfly exhaust throttling valve [66] and a transfer port throttling [67]. Then the prototype two-stroke CAI ported DI engine was built and showed significant reduction in NOx emissions and fuel consumption compared to its four-stroke counterpart of equivalent power output [68]. In parallel, CAI operation was demonstrated on a two-stroke ported motorcycle engine by means of residual gas trapping through a variable exhaust port timing and exhaust throttling [69]. Then its first industrial application was in Japan in 1996 and in Europe in 1998 [31]. In addition, research was carried out on CAI with different fuels in two-stroke ported engines [70, 71].

It was not until the 2/4SIGHT concept (two-stroke / four-stroke switchable engine) in 2003 that CAI was achieved on a poppet valve engine running two-stroke cycle but

within a relatively limited operating range [72, 73, and 22]. Apart from this work, very little studies were carried out on two-stroke CAI in poppet valve engines. The advantages of poppet valve two-stroke engine have been stated in previous sections. In 2007, Kim compared the four-stroke CAI and two-stroke CAI operation in a poppet valve engine equipped with electromagnetic valvetrain [74]. Although the results showed CAI operating range was extended in two-stroke cycles, two-stroke CAI didn't exhibit advantage compared to the four-stroke exhaust gas rebreathing CAI operation. However, detailed investigations and analysis were not carried out.

2.4 Summary

This chapter briefly described the development history of vehicles and engines. From the developing trend of the emission legislations, it can be seen that there has been the demand for the automotive engine to output higher power but lower emissions while consuming less fuel. It is this motivation that is pushing the evolution of the engine technologies.

The invention and development of new technologies will promote the progress of other relevant technology. This chapter highlighted some internal combustion technologies that are relevant to this work, including two-stroke cycles, four-stroke cycles, variable valve actuation, direct injection, engine downsizing and boosting technologies.

In order to break through the efficiency and emission limits of conventional gasoline and diesel engines, a new combustion mode of CAI was introduced. Literature survey of the research on CAI combustion highlighted its characteristics and advantages, the approach to achieve CAI in the engine, the challenges of implementing CAI in product engines and the history of the research of CAI on two-stroke and four-stroke engines. In particular, it has identified that systematic studies on the operation of a two-stroke direct injection engine with inlet and exhaust valves should be carried out to explore the synergy of such an engine design and the autoignition combustion process for maximum benefit in fuel economy and emission reductions.

Chapter 3

Experimental Facilities

Chapter 3 Experimental Setup and Test Facilities

3.1 Introduction

This chapter describes the experimental setup and test facilities used to obtain all measurements and data. The experimental setup in this work composes of a single cylinder engine, the engine testbed, supercharging facility, measurement devices and a data acquisition system. The schematic of complete setup is shown in Figure 3.1.

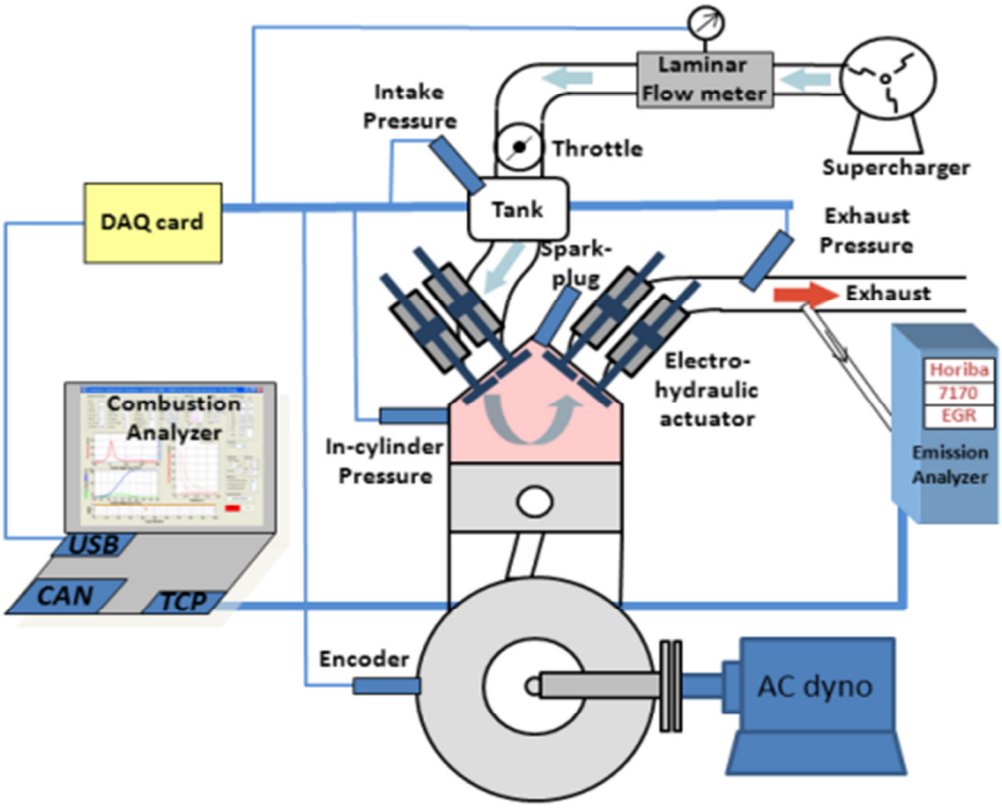

Figure 3.1 Schematic of Experimental Setup

3.2 Camless two/four-stroke switchable DI engine and the valve train system

3.2.1 Single Cylinder Engine

A single cylinder engine was designed and commissioned to operate in either four-stroke or two-stroke cycles through an electrohydraulic valvetrain system. The engine

comprises of a standard Ricardo single cylinder research engine crankcase and a special designed cylinder head to accommodate 4 sets of electrohydraulic valve actuation devices. The camless two/four-stroke switchable DI engine is shown in Figure 3.2, of which the specifications are shown in Table 3.1. The engine is mounted on a seismic block to damp out the first order vibration and driven by an AC motor so that both motored and fired operation could be performed. The coolant and oil are supplied by fully automated coolant and oil conditioning circuits.

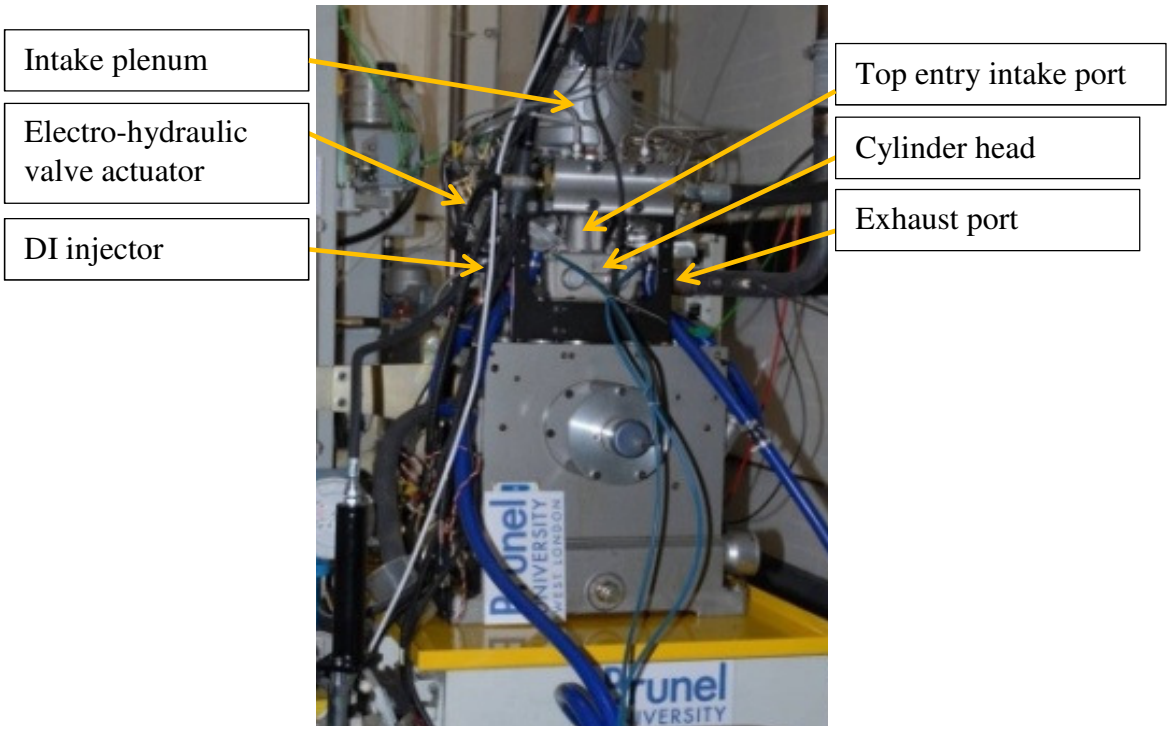

Figure 3.2 Camless Two/Four-stroke Switchable DI Engine

Table 3.1Engine Specifications

Bore × Stroke	81.6mm×66.94mm
Swept volume	0.35L
Compression ratio	11.78:1
Combustion chamber	Pent roof / four valves
Valve train	Electro-hydraulic actuation
Fuel injection	Side Direct injection
Max speed	6500 rpm
Max peak cylinder pressure	120 bar
Intake port	Vertical

As the engine is designed for two-stroke operation, two individual vertical intake ports, as shown in Figure 3.3, are adopted in the cylinder head design to produce reverse tumble flow[22, 75]. This forces air to move in an anti-clock wise pattern away from the exhaust valves and hence provides higher scavenging efficiency. The scavenging process and its related air short-circuiting issue will be discussed in detail in Chapter 4.

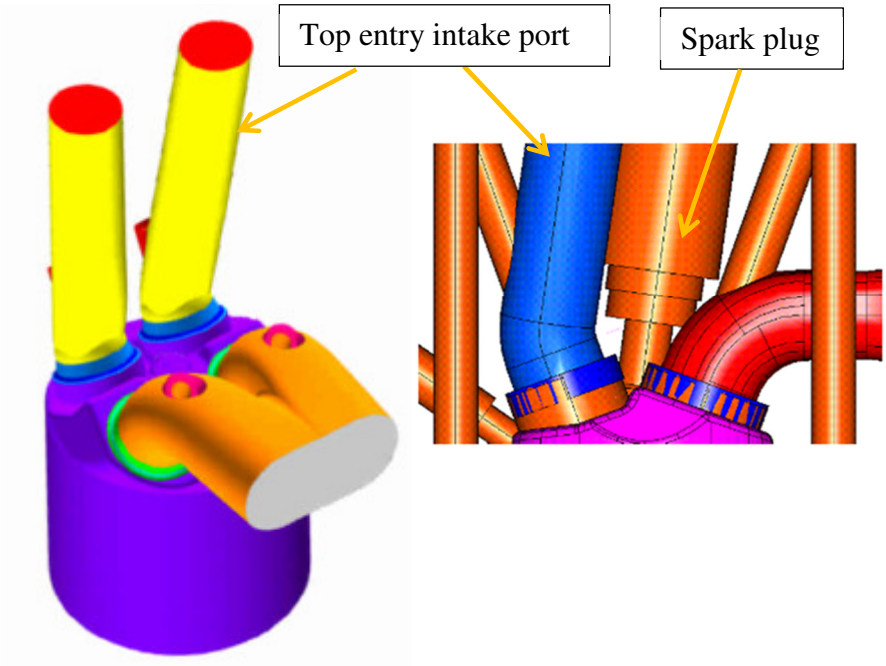

Figure 3.3 Vertical Intake Port Design

Figure 3.4 shows the combustion chamber and piston crown design. In order to increase the exhaust flow at boosted conditions and improve gas exchange efficiency, the two exhaust ports are designed larger than intake ports. The injector is located below the two intake valves. In order to allow intake and exhaust valves to open at 3.5mm lift at TDC for extreme operating strategies while keeping the high compression ratio at 11.78, four valve pockets were designed on the piston crown.

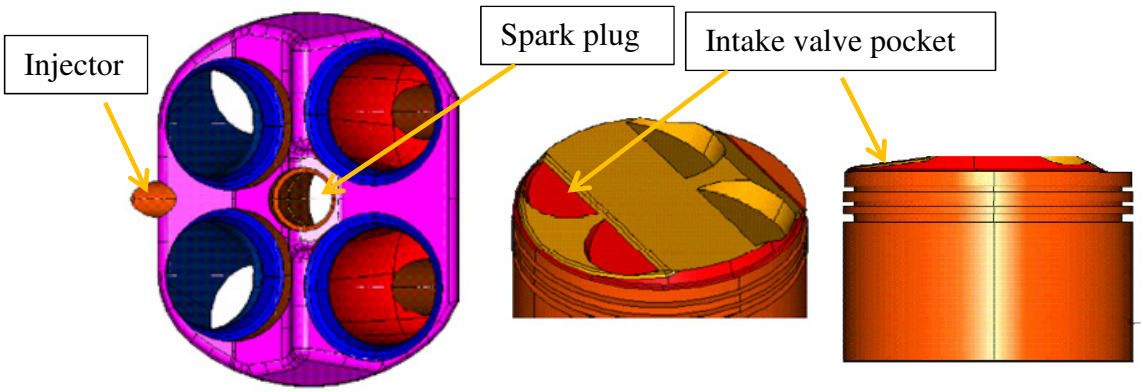

Figure 3.4 Combustion Chamber and Piston Crown

3.2.2 Electrohydraulic Valvetrain System

An electro hydraulic valvetrain system is mounted on the cylinder head to enable independent control of the valve timings and lifts. Each valve is attached to an electrohydraulic actuator which allows valve motion to vary with engine speed to meet set limits at every speed and position. The valve is screwed in a plunger in the actuator. A fast response Moog servo valve is mounted on the side of the actuator and switches the high pressure hydraulic oil circuit. The hydraulic oil pushes the plunger up and down in the cylinder of the actuator. The maximum allowable peak valve velocity is about 4.5 m/s. The variable valve lift range is from 0 to 9.5mm. The valve lift is measured by a Linear Variable Differential Transformer (LVDT) Positional feed-back from the plunger and engine valve assembly is continually provided by the LDTV, which allows actual profiles to be continually monitored and corrected from cycle-to-cycle, to ensure accuracy and repeatability. The valve lift profile during the valve train test in four-stroke operation at engine speed from 1000rpm to 6500rpm is shown in Figure 3.6.

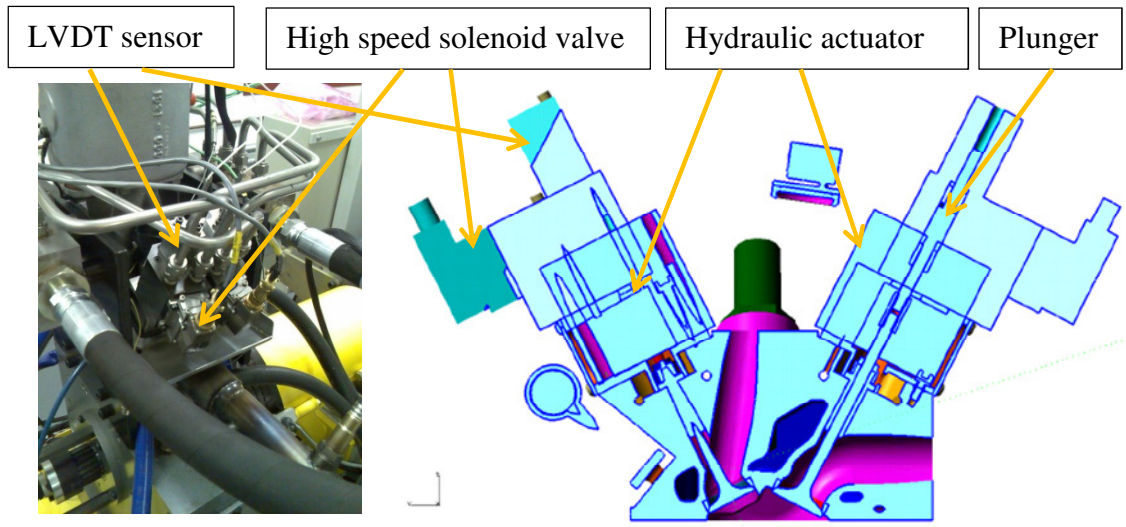

Figure 3.5 Electrohydraulic Valve Actuator and its Cross Section Drawing

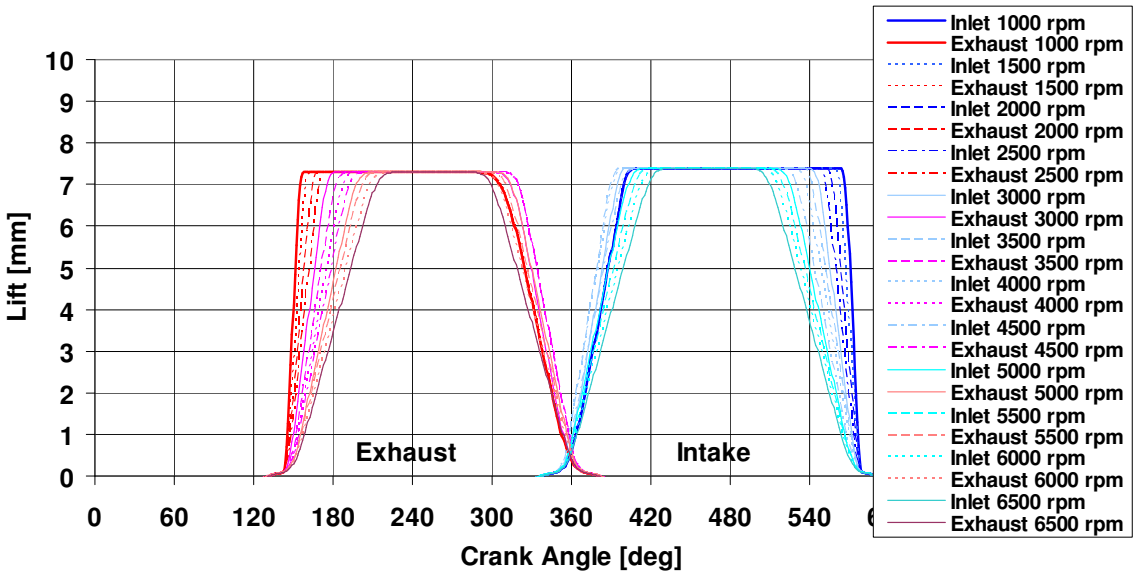

Figure 3.6 Valve Lift Profiles in Four-stroke Operation

The high-pressure oil is supplied by a hydraulic pump unit shown in Figure 3.7. It comprises of a variable delivery piston hydraulic pump rated at 18.5KW and 34l/min delivery at 280bar. It is equipped with 3 micron on-line and 10 micron off-line filtration system, using ISO 32 hydraulic oil from a 225l oil tank supplied by DGB Hydraulics Ltd. It includes a 10l bladder accumulator to maintain pressure during a power cut out and a load control valve powered by UPS. Feeds and drain manifolds are mounted on the engine with oil pressure sensor incorporated into feed manifold.

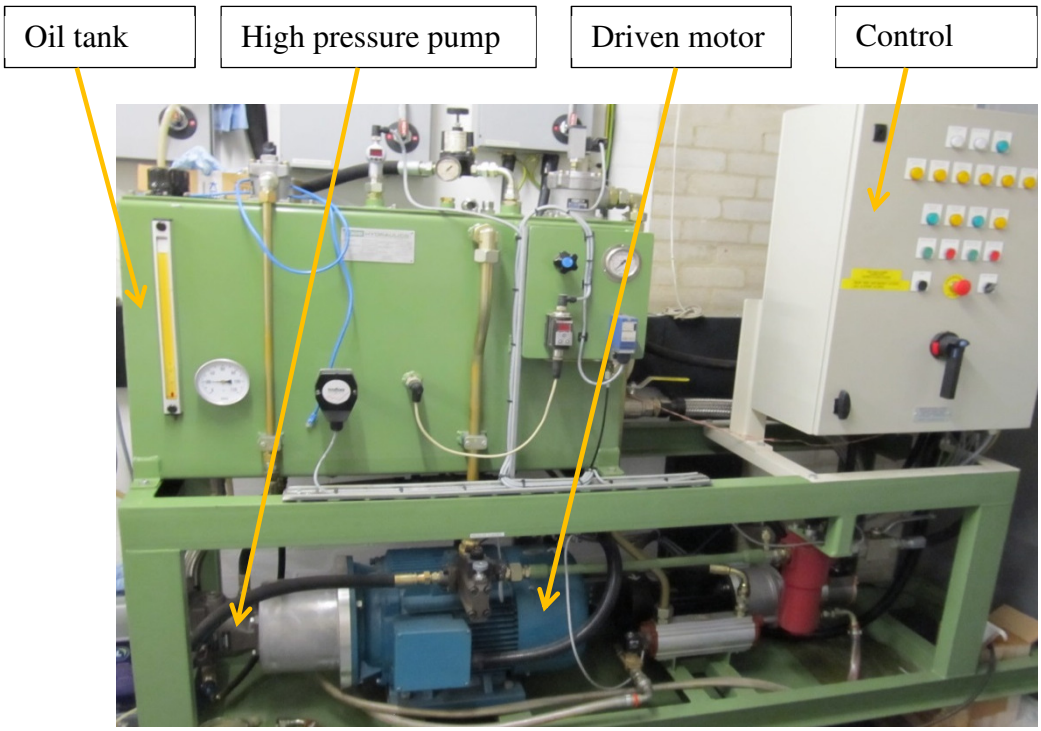

Figure 3.7 Hydraulic Pump Unit

Each valve actuator is controlled by an individual control circuit. So there are four sets of control circuits in the valve control unit (VCU) as shown in Figure 3.8. The hydraulic valve train does not have a physical cam ramp to control opening and closing events. In order to protect the valve and valve seat, a 'soft-landing' strategy is incorporated in the valve control program, which also limits seating velocity at 0.32mm lift to the velocity of 0.009mm/deg CA which is equivalent to 0.054 m/s @ 1000rpm, 0.243 m/s @4500rpm and 0.351 m/s @6500rpm.

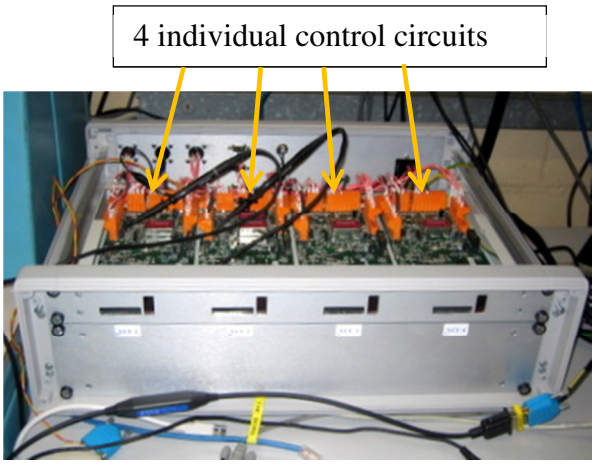

Figure 3.8 Valve Control Unit

3.2.3 Fuelling System

The gasoline fuel supply and injection system comprises of a direct gasoline injector installed on the side of combustion chamber below the two intake valves, a low-pressure fuel pump, a high-pressure fuel pump, a low pressure regulator, a high pressure relief valve, a common rail and a fuel heat exchanger, as shown schematically in Figure 3.9. Fuel is supplied from a 25 litre tank mounted on the test cell wall and pressurised by a low-pressure pump to 3.5bar and then pumped to 100bar by a high pressure pump before flowing into the common rail. When ethanol blended fuel is used, it is first pre-mixed and then poured into the tank. The low-pressure pump keeps circulating the fuel in the tank to prevent separation of the fuel blends. The high-pressure pump is electrically driven by a fixed speed AC electric motor and the fuel pressure is monitored by the ECU using a fuel rail pressure sensor and regulated by a high-pressure relief valve, set at 100bar. A heat exchanger is used to remove the excess heat from the pressurised-fuel return in order to maintain a constant fuel temperature. An instantaneous fuel flow meter is installed between the high pressure fuel pump and injector for the measurement of fuel flow rate.

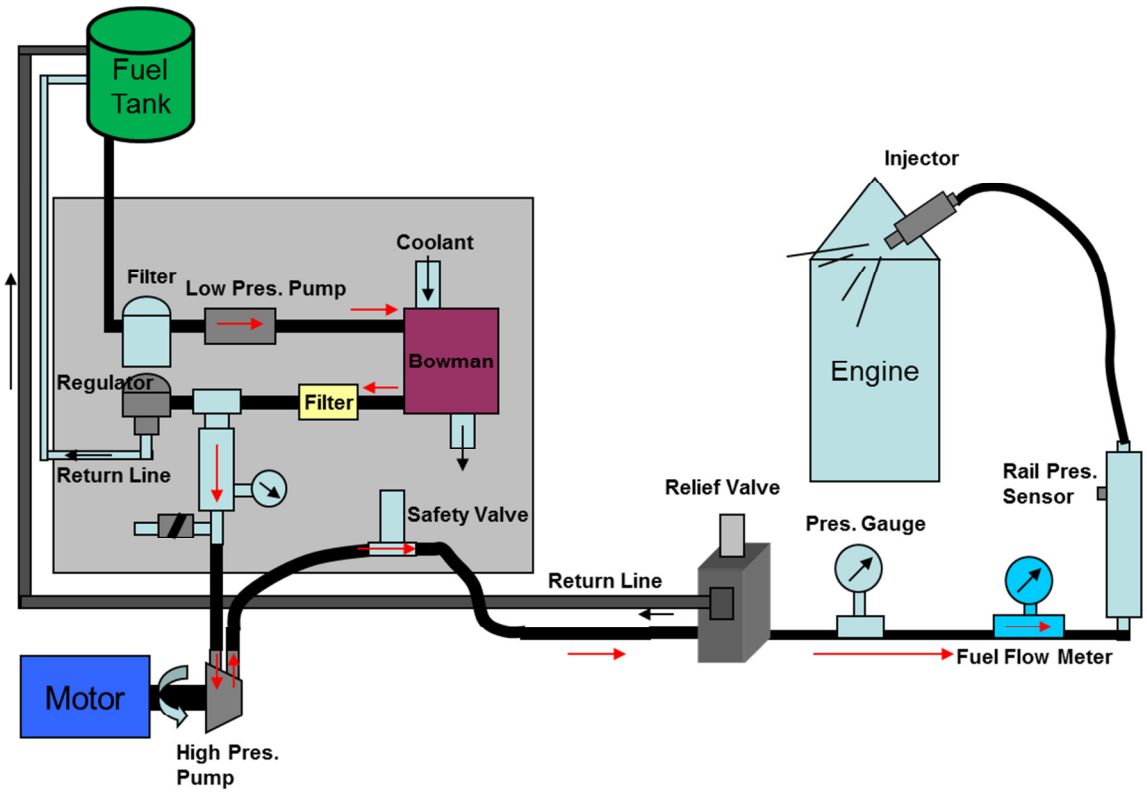

Figure 3.9 Fuel Supply Circuit Diagram

The fuel is injected by a Denso GDI injector mounted under the intake port at an injection pressure of 100bar. The GDI injector is the second generation solenoid GDI injector with a double slit nozzle and is used on Lexus IS series cars since 2007. The injector and its spray pattern are shown in Figure 3.10 [76]. This is designed to form a double thin fan shape spray in the cylinder, as shown in Figure 3.11. The injection mass flow rate was calibrated at the injector pressure of 120bar and 150bar by engine supplier, as shown in Figure 3.12.

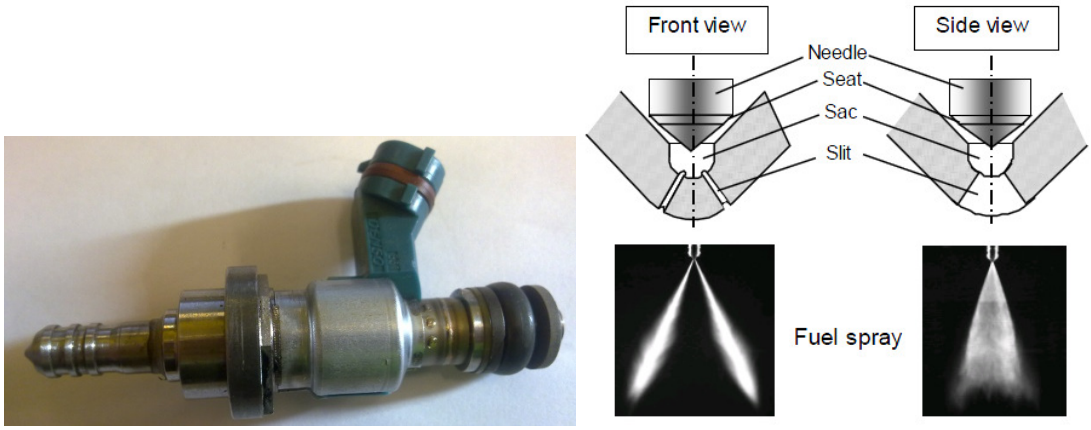

Figure 3.10 Double Slit Solenoid GDI Injector and its Spray Pattern

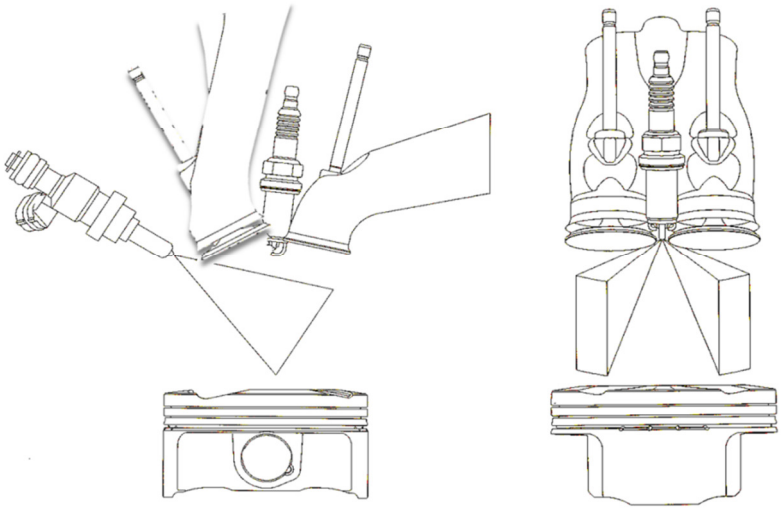

Figure 3.11 Double-fan Spray in Combustion Chamber

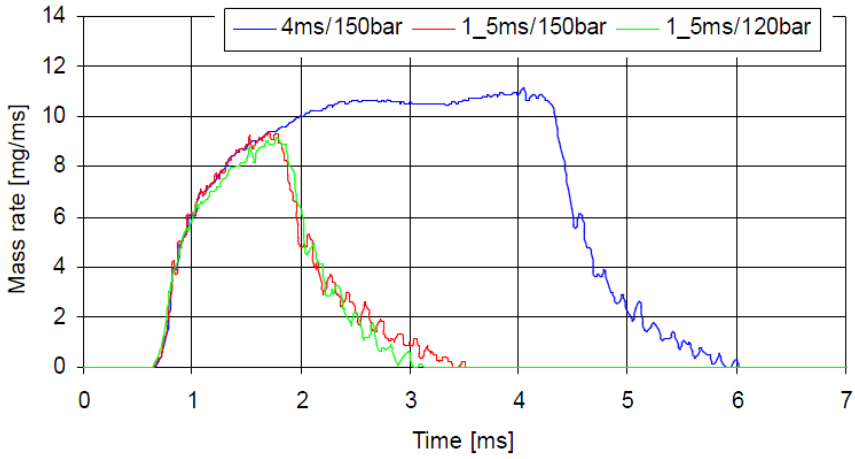

Figure 3.12 Injector Mass Flow Rate Calibration

3.2.4 Engine Control System

The engine control system used in this work comprises of an engine control unit (ECU), a VCU, and user interface, INCA. As shown in Figure 3.13, the ECU controls spark timing via a pen coil mounted on the spark plug, an injector via a DI driver, and an electronic throttle. VCU controls the four electro hydraulic valves and communicates with the ECU via a high speed CAN bus. User can input all the operating parameters including spark timing, injection timing and pulse width, valve timings and lifts via a calibration interface program, INCA.

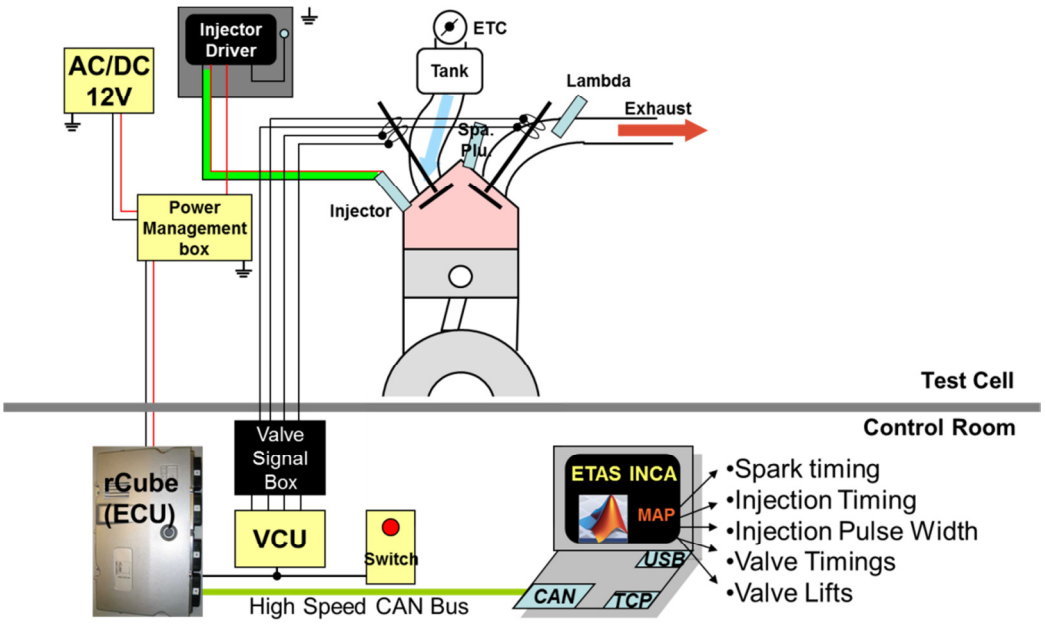

Figure 3.13 Engine Control System Diagram

Figure 3.14 shows the INCA interface where the user can monitor engine operating conditions and input engine control parameters. In the ECU, there are 4 sets of engine control parameter maps, which are for four-stroke SI, four-stroke CAI, two-stroke SI and two-stroke CAI operations. All sets of the maps are switchable when engine is running for mode switching tests. The two intake and two exhaust valves can be operated individually, in which more complex valve events can be performed and more advanced engine operating mode can be achieved. For example, for exhaust gas rebreathing CAI operation, one exhaust valve can open and close as normal and another exhaust valve can open during the intake stroke, so that the exhaust gas can be sucked back into cylinder for initiating CAI combustion in the next cycle.

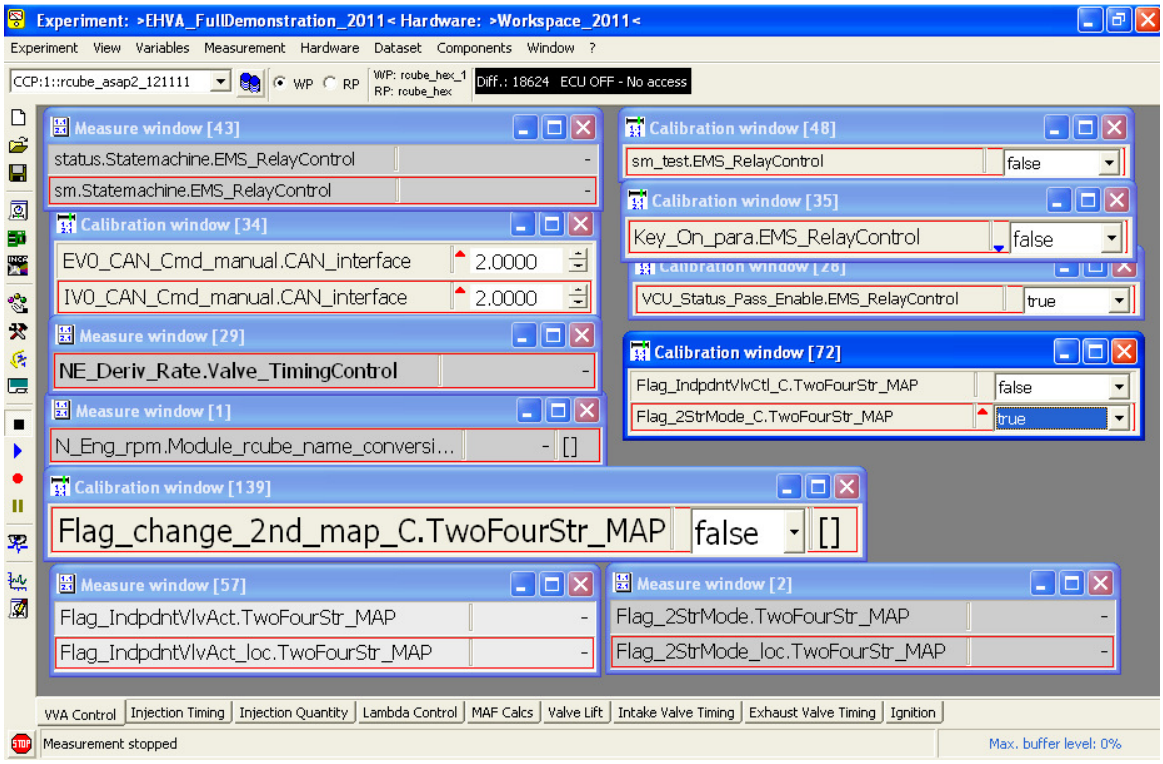

Figure 3.14 INCA Interface

The most common valve profiles for two-stroke SI and CAI operation are illustrated in Figure 3.15. In two-stroke SI operation, in order to make use of the momentum of the fresh charge and achieve the post-scavenging, the exhaust valve closes after the intake valve close. In two-stroke CAI operation, in order to trap more burnt gas in the cylinder, both the intake and exhaust valve durations are shortened. The amount of the residual gas is controlled principally by the exhaust valve closure and varied depending on the requirement of the operation conditions. In two-stroke operations, fuel injection is timed

to take place immediately after the valve closure in order to maximize the period of evaporation and atomization.

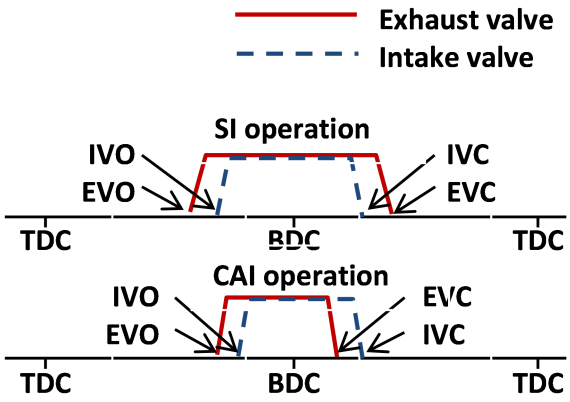

Figure 3.15 Sketch of Valve Profiles for Two-stroke SI and CAI Operation

3.3 Dynamometer System

The dyno system used in this work is supplied by CP engineering and comprises an AC motor, an inverter, a coolant and oil conditioning circuit and a remote control PC with an operating software. The AC motor shown in Figure 3.16 is rated at 40KW power and 6000rpm maximum speed capable of motoring and regeneration modes. A coolant and oil conditioning circuit regulates coolant temperature and oil pressure and temperature. The oil pump was employed to supply pressurised oil of 3.5bar to the engine.

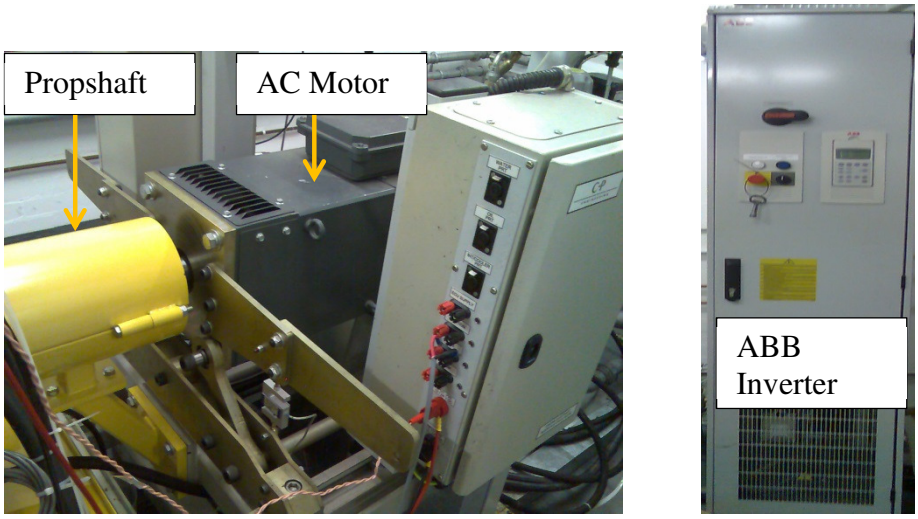

Figure 3.16 AC Dynamometer and Inverter

The dynamometer is remotely controlled by a PC operating with CADET V12 software. The software enabled the automatic and manual control modes of the dyno, data logging, low and high alarm level shut down and the dyno speed selection. It also monitors transient engine speed and torque, as well as oil temperature and pressure and coolant temperature. The user interface is shown in Figure 3.17. In most of tests in this work, the coolant and oil temperature was set to 80degC.

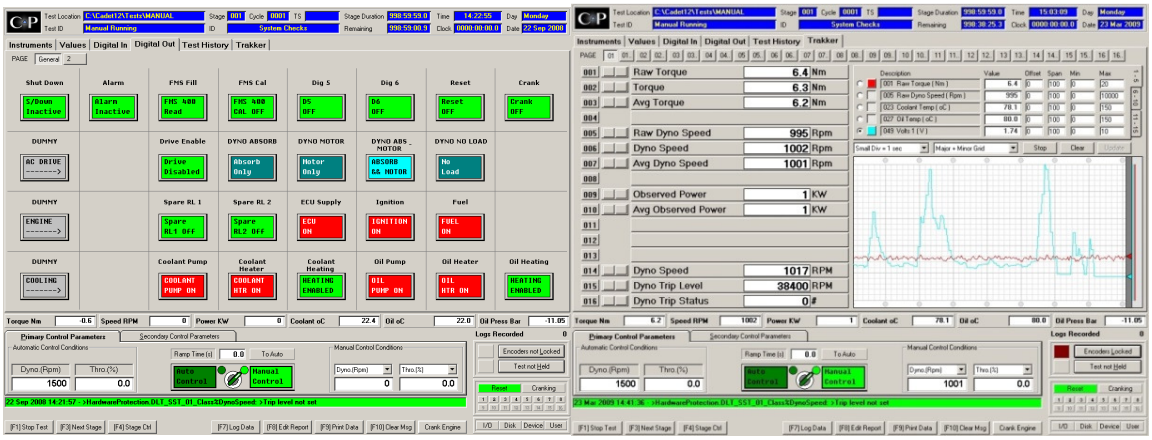

Figure 3.17 Dynamometer Control Software Interface

3.4 Supercharging System

The supercharging system used for this study is connected to the engine's intake system to supply the compressed air at a pre-set boost pressure and temperature via closed loop control of heaters and heat exchangers. The supercharger is an AVL type 515 rotary vane type compressor as shown in Figure 3.18. The remote supercharger controller enables the temperature and pressures of the charged air to be controlled. The control range of the charged air temperature begins at 15 degC above the cooling water temperature and extends up to 130 degC. The control range of the air pressure extends from 1.1bar to 3.2bar abs. The supercharging equipment provided air flow up to a maximum of 300m^3/h at 20 degC and 1 bar abs.

Figure 3.18 AVL Supercharger and its Remote Controller

3.5 Measurement System

The measurement system includes in-cylinder pressure measurement, instantaneous intake and exhaust pressure, steady temperature measurement, air and fuel flow rate measurement, linear lambda measurement and exhaust emissions analysis, as shown in Figure 3.1.

a) In-cylinder pressure transducer and charge amplifier

The instantaneous in-cylinder pressure was measured by a water cooled piezoelectric pressure transducer (Kistler 6061B) with a measurement range of 0-250 bar gauge and sensitivity of -25 PC/bar installed on the cylinder head. The sensor outputs a charge signal which is converted into a voltage signal by a charge amplifier (Kistler Type 5011), as shown in Figure 3.19.

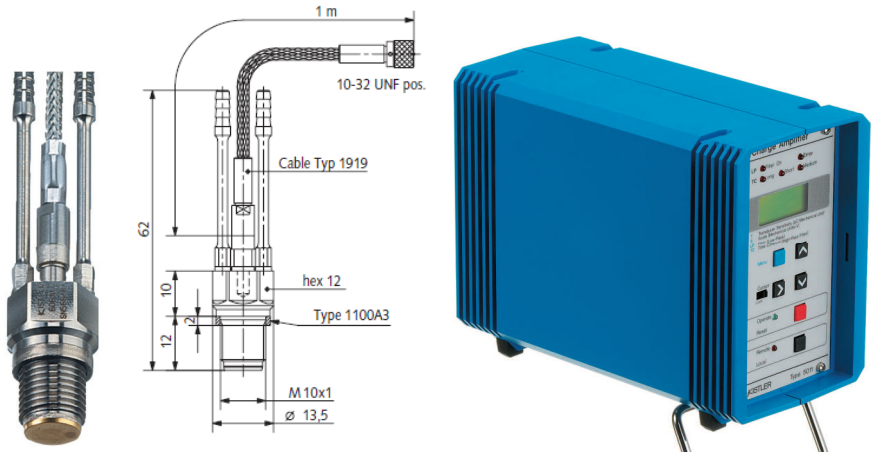

Figure 3.19 Kistler 6061B Pressure Transducer and 5011A Charge Amplifier

b) Intake and Exhaust Pressure and Temperature

Both the instantaneous intake and exhaust pressures were measured by two Kistler piezo resistive pressure transducers installed in the intake runner and exhaust runner respectively, as shown in Figure 3.20. The intake pressure transducer, type 4007BA20F, can measure up to 20bar absolute pressure and is capable of continuous high-temperature operation up to 200 degC. It is connected to a Kistler amplifier, Type 4618AO with pressure and temperature output. The exhaust pressure transducer, type 4007BA5F, can measure absolute pressure up to 5bar. The exhaust pressure transducer is mounted in a cooling adaptor, type 7525A2, to prevent the damage from the high exhaust-gas temperature.

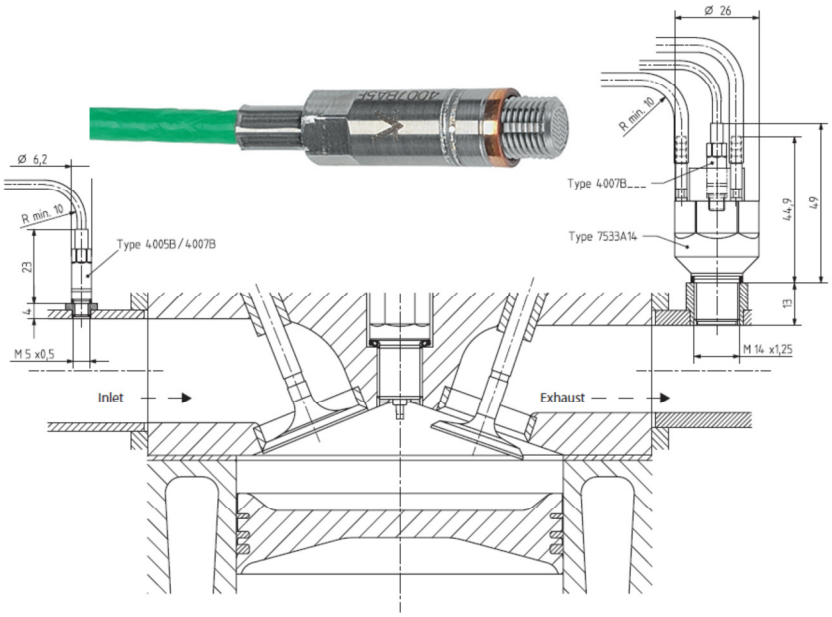

Figure 3.20 Kistler Type 4007B Piezo-resistive Pressure Transducer and its Installation for Instantaneous Intake and Exhaust Pressure Measurement

Intake and exhaust temperature are measured by a standard K- type thermocouples at intake manifold and exhaust port.

c) Fuel flow meter

The fuel flow rate is measured by a Coriolis mass flow meter, type PROMASS 83A, supplied by Endress Hauser at high pressure line before common rail. The flow meter

shown in Figure 3.21 must be installed at the lowest level of the whole fuelling system to avoid the bubbles coming into it and affect the reading. It outputs frequency and current signals. In this work the current signal is converted into a voltage signal and then logged by the data acquisition system.

Figure 3.21 Coriolis Mass Flow Meter

d) Intake air flow meter

A laminar air flow meter is installed in the engine's intake system to measure the intake mass flow rate. The air flow meter shown in Figure 3.22, type HFM-200 LFE, is supplied by Teledyne Hastings Instruments and Chell Instruments with the measuring range of 0-1500 standard litre per minute and measuring uncertainty of 0.73%.

Figure 3.22 Laminar Air Flow Meter

e) Lambda sensor

The air fuel ratio for this study is measured by a wide band lambda sensor (Bosch UEGO LSU4.0) in the exhaust pipe.

f) Gaseous emission analyser

The exhaust emissions are analysed by a Horiba 7170DEGR gas analyser system which sampled the exhaust gases from the exhaust manifold. The concentration of CO, CO_2, O_2, THC and NOx in the exhaust gas are analysed and outputted via LAN port. The readings are logged on cycle basis and averaged over 100 consecutive engine cycles.

It is worth pointing out that the C, H, O atom number ratio should be reset in AFR set menu when different fuel is used. Table 3.2 and Table 3.3 show the fuel property of E15 and E85 respectively and the calculations used for working out C, H, O atom number ratio.

Table 3.2 E15 Fuel Properties

Fuel	**Ethanol**			**Gasoline**			**E15**		
Volume [ml]	15			85			98.70		
Density [g/ml]	0.789			0.72			0.74		
Weight [g]	11.835			61.2			73.035		
	C	**H**	**O**	**C**	**H**	**O**	**C**	**H**	**O**
Atom number	2	6	1	8.26	15.5	0	6.22	12.41	0.3
Mole number	0.257			0.534			0.79		
LHV [kJ/g]	26.9			43			40.39		
A/F	8.9955			14.603			13.69		

Table 3.3 E85 Fuel Properties

Fuel	**Ethanol**			**Gasoline**			**E85**		
Volume [ml]	85			15			99.83		
Density [g/ml]	0.789			0.72			0.78		
Weight [g]	67.065			10.8			77.865		
	C	**H**	**O**	**C**	**H**	**O**	**C**	**H**	**O**
Atom number	2	6	1	8.26	15.5	0	2.38	6.577	0.9
Mole number	1.4579			0.0942			1.55		
LHV [kJ/g]	26.9			43			29.133		
A/F	8.996			14.60			9.77		

3.6 Data Acquisition System

All the experimental test data is analysed and logged by an in-house data acquisition system, which is developed at Brunel University by the author.

a) Hardware

The hardware connection is shown in Figure 3.23. A high speed A/D card and a multi-serial card are connected to a PC via USB port. The Horiba Emission analyser is connected to the same PC via LAN port and its communication protocol is TCP and UDP. The ECU is connected to the PC via PCMCIA port. Therefore, the data logged from every connection can be synchronised on the cycle basis in the software.

The high speed card used for this study is a National Instrument (NI) USB-6353 high speed A/D card with 32 -10~ +10V A/D channels and external clock trigger function, as shown in Figure 3.24. The maximum sampling speed is 1Mega samples per second. In this study, only 18 channels are used and the channel definition is shown in Table 3.4. An encoder with the resolution of 1 pulse per CA is coupled to the engine crankshaft and produces the crank angle signal (TTL) and TDC reference signal (one pulse per revolution). The valve lift signal from LVDT sensors is converted into single ended voltage by an amplifier and connected to the A/D card. The lambda sensor signal is conditioned and digitalised by a Motec Unit and sent to multi-serial card at the rate of

20Hz. The thermocouple signal has to be converted by a thermocouple conditioner shown as green box in Figure3.24 before it can be logged by the A/D card.

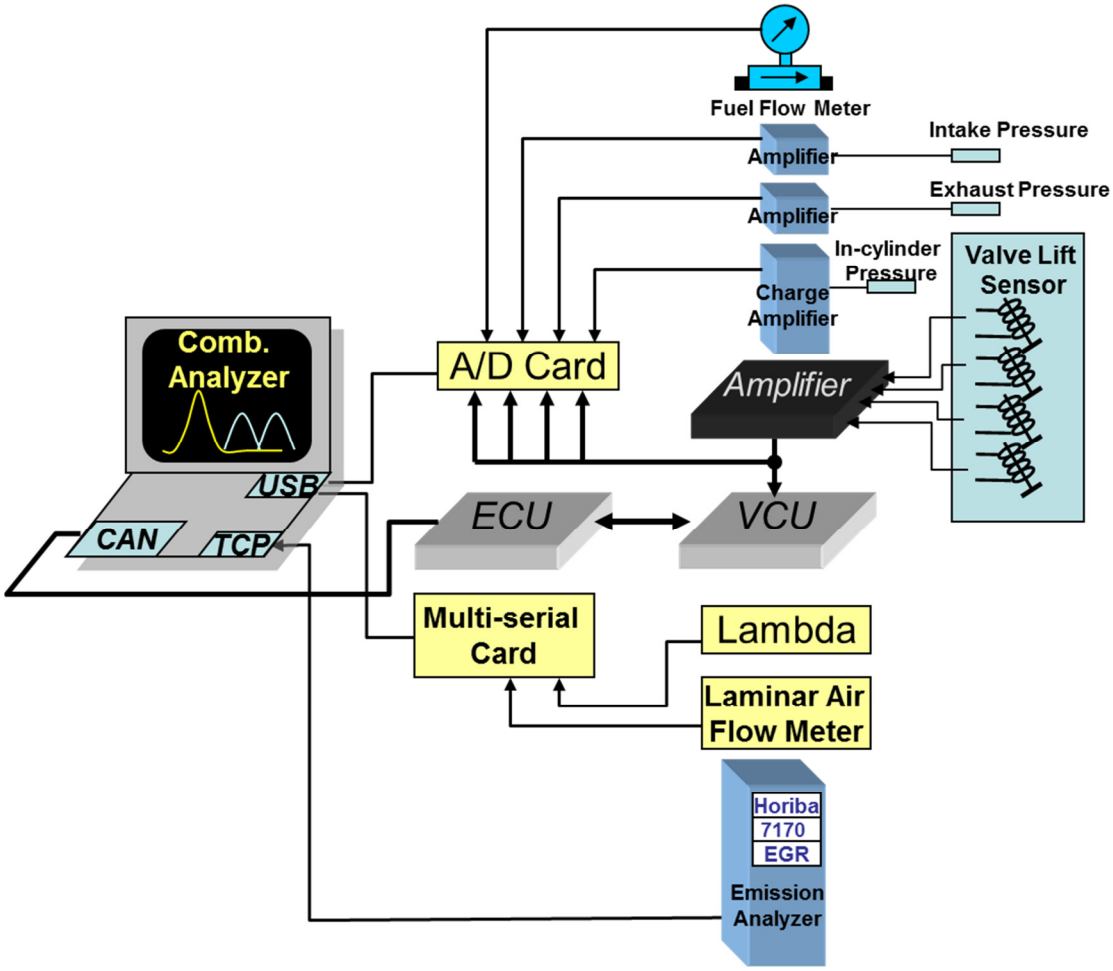

Figure 3.23 Diagram of Data Acquisition System

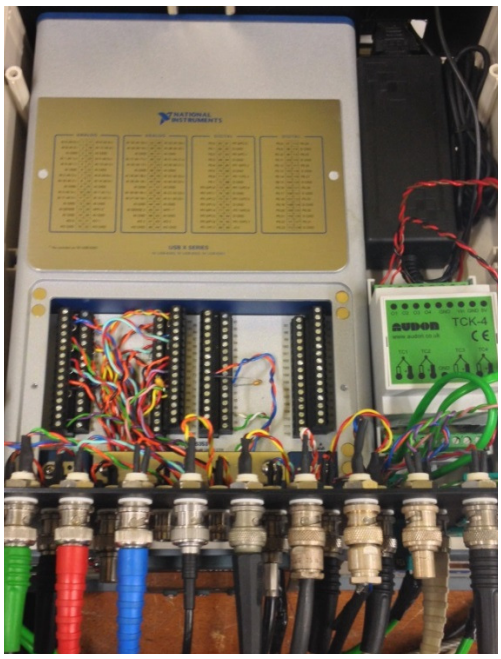

Figure 3.24 DAQ Card

Table 3.4 Channel Definition in DAQ Card

Channel No.	**Signal Name**
1	Exhaust valve 1 lift
2	Exhaust valve 2 lift
3	Intake valve 1 lift
4	Intake valve 2 lift
5	In-cylinder pressure
6	TDC reference
7	Intake pressure
8	Exhaust pressure
9	Injection
10	Spark
11	Torque
12	Speed
13	Fast UEGO
14	Air flow rate
15	Fuel flow rate
16	Fast CO2
17	Intake temperature
18	Exhaust temperature

b) Software

A ‘Transient Combustion Analyser’ programme was developed by the author. In addition to data logging, the software performs on-line calculation and display of the heat release, combustion characteristics, fuel consumption, specific emissions and efficiencies, as shown in Figure 3.25.

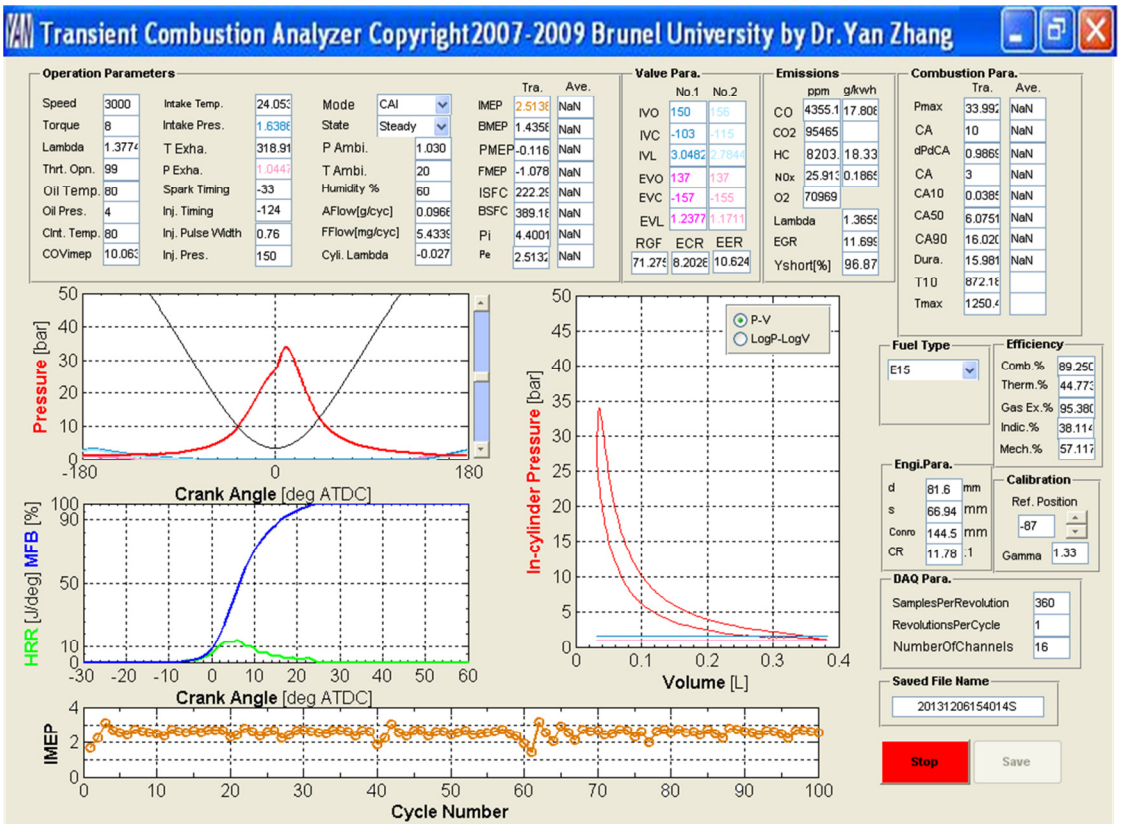

Figure 3.25 Transient Combustion Analyser Panel

The program interface is developed in GUI Matlab and the relevant calculations are coded using ‘m code’ due to the advantage of large matrix calculation in Matlab. Only the data called from low level A/D card buffer is through NI DAQmax.

The cylinder pressure transducer is a piezoelectric sensor, which outputs a charge referenced to an arbitrary ground and then the charge signal is converted into a voltage signal by a charge amplifier. The relative cylinder pressure must be then converted into an absolute pressure. The conversion process usually is referred to as ‘pegging’. In this work, the in-cylinder pressure signal is pegged on the intake abs pressure [77]. This

involves setting the cylinder pressure at intake bottom dead centre equal to intake manifold pressure, which is measured by a piezo-resistive absolute pressure transducer.

In the engine, there is always a difference between thermodynamic TDC and mechanical TDC due to the presence of heat transfer and gas leakage issues. The difference is referred as 'thermodynamic heat loss angle', which reflects the heat loss during compression and expansion process. In this study, the thermodynamic TDC was calibrated using motoring in-cylinder pressure [78] at the engine speed of 1500rpm. It was observed that the thermodynamic heat loss angle was calculated to be 0.8deg CA at 1500rpm.

In order to avoid piston and valve interference, the piston position indicated by the black line and valve lifts by the blue lines are shown in the top left graph.

The calculations used in the program regarding heat release, combustion characteristics, fuel consumption, specific emissions are from [77, 78]. In addition, detailed analyses of various efficiencies have been included to assist in the identification of loss at each stage of the energy conversion process.

The net indicated mean effective pressure is calculated

$$\text{IMEP}=\begin{cases}\int_{-180}^{540}\frac{p}{Vs}\dot{V}(\varphi)d\varphi & (4-stroke)\\ \int_{-180}^{180}\frac{p}{Vs}\dot{V}(\varphi)d\varphi & (2-stroke)\end{cases} \qquad 3\text{-}1$$

The gross indicated mean effective pressure is given by

$$\text{IMEP}_{\text{gross}}=\int_{-180}^{180}\frac{p}{Vs}\dot{V}(\varphi)d\varphi \qquad 3\text{-}2$$

where,

Vs is the displacement volume.

The pumping mean effective pressure is defined by

$$\text{PMEP}=\text{IMEP}-\text{IMEP}_{\text{gross}} \qquad 3\text{-}3$$

and the

$$\text{gas exchange efficiency} = \text{IMEP}_{\text{gross}} / \text{IMEP} . \quad (3\text{-}4)$$

The combustion efficiency is defined as the ratio of the heat released from the fuel to the chemical energy of the fuel,

$$\eta_{Combustion} = \frac{Q_1}{E_{fuel}} = 1 - \frac{G_{CO} * LHV_{CO} + G_{HC} * LHV_{HC}}{Fuel\ flow\ rate * LHV} \quad (3\text{-}5)$$

where,

Q_1 is the heat released by fuel

E_{fuel} is the chemical energy of fuel

G_{CO} is CO emission mass flow rate

LHV_{CO} is the low heat value of CO, 10.1 [kJ/g]

G_{HC} is HC emission mass flow rate

LHV_{HC} is the low heat value of HC, 43 [kJ/g]

LHV is Low heat value of fuel

The thermodynamic efficiency is defined as the ratio of the gross work of the cycle to the heat leased by fuel,

$$\eta_{Thermodynamic} = \frac{W_{Gross}}{Q_1} = \frac{IMEP_{Gross} * V_s}{Fuel\ flow\ rate * LHV * \eta_{Combustion}} \quad (3\text{-}6)$$

where,

W_{Gross} is the gross work of the cycle

$IMEP_{Gross}$ is the gross indicated mean effective pressure

V_s is the displacement volume

The indicated efficiency is defined as the ratio of the gross work of the cycle to the chemical energy of fuel, and its formula is:

$$\eta_{Indicated} = \frac{W_{Gross}}{E_{fuel}} = \eta_{Thermodynamic} * \eta_{Combustion} \quad (3\text{-}7)$$

The compression work consumed by the supercharger is calculated as follows,

$$\text{Wc}=Air\ flow\ rate * Cp * T1 * \left[\left(\frac{P2}{P1}\right)^{\frac{\gamma-1}{\gamma}} - 1\right] / \eta_c / \eta_{mechanical} \quad \text{3-8}$$

where,

For the air, Cp=1.012 J/(g.K) [78]

$\gamma = 1.4$

Compressor efficiency $\eta_c = 60\%$ [78]

Compressor Mechanical efficiency $\eta_{mechanical} = 90\%$ [78]

T1 Supercharger inlet temperature

P1 Supercharger inlet pressure

P2 Supercharger outlet pressure

Finally, the overall mechanical efficiency is determined by

$$\eta_{mech} = (\text{BMEP} - \text{Wc} / \text{Vs}) / \text{IMEP} \quad \text{3-9}$$

which includes the additional compression work required by a supercharger.

3.7 Summary

This chapter presented the details of the 2/4-stroke GDI engine and its relevant hydraulic valve system, fuelling system and control system used during all the experimental tests. This is followed by the dyno system and supercharging system used to serve the engine. The operating principle of all the main sensors and analysers was explained. In the last section, the in-house data acquisition system and the parameter definition and calculations were also explained.

Chapter 4

Cycle-resolved Air Short-circuiting and Residual Gas Measurement

Chapter 4 Cycle-resolved Air Short-circuiting and Residual Gas Measurement

4.1 Introduction

This chapter introduces the air short-circuiting phenomenon in two-stroke engines which has a strong impact on the engine combustion, performance and emissions. This is followed by the development and application of the methods to detect and measure the air short-circuiting on a cycle-resolved basis. In order to measure the residual gas fraction in a two-stroke engine and investigate the effect of residual gas fraction on CAI combustion and engine performance, a cycle-resolved residual gas measurement technique is implemented and applied to the single cylinder engine.

4.2 Air Short-circuiting in Two-stroke Engines and its Measurement

In a typical two-stroke engine, there is a significant overlap between the intake and exhaust processes, as shown in Figure 2.1, during which the burnt gases can be scavenged from the cylinder by fresh charge. As a result, some of the fresh charge can pass directly across the combustion chamber and into the exhaust port during the overlap period, as shown in Figure 4.1. This phenomenon is referred to as air short-circuiting and its presence in the two-stroke engine operation can lead to a number of drawbacks, including

1) Reduction in scavenging efficiency and increase in the gas exchange loss.
2) Increase in fuel consumption and uHC emissions in port fuel injection engines and carburetted engines.
3) False reading of the relative air to fuel ratio (lambda) in the exhaust pipe and fuel rich combustion, accompanied with higher fuel consumption and higher emissions.
4) Reduction in the conversion efficiency of a three-way catalyst.

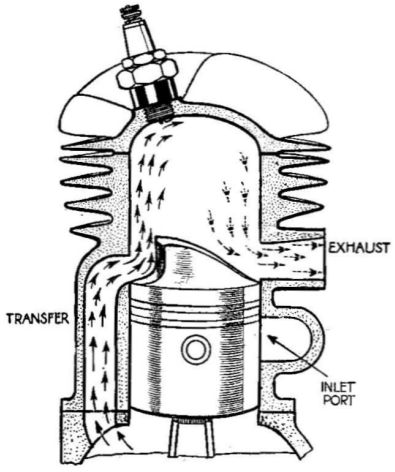

Figure 4.1 Short-circuiting of the Fresh Air during Scavenging Process

In the history of developing and improving two-stroke engines, researchers had long recognised the issue of short-circuiting during the scavenging process in two-stroke engines and resolved to measure short-circuiting and scavenging efficiency through liquid simulation techniques [79, 80] in the model engine and gas visualization technology in the motored engine operations [81, 82]. Although some other methods for the measurement of the scavenging efficiency of the port scavenged two-stroke engine had also been attempted [83-85], the first widely used experimental method to measure the short-circuiting was proposed by Jante [86] using the distribution of the gas velocity measured by the pitot tubes first in motored conditions, and then it was further developed for measurement under firing conditions [87]. Another experimental method for determining the scavenging efficiency using the measurement of the oxygen concentration was postulated in the late 1940s [88]. Based on this method, the scavenging flow was further assessed by the measurement of scavenging, trapping and charging efficiency as a function of scavenge ratio [89]. Then the efficiencies of loop, cross, and uniflow scavenging were compared using this parameter [90].

4.3 Cycle-resolved Air Short-circuiting Measurement by Fast UEGO

In the tailpipe, the short-circuiting rate (y_{short}) can be defined as the ratio of the mass flow of short-circuited air to the mass flow of the exhaust gas, as shown in equation (4-1).

$$y_{short} = \frac{A_s}{A_e} \quad \text{4-1}$$

where:

A_s: Mass flow rate of short-circuited air

A_e: Mass flow rate of exhaust gas

According to the mass conservation equation (4-2),

$$\boldsymbol{A_e = A_s + A_c + A_f} \quad \textbf{4-2}$$

where:

A_c: Mass flow rate of the combusted air

A_f: Mass flow rate of fuel

y_{short} can be represented by equation (4-3).

$$\boldsymbol{y_{short} = \frac{A_s}{A_s + A_c + A_f}} \quad \textbf{4-3}$$

Unless the instantaneous mass flow rate, A_s, is measured directly in the exhaust, the short-circuiting rate cannot be calculated from equation (4-3).

Since it is known that the short-circuited air coming into the exhaust pipe dilutes the exhaust gases and also causes an increase in oxygen concentration. In this case, the widely used oxygen sensor on the exhaust pipe cannot accurately reflect the lambda value. Equation (4-4) and (4-5) show the difference between the measured lambda in the tailpipe (λ_{tp}) and the actual lambda in the engine cylinder (λ_c).

$$\boldsymbol{\lambda_{tp} = \frac{A_s + A_c}{A_f} / AFR_{stoichiometric}} \quad \textbf{4-4}$$

$$\boldsymbol{\lambda_c = \frac{A_c}{A_f} / AFR_{stoichiometric}} \quad \textbf{4-5}$$

where,

$\boldsymbol{AFR_{stoichiometric}}$ is the stoichiometric air to fuel ratio.

By substituting equation (4-4) and (4-5) into equation (4-3), short-circuiting rate can be presented as a function of λ_{tp} and λ_c, as shown in equation (4-6)

$$y_{short} = \frac{\lambda_{tp} - \lambda_c}{\lambda_{tp} + AFR_{stoichiometric}^{-1}} \qquad \textbf{4-6}$$

The exhaust lambda (λ_{tp}) can be measured by a standard lambda sensor in the exhaust pipe. The in-cylinder lambda (λ_c) can be measured from exhaust port close to cylinder. If the exhaust gas is sampled before intake process begins, the measured lambda will be the same as the in-cylinder lambda (λ_c). When fresh air comes into and across the cylinder, the lambda value will start to increase because of the dilution effect of the fresh air, as shown in Figure 4.2.

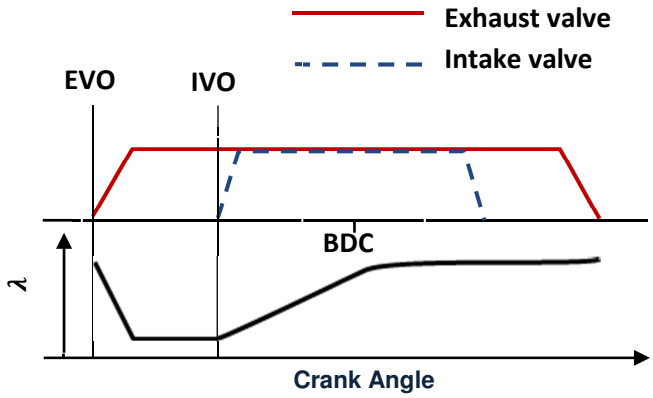

Figure 4.2 Lambda Variations during Scavenging Process

In order to obtain the lambda variation against crank angle, the standard wide band lambda sensor was modified. Firstly, the two original protection caps were removed as shown in Figure 4.3. Then the sensor was fitted into a fast sampling head to increase the speed of delivery of the sampled gas from exhaust port to the modified lambda sensor, as shown in Figure 4.4. Figure 4.5 shows the structure of the fast sampling head. In the fast sampling head, there are two chambers: constant pressure chamber and lambda sensor chamber. The pressure in the two chambers is kept constant by the two vacuum regulators to stabilise the sample flow and eliminate the exhaust pulsation effect. The pressure in the constant pressure chamber is 0.7bar absolute and the pressure in the lambda sensor chamber is 0.65bar absolute. Between the two chambers there is a

capillary with 0.12mm inner diameter, which assures the steady sample flow stream towards the lambda sensor orifice and minimises the measuring error caused by the fluctuation of the sample flow.

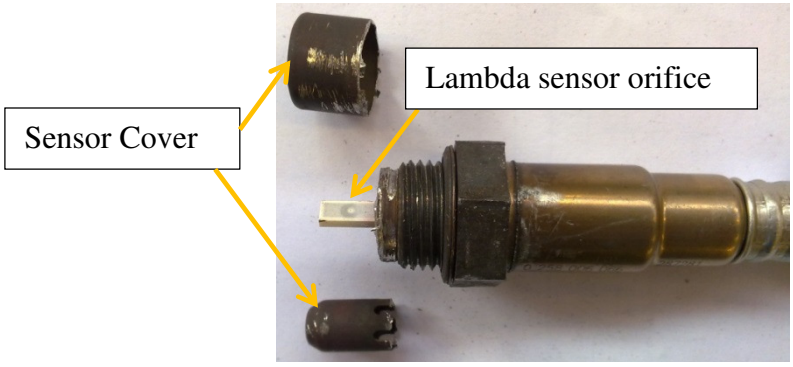

Figure 4.3 Modified Wide Band Lambda Sensor

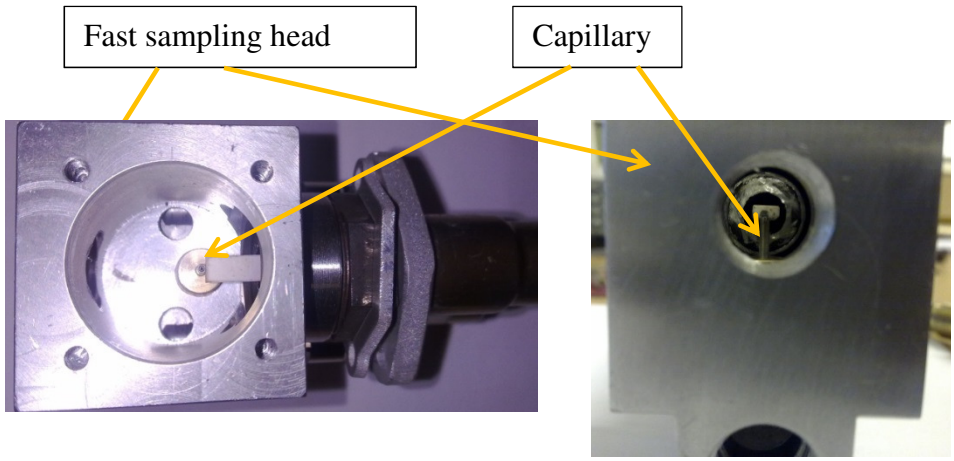

Figure 4.4 Installation of Modified Lambda Sensor in a Fast Sampling Head

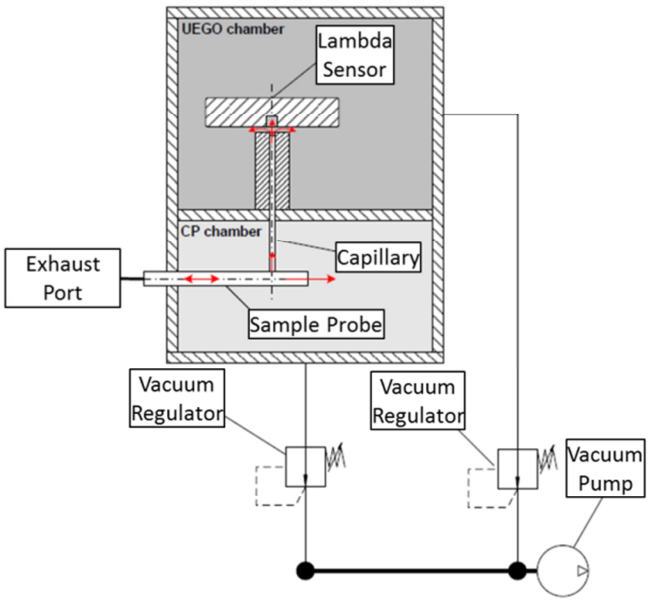

Figure 4.5 Sketch of the Structure of the Fast Sampling Head

In order to catch the first portion of the exhaust gas which has the same oxygen concentration as the in-cylinder burned gas, the exhaust gas must be sampled very close to the exhaust valve before it mixes with the exhaust gases from the previous cycle in the exhaust port. A thin sampling probe was made and positioned in the exhaust port, as shown in Figure 4.6. In addition to the fast lambda sensor, a standard lambda sensor is also required to measure the averaged lambda in the exhaust pipe. The installation of the fast and standard lambda sensors is shown in Figure 4.7.

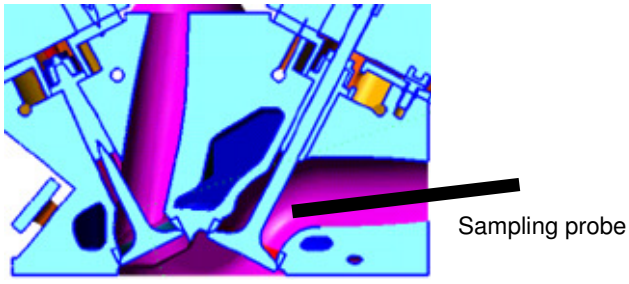

Figure 4.6 Sketch of the Installation of the Sampling Probe

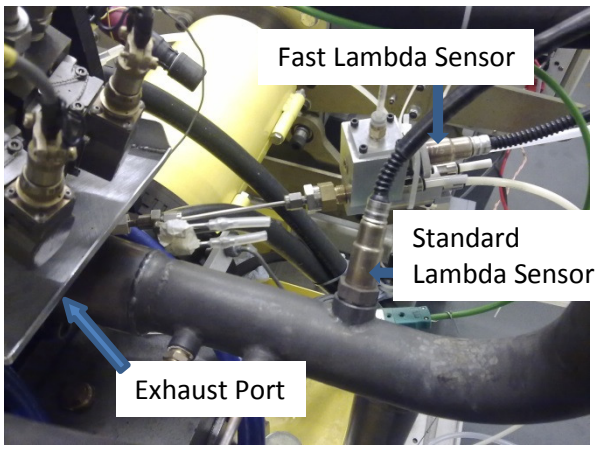

Figure 4.7 Installation of the Fast UEGO and Standard Lambda Sensors

Figure 4.8 shows the time-resolved fast lambda output at 1500rpm. As expected, the lambda curve has a valley in each engine cycle. The lowest value in the valley reflects the cylinder lambda of this engine cycle, although there is an approximately 40ms delay from the Exhaust Valve Open (EVO) to the start of the drop on the lambda signal. The delay includes the time that exhaust gas travels from the cylinder into exhaust port and then through the sampling probe into the fast UEGO sample head, and eventually reaches the orifice on the UEGO sensor, and the time the UEGO sensor converts the oxygen concentration into a current signal. By this method the cylinder lambda can be identified and thus the short-circuiting rate in each single engine cycle can be calculated via Equation (4-6).

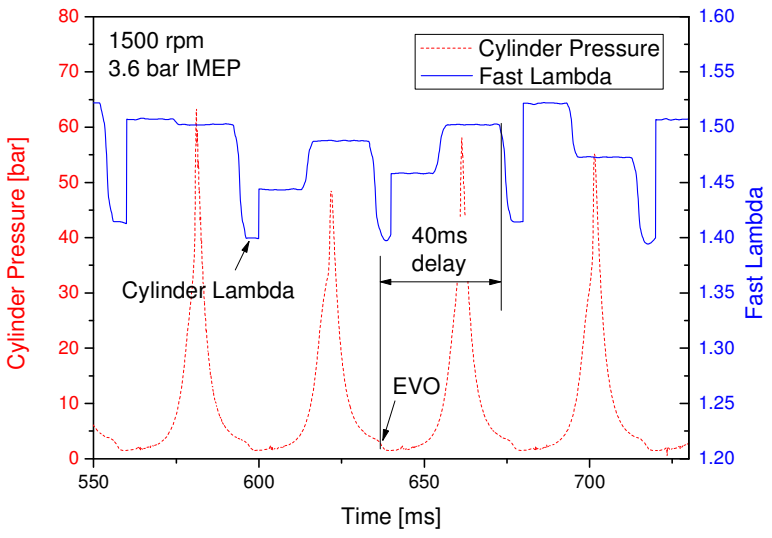

Figure 4.8 In-cylinder Pressure and Fast Lambda VS Time

4.4 Cycle-resolved Air Short-circuiting Measurement by Fast NDIR

An alternative method for measurement of the cycle-resolved short-circuiting rate in a firing two-stroke engine is also proposed and tested. It is based on the measurement of CO_2 concentrations in the intake and exhaust, as given in Equation (4-7) [91].

$$y_{short} = \frac{[CO_2]_b - [CO_2]_{tp}}{[CO_2]_b - [CO_2]_a} \qquad \textbf{4-7}$$

where:

$[CO2]_b$: CO2 concentration in the cylinder after combustion

$[CO2]_{tp}$: CO2 concentration in the tailpipe

$[CO2]_a$: CO2 concentration in the intake

In this case, the $[CO2]_{tp}$ and $[CO2]_a$ can be measured directly by the standard emission analyser from the exhaust pipe and intake pipe respectively. Ideally, $[CO2]_b$ should be measured via a fast acting in-cylinder sampling valve right after combustion but before exhaust valves open during the expansion stroke. On a four-valve modern gasoline engine of a small displacement volume, there is no extra space to mount the in-cylinder sampling valve in the cylinder head.

Instead, $[CO2]_b$ can be measured from the exhaust port close to the exhaust valves. When the exhaust gas is sampled before the intake process begins, the measured CO_2 concentration will be the same as that in the cylinder after combustion. But the CO_2 concentration will be diluted by the short-circuited air during the overlap period of the intake and exhaust processes. Figure 4.9 shows schematically the temporal CO_2 concentration in the exhaust port during the exhaust process of the two-stroke operation, together with the valve timing diagram of the two-stroke operation. When the exhaust valves open, there will be a rapid rise in the CO_2 concentration from A to B as the first portion of the burnt gas comes out of the cylinder. After reaching its maximum, CO_2 concentration will remain constant in the period between B to C until the intake valves open. As soon as the short-circuiting of fresh air into the exhaust occurs, the exhaust gas will be diluted and the CO_2 concentration will start to fall, as indicated by the period from C to D. The CO_2 concentration between B and C can thus be considered as $[CO_2]_b$.

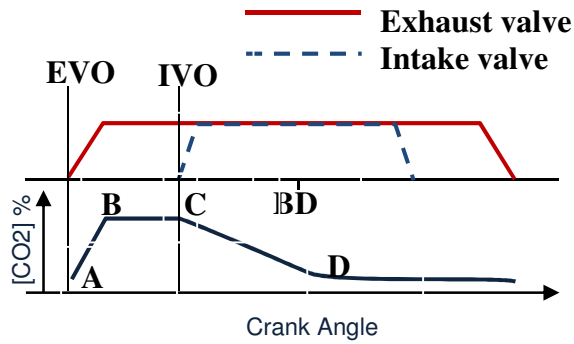

Figure 4.9 Variation of the CO2 concentration at the Back of Exhaust Valve

In this work, the same sampling probe was used as shown in Figures 4.6 and 4.7. A fast response CO_2 analyser type NDIR500 from Cambustion Ltd was used to measure the instantaneous CO2 concentration through the sampling probe.

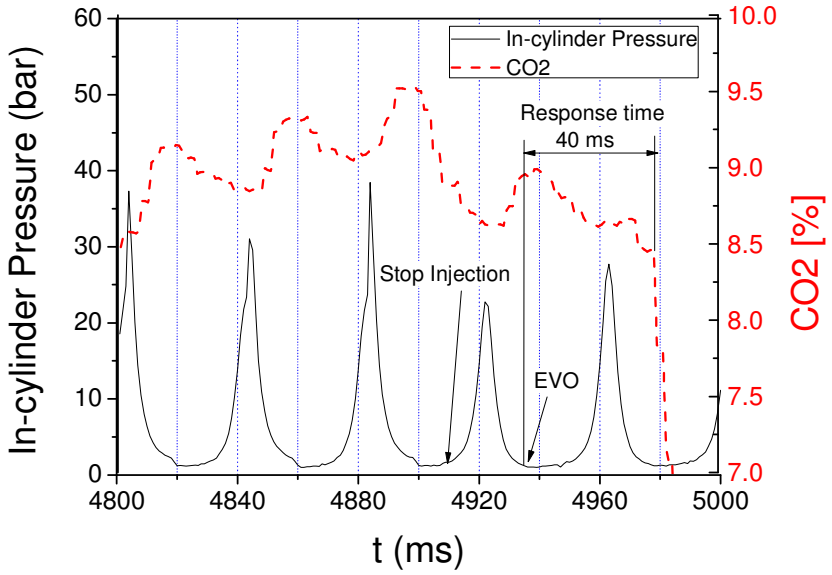

Figure 4.10 In-cylinder Pressure and CO2 Concentration Vs Time

In order to obtain the cycle-resolved measurement, the response speed of the CO_2 analyser is essential to obtain the instantaneous $[CO2]_b$ for calculating the short-circuiting rate through equation (4.7). The CO_2 measurement delay time of the whole system, including the time for the sampled gas going through the sampling probe and the exhaust gas travelling from the exhaust valve to the sampling probe, was investigated by simply switching off the injection in a cycle. The in-cylinder pressure and the CO_2

concentration were logged simultaneously and shown in Figure 4.10. The injection was switched off in the cycle at 4920ms, where no combustion took place. The response time of the fast CO_2 measurement system was then estimated from the exhaust valve opening time to the sudden drop of the CO_2 concentration, which was measured at approximately 40ms.

An example of the actual sample measurement taken at the operation condition shown in Table 4.1 is given in this section.

Table 4.1 Sample Operating Condition

Engine speed	1500rpm
Engine load	IMEP=3.245bar
Intake pressure	1.17bar abs
Exhaust Lambda	1.02
Injection timing	-140 deg ATDC
Injection duration	1.00 ms
CO2 concentration in tailpipe measured by Horiba 7170DEGR	CO2tp=11.214%
CO2 concentration in intake manifold	CO2a=0.04%

Figure 4.11 shows the CO_2 concentration measured by the Fast NDIR500 analyser over 100 consecutive cycles. It can be seen that there is a noticable rise after exhaust valve opens followed by a constant valve lift for 30/40 degree crank angles. The sampling window was thus chosen as from 250 to 275 deg ATDC.

By averaging CO_2 concentration in the sampling window, the CO2b can be obtained in each engine cycle and is shown in Figure 4.12. As the CO_2 concentration in the tailpipe (CO2tp) is 11.214% and the CO_2 concentration in the intake manifold is 0.04%, according to Equation 4-7, the short-circuiting rate for each cycle can be calculated and is also shown in Figure 4.12. By averaging over 100 consecutive cycles, the averaged short-circuiting rate at this operating condition is determined to be 2.79%, where the CoV_{yshort} is 20.57% .

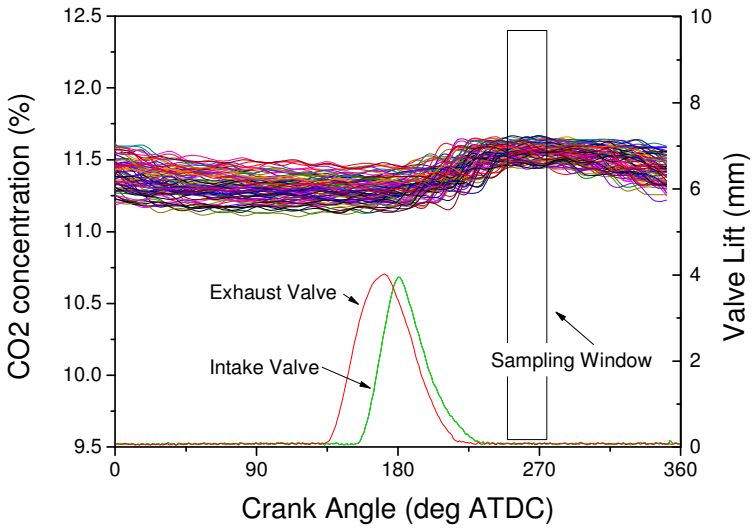

Figure 4.11 Time-resolved CO_2 Concentration over 100 Consecutive Engine Cycles

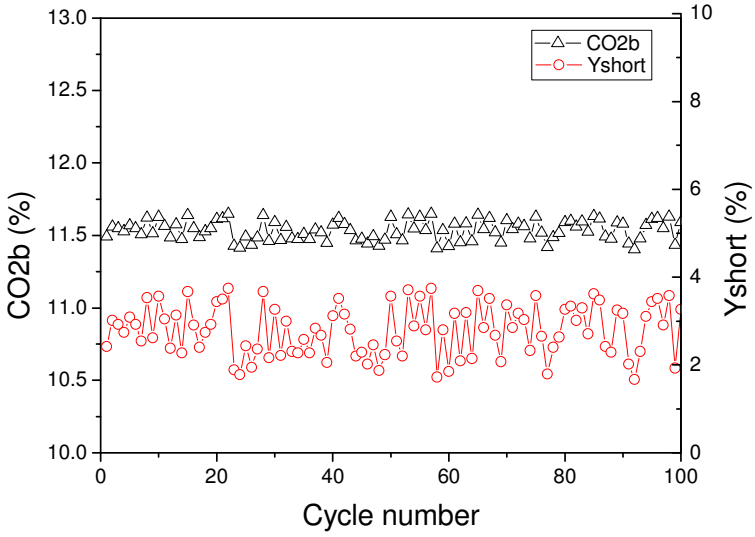

Figure 4.12 $CO2_b$ and Y_{short} in 100 Consecutive Engine Cycles

Once the short-circuiting rate is identified, the in-cylinder lambda can be calculated using equation (4-8).

$$\lambda_c = \frac{(AFR_{stoichiometric} \cdot \lambda_{tp} + 1)(1 - y_{short}) - 1}{AFR_{stoichiometric}} \qquad \textbf{4-8}$$

4.5 Cycle-resolved Residual Gas Measurement by Fast NDIR

Often, internal exhaust gas recirculation (EGR) is used instead of external EGR in modern gasoline engines with variable valve timing (VVT) devices for better transient performance and reduced accessories. The amount of residual gas retained within the cylinder is important because, apart from suppressing NOx formation, it also increases the engine's susceptibility to knock at full-load and, to some extent, aids fuel vaporisation (which is especially of interest to reduce particulate emissions during DI gasoline engine warm-up).

An accurate prediction of residual burned gas within the combustion chamber is important to quantify for development of modern engines, especially so for those with internally recycled burned gases and CAI operations. Especially in two-stroke engines, the gas exchange process is assessed by the scavenging efficiency and trapping efficiency [14].

When considering CO_2 as the tracing gas, the RGF value can be calculated from the ratio of CO_2 concentration during compression ($[CO_2]_{in}$) to that in exhaust stroke ($[CO_2]_{ex}$). [91]

$$\boldsymbol{RGF = \frac{[CO_2]_{in}}{[CO_2]_{ex}} \times 100\%} \qquad \textbf{4-9}$$

The CO_2 concentration in the exhaust can be measured by a standard emission analyser from the exhaust pipe.

In order to sample the gas in the cylinder while engine is operating with combustion, the original spark plug was replaced by an offset electrode spark plug and sample probe combination as shown in Figure 4.13. The ignition coil used was the original production 'pencil' type coil. A Cambustion NDIR 500 fast CO_2 analyser was configured for in-cylinder sampling and was connected to the sampling probe for instantaneous CO_2 concentration measurement, drawing its sample from the plug's electrode location. The output CO_2 signal was logged simultaneously with in-cylinder pressure.

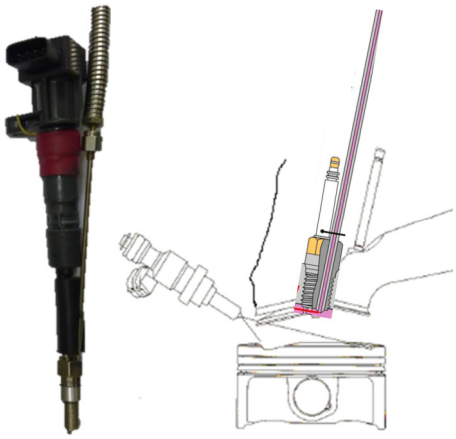

Figure 4.13 Spark Plug and Sample Probe Combination and its Installation on the Engine

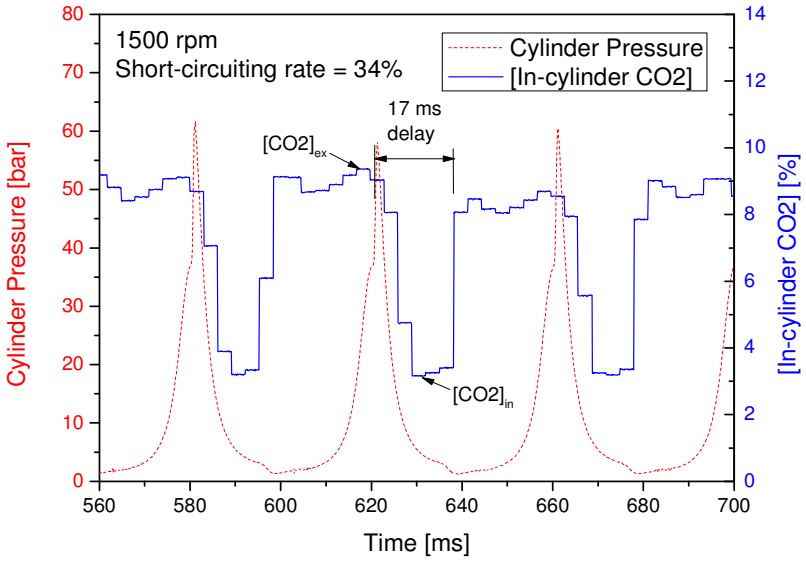

Figure 4.14 In-cylinder Pressure and CO2 Concentration Vs Time

Figure 4.14 shows the variation of in-cylinder CO_2 concentration and pressure trace when the engine was running in two-stroke CAI operation at 1500rpm. The peak cylinder pressure is associated with the compression and combustion processes. Initially, the in-cylinder CO_2 concentration stays at a constant value of about 9.5% (similar to the exhaust CO_2 concentration) but with a short-duration fall corresponding to the opening of the exhaust valve before it recovers to the exhaust CO_2 concentration. The CO_2 minima every 360CAD corresponds to the trapped CO_2 within the burned gas measured during the latter part of the compression stroke. Figure 4.14 shows this to be approximately 3% CO_2. The interval during which this gas is available to the fast NDIR is short and the

next combustion event rapidly presents new burned gas concentrations to the analyser resulting in the rapid increase to around 9% CO_2 once again. The data shown in Figure 4.14 has not been corrected for transport delay which will be discussed later. In order to explain such variations in the in-cylinder CO_2 concentration, it is important to understand the mixture formation process as well as the fluid transfer process involved in the sampling process. During the intake process, the residual burned gas is diluted with fresh air entering the cylinder, hence the CO_2 concentration decreases and reaches its minimum at the end of the intake process. Since the sampling probe was placed next to the spark plug, the burned gas is compressed into the sampling probe as soon as the combustion starts, which causes the CO_2 concentration to rise rapidly. However, after the gas enters the sampling probe, it takes a finite amount of time to reach the NDIR detector of the fast CO_2 analyser, where the gas is registered and analysed. The in-cylinder CO_2 concentration curve is shifted from the pressure curve. The CO_2 signal delay in the sampling system counted from the peak pressure to the sudden increase in CO_2 concentration is about 17ms.

According to above analysis, the cycle resolved RGF is determined by the quotient of the minimum and maximum value of in-cylinder CO_2 concentration measured during the firing cycle as shown in Figure 4.14.

4.6 Summary

The present chapter describes the 'air short-circuiting' phenomenon that commonly occurs during the scavenging process in two-stroke engines. In order to detect and quantify the short-circuiting rate, two cycle-resolved methods are proposed and evaluated. The first one is based on oxygen concentration measurement via a low cost modified fast lambda sensor and the other is based on the CO_2 concentration measurement via the NDIR fast CO2 analyser. In addition, a cycle resolved residual gas fraction method is also described in this chapter. The impact of short-circuiting on engine performance, combustion and emissions will be discussed in Chapter 5.

Chapter 5

Two-Stroke CAI Operation

Chapter 5 Two-Stroke CAI Operation

5.1 Introduction

Two-stroke CAI combustion was accomplished by means of residual gas trapping via reduced overlap between exhaust and intake valve openings. In order to utilise the widely used 3-way catalyst on the production engine, the engine experiments were carried out at exhaust lambda 1. The operating range of two-stroke CAI will be presented and discussed in this chapter. The effect of spark ignition and boost pressure will then be analysed. The specific fuel consumption and emissions results from the two-stroke poppet valve engine operation will be shown. These results will also be compared with engine baseline in Chapter 6. Its lean operation under boosted conditions will be discussed in Chapter 8.

5.2 Two-stroke CAI Combustion at Lambda 1.0

As explained in Chapter 2, in the four-stroke engine operating in CAI mode by means of residual gas trapping, the exhaust gas was trapped in the cylinder by closing exhaust valve earlier. When the engine runs natural aspirated, the engine output load is mainly controlled by the exhaust valve closing timing, as the amount of fresh charge sucked into the cylinder in each cycle is determined by how much exhaust gas was trapped in the cylinder in the last cycle. Therefore, it's necessary that the engine has variable valve timing.

However, in two-stroke engine operating in CAI mode by means of residual gas trapping, the variable valve timing is less necessary to engine load control, as it is controlled by scavenging ratio, namely boosted pressure. During the scavenging process, the fresh charge not only displaces the exhaust gases but also mixes with them at the same time. Therefore, the residual gas is retained in the cylinder because of insufficient scavenging. In order to reduce the scavenging ratio and retain the residual gas in the cylinder, the intake and exhaust valve opening duration was shortened to 60 deg CA and lift was shortened to 7mm at 1000rpm. The Exhaust Valve Open (EVO) and Intake Valve Close (IVC) were fixed symmetric to BDC and the valve overlap was kept at 40 deg CA at 1000rpm so the engine load and scavenging can be individually controlled by the

boosting pressure. This strategy can be further transplanted onto the product two-stroke engine with a cam driven valvetrain.
The DI timing was set at 140 deg CA BTDC, which is just after the IVC timing to avoid the fuel being injected onto the back of intake valves, and is also the earliest feasible timing for homogeneous air fuel mixture. The injection pressure was maintained 100bar throughout the study.

When running the tests, the coolant and oil were pre-heated and their temperature was kept at 80 degC through an individual coolant and oil conditioning unit. In the starting process, the engine was motored by the AC dyno to a certain speed before turning on the spark and injection.

5.2.1 Operating Range

The operating range of the two-stroke CAI in terms of engine speed and load was investigated on the camless GDI engine. Experiments were carried out by varying the engine speed from 800 rpm to 3000rpm at different engine loads. As shown in Figure 5.1, the operating range of CAI combustion is enveloped by 3 limits, (i) the knock limit on the low speed high load boundary, (ii) the gas exchange limit on the high speed and high load boundary and (iii) the misfire limit on the low load boundary. The knock limit is defined by the threshold of the in-cylinder pressure rise rate. The misfire limit is defined by the operating condition when the engine operation became intermittent due to large number of misfiring cycles. Based on the previous study [92], the maximum rate of pressure rise dP /dCA was limited to 5 bar/CA in order for the engine to operate with similar noise levels to the SI engine. At each engine speed the engine load was varied from low to high by increasing the intake pressure and hence the scavenging rate in the two-stroke engine operation. The intake pressure distribution over the operation range is shown in Figure 5.3a. It should be pointed out that the maximum IMEP on this two-stroke engine with CAI operation is 7.8bar at 1500rpm, which is equivalent to 15bar IMEP for a four-stroke engine. It is expected that the upper load region can be further expanded with lean boost and/or external EGR as well as optimized valve timings.

Because the valves are operated independently from the engine's own rotation by the electro-hydraulic actuation, for a given intake and exhaust valve profiles, the opening

durations remain constant in ms but they will become less in terms of deg CA as the engine speed increases. In addition, due to the finite opening and closing speeds of the electro-hydraulic valves, the valves cannot reach their maximum lift at 1500rpm and above in the two-stroke mode, as shown in Figure 5.2. Although the valve durations were increased at higher engine speed operations to compensate for the reduction in air flow rate caused by the reduced valve lift, it is still not sufficient for high load operation. This is the main cause of the presence of the gas exchange limit formed on the operating range envelop.

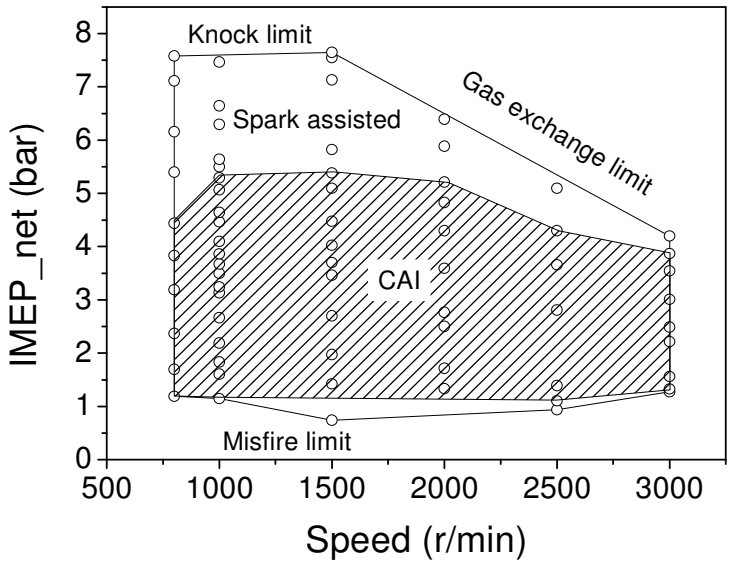

Figure 5.1 Operating Range for Two-stroke CAI Operation with Exhaust Lambda 1.0

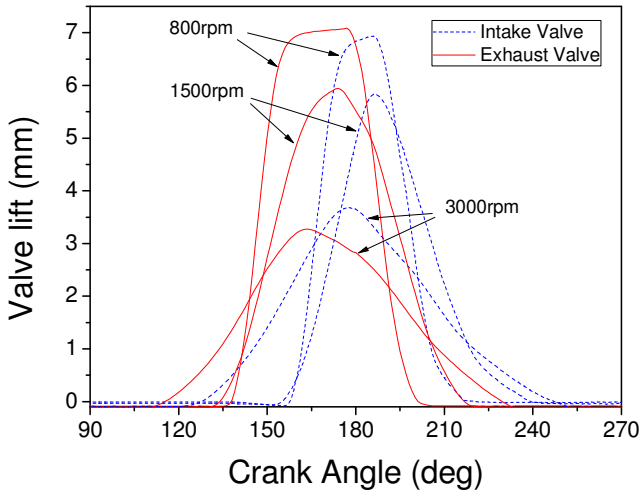

Figure 5.2 Valve Profiles at 800rpm, 1500rpm and 3000rpm

It also can be seen from Figure 5.1 that the operating range comprises of pure CAI from almost idle operations to part load conditions from 800rpm to 3000rpm and spark assisted CAI operation at both higher load and idle regions. Although there was no noticeable effect of spark ignition seen on the combustion process within the CAI operating range, the spark was kept on but the spark timing was set at TDC. The pure CAI operating zone is sandwiched by 2 regions of the spark assisted CAI operation, where the combustion cannot continue without spark. However, the effects of the spark on the spark assisted CAI operation zone at higher load and idle conditions are different, which can be seen from the spark timing distribution over the operating range in Figure 5.3b. In the high load spark assisted CAI operation, as the thermal load increased with the engine load, combustion became faster and the pressure rise rate was greater. The spark timing was thus retarded to prevent knock. In the spark assisted CAI operation at idle, the spark timing was advanced before TDC to help to stabilize the combustion process.

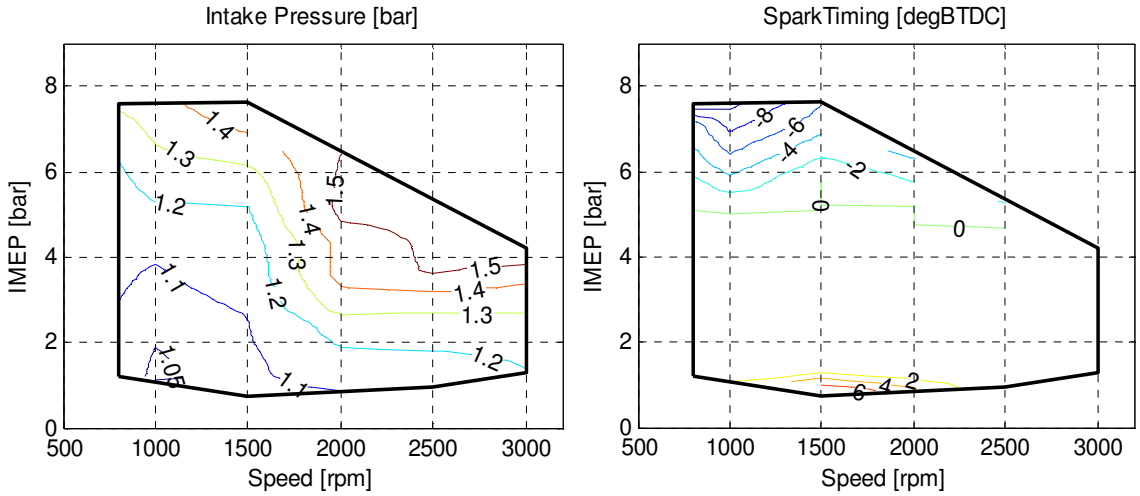

a) **b)**

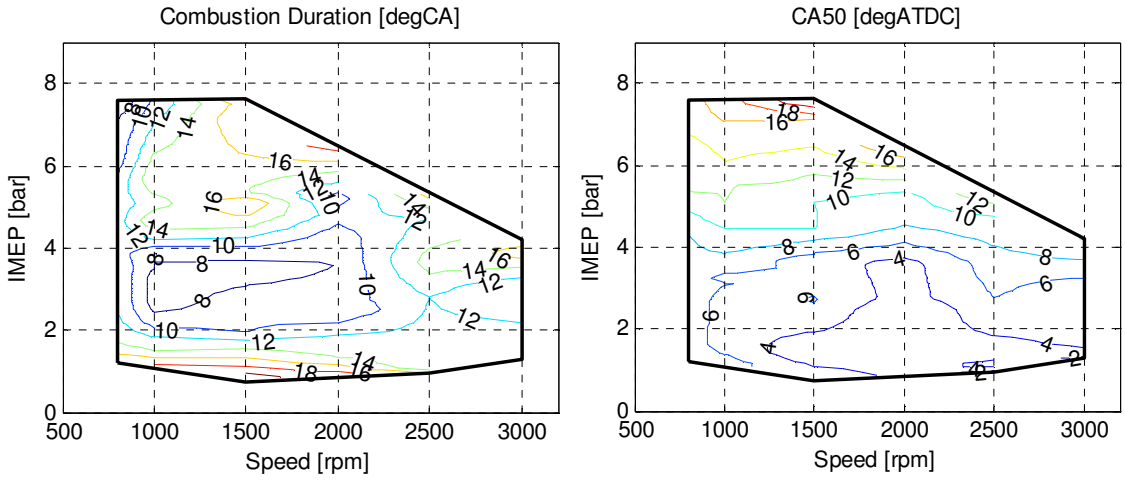

Figure 5.3 Intake Pressure, Spark Timing, Combustion Duration and CA50 over the Operating Range

5.2.2 Performance and Emissions at exhaust lambda 1.0

Figure 5.3c shows the combustion duration over the CAI operating range, which in this paper is defined as the deg CA from 10% mass fraction burnt to 90% mass fraction burnt. It can be seen that the combustion speed was the highest at low speed mid-load operation in the pure CAI operation zone, where the combustion duration was less than 8 CA. When the engine speed increased, the combustion speed increased but the combustion duration in deg CA increased by a few degrees. At low load operation, the combustion duration became longer because the combustion process was slowed down due to dilution by the large amount of the residual gases, of which the quantity was mainly determined by the intake pressure and air flow rate. In the spark assisted CAI operation above the pure CAI operation range, the combustion duration was longer and the heat release process was slower due to retarded combustion phasing of CA50 as shown in Figure 5.3d, the crank angle at which 50% mass fraction is burnt. It is noted that at the higher load region of low engine speeds, although the combustion phase was retarded to 16 or 18 degree ATDC, the combustion speed was still high enough to cause excessive pressure rise due to insufficient dilution effect of less residual gas at lower engine speed. Therefore, it is envisaged that the upper load region can be extended further by introducing leaner mixture at higher boost and/or externally cooled EGR. The results shall be presented in a future publication.

Figure 5.4a shows the Indicated Specific NOx (ISNOx) emission values over the CAI operating range. It can be seen that the NOx emissions under pure CAI operation were below 2g/KWh due to the dilution of the large amount the residual gas in the cylinder. When the load increased and the operating mode transferred from pure CAI to spark assisted CAI, more NOx emissions were produced because of the reduction in the residual gas fraction and the increase in the in-cylinder temperature. At the knock limit boundary, the NOx emissions increased to 6 g/kWh.

Figure 5.4b shows the distribution of Indicated Specific CO (ISCO) emission over the CAI operating range. It can be seen that the CO emission was very high and its value tended to be higher at higher load and higher speed where the intake pressure was higher as shown in Figure 5.4a. Such results are likely to be caused by the air short-circuiting prevalent in the two-stroke operation. During the gas exchange process in the two-stroke engine operation, there is a valve overlap when both of the intake and exhaust valves are open to achieve the scavenging. During this period, a portion of the intake fresh air can flow across the combustion chamber and into the exhaust directly. The portion of the fresh air dilutes the exhaust gas and leads to the measurement of the air to fuel ratio in the exhaust pipe to be leaner than the actual air to fuel ratio of the in-cylinder mixture. Therefore, the mixture in the cylinder during the combustion process is richer than that measured from the exhaust pipe. Figure 5.5 shows the effect of the short-circuiting on the relative air to fuel ratio (Lambda). The in-cylinder lambda ($Lambda_c$) was derived from the measurement of instantaneous CO_2 concentration in the exhaust port with a fast response Cambustion CO_2 analyser as to be described in Chapter 4, whereas the lambda in the tailpipe($Lambda_{tp}$) was measured by a lambda sensor. It can be seen that the short-circuiting rate increased with the intake pressure for the fixed valve timings. As a result, the in-cylinder lambda ($Lambda_c$) became increasingly richer while the lambda in the tailpipe ($Lambda_{tp}$) was ketp at 1. Thus the CO emissions would be expected to increase with the intake pressure when the exhaust lambda signal is used as a feedback for the air fuel ratio control on the two-stroke engine.

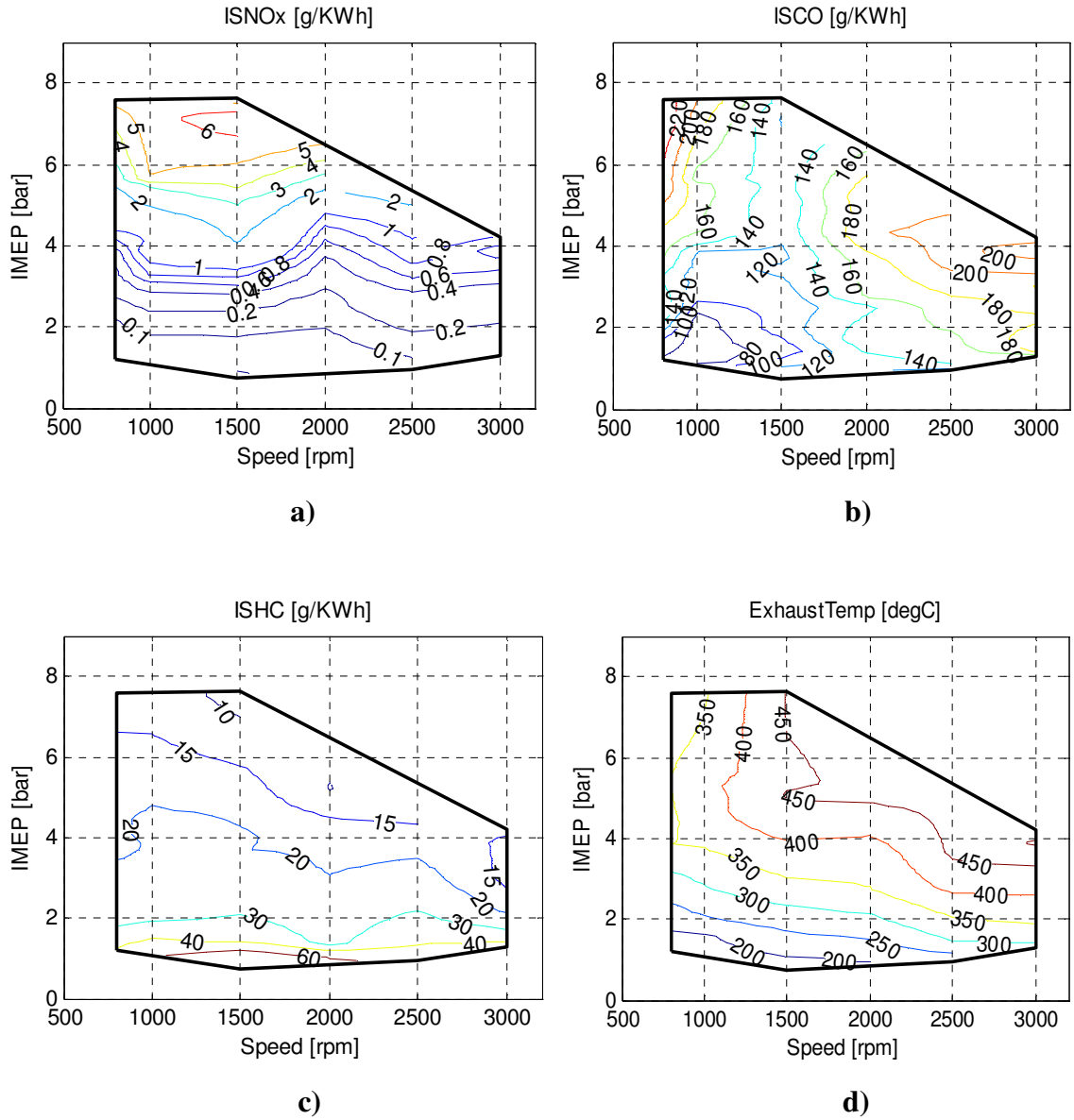

Figure 5.4 ISNOx, ISCO, ISHC, and Exhaust Temperature over the Operating Range

Figure 5.4c shows the distribution of Indicated Specific uHC (ISHC) emissions over the CAI operating range. The value varied from 10 g/kWh to 60 g/kWh depending on the engine load. The high values of uHC emission were caused by richer mixture whilst the exhaust lambda was maintained at 1.0 because of the short-circuiting process discussed above. Since the oxidation rate of the uHC during the combustion process in the cylinder is mainly determined by the in-cylinder temperature. When in-cylinder temperature increases, more uHC is converted to the CO_2 and H_2O. Therefore, the distribution of the uHC emission is much related to that of the exhaust temperature, as shown in Figure 5.4d.

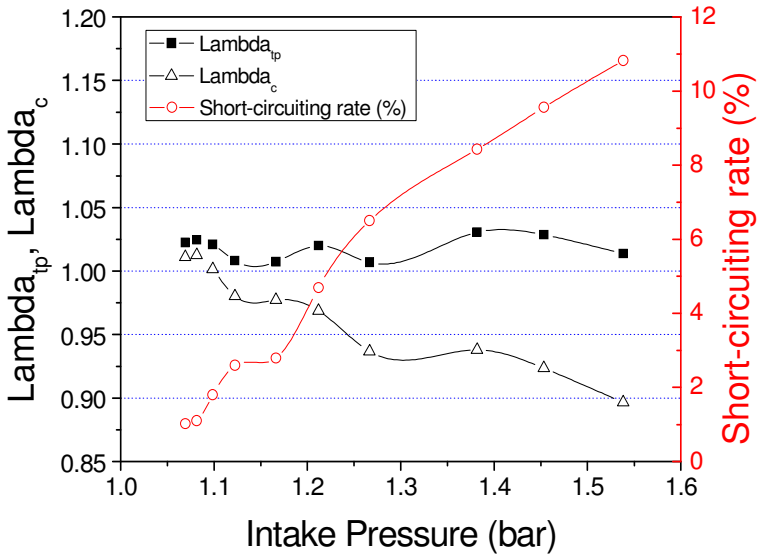

Figure 5.5 Effect of Short-circuiting on the Measurement of Lambda at 1500rpm

Figure 5.6 shows the distribution of Indicated Specific Fuel Consumption (ISFC) over the operating range. Within the pure CAI operating range, the ISFC varied from 270 g/kWh to 320 g/kWh depending on the engine load. Above the pure CAI operation, the fuel consumption increased with engine load because of the delayed combustion and too rich mixture caused by the short-circuiting stated above.

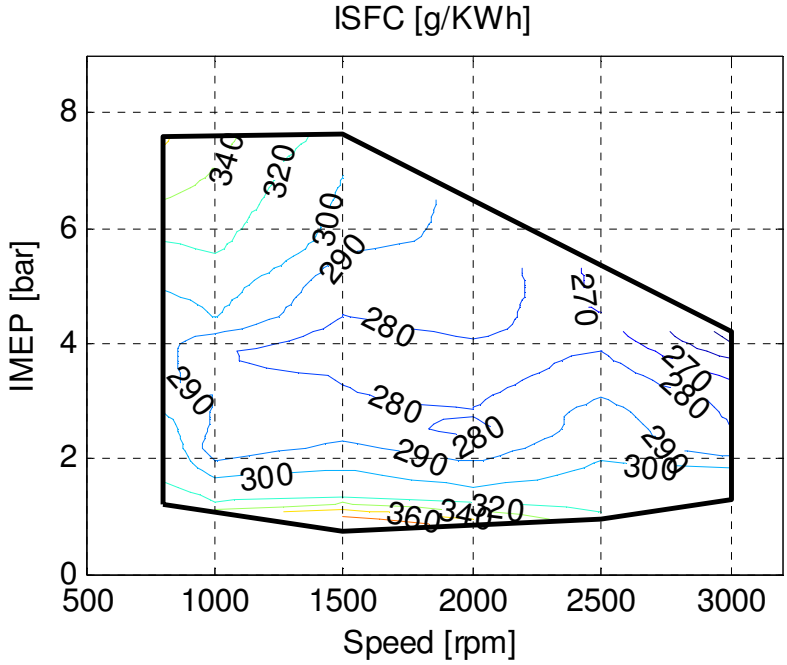

Figure 5.6 ISFC over the Operating Range

5.3 Short-circuiting Effects on Two-stroke CAI Combustion and Emissions

The effect of the air flow rate on the short-circuiting was investigated by changing the boost pressure and hence the engine power output. Figure 5.7 compares the concentration of CO_2 sampled at the exhaust valve under different load conditions over two engine cycles. It can be seen that the variation of the CO_2 concentration, within one engine cycle between 40ms at 1500rpm in the two-stroke mode, increases with engine load. This indicates that the short-circuiting rate becomes higher when the boost pressure and engine load increase. Figure 5.8 shows the corresponding short-circuiting rate calculated using Eq.4.7. More detailed information on the actual measurements and data processing is given in Chapter 4. In the two-stroke CAI mode, the engine load is mainly determined by the intake pressure when the valve timings and lambda are fixed. It can be seen that the short-circuiting rate increases in proportion to the intake pressure. This can be readily explained by the fact that at higher boost pressures, higher air flow velocity causes more air to flow from the near side of the intake valves directly across the combustion chamber to the exhaust valves and the exhaust port. When the intake pressure was varied from 1.06bar to 1.38bar, the IMEP increased from 1.16bar to 5bar. At low load operation, the intake air flow rate curve follows the IMEP curve and the short-circuiting rate is below 5%. When the IMEP is over 4bar, the difference between the IMEP and air flow rate becomes bigger, indicating a portion of the intake air didn't participate in the combustion and entered the exhaust pipe directly. In this case, the short-circuiting rate is over 5%. The dispersion of the short-circuiting rate shown in Figure 5.8 indicates that the cycle-to-cycle variation of the short-circuiting rate increases with the air flow rate.

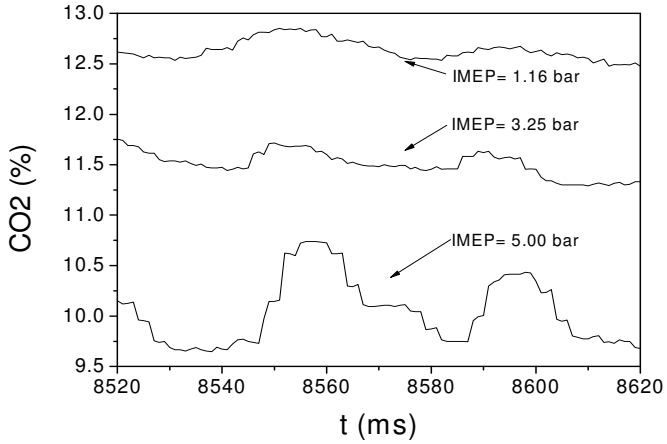

Figure 5.7 CO2 Concentration at the Exhaust Valve at 1500rpm Vs Time

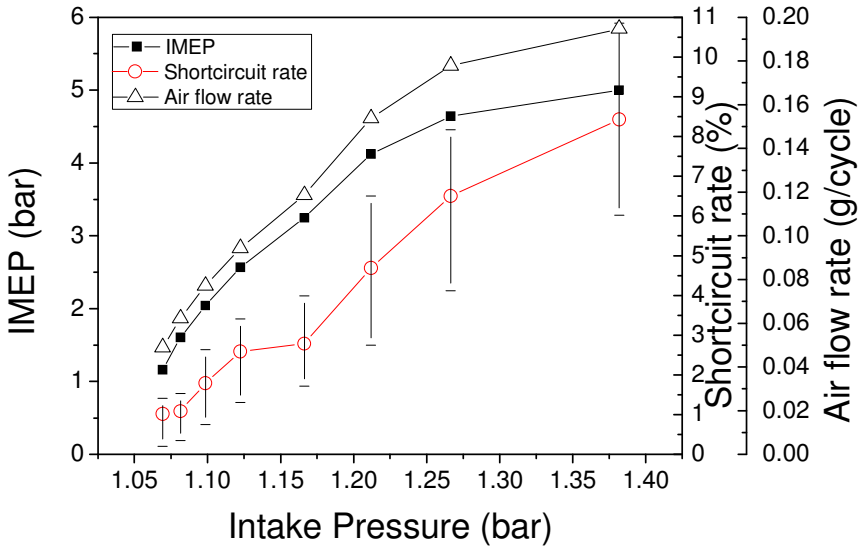

Figure 5.8 IMEP, short-circuiting rate and air flow rate at 1500rpm VS. intake pressure

Because of the dilution of the exhaust gas by the short-circuited air, measurements of the relative air-fuel ratio by a lambda sensor will be adversely affected. In order to investigate the effect of the short-circuiting on the exhaust lambda measurement, further engine tests were carried out at constant load (3.6bar IMEP) and speed (1500rpm) with the same valve timings shown in Figure 5.2. The exhaust lambda value was varied from 1.0 to 1.44 by increasing the intake pressure and reducing the fuelling rate, as shown in Figure 5.9.

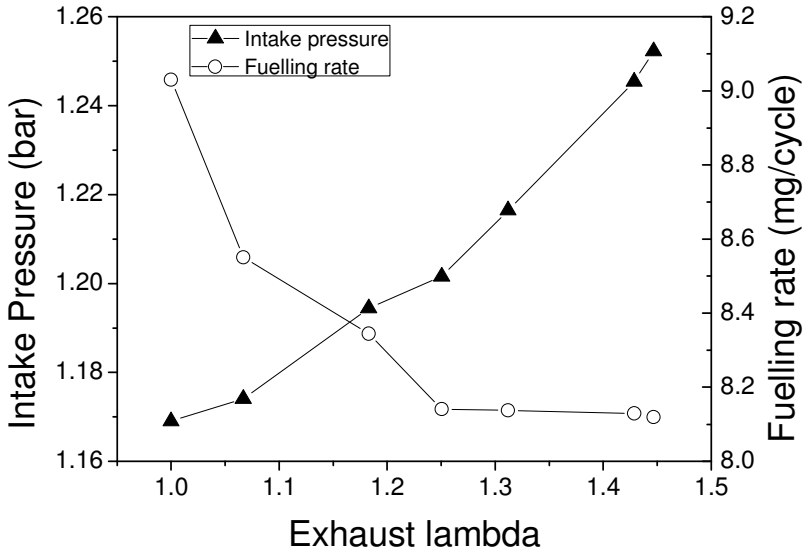

Figure 5.9 Intake Pressure and Fuelling Rate Vs Lambda$_{tp}$

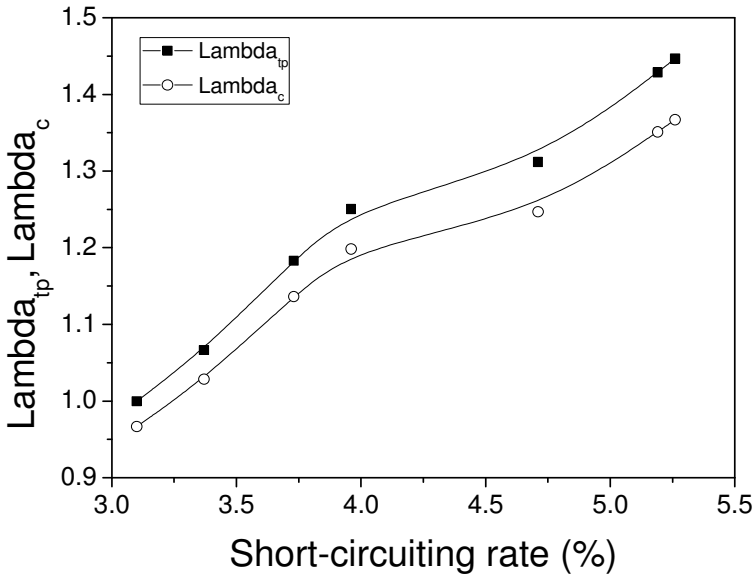

Figure 5.10 Effect of Short-circuiting on the Difference between the Measured Exhaust Lambda and In-cylinder Lambda Values

In order to work out the relative air to fuel ratio in the cylinder, Equations 4-6 can be rearranged so that the in-cylinder lambda (λ_c) can be worked out from the Lambda sensor's reading and the short-circuiting rate, Equation 4-8.

Figure 5.10 plots the $lambda_c$ and $lambda_{tp}$ as a function of the short-circuiting rate. It can be seen that the in-cylinder lambda value was always lower than the exhaust lambda due to the presence of additional short-circuited air in the exhaust. In addition, when the measured exhaust lambda was 1, the in-cylinder lambda value was about 0.96 at this operation condition. This explains the high CO and uHC emissions seen in Figure 5.11 when the closed-loop controlled stoichiometric operation was adopted at this operating point. The stoichiometric combustion took place when the exhaust lambda was 1.04. This is further supported by the measured CO_2 concentration in the exhaust shown in Figure 5.12, which peaked at around the exhaust lambda value of 1.07. CO and HC emissions reached their lowest value at the exhaust lambda of 1.14 and the calculated in-cylinder relative air to fuel ratio of 1.1. It is interesting to note that both the maximum NOx concentration in Figure 5.11 and the highest combustion efficiency in Figure 5.13 occurred at the in-cylinder lambda value of 1.1. In addition, it is noted that the shortest combustion duration or the fastest combustion took place with the relative leaner air fuel mixture as well. In theory, if the mixture were homogeneous, one would expect the maximum combustion efficiency with stoichiometric mixture and that the maximum

flame speed with slightly rich mixture. However, both the combustion efficiency and flame speed reached their maximum with an overall leaner mixture in the current experiments. Thus it indicates that stratified charge combustion could have taken place in the cylinder with stoichiometric mixture in most regions, due to the fact that there may not be enough time to form a homogeneous mixture when the injection took place during the compression stroke after the closure of the intake valves.

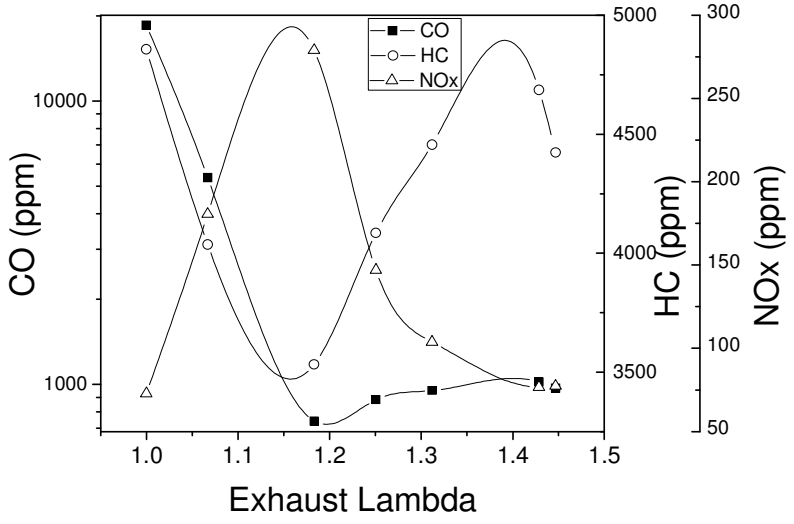

Figure 5.11 Effect of Lambda on CO, HC and NOx Emissions

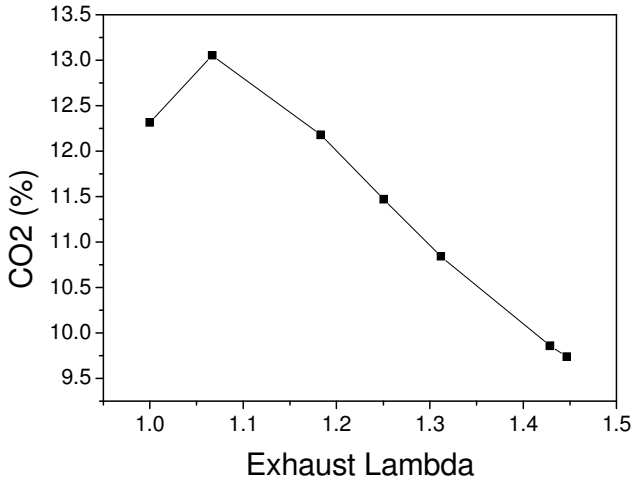

Figure 5.12 Effect of Lambda on CO2 Emissions

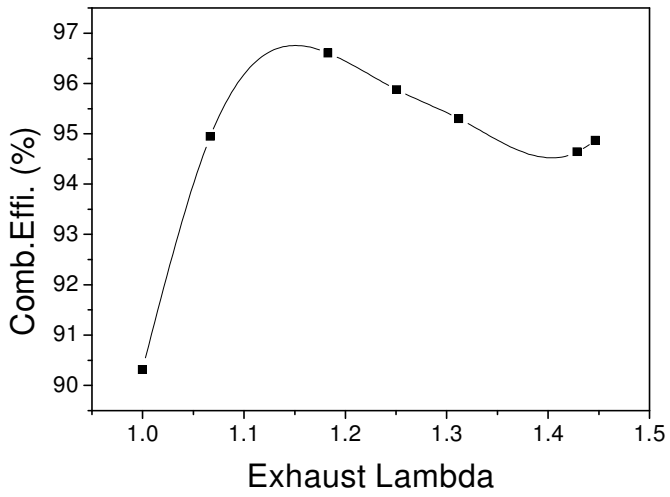

Figure 5.13 Effect of Lambda on Combustion Efficiency

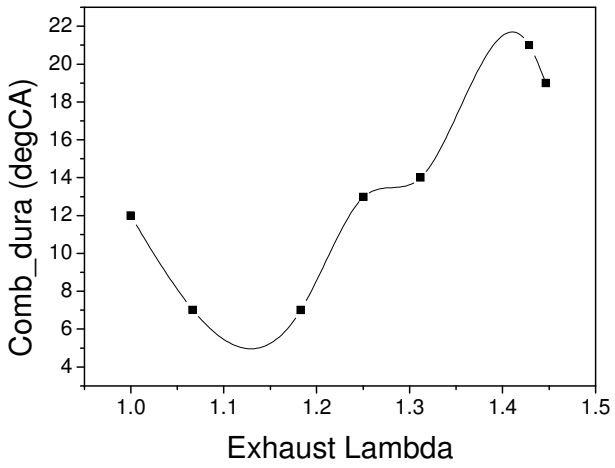

Figure 5.14 Effect of Lambda on Combustion Duration

The main findings of this section can be summarised as follows:

1) The results at constant engine speed shows that the short-circuiting rate increased from 1% at minimum load to about 8% at 5 bar IMEP when the boost pressure was increased from 1.05 bar to 1.4 bar.

2) The measured short-circuiting rate was then used to determine the in-cylinder relative air to fuel ratios from the lambda sensor readings. At 3.6 bar IMEP at 1500rpm, the difference between the exhaust lambda and the in-cylinder lambda remained relatively constant at 0.4 when the boost pressure was increased from 1.17bar to 1.25bar.

3) The combustion and emission results show that maximum combustion efficiency and lowest CO and uHC emissions occurred with a relatively lean overall in-cylinder mixture, indicating the presence of stratified charge combustion whilst the maximum CO_2 concentration was obtained with a stoichiometric in-cylinder mixture.

5.4 Summary

In this chapter, two-stroke CAI combustion was studied at exhaust lambda 1. It is demonstrated that a wider range of CAI operation could be achieved at engine speeds from 800rpm to 3000rpm and with engine load from idle to 7.8bar IMEP, which is equivalent to 15.6 bar IMEP on the four-stroke operation. In the CAI operational range, the NOx emission was very low and the specific fuel consumption was also low. Due to the short-circuiting, the in-cylinder mixture was too rich for complete combustion when the exhaust lambda was controlled at 1.0 and hence higher CO and uHC emissions were observed.

The air short-circuiting rate was quantified and used to determine the in-cylinder relative air to fuel ratios from the lambda sensor readings. The combustion and emission results show that maximum combustion efficiency and lowest CO and uHC emissions occurred with a relatively lean overall in-cylinder mixture whilst the maximum CO_2 concentration was obtained with a stoichiometric in-cylinder mixture.

Chapter 6

Further Analysis of two-stroke CAI Combustion and Comparison with other Combustion modes

Chapter 6 Further Analysis of Two-stroke CAI Combustion and Comparison with other Combustion Modes

6.1 Introduction

Since direct injection was used, the injection timing would affect the mixture formation and subsequent combustion, in the first part of this chapter the effect of injection timing is discussed on CAI combustion during two-stroke and four-stroke operations. In order to evaluate its relative merits, the performance and emissions of the two-stroke CAI combustion operation was compared with several other four-stroke combustion modes.

6.2 Injection Timing Effects on CAI Combustion

Effects of the injection timing were investigated and analysed for the three CAI combustion modes in terms of combustion, performance and emissions. The CAI combustion operation was realised by means of three different operating strategies, as shown in Figure 6.1. The valve timings and maximum valve lift and other engine operating conditions are given in Table 6.1. They are four-stroke Negative Valve Overlap (NVO) CAI operation, four-stroke exhaust rebreathe CAI operation and two-stroke CAI operation.

Case 1: Four-stroke NVO CAI operation

In four-stroke NVO CAI operation mode, the burnt gases are trapped in the cylinder by earlier closure of exhaust valves. To avoid the backflow of the burnt gases entering the intake port, the intake valve opening time is retarded so that it is symmetric to the exhaust valve closing time on the gas exchange TDC. For homogeneous mixture operation, the injection timing can be altered from exhaust valve closure to intake valve closure, as shown in Figure 6.2.

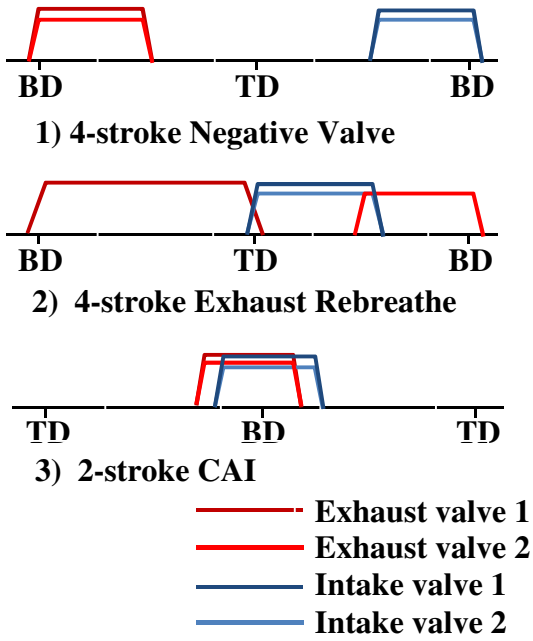

Figure 6.1 Valve Timings for Four-stroke and Two-stroke CAI Operations

Table 6.1 Valve Timings and Lifts for each Operating Mode

Mode	IVO	IVC	EVO		EVC		IVL	EVL
4strNVO	100deg ATDC	0deg ABDC	10deg BDC		100deg BTDC		5.5mm	7.8mm
4strReB	5deg BTDC	80deg BBDC	Valve1	Valve2	Valve1	Valve2	6.0mm	7.8mm / 8.0mm
			10deg BDC	45deg ATDC	0deg ATDC	0deg ABDC		
2strCAI	17deg BBDC	60deg ABDC	40deg BBDC		12deg ABDC		4.0mm	3.8mm

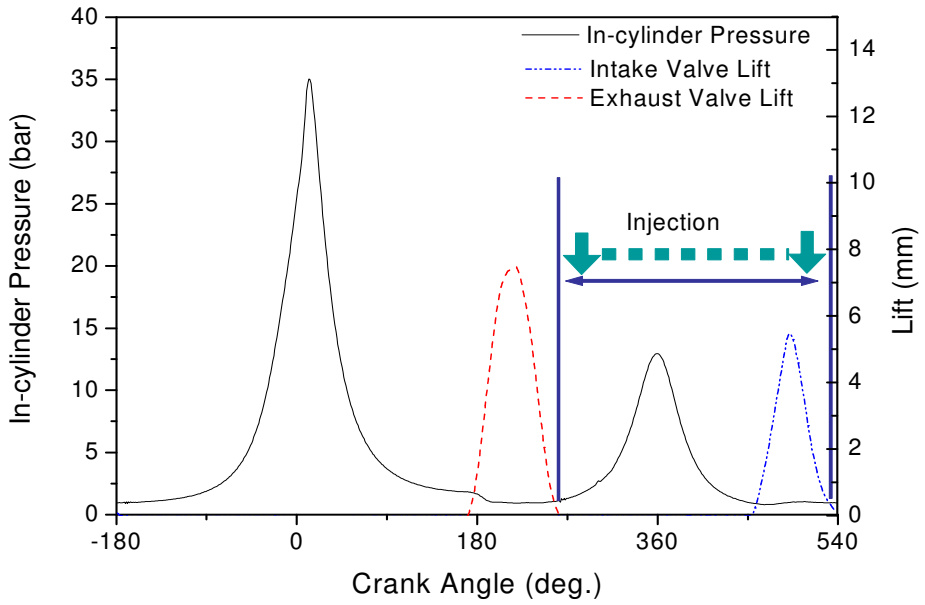

Figure 6.2 Injection Timing in Four-stroke NVO CAI Operation

Case 2: Four-stroke exhaust rebreathe CAI operation

Another way to recirculate exhaust gases in the four-stroke operation is to suck back the exhaust gases from the exhaust ports by reopening the exhaust valve during the intake stroke. As the electro-hydraulic valve train system installed on the engine allows independent valve control, exhaust valve 1 is actuated to open as normal and exhaust valve 2 is delayed to open during the intake stroke in order to suck the exhaust gas back into the cylinder. In this operation mode, the injection timing is varied from the exhaust valve 1 closure to the intake valve closure, as shown in Figure 6.3.

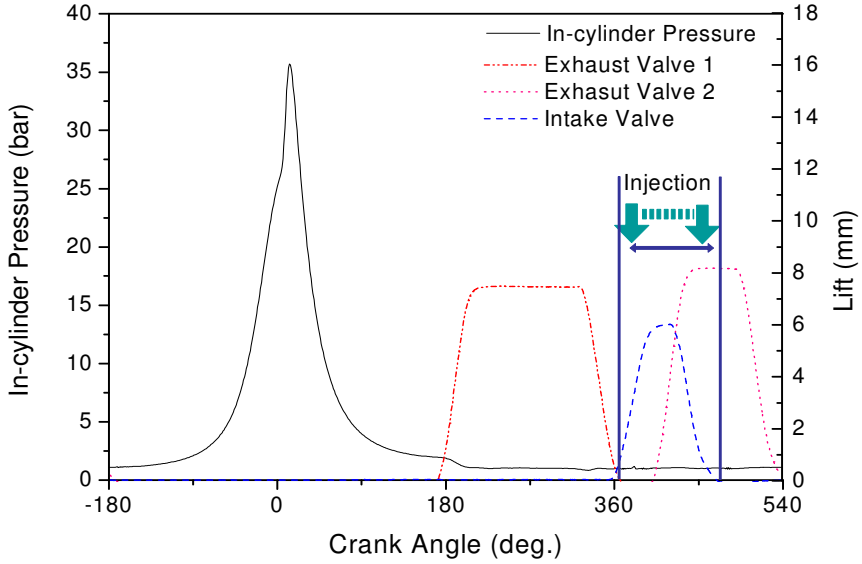

Figure 6.3 Injection Timing in Four-stroke Exhaust Rebreathe CAI Operation

Case 3: two-stroke CAI operation

As discussed in Chapter 5, in order to retain a portion of the exhaust gases in the cylinder to achieve two-stroke CAI combustion, the exhaust valve closure is advanced. The injection timing is varied from the exhaust valve closure (-150deg ATDC) to the intake valve closure (-100deg ATDC), as shown in Figure 6.4.

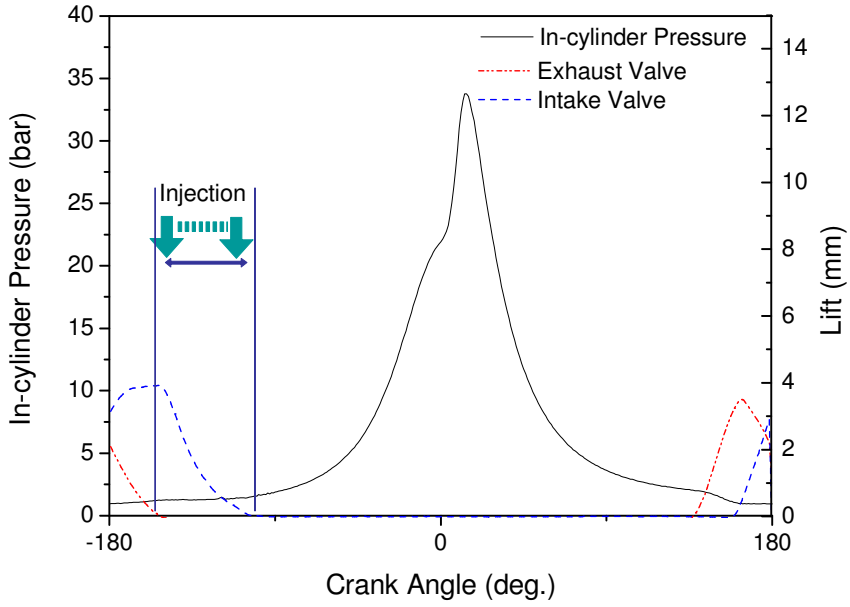

Figure 6.4 Injection Timing in Two-stroke CAI Operation

6.2.1 Effect of Injection Timings on the Air Flow Rate

In Figure 6.5, the measured air flow rate, denoted by the square symbols, is plotted as a function of the fuel injection timing for the four-stroke NVO CAI operation. The pink line at the bottom-left of the graph is the last part of the exhaust valve lift curve. The intake valve lift curve is located around 490deg ATDC. It is noted that the air flow rate decreases as the injection timing is retarded towards TDC during the negative valve overlap period and then rises after TDC to reach another peak at 440deg ATDC.

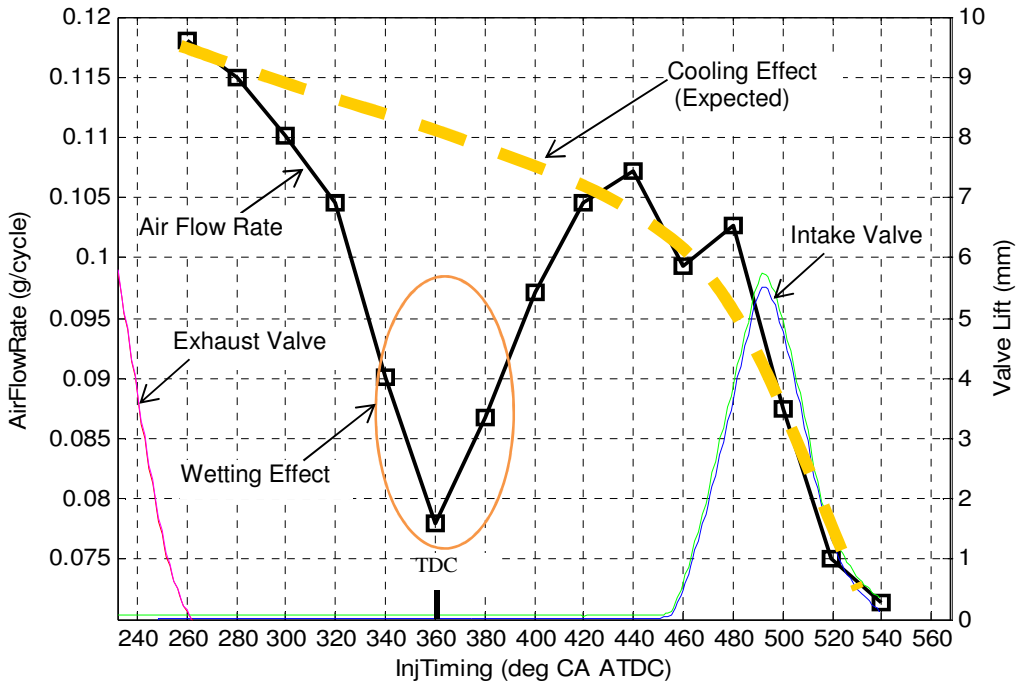

Figure 6.5 Effect of Injection Timing on Intake Air Flow Rate in Four-stroke NVO CAI Operation (1500rpm, Lambda=1)

It is known that when liquid fuel is injected directly into the cylinder, its evaporation cools down the charge and brings down the gas temperature. This so-called charge cooling effect is expected to increase the air flow rate into the cylinder. When fuel is injected earlier in the NVO period, there is more time for the liquid fuel to evaporate and hence a greater charge cooling effect to reduce the cylinder charge temperature and pressure. In turn, this will lower the pressure at IVC so that more air can be inducted into the cylinder. If this is the sole reason, one would expect a monotonic decrease in air flow rate with retarded injection timing during the NVO period. However, the presence of the significant dip in the air flow rate at TDC suggests that a more dominant process has taken place. As described in Chapter 3, the Denso high pressure fuel injector is located below the two inlet valves and it is characterized with a fan shaped fuel spray. At TDC, some of the liquid fuel will reach the piston surface and form liquid film on the piston top that will not participate in the evaporation and hence charge cooling process as much as the air borne fuels. Hence the temperature and pressure at the subsequent IVC timing will be higher, hindering the air flow into the cylinder. This phenomenon remains dominant until 440deg ATDC, when the charging cooling effect becomes dominant again. As a result, during the intake process when the intake valves are open the air flow rate drops with retarded injection timing as less time is available for evaporation and hence

charge cooling to take place. Impingement from the high pressure fuel injection is responsible for the sudden decrease in the air flow rate.

Figure 6.6 shows the effect of injection timing on the intake air flow rate in the four-stroke exhaust rebreathe CAI operation. The red line on the left is the first exhaust valve lift curve and the pink line on the right shows the second exhaust valve opening duration and timing. In this case, the intake air flow doesn't change as much as that during NVO CAI operation. The reason is that the intake air flow rate is much less affected by the amount of residual gases, as the recirculated exhaust gases come into the cylinder through the second exhaust valve towards the end of the intake process. Therefore, the in-cylinder temperature and pressure during the exhaust rebreathing period have little effect on the intake air flow rate. In addition, as fuel is injected into the fresh air at ambient temperature, the fuel evaporation process is much slower and hence less charge cooling takes place during the intake process. In addition, since the fuel injection take place after TDC, the liquid fuel impingement is absent.

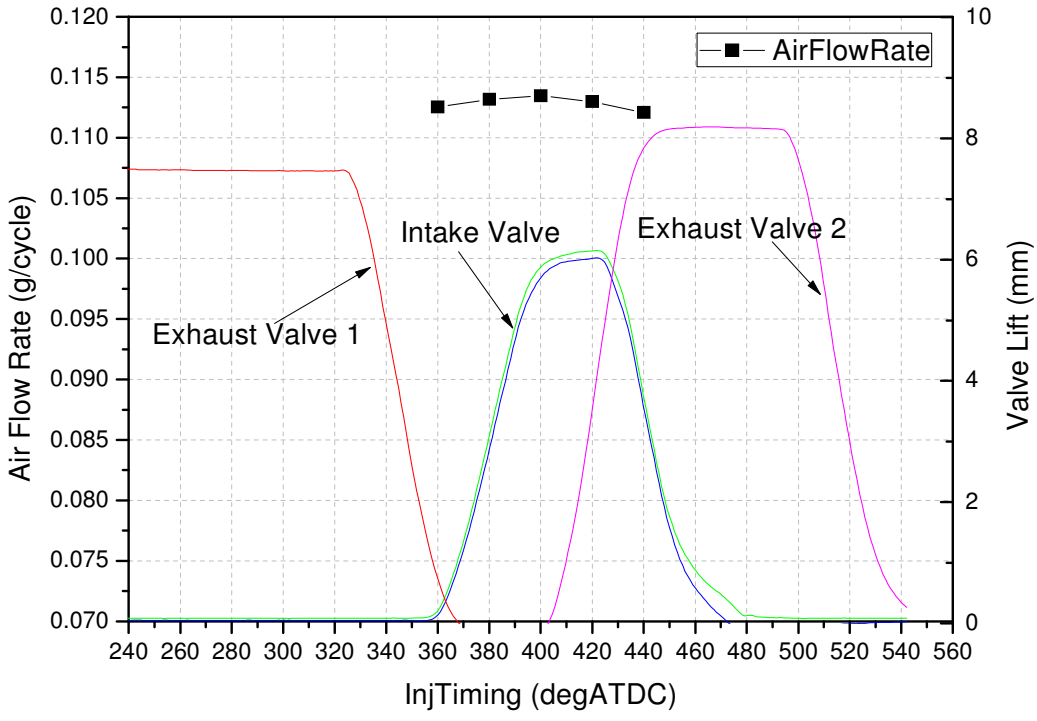

Figure 6.6 Effect of Injection Timing on Intake Air Flow Rate in Four-stroke Exhaust Rebreathe CAI Operation (1500rpm, Lambda=1)

In Figure 6.7, it can be seen that during the two-stroke CAI operation mode, the exhaust valves are shown to close around -150deg ATDC and the intake valves remain open until

-100deg ATDC. The air flow rate decreases slightly as the fuel injection is retarded from EVC at -150deg ATDC as the amount of charging cooling is reduced with less time available during the intake process. Since some of the fuel is injected into the hot residual gases as well as the fresh air, the fuel evaporation is faster than the four-stroke exhaust rebreathing CAI operation but less than that of the four-stroke NVO CAI condition. As a result, the charge cooling effect lies between the four-stroke NVO CAI mode and four-stroke exhaust rebreathe CAI mode.

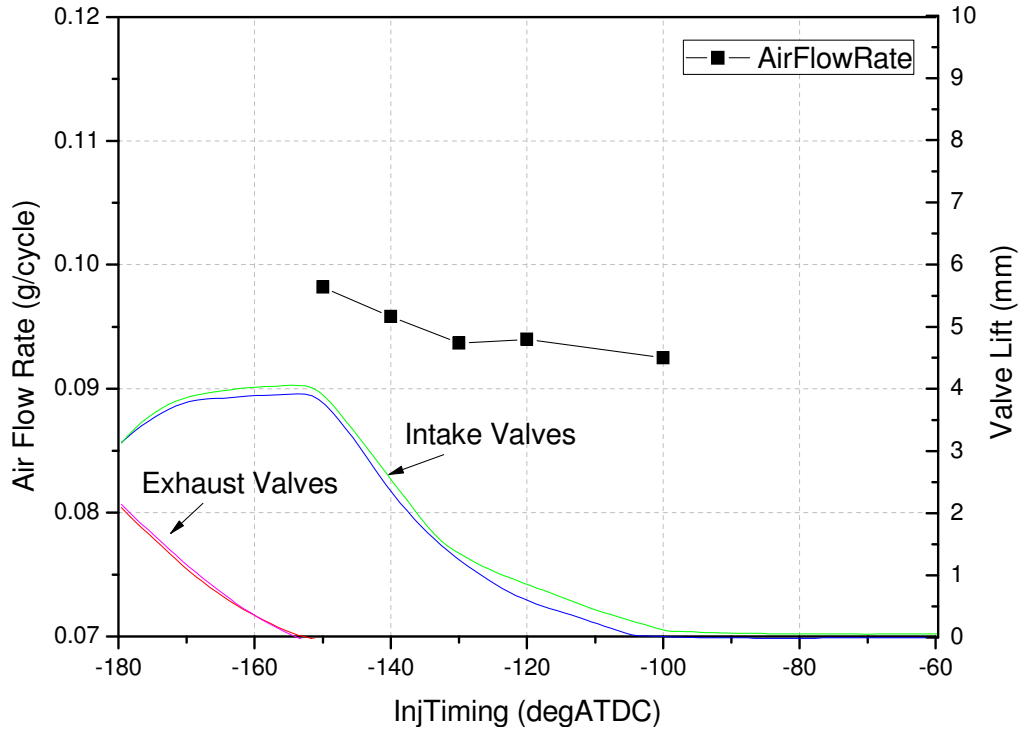

Figure 6.7 Effect of Injection Timing on the Intake Air Flow Rate in Two-stroke CAI Operation (1500rpm, Lambda=1)

6.2.2 Effect of Injection Timings on Emissions

Due to the dilution of the large amount of exhaust gases in the combustion process, the measured NOx emissions are very low and below 100ppm. However, CO and HC emissions are high and vary significantly with injection timings. As shown in Figure 6.8 and Figure 6.9, CO and HC follow the same trend with the injection timing during the four-stroke NVO CAI operation. The CO and HC emissions reach a peak at TDC because of the liquid fuel impingement. The second peak at IVC is likely a result of the

interaction of the intake flow and the spray. As explained in Chapter 3, the engine is designed with vertical intake ports so that a reversed tumble flow can be formed to avoid short-circuiting during two-stroke operation. When the fuel injection timing coincides with the opening of the intake valves, the fuel spray is subject to incoming air flows at high speeds and deflected towards the piston, hence liquid impingement occurs on the piston crown. The rise in the CO and HC emissions with injection timing during the compression stroke is caused by the inhomogeneous mixtures due to insufficient mixing time of later injections.

In comparison, there are less HC and CO emissions from the four-stroke exhaust rebreathe CAI operation. Since the gas motion is more vigorous in exhaust rebreathe CAI operation c.f. four-stroke NVO CAI operation, the mixing process is largely improved. So the CO emission is lower even when the fuel is injected onto the piston crown, as shown in Figure 6.10. However, some of the fuel film on the piston crown still cannot be burned and leads to the high HC emissions evident in Figure 6.11. The peak in CO emissions at the latest injection, when the second exhaust valve opens, could be caused by the fuel injection into the recirculated exhaust gases, which results in incomplete combustion.

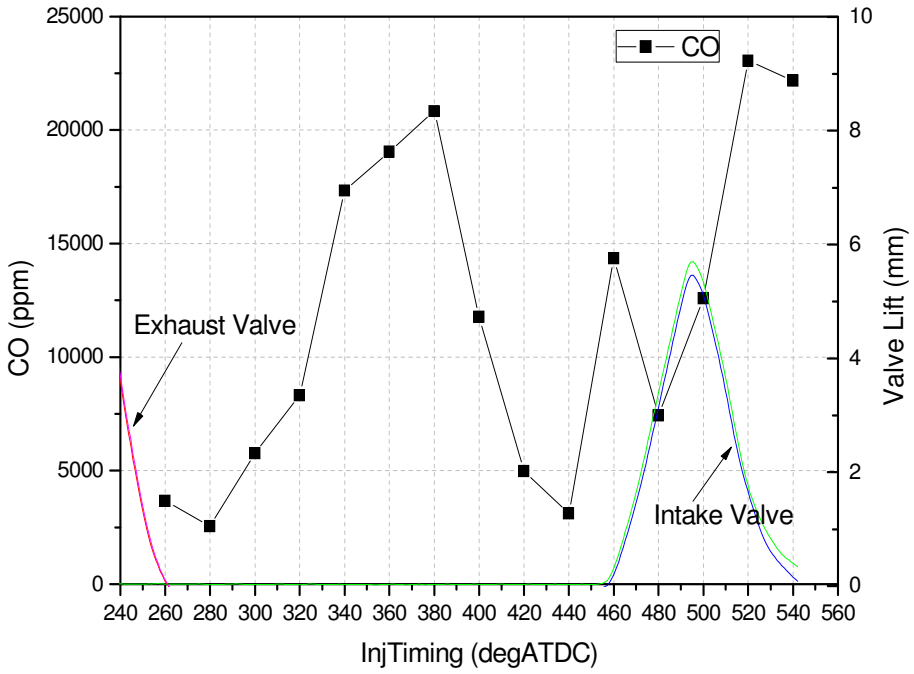

Figure 6.8 Effect of Injection Timing on CO Emissions in Four-stroke NVO CAI Operation (1500rpm, Lambda=1)

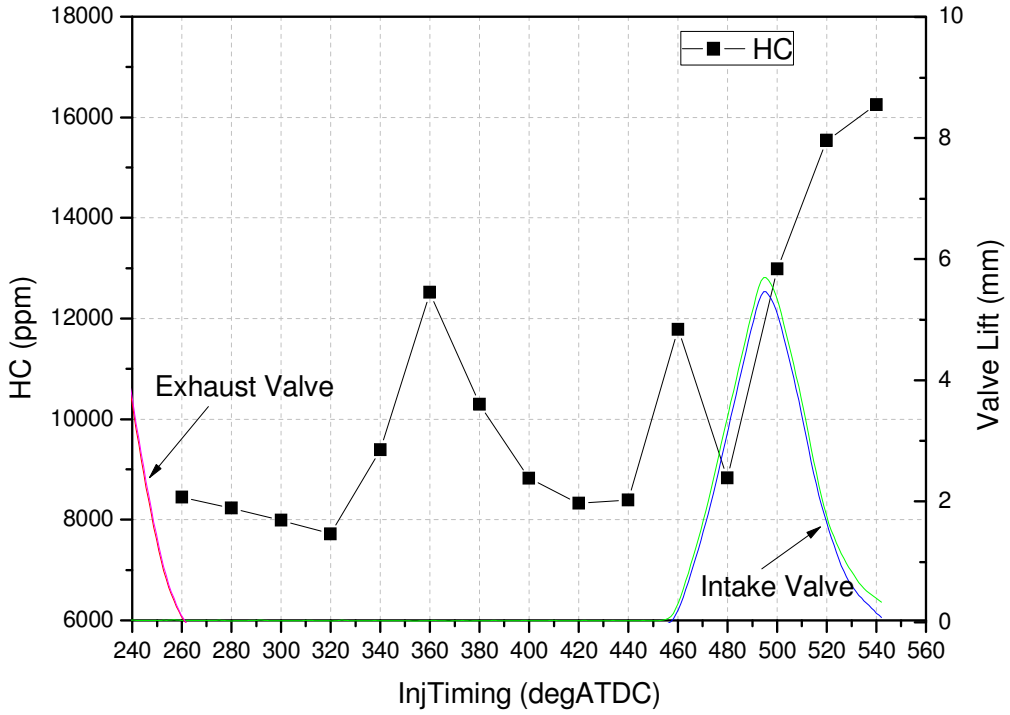

Figure 6.9 Effect of Injection Timing on HC Emissions in Four-stroke NVO CAI Operation (1500rpm, Lambda=1)

In the two-stroke CAI operation mode, the injection timing is retarded to the compression stroke to avoid fuel short-circuiting. Compared with the four-stroke operation modes, the fuel has less time to evaporate and atomize, resulting in the poor mixing and subsequent too rich combustion at some spots in the combustion chamber. This is reflected in the higher CO and HC emission data shown in Figure 6.12 and 6.13. As the injection timing is further retarded, the shorter mixture preparation time becomes, and higher HC and CO emissions result.

6.2.3 Effect of Injection Timing on CAI Combustion Process

Injection timing also affects the CAI combustion process through the charge cooling effect, piston wetting effect and mixing. In order to analyse the combustion process, the combustion parameters, such as CA10 (10% mass fraction fuel burnt crank angle), CA50 (50% mass fraction of fuel burnt crank angle) and CA10-90 (crank angles from 10% to 90% mass fraction fuel burnt), were calculated from the in-cylinder pressure and analysed for different injection timings in 3 CAI operation modes.

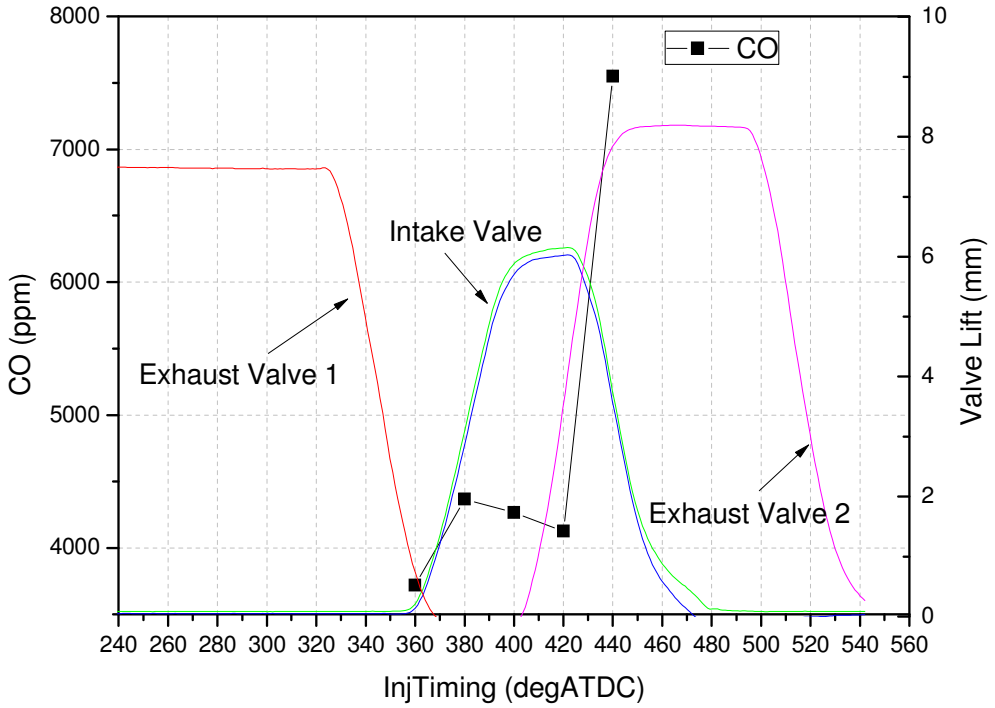

Figure 6.10 Effect of Injection Timing on CO Emissions in Four-stroke Exhaust Rebreathe CAI Operation (1500rpm, Lambda=1)

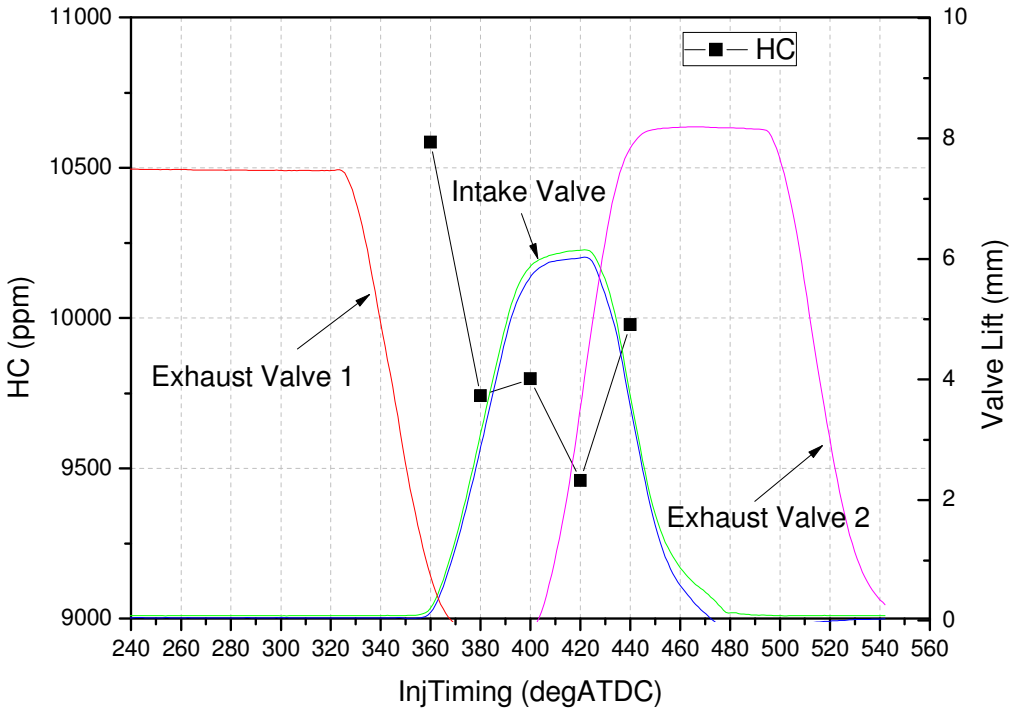

Figure 6.11 Effect of Injection Timing on HC Emissions in Four-stroke Exhaust Rebreathe CAI Operation (1500rpm, Lambda=1)

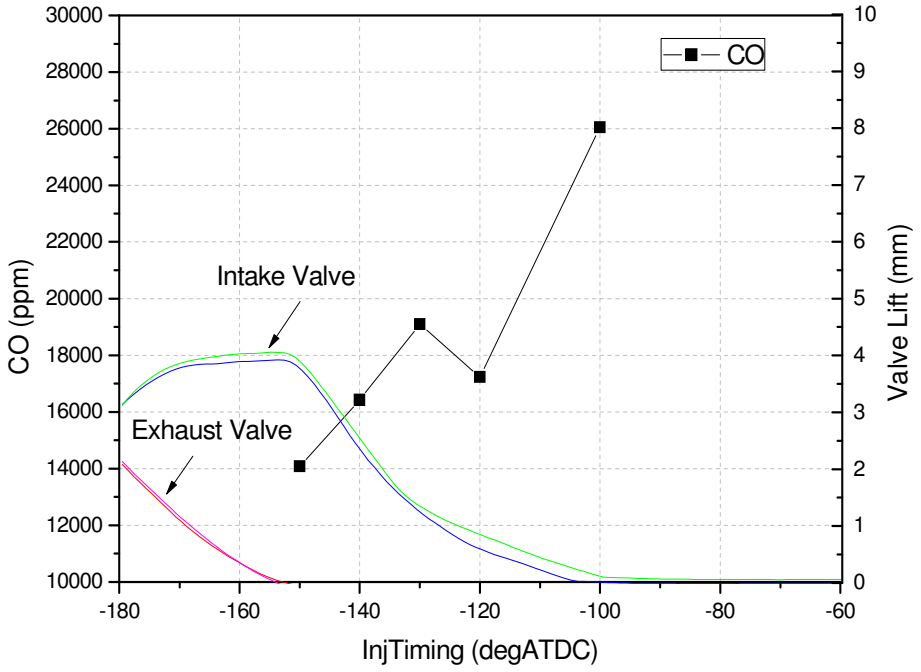

Figure 6.12 Effect of Injection Timing on CO Emissions in Two-stroke CAI Operation (1500rpm, Lambda=1)

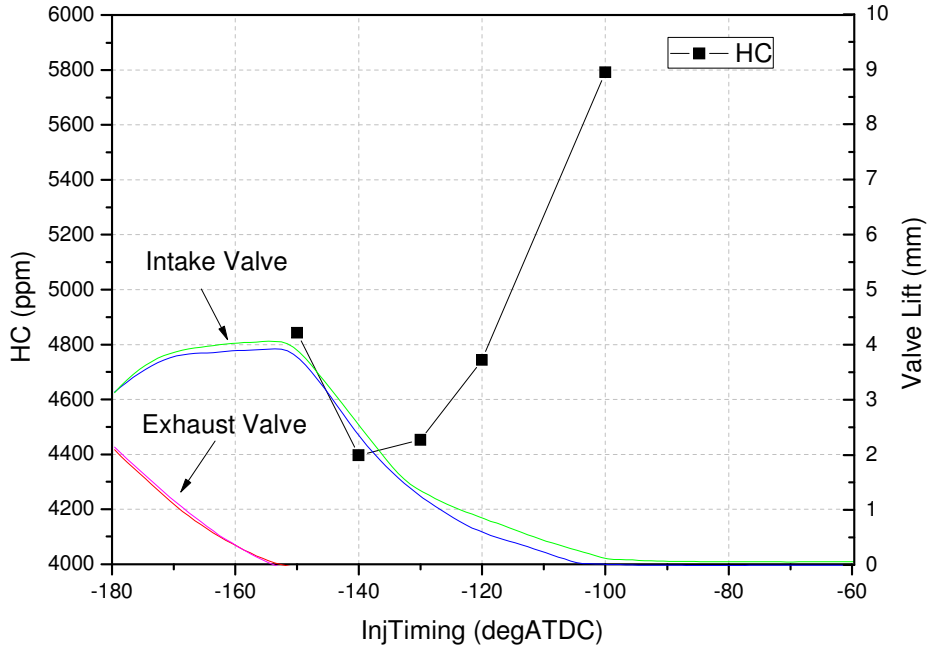

Figure 6.13 Effect of Injection Timing on HC Emissions in Two-stroke CAI Operation (1500rpm, Lambda=1)

Figure 6.14a shows the effect of injection timing on CA10, the start of combustion process, in the four-stroke NVO CAI operation mode. When fuel is injected around

360deg ATDC (gas exchange TDC), the start of combustion is retarded due to the contribution of the piston wetting effect as first mentioned above. However, looking at the CA10-90 shown in Figure 6.14b, which indicates the combustion duration, it can be found that the combustion speed is faster when fuel is injected around the gas exchange TDC because of the heating effect of the residual gas, since the intake air flow rate drops and residual gas fraction increases when the injection timing is around gas exchange TDC, as shown in Figure 6.5.

In the four-stroke exhaust rebreathe CAI operation, the injection timing has less effect on start of combustion as the wetting effect becomes weaker in front of the higher air motion in the cylinder, but the later injection of the fuel leads to the longer combustion duration due to the fuel injection into the recirculated exhaust gases, as shown in Figure 6.15.

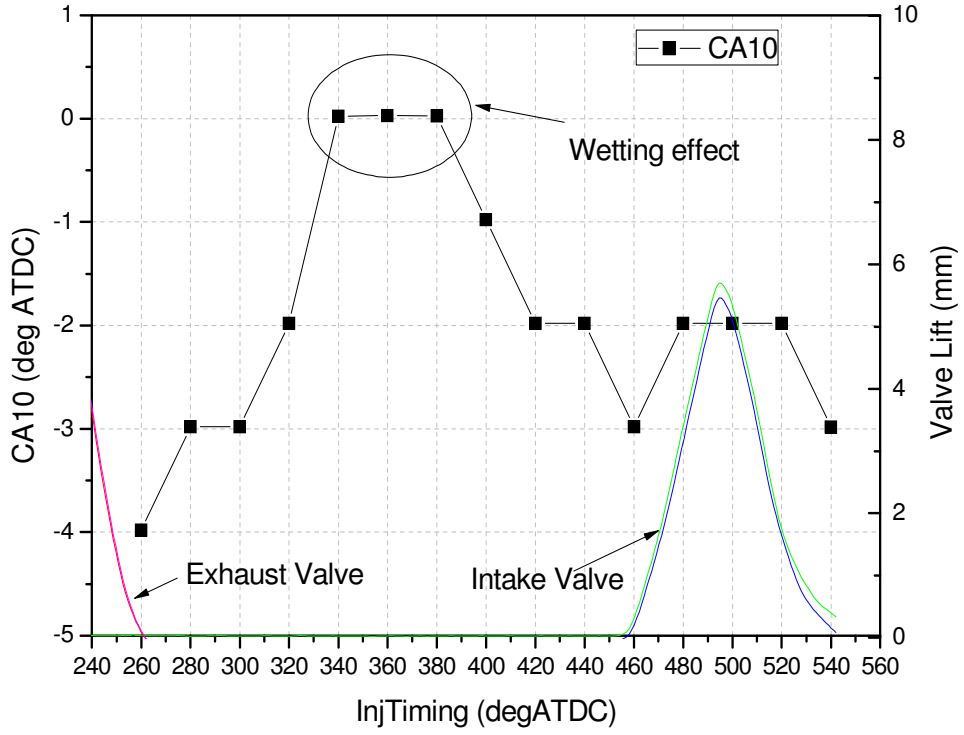

a)

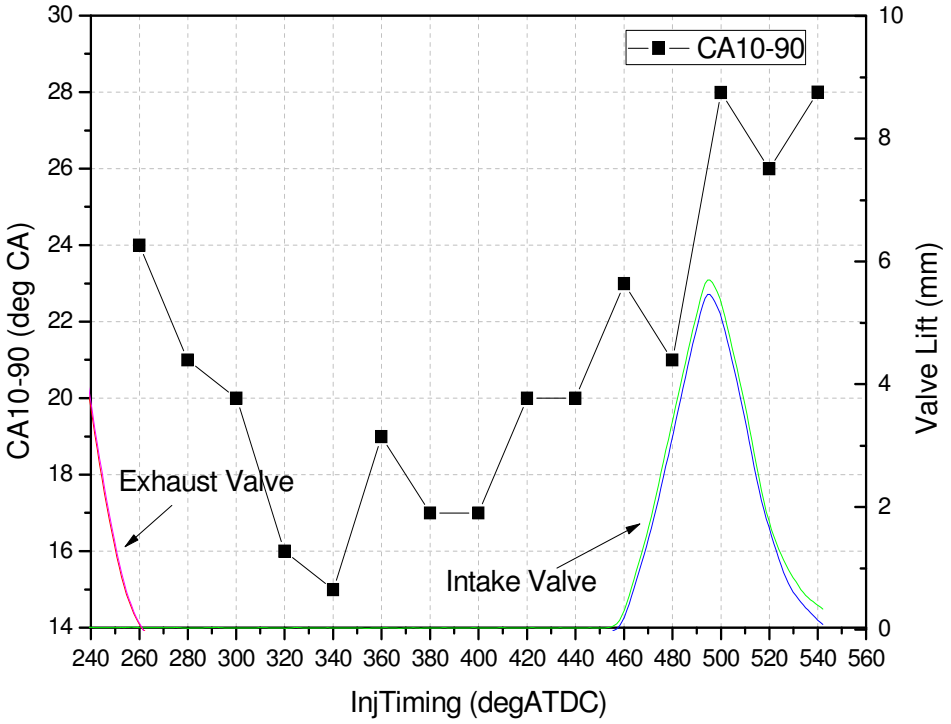

b)

Figure 6.14 Effect of Injection Timing on CA10 and CA10-90 in Four-stroke NVO CAI Operation

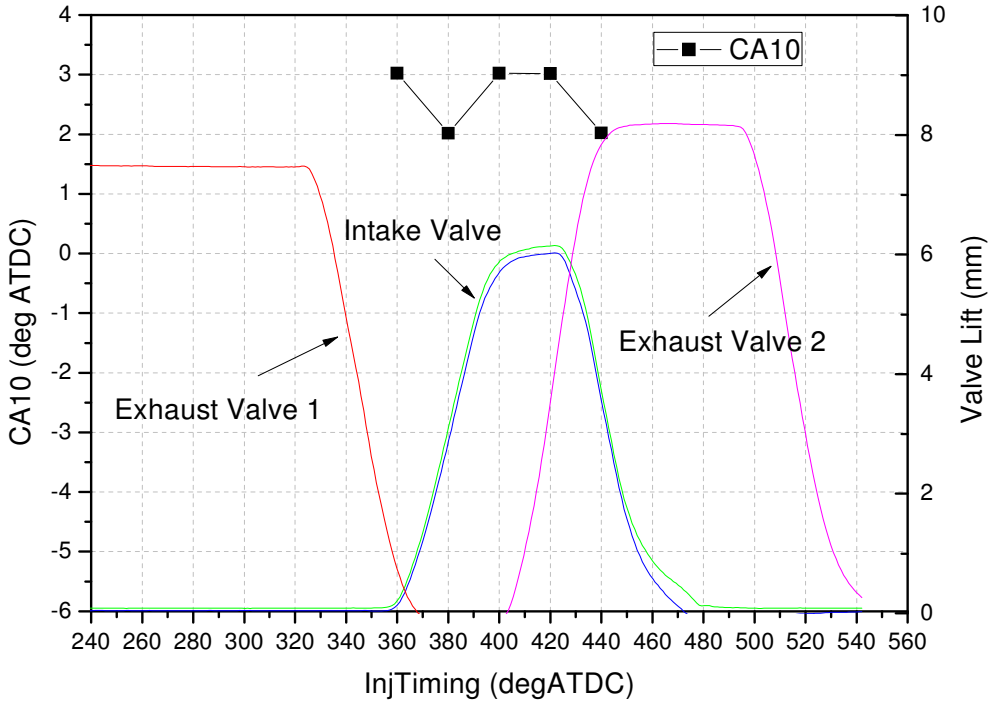

a)

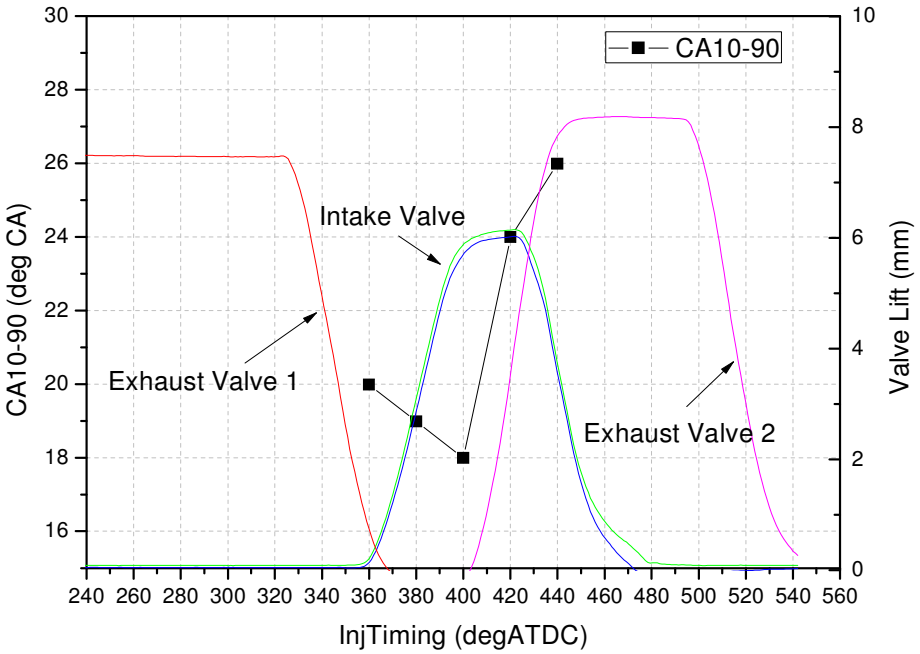

b)

Figure 6.15 Effect of Injection Timing on CA10 and CA10-90 in Four-stroke Exhaust Rebreathe CAI Operation

In two-stroke CAI operating mode, the combustion process is mainly determined by the extent of the air fuel mixing process, as the fuel has less time to evaporate and mix with the air in the cylinder when injection is in the compression stroke. As shown in Figure 6.16a, the later the fuel is injected, the more retarded the combustion phasing as represented by CA50. The retard in the combustion phase also results in the longer combustion duration shown in Figure 6.16b. Even when the spark was switched on to bring the combustion phase forward and the injection timing at –100deg ATDC, the combustion speed was hardly affected.

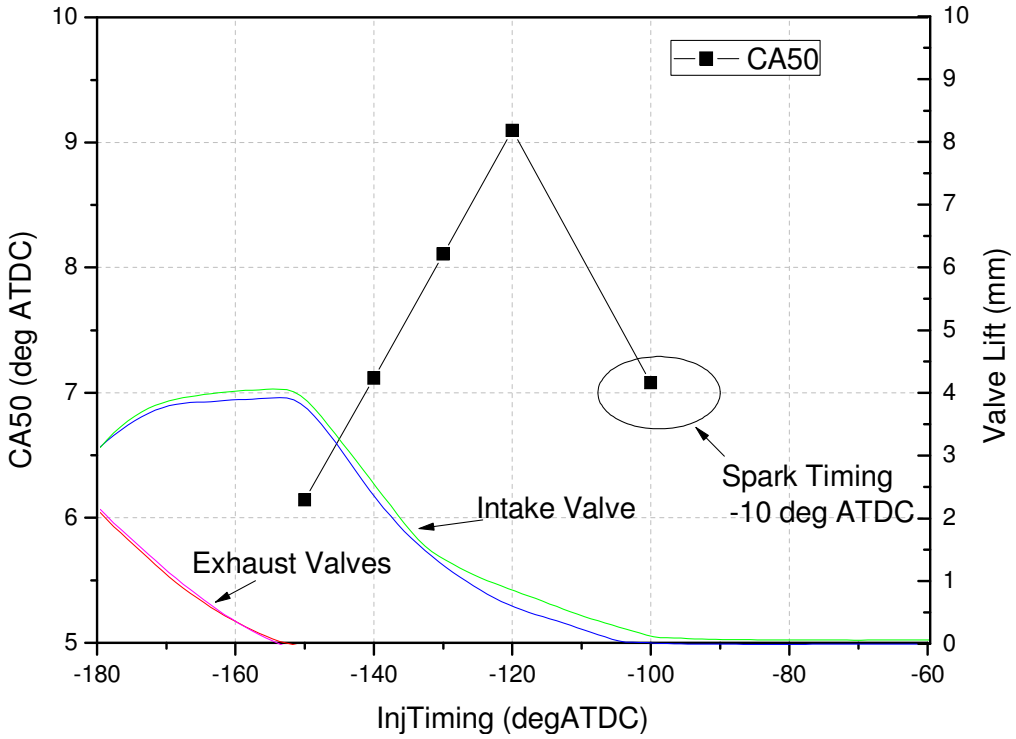

a)

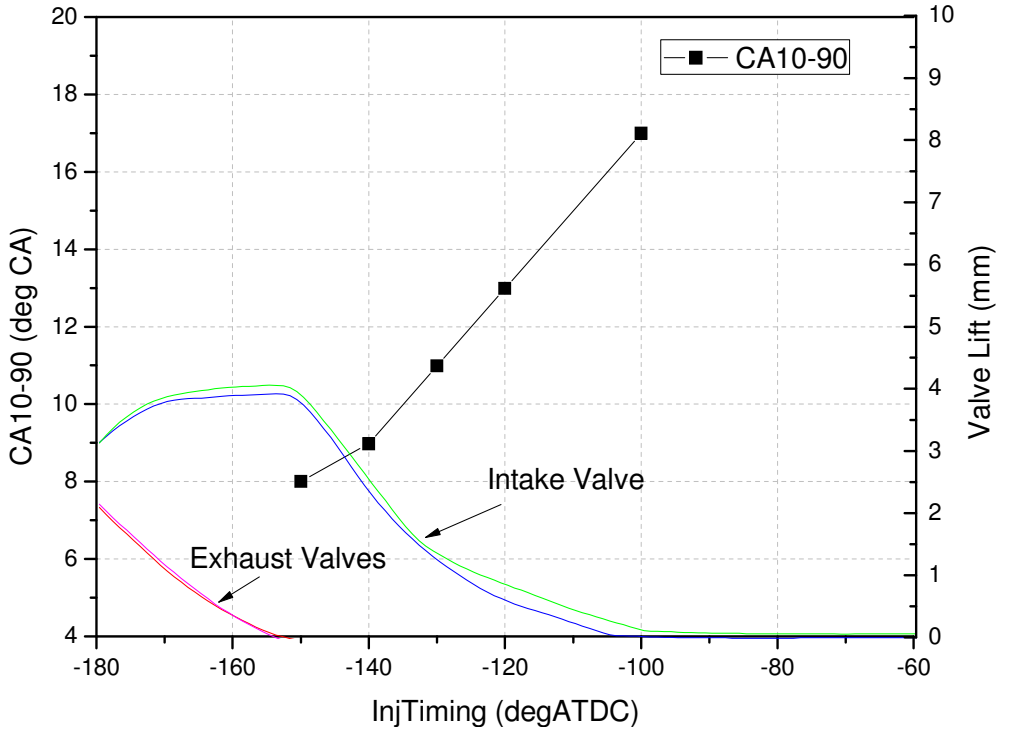

b)

Figure 6.16 Effect of Injection Timing on CA50 and CA10-90 in Two-stroke CAI Operation

In this section, effects of the injection timing on three CAI operation modes are analysed in detail. The charge cooling and piston wetting effects have been identified as the main causes of the changes in air flow, emissions and the combustion process. The main findings can be summarised as follows:

(1.) The charge cooling effect, which increases the intake air flow rate, is most significant during four-stroke NVO CAI operation when the hot residual gas is compressed to vary the temperature. It is of little consequence in the case of four-stroke exhaust rebreathing CAI operation. As fuel is injected into the mixture of cold air and hot residual gas in two-stroke mode, the charge cooling effect is noticeable but much less than that during four-stroke NVO CAI operation.
(2.) When the fuel is injected near to TDC, liquid fuel impingement impedes the fuel evaporation and reduces the charge cooling effect, in particular in four-stroke NVO CAI mode. The liquid fuel impingement leads to higher HC emissions.
(3.) The interaction of the fuel spray and incoming air or recirculated exhaust gases also affects the HC and CO emissions. This should be taken into account in the design of the fuel injector and its location as well as when developing the fuel injection strategies to be used.
(4.) Compared with residual gas trapping, rebreathing of the exhaust gases gives higher air motion in the cylinder and hence improved mixing.
(5.) For two-stroke CAI operation, it is necessary to improve the fuel evaporation and mixing process through multiple injections using a faster piezo injector.
(6.) The injection timing has less effect on the start of combustion unless the fuel impingement is significant in four-stroke NVO CAI and exhaust rebreathe CAI operation. In two-stroke CAI operation, the injection timing significantly affects the combustion phase and duration due to the shortened mixing time from the fuel injection to ignition.

6.3 Comparison between Two-stroke, Four-stroke, SI and CAI Operations

In order to evaluate the relative performance of two-stroke CAI operation, six other operating modes were performed on the same engine and compared. The seven engine

operating modes, including: four-stroke throttle-controlled SI, four-stroke intake valve throttled SI, four-stroke positive valve overlap SI, four-stroke negative valve overlap CAI, four-stroke exhaust rebreathing CAI, two-stroke CAI and two-stroke SI, were achieved through different combinations of valve timings and durations Their performance and emission characteristics were analysed and compared at a typical engine calibration operating condition of 1500rpm and 3.6bar IMEP in four-stroke or 1.8bar IMEP in two-stroke.

6.3.1 Operating modes

Figure 6.17 and Table 6.2 shows the valve timings and injection timings used in different operating modes. In addition, during the four-stroke mode operations, the supercharger was turned off and the intake air was drawn from ambient. For the two-stroke mode operations, the compressed air supply from the supercharger was connected to the intake system to provide the boost air.

Mode 1: Four-stroke throttle-controlled SI mode

This is the conventional spark ignition mode used in the production gasoline engines. Engine load is controlled by the throttle opening, and its combustion process is initialized by the spark discharge followed by flame propagation. The engine was operated in this mode to obtain the baseline data. At part load, the partially closed throttle results in significant increase in the pumping loss, the main cause for the poor fuel economy of current SI gasoline engines. In this engine operation mode, the fuel was injected earlier in the intake stroke to obtain a homogeneous mixture. To prevent wetting the piston crown, the start of injection timing used in this paper was set to 300 deg. CA before combustion TDC.

Mode 2: Four-stroke intake valve throttled SI mode

In order to reduce the pumping loss caused by the partially closed intake throttle at part load, intake valve opening duration can be used to regulate the amount of air into the cylinder with Wide Open Throttle (WOT). In this work, the intake valve opening (IVO) was fixed at normal timing and the IVC was varied to throttle the intake air flow.

Mode 3: Four-stroke positive valve overlap SI mode

In this case, IVO takes place before TDC and EVC after TDC to create a positive overlap between the intake and exhaust valve opening periods. As the intake valve opens in the exhaust stroke, a portion of exhaust gas enters the intake port and will sucked back into the cylinder in the intake stroke. The exhaust valve closes after TDC so that some exhaust gas will be sucked back into the cylinder. In this work, the intake and exhaust valve lifts were reduced to 3mm to avoid contact of the piston and valves around the gas exchange TDC. The intake throttle was used as the principal means to control the engine load but it was adjusted to a wider opening position than that of four-stroke throttle-controlled SI operation in order to inhale the correct amount of air in the cylinder with the recycled exhaust gas present.

Mode 4: Four-stroke negative valve overlap CAI mode

Another way to obtain internal EGR is to trap a portion of the burnt gas in the cylinder by earlier closing of the exhaust valve. To minimize backflow the intake valve then opens later. A negative valve overlap period is formed and the residuals are recompressed around the gas exchange TDC. In this case, intake air flow rate is dependent on the amount of the trapped residuals, which can be controlled by varying exhaust valve closing. Therefore, the throttle can be kept wide open and hence the pumping losses are reduced. As the exhaust valve closes earlier, the fuel injection timing can be advanced into the exhaust stroke for better evaporation and atomization. In this work, the start of fuel injection timing was fixed at 440deg CA before combustion TDC.

Mode 5: Four-stroke exhaust rebreathe CAI mode

Another way to obtain the internal EGR is to secondarily open the exhaust valve during the intake stroke, so a portion of the exhaust gas can be sucked back into the cylinder from the exhaust manifold. This increases the challenge to the valve system as the exhaust valve needs to open twice within one engine cycle. To achieve this valve event, in this work, the two exhaust valves were actuated individually. One exhaust valve opened as normal and the other one in the intake stroke. The air flow rate in this mode was also controlled by the intake valve duration with WOT.

Mode 6: Two-stroke CAI mode

When both of the intake and exhaust valves open twice around each BDC within 720 deg. CA, the engine operation mode becomes two-stroke operation. On the poppet-valve engine, owing to the characteristic of the incomplete scavenging in two-stroke mode, a large amount of the residual gases is trapped in the cylinder when the exhaust valve closes earlier. In this mode the engine load was determined by the boost pressure. Fuel was injected after the exhaust valve closing and before the intake valve closing for better mixing through longer mixture preparation period and the interaction between the intake air and fuel injection. The start of injection timing was set to 140deg CA BTDC.

Mode 7: Two-stroke SI mode

As a basis for comparison, two-stroke SI mode was also studied in this work. It was realised by extended exhaust period to maximise the scavenging efficiency. Engine load, similar to two-stroke CAI mode, was also determined by the boost pressure. As less burnt gas was retained in the cylinder, the boost pressure requirement was reduced at the same engine load compared to the two-stroke CAI mode.

In order to compare the results in different operating modes, the engine was operated at a common operating condition of 1500rpm 3.6bar IMEP. All the equations used to calculate efficiencies are shown in Chapter 3.6. The pressure-volume diagrams at this load are shown in Figure 6.18 for the seven operating modes.

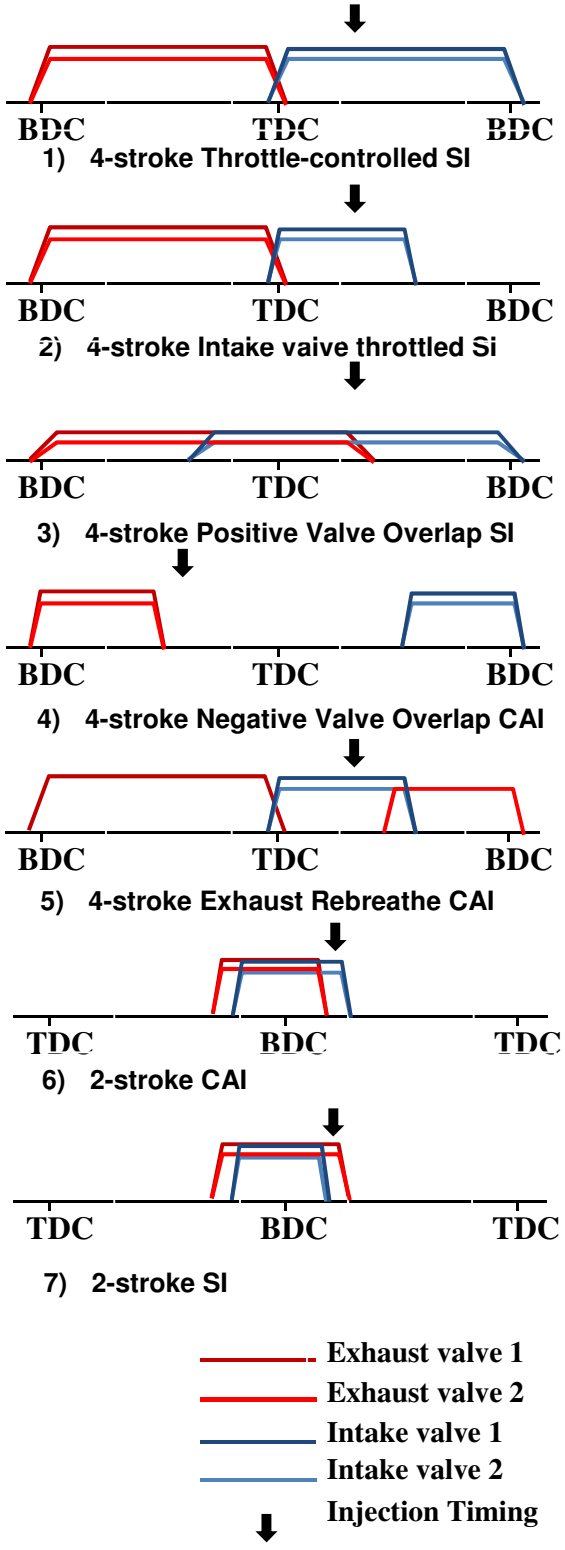

Figure 6.17 Valve Timings and Injection Timings for the 7 Operating Modes

Table 6.2 Valve Timings for each Operating Mode

Mode	IVO	IVC	EVO		EVC	
4strThrSI	5deg BTDC	0deg ABDC	10deg BDC		0deg ATDC	
4strIVLSI	5deg BTDC	100deg BBDC	10deg BDC		0deg ATDC	
4strPVOSI	30deg BTDC	0deg ABDC	10deg BDC		25deg ATDC	
4strNVO	100deg ATDC	0deg ABDC	10deg BDC		100deg BTDC	
4strReB	5deg BTDC	80deg BBDC	Valve1	Valve2	Valve1	Valve2
			10deg BDC	45deg ATDC	0deg ATDC	0deg ABDC
2strCAI	17deg BBDC	60deg ABDC	40deg BBDC		12deg ABDC	
2strSI	40deg BBDC	40deg ABDC	60deg BBDC		60deg ATDC	

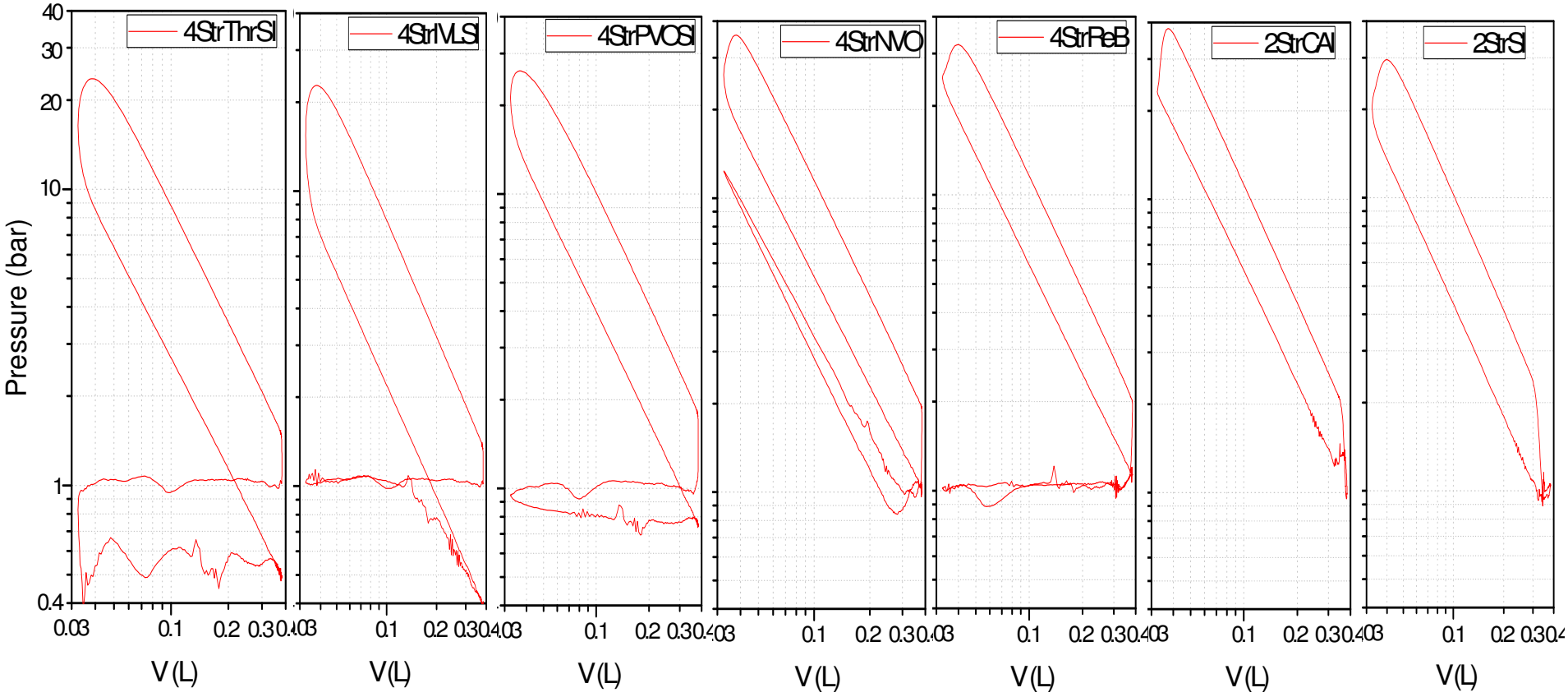

Figure 6.18 P-V Diagram for 7 Operating Modes

6.3.2 Gas Exchange Efficiency

As mentioned previously, in conventional throttle controlled SI mode, high pumping work occurs as a vacuum is created in the intake system at part-load due to the partially closed throttle. To quantify the pumping work in the seven operating modes, PMEP was calculated from the in-cylinder pressure data during the gas exchange process. As shown in Figure 6.19, when the throttle is replaced by the intake valve to control the engine load, PMEP is reduced by 0.2bar, which contributes 4% gain in gas exchange efficiency as shown in Figure 6.20. The PMEP is further reduced by allowing the exhaust gas to be sucked back into the cylinder in the four-stroke positive valve overlap SI mode. In four-stroke negative valve overlap mode, PMEP slightly increases due to the heat loss during the recompression process. The PMEP of the four-stroke exhaust rebreathe mode is the lowest because of almost zero intake and exhaust pressure difference. Therefore, the gas exchange efficiency is nearly 100% in this mode. In two-stroke operation modes, the pumping loss during the gas exchange process is zero, but the energy consumed by the supercharger is calculated and included in the Friction Mean Effective Pressure (FMEP) shown in the section of mechanical efficiency and Brake Specific Fuel Consumption (BSFC).

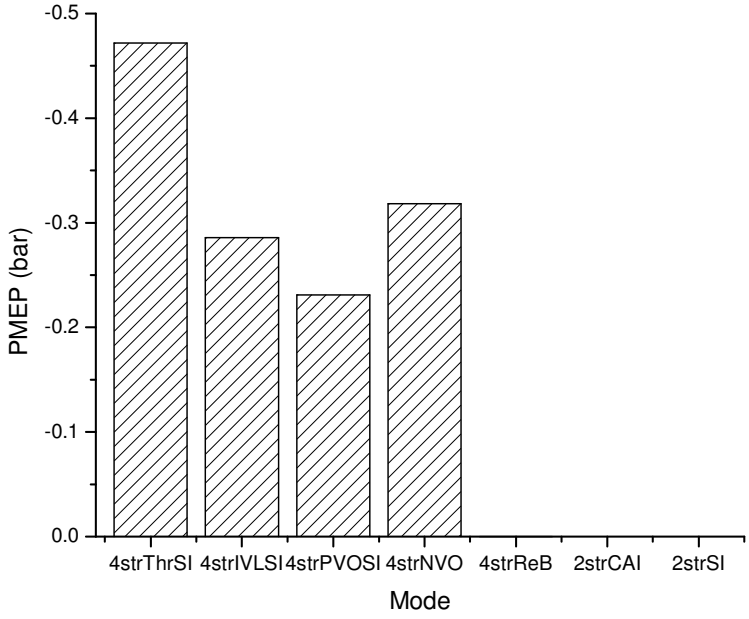

Figure 6.19 PMEP of the 7 Operating Modes

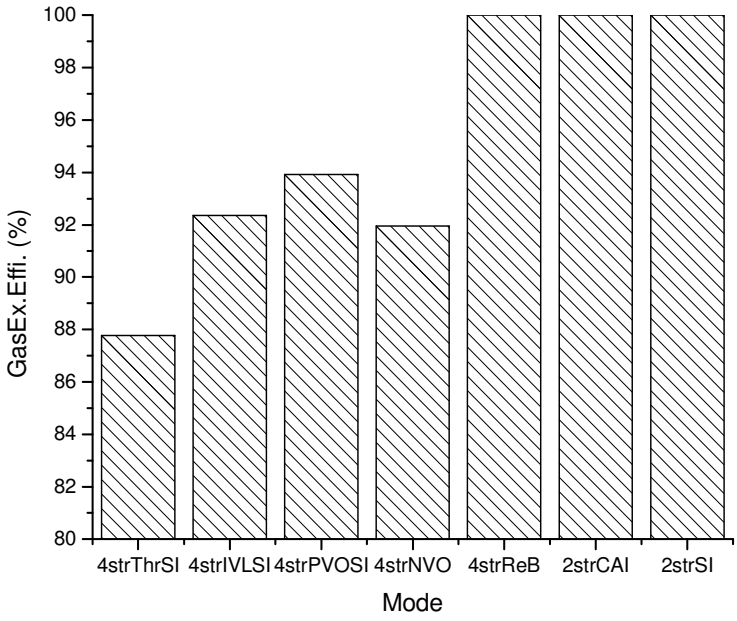

Figure 6.20 Gas Exchange Efficiency of the 7 Operating Modes

6.3.3 Combustion Efficiency

Comparison of the combustion efficiency, which is calculated from the fuelling rate and emissions data, reflects the quality of the mixing and atomization of the fuel in the cylinder before ignition. From Figure 6.21, it can be seen that the combustion efficiency of four-stroke intake valve throttled SI is lower than that of the other four four-stroke modes probably due to the worse atomization in the low in-cylinder temperature caused by the expansion after the intake valve closing in the intake stroke. In four-stroke exhaust rebreathe mode, the exhaust gas comes back in the cylinder during the intake stroke. This upset the air motion and mixing process in the cylinder and made the combustion efficiency the second lowest in four-stroke modes. Combustion efficiency of the four-stroke negative valve overlap is the highest because of the better and longer mixing and atomization since the fuel is injected in the exhaust stroke. The high temperature of the trapped residual and the recompression process helps mixing and atomization. In two-stroke SI mode, the combustion efficiency is the lowest due to the shortened time of evaporation, as the start of injection timing is retarded to 140 deg. CA BTDC. The high CO emissions, shown in Figure 6.26, in two-stroke mode reflects that diffusion combustion caused by the poor mixing process takes place in the cylinder. In the case of two-stroke CAI mode more burnt gas is retained in the cylinder, which gives higher in-

cylinder temperature and helps the mixing process. The CO emissions are lower than that of two-stroke SI mode.

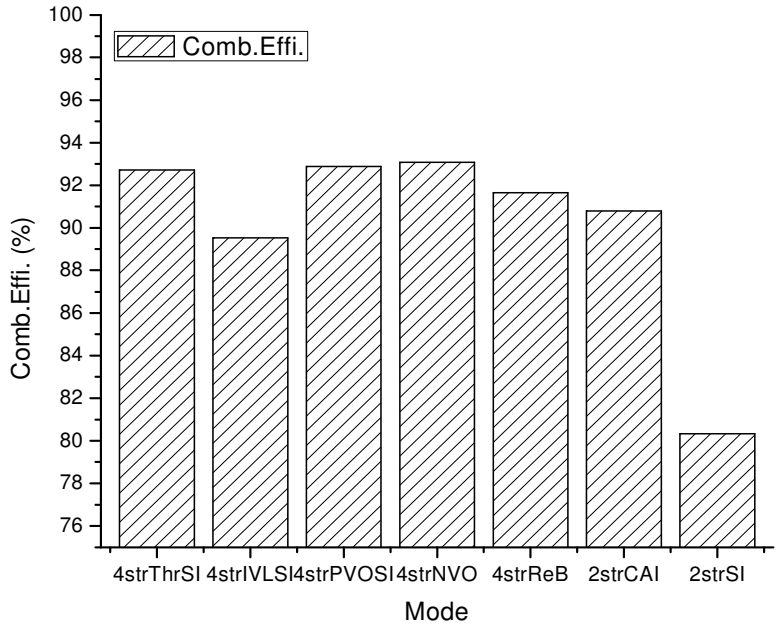

Figure 6.21 Combustion Efficiency of the 7 Operating Modes

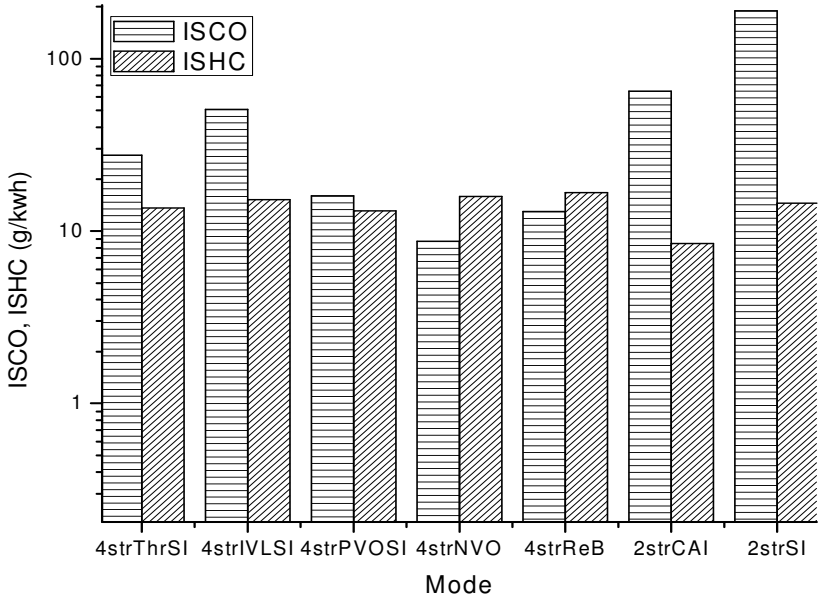

Figure 6.22 ISCO and ISHC of the 7 Operating Modes

6.3.4 Thermodynamic Efficiency

Figure 6.23 shows the gross indicated thermodynamic efficiency of the seven modes, which is calculated from the ratio of the gross work in the compression and expansion stroke to the heat released from the combustion process. A lot of factors can affect the thermodynamic efficiency of the internal combustion engine. In this work, it's mainly determined by the effective compression ratio, expansion ratio, combustion phase and duration, specific heat ratio and heat transfer to the wall. The results show very similar thermodynamic efficiencies between four-stroke throttle controlled SI and intake valve throttled SI mode, since their combustion phase and duration are almost identical as shown in Figure 6.24. In four-stroke positive valve overlap SI mode, the presence of burnt gas slows down the flame propagation speed and hence the lower thermodynamic efficiency. Figure 6.24 also shows that the combustion duration of four-stroke negative valve overlap CAI and exhaust rebreathe CAI modes are shorter than that of four-stroke SI mode, which tends to increase the thermodynamic efficiency of such operating modes as the heat addition process becomes akin to the constant volume process. In addition, low combustion temperature in the CAI modes also contributes to the high thermodynamic efficiencies seen for such operations.

In two-stroke mode, the low thermodynamic efficiency is mostly caused by the low effective expansion ratio due to the early opening of the exhaust valves. This suggests that it may be possible to improve the thermodynamic efficiency of this two-stroke mode by increasing the expansion process through retarded exhaust valve opening. Such change may not be desirable for the SI combustion due to the deteriorating scavenging process but it could be implemented for CAI combustion which relishes the presence of hot residual gases.

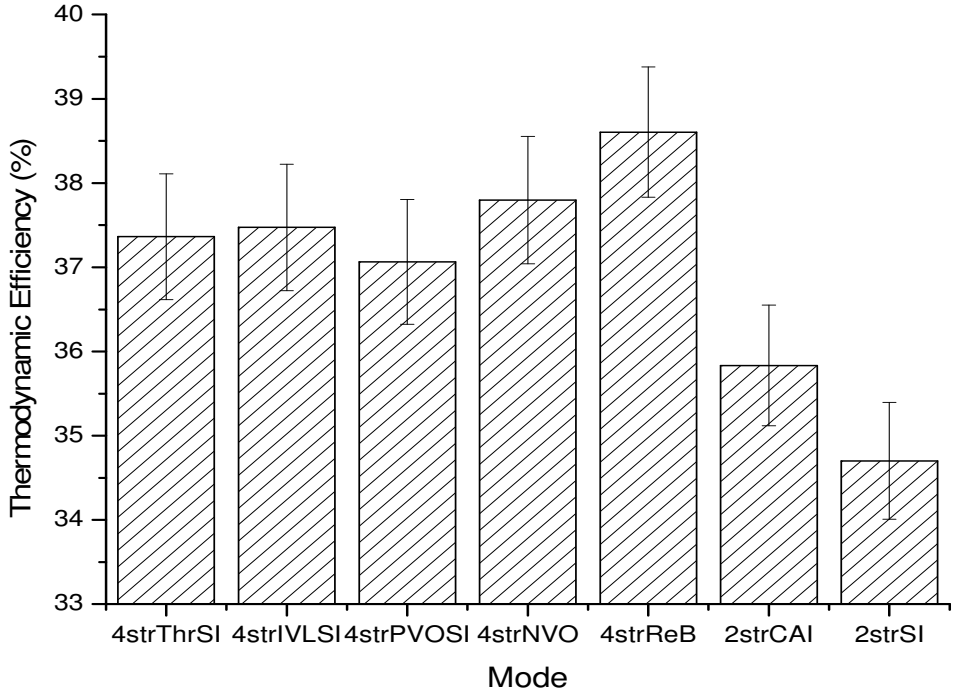

Figure 6.23 Gross Indicated Thermodynamic Efficiency of the 7 Operating Modes

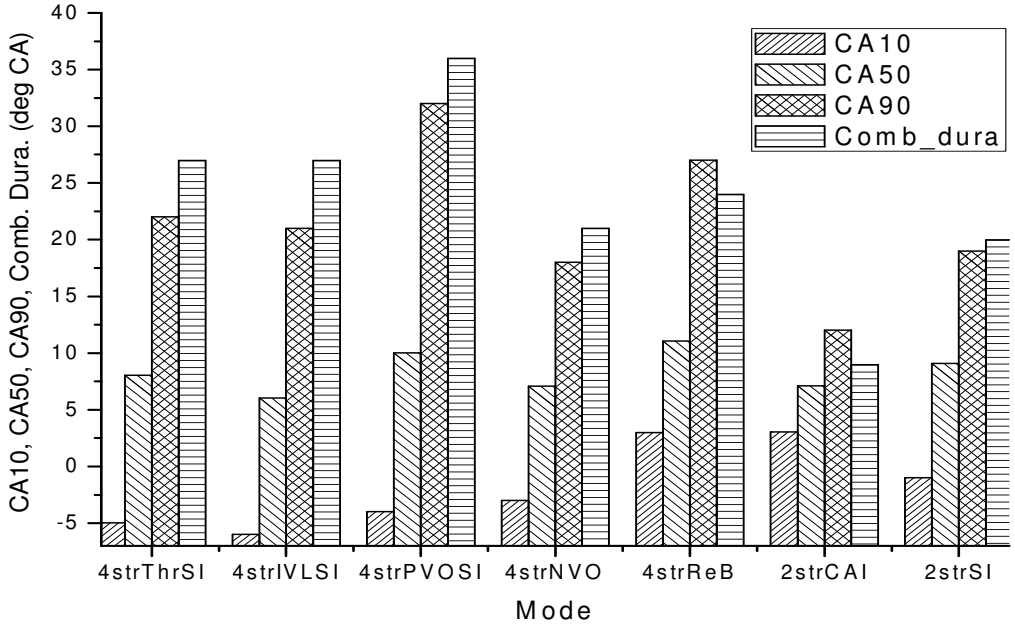

Figure 6.24 CA10, CA50, CA90 and Combustion Duration of the 7 Operating Modes

6.3.5 Net Indicated Efficiency

Combining the efficiencies above, the net indicated efficiency can be worked out and their values are shown in Figure 6.25. Figure 6.26 shows the ISFC of the seven operating modes, which is calculated from the ratio of fuelling rate to the indicated power.

In four-stroke modes, the net indicated efficiency of throttle controlled SI is the lowest due to the high pumping loss and low thermal efficiency, hence the higher fuel consumption. Intake valve throttled SI mode increases the net indicated efficiency by less than 1% at this operating condition since the reduced pumping work is offset by the reduction in the combustion efficiency. With reduced pumping loss, four-stroke positive valve overlap SI mode exhibits the same indicated efficiency as four-stroke negative valve overlap mode. Four-stroke CAI operation with exhaust rebreathing shows the highest net indicated efficiency and thus the lowest fuel consumption, due to the absence of pump loss and faster combustion.

In two-stroke CAI mode, the indicated efficiency is higher than that of the four-stroke throttle control SI and intake valve throttled SI due to reduced pumping loss. Two-stroke SI has the lowest indicated efficiency of the seven operating modes due to its low combustion efficiency and thermodynamic efficiency.

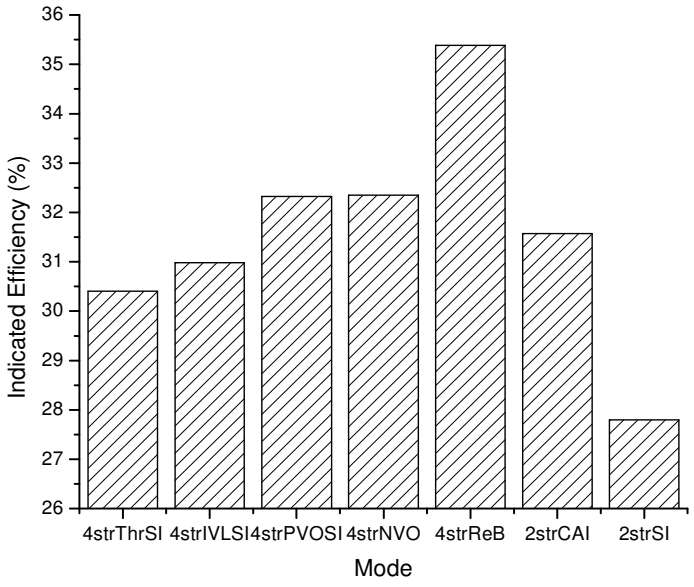

Figure 6.25 Indicated Efficiency of the 7 Operating Modes

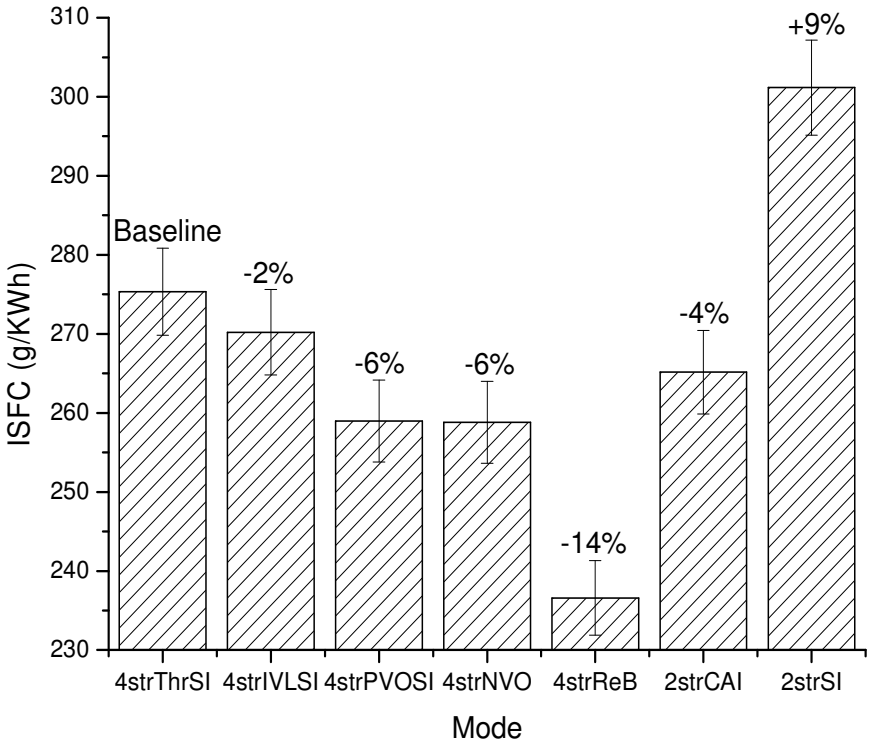

Figure 6.26 ISFC of the 7 Operating Modes

6.3.6 Emissions

CO and HC emission have been shown in Figure 6.22. From the emission data, we can see CAI combustion generates similar CO or HC emissions to those of SI operations. High CO and HC emissions are mainly caused by the poor mixing or substantial diffusion combustion from any liquid fuel film on the piston crown. It is noted that as the injection takes place earlier CO emissions tend to fall due to the longer mixing period. There is no obvious evidence in fuel short-circuiting in the two-stroke modes as was the case of conventional port injected two-stroke engine operations.

From the NOx emissions data shown in Figure 6.27, it can be seen that compared with conventional throttle controlled SI combustion four-stroke intake valve throttled SI combustion produces slightly lower NOx emissions owing to the lower in-cylinder temperature caused by the Miller cycle. With the dilution of burnt gas in four-stroke positive valve overlap SI, negative valve overlap CAI and exhaust rebreathe CAI, the NOx emissions can be significantly reduced. In two-stroke SI mode, the NOx is less than

four-stroke throttle controlled SI mode because of high burnt gas retained in the cylinder inherently caused by the in-complete scavenging of two-stroke mode.

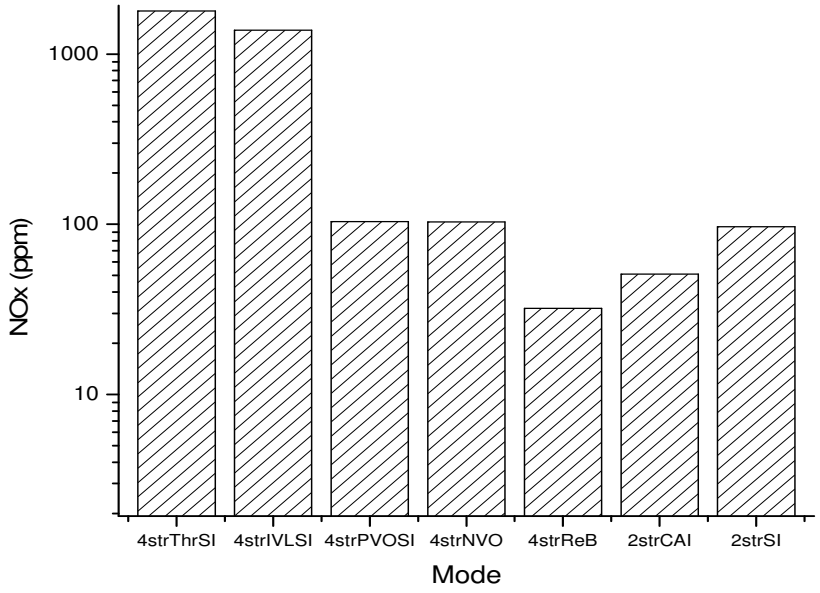

Figure 6.27 NOx Emissions of the 7 Operating Modes

6.3.7 Mechanical Efficiency and BSFC

FMEP calculated from the difference between engine brake output and indicated output, is shown in Figure 6.28. For two-stroke operation modes, the work consumed by the supercharger for scavenging is calculated from the pressure difference between the inlet and outlet port of the supercharger and included in the FMEP. In four-stroke operation modes, intake valve throttled SI operation has lowest friction due to the lower in-cylinder pressure of the Miller cycle. The FMEP of two-stroke operation modes is much lower than that of four-stroke operation modes because of the halved number of strokes. This contributes to a 10% increase in Mechanical efficiency of two-stroke CAI and 13% for two-stroke SI, as shown in Figure 6.29. The 3% difference is caused by more energy being consumed by the supercharger in two-stroke CAI operation mode, as higher intake pressure is required for delivering the fresh air into the cylinder.

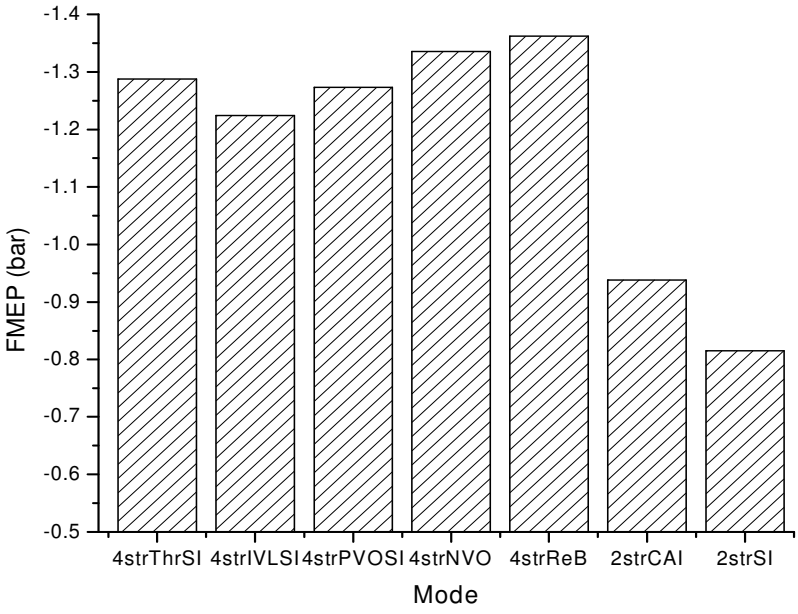

Figure 6.28 FMEP of the 7 Operating Modes

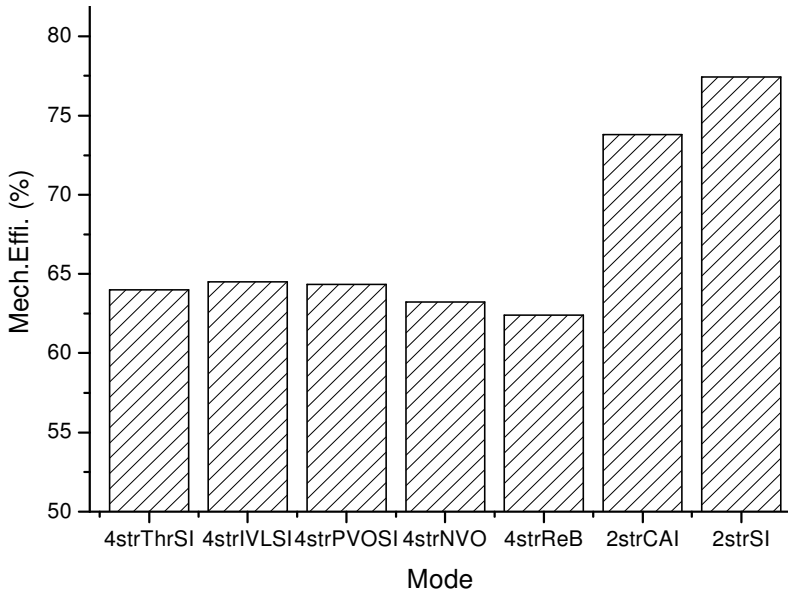

Figure 6.29 Mechanical Efficiency of the 7 Operating Modes

Figure 6.30 shows the BSFC in the seven operating modes, which is calculated from the ratio of the fuelling rate to the brake power obtained from the engine crankshaft. This reflects the total fuel consumption after taking the friction loss and the supercharger power into account. Now the two-stroke CAI operation mode has the best fuel economy and reduces the fuel consumption by 19% compared with four-stroke throttle controlled SI operation mode.

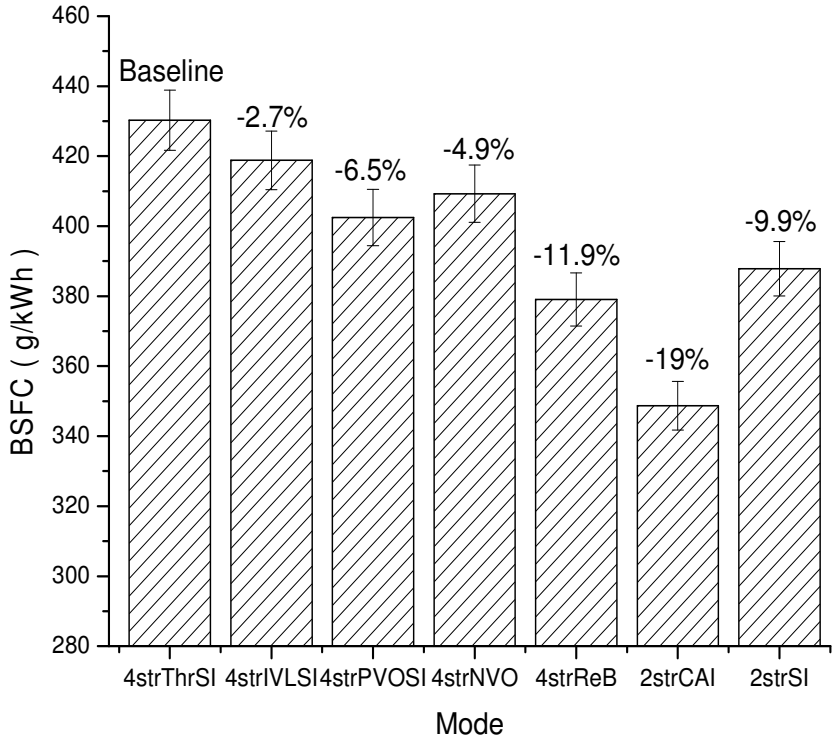

Figure 6.30 BSFC of the 7 Operating Modes

The main findings of this section can be summarised as follows:

1. Four-stroke throttle controlled SI operating mode has the highest pumping loss due to the partially closed throttle. Four-stroke exhaust rebreathe CAI operating mode has the lowest pumping loss because of recirculating the exhaust gases during the intake stroke.
2. Four-stroke throttle controlled SI, positive valve overlap SI and NVO CAI have the higher combustion efficiency. Two-stroke SI has the lowest combustion efficiency.
3. Four-stroke exhaust rebreathe CAI has the highest indicated efficiency due to the lowest pumping losses and higher thermodynamic efficiency caused by the shorter combustion duration. Two-stroke SI has the lowest indicated efficiency due to the low combustion efficiency and thermodynamic efficiency.
4. Two-stroke operating modes produce more CO emissions due to shortening the mixing process. Without the dilution of exhaust gases, four-stroke throttle controlled SI and intake valve throttled SI combustion produce more NOx emission.
5. Two-stroke CAI operating mode provides the lowest fuel consumption due the low friction loss.

6.4 Summary

In this chapter, the effect of direct fuel injection timing on engine performance, combustion and emissions was investigated in 3 CAI operating modes. The charge cooling effect of direct fuel injection is most significant during four-stroke NVO CAI operation. Its effect is also noticeable in two-stroke CAI operation but negligible in four-stroke exhaust rebreathing CAI operation. The injection timing has less effect on the start of combustion unless the fuel impingement is significant in the four-stroke NVO CAI and exhaust rebreathe CAI operation. In the two-stroke CAI operation, the injection timing significantly affects the combustion phasing and duration due to the shortened mixing time from the fuel injection to ignition.

For further estimating two-stroke CAI operation, 7 operating modes were performed on the same engine, including either two-stroke or conventional four-stroke engine operations. It is found that the two-stroke CAI operation mode incurs the lowest fuel consumption at the part-load condition tested.

Chapter 7

Ethanol Blends CAI in Two-stroke Operation

Chapter 7 Ethanol Blends CAI in Two-stroke Operation

7.1 Introduction

In this chapter, CAI combustion with ethanol blended gasoline is demonstrated over different engine speed and load conditions in the two-stroke poppet valve DI engine. Detailed analysis of effect of ethanol on combustion process, emissions and efficiencies are performed and presented when the engine was operated with measured exhaust lambda at 1.0.

7.2 Ethanol Content Effects on CAI Combustion and Emissions

In order to compare the results between burning pure gasoline and ethanol blended gasoline, the engine test conditions were kept the same as that explained in Chapter 5. The experiments were performed with E15 (15% ethanol in gasoline by volume) and E85 (85% ethanol in gasoline by volume) while the valve timings, boost pressure, injection timing, and spark timing were all kept the same, only the injection duration were changed to keep the exhaust lambda 1.0 while injecting ethanol blended fuels.

First of all, the ethanol content effect on CAI combustion process was investigated. Figure 7.1 shows 50% mass fraction burnt crank angle (CA50) as a function of the engine load, IMEP, at 2000rpm with gasoline, E15 and E85. It can be seen that the combustion phase was retarded with increasing engine load in most cases. As explained previously, load in the two-stroke CAI operation was determined by the scavenging rate. As the load increased, there was more fresh charge but less residual gas trapped, resulting in the lower in-cylinder temperature. Therefore, the start of autoignition combustion was delayed until the charge temperature was compressed to the autoignition temperature. At the highest load conditions, autoignition could not start and spark ignition was introduced at 8 deg after TDC to initiate the combustion process. At the low load conditions, the start of combustion for E15 and E85 advanced slightly as the load was changed from 1 bar IMEP to 2 bar IMEP. At such low load, the largest amount of burned gas was trapped and the burned gas temperature was at their lowest value. In addition, there was a relative large percentage of unburned or partially burned fuel in the trapped charge which

could contribute to the autoignition chemistry leading to the start of the high temperature combustion reactions. Since the autoignition process is affected by the charge dilution, temperature, and chemical species in the cylinder charge, the small changes observed could have been caused by any of these factors.

As shown in Figure 7.2, the combustion duration of all three fuels initially decreased with load due to smaller dilution effect by the reduced amount of burned gas trapped in the cylinder at higher load. Beyond 4.2 bar IMEP, E15 and E85 showed increased combustion duration. At such high load conditions, spark ignition was critical to initiate the combustion process in the form of flame propagation. Because of the relatively high temperature of the end gas region, multiple autoignition combustion would take place in conjunction with the flame propagation. This can be illustrated by the mass fraction burned curves at 4.2 bar and 6.6 bar IMEP values for E85 plotted in Figure 7.3. It can be seen that the heat release process is characterised by a relatively slow first part and then followed by a faster second part. As previous studies have shown [93, 94], the two stage heat release process was a result of the hybrid combustion of flame propagation and multiple autoignition burning in the spark assisted CAI region. As the load increased beyond 4.2 bar IMEP, flame propagation became dominant over the multiple autoignition combustion and accounts for a greater part of the combustion and heat release process, resulting in an increase in the overall combustion duration.

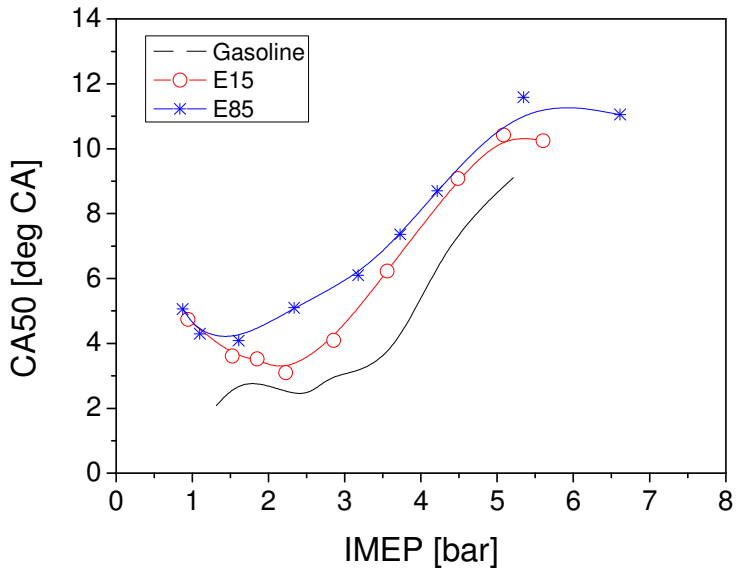

Figure 7.1 CA50 in Two-stroke CAI Operation at 2000rpm

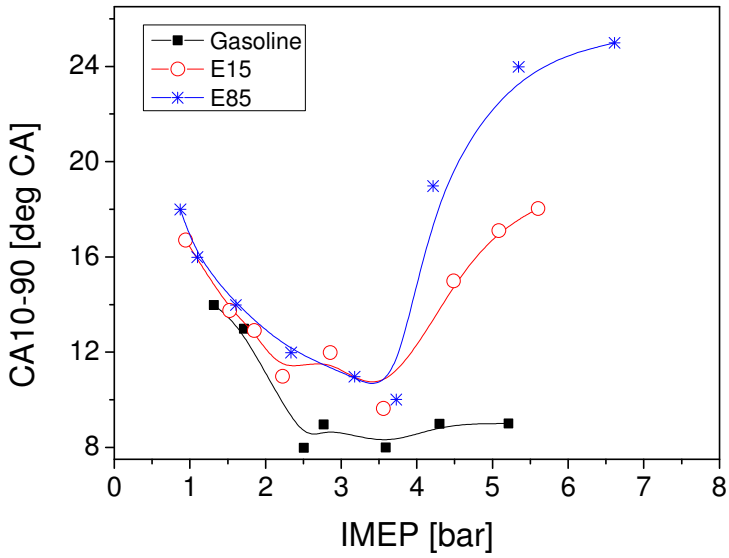

Figure 7.2 CA10-90 in Two-stroke CAI Operation at 2000rpm

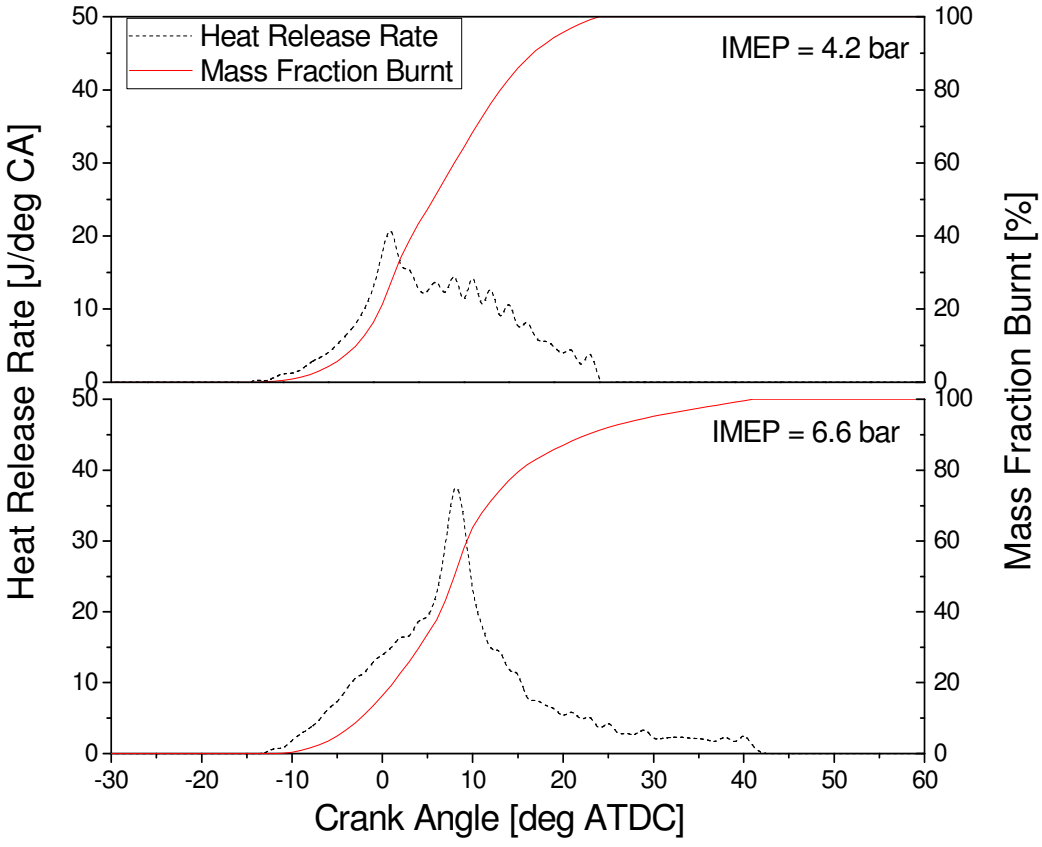

Figure 7.3 Heat Release Rate and Mass Fraction Burnt of E85 at 2000rpm

Figure 7.4 shows the unburned hydrocarbon (uHC) emissions as a function of engine output at 2000rpm. The presence of ethanol reduced the uHC emissions throughout the load range. E85 produced about 50% less uHCs than gasoline due to the oxygen in the

fuel. As the combustion temperature became higher with load, more complete combustion could take place and hence less uHC emissions. As reported by the authors [95], the uHC emissions from the two-stroke CAI combustion was not much different from the four-stroke SI operations in the same engine. One major source of uHCs from this engine is due to the inadequate optimisation of fuel spray and combustion chamber design, which resulted in fuel impingement on the piston and cylinder wall. It is expected that multiple fuel injection from a fast acting injector at higher injection pressure together with an appropriate designed piston top would lead to significant reduction in the uHC emissions.

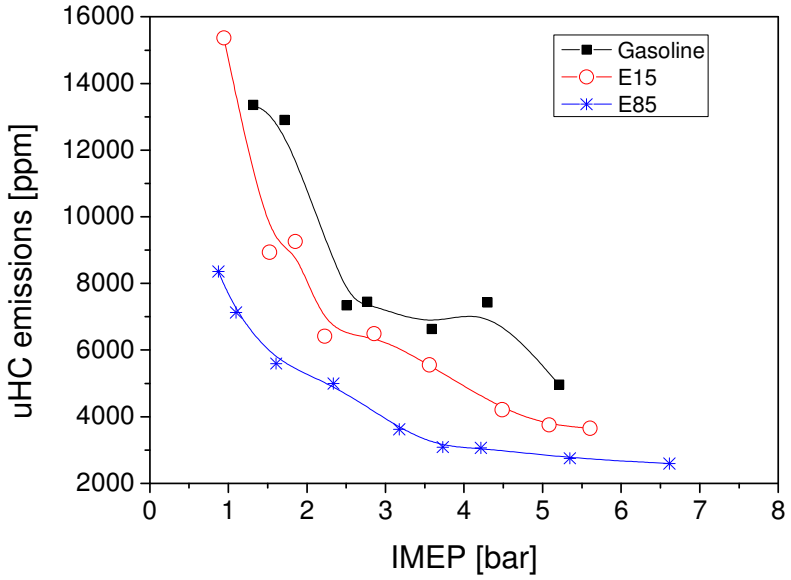

Figure 7.4 uHC Emissions in Two-stroke CAI Operation at 2000rpm

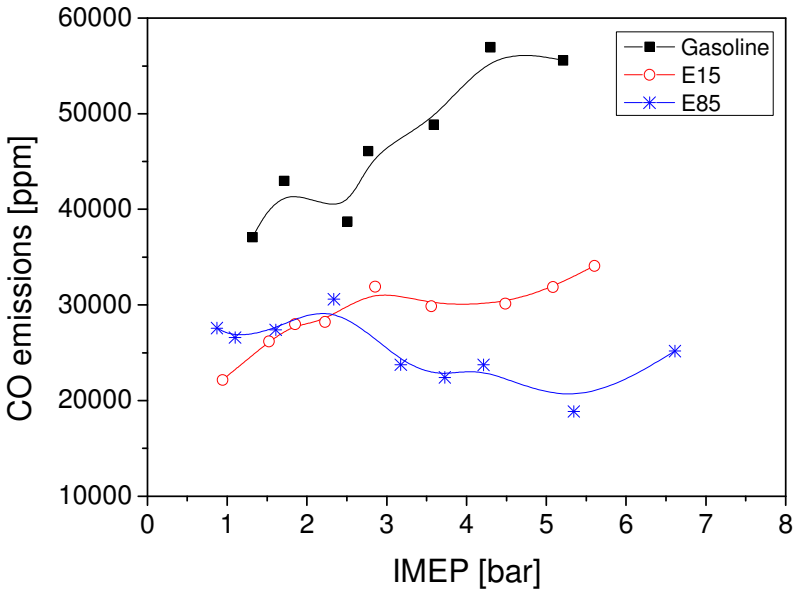

Figure 7.5 CO Emissions in Two-stroke CAI Operation at 2000rpm

The CO emission results in Figure 7.5 show that E15 and E85 fuels produce less CO emissions, particularly at high load conditions, because of the more effective oxidation reactions of oxygenated ethanol. It is noted that gasoline produced significantly more CO at higher load whilst the CO emissions from E15 and E85 fuels remained relatively insensitive to the load. In order to explain the results, it is necessary to understand the air short-circuiting and its effect on in-cylinder air/fuel ratio. As described in Chapter 5, there was an overlap period between the intake process and exhaust process in the two-stroke CAI mode operation. During this overlap period, it is likely that a fraction of air could flow directly out of the exhaust valves, a phenomenon known as air short-circuiting. As shown in Figure 5.8, the short-circuiting rate increased with the engine load or boost pressure, combustion took place with richer fuel and air mixture at higher load, resulting in higher CO emissions with gasoline as shown in Figure 7.5. When ethanol was introduced, the stoichiometric air to fuel ratio decreased. Hence less air at lower boost pressure was needed, reducing the short-circuiting rate. At low loads, the effect of ethanol on improving CO emissions becomes less significant because of the lower short-circuiting rate and lower combustion temperature of ethanol.

Figure 7.6 shows the NOx emissions in the two-stroke CAI operation fuelled with gasoline, E15 and E85 at an engine speed of 2000rpm. E85 reduced NOx emissions at high loads mainly due to the cooling effect of ethanol. However, this effect became less significant at low loads as the combustion temperature and NOx emission were very low (less than 100ppm).

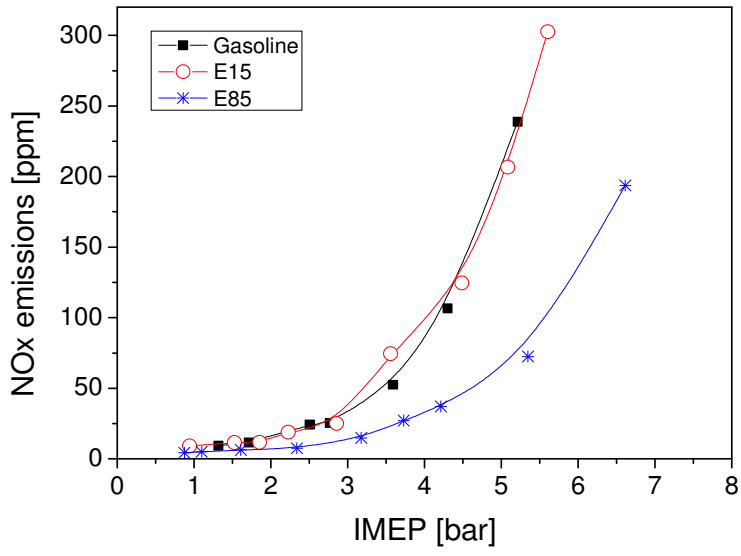

Figure 7.6 NOx Emissions in Two-stroke CAI Operation at 2000rpm

7.3 Ethanol Content Effects on Two-stroke CAI Operating Range

The load-speed operating range of two-stroke pure CAI of gasoline, E15 and E85 was investigated when the exhaust lambda was set to 1.0. The operating ranges of CAI combustion are shown in Figure 7.7. The engine speed was varied from 800rpm to 3000rpm, and the load was varied from the minimum to the maximum by adjusting the intake pressure. With the same valve timings, by increasing the intake pressure, more fresh air is inducted and more exhaust gases are displaced, resulting higher power output. The pure CAI operation is defined as operational conditions where spark ignition doesn't have any effect on the combustion phase. At low load operation, the boost pressure was lower, less exhaust gas was scavenged. The very high residual gas fraction led to unstable combustion and misfire, which limited the operation range at low load boundary. It is noted that at low speed, the more ethanol was blended in the gasoline, the more difficult the mixture could get auto ignited due to the low mixture temperature caused by the charge cooling effect of ethanol injection. Therefore, the low load boundary of E85 occurred at higher IMEP values than that of gasoline and E15 at 800rpm. When the engine speed increased, the difference in the low load CAI limits between gasoline and its mixture with ethanol disappeared because of the reduced heat loss and higher thermal loading at higher engine speeds.

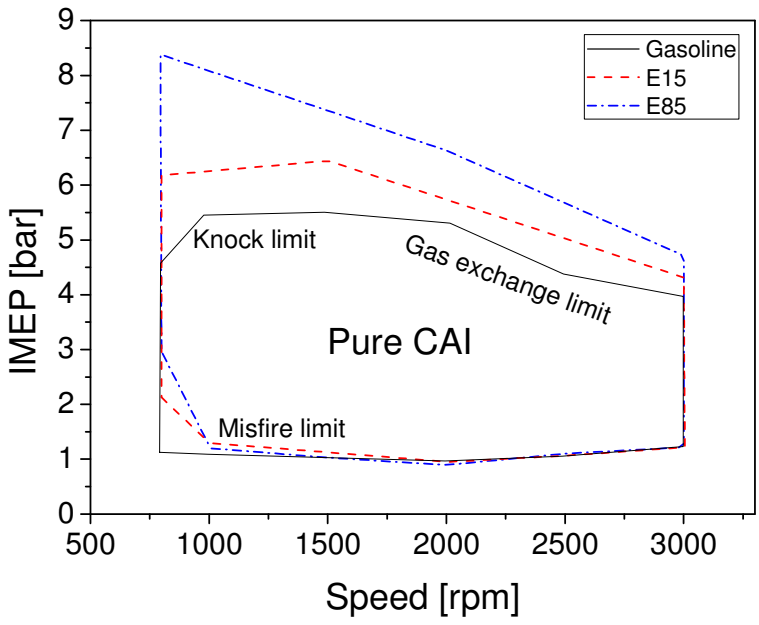

Figure 7.7 Operating Range of Two-stroke CAI Fuelled with Gasoline, E15 and E85

At 1000 rpm, when IMEP was over 5.3bar, combustion became very rapid and the rate of pressure rise exceeded the pre-defined knock limit of 5bar/CA. This is because the combustion process was accelerated due to the higher in-cylinder temperature and less dilution of the residual gases at higher load conditions, as shown in Figure 7.8. It can be seen that the knock limit was extended by 0.7bar to 6.2 bar IMEP when blending 15% ethanol in gasoline. E85 further extended the load range by 3bar to 8.5 bar IMEP. This is a result of slower heat release rate of ethanol than gasoline, as shown in Figure 7.9. In the case of gasoline, the upper load boundary moved up slightly as the engine speed was changed from 800rpm to 1000rpm, as to be explained later.

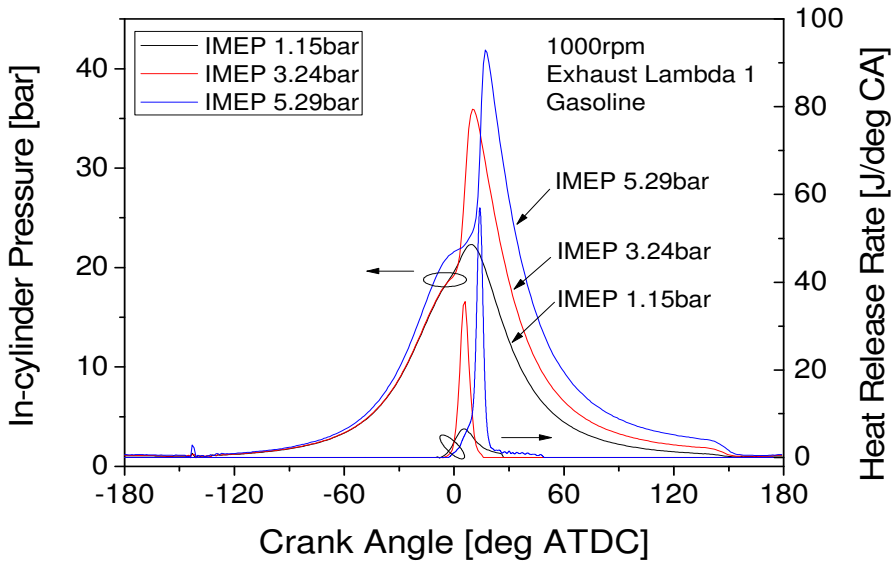

Figure 7.8 In-cylinder Pressure and Heat Release Rate at 1000rpm and Different Loads

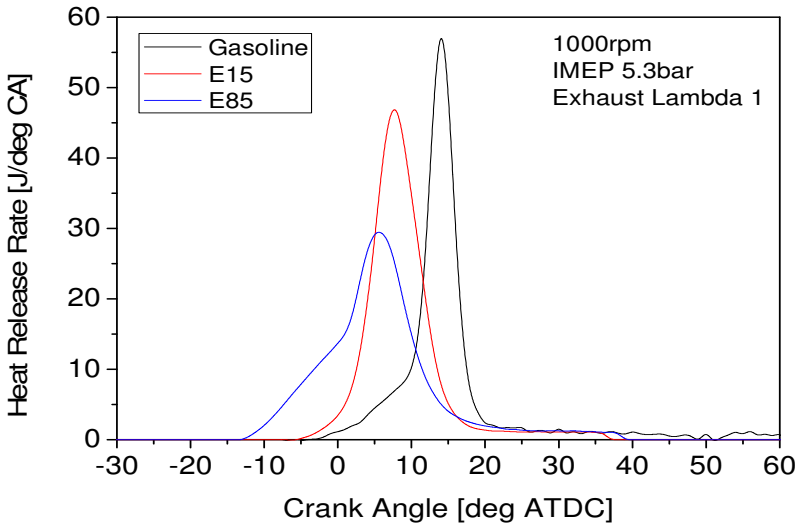

Figure 7.9 Heat Release Rate of Gasoline, E15 and E85 at 1000rpm and 5.3bar IMEP

For all three fuels, it is noted that the upper load limits would fall with the engine speed. For gasoline and E15, this occurred at 2000rpm and 1500rpm respectively, whilst E85 fuel exhibited continued decrease in the upper load limit of CAI operation with the engine speed. This can be explained by the flow characteristics of the camless valve actuation system. Because the valves were operated independently from the engine's own rotation by the electro-hydraulic actuation, for a given intake and exhaust valve profile, the valve opening durations remained constant in mille-seconds but they became less in terms of crank angles as the engine speed increased. In addition, due to the finite opening and closing speeds of the electro-hydraulic valves, the valves could not reach their maximum lift at 1500rpm and above in the two-stroke mode. Although the valve durations were increased at higher engine speed operations to compensate for the reduction in the air flow rate caused by the reduced valve lift as shown in Figure 5.2, it is still not sufficient for the high load operation. This resulted in the gas exchange limit at higher speeds on the CAI operating range. Because ethanol has a lower stoichiometric air fuel ratio than gasoline, the addition of ethanol reduced the amount of air required for combustion and hence could produce more output for the same amount of air trapped in the cylinder than gasoline. This is illustrated by the air flow rate values for gasoline (Figure 7.10a), E15 (Figure 7.10b), and E85 (Figure 7.10c). Therefore, at 3000rpm, E15 extended the gas exchange limit by half bar IMEP and E85 1.5bar IMEP, compared with gasoline CAI operating range.

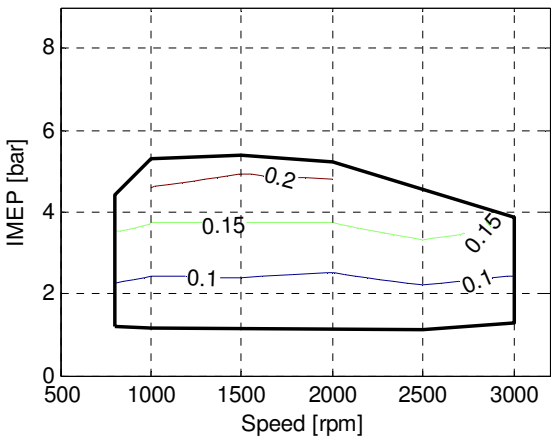

a) Gasoline

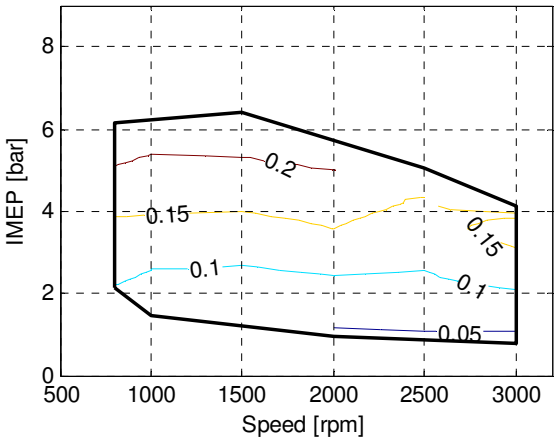

b) E15

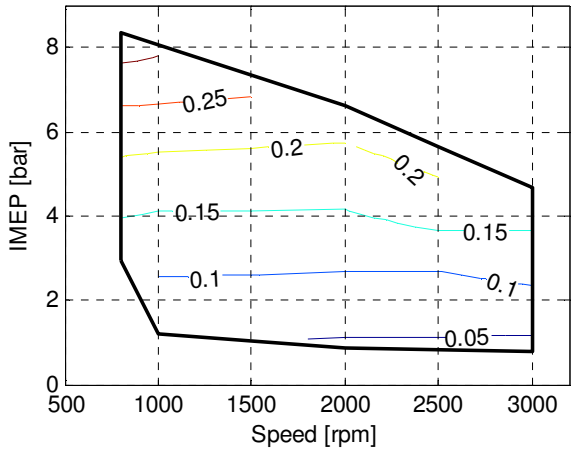

c) E85

Figure 7.10 Air Flow Rate [g/cycle] over Two-stroke CAI Operating Range

7.4 Ethanol Content Effects on Efficiencies of Two-stroke CAI Operation

In order to compare the fuel economy and take into account of the different calorific values of gasoline and ethanol, combustion efficiency, thermodynamic efficiency and indicated fuel conversion efficiency are calculated and analysed for gasoline and its blends with ethanol.

Figure 7.11 shows their combustion efficiency values in the two-stroke CAI operation at 2000rpm. It can be seen that the combustion efficiency is relatively low on this engine due to the rich air/fuel mixture in the cylinder caused by the short-circuiting of the air and non-optimized injection system, as mentioned above. However, compared with gasoline, the combustion efficiency was improved by 3-5% by blending 15% ethanol in the gasoline. Further increasing ethanol concentration to 85% in the fuel could further improve the combustion efficiency at high load operation, but at low load operation the low temperature of the mixture caused by the higher latent heat value of ethanol led to lower combustion efficiency. This is also reflected by the higher CO emissions of E85 at low load shown in Figure 7.5.

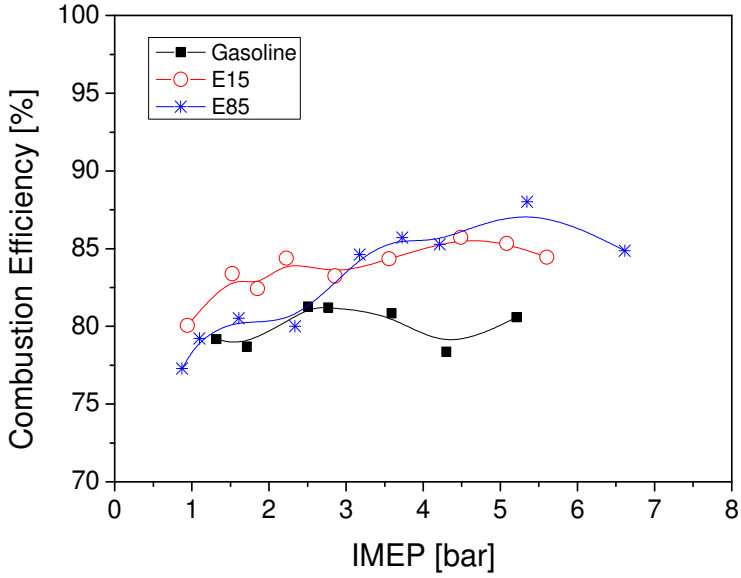

Figure 7.11 Combustion Efficiency in Two-stroke CAI Operation at 2000rpm

The best thermodynamic efficiency was obtained with E85 at high load operation, shown in Figure 7.12. This was the result of optimised combustion phasing as shown in Figure 7.1 and reduced heat loss during the combustion process because of the lower charge and combustion temperature of ethanol. The presence of ethanol had little effect at low load operations.

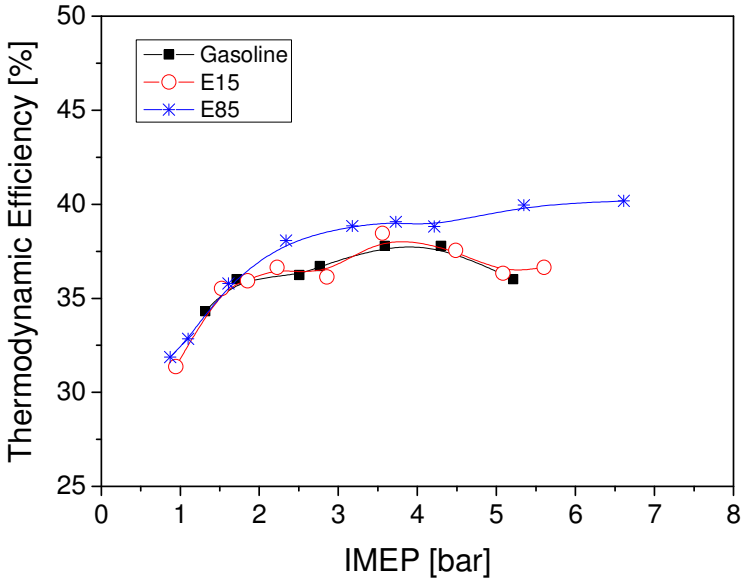

Figure 7.12 Thermodynamic Efficiency in Two-stroke CAI Operation at 2000rpm

Figure 7.13 shows the combined effect of combustion efficiency and thermal efficiency, as measured by the indicated fuel conversion efficiency. At 5bar IMEP and 2000rpm, the indicated efficiency can be improved by 5% with E85 and 2% with E15.

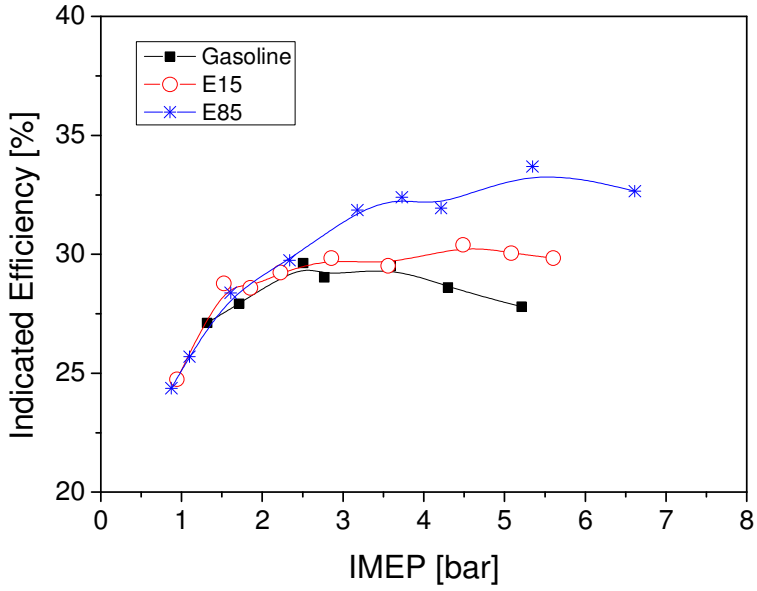

Figure 7.13 Indicated Fuel Conversion Efficiency in Two-stroke CAI Operation at 2000rpm

7.5 Summary

In this Chapter, CAI combustion of gasoline with ethanol was suited over a wide range of speed and load when the exhaust lambda was set to 1.0. Their combustion and heat release characteristics, emissions, and their combustion and thermodynamic efficiencies were determined and analysed. The results show that

(i) The presence of ethanol allowed CAI combustion to be extended to higher load conditions. In the case of E85 the maximum IMEP of 8.4bar was obtained at 800rpm. Further improvement in the high load range at higher engine speeds can be achieved with a faster camless system or mechanical camshafts.

(ii) CO, uHC and NOx emissions are significantly reduced by injecting ethanol blended fuels. E85 has greater effect on the emission reduction than E15.

(iii) Both combustion efficiency and thermodynamic efficiency are improved by the presence of ethanol because of the optimum combustion phasing and lower heat loss. E85 improved indicated fuel conversion efficiency by over 5% at 2000rpm.

Chapter 8

Lean Boost CAI Operation

Chapter 8 Lean Boost CAI Operation

8.1 Introduction

One of the key issues associated with the two-stroke cycle is the short-circuiting phenomenon, in which some of the intake air or air fuel mixture can flow directly into the exhaust port during the scavenging process [95]. Although the fuel short-circuiting issue can be solved by direct fuel injection into the cylinder, the air short-circuiting cannot be completely eliminated. The short-circuited air can skew the reading of the lambda sensor in the exhaust pipe, resulting in an enriched in-cylinder air and fuel mixture. In order to correct for the over-rich mixture combustion, further engine experiments were conducted without the constraint of constant lambda value measured in the engine exhaust.

In this Chapter, the engine performance, combustion and emission characteristics with the lean boost strategy will be presented and analysed. The effect of valve timing on residual gas fraction, in-cylinder lambda, effective expansion ratio, and effective compression ratio is discussed. The effect of ethanol content on CAI combustion is given. Significant improvements in combustion efficiency and fuel conversion efficiency as well as large reductions in CO and uHC emissions are achieved by lean boost and optimised valve timings.

8.2 Intake Pressure Effects on In-cylinder Lambda and Trapping Efficiency

In order to achieve the two-stroke cycle operation, compressed air is required to achieve the scavenging process during the valve overlap period. Figure 8.1 shows the intake pressure values for exhaust lambda 1 and lean boost CAI operations as well as their operational range. At each engine speed the engine load was varied from low to high by increasing the intake pressure and hence the scavenging rate in the two-stroke engine operation. The two-stroke CAI combustion was achieved over the engine speed range from 800 rpm to 3000rpm. The CAI combustion is enveloped by 3 limits, (i) the knock limit on the low speed high load boundary on the top left region, (ii) the gas exchange limit on the high speed and high load boundary in the top right region, and (iii) the misfire limit on the low load boundary at the bottom. The knock limit is defined by the

threshold of the in-cylinder pressure rise rate. According to [92], the maximum rate of pressure rise dP/dCA was limited to 5bar/CA in order for the engine to operate with similar noise levels to the production gasoline engine. The misfire limit is defined by the operation condition when the engine operation became intermittent due to large number of misfiring cycles. It should be pointed out that the maximum IMEP on this two-stroke engine with CAI operation is 7.8bar at 1500rpm, which is equivalent to 15.6 bar IMEP on the four-stroke engine.

Because the valves were operated independently from the engine's own rotation by the electro-hydraulic actuation, for a given intake and exhaust valve profiles, the opening durations remained constant in milliseconds but the number of crank angles became less as the engine speed increased. In addition, due to the finite opening and closing speeds of the electro-hydraulic valves, the valves could not reach their maximum lift at 1500rpm and above in the two-stroke mode. Although the valve durations were increased at higher engine speed operations to compensate for the reduction in the air flow rate caused by the reduced valve lift, it is still not sufficient for the high load operation. This is the main cause to the presence of the gas exchange limit formed on the operating range envelop.

The engine load was regulated by the intake pressure in both the exhaust lambda 1 mode and lean boost mode. The boost pressure in the lean boost mode was selected at each operating point to give the minimum indicated fuel consumption. As Figure 8.1 shows, higher intake pressure was required in the lean boost mode in order to allow more exhaust gas to be scavenged. In addition, the difference in intake pressures between the exhaust lambda 1 mode and lean boost operation becomes more pronounced at higher load. For example, the intake pressure difference at 1000rpm 2bar IMEP was about 0.25bar and it increased to 0.77bar at 7bar IMEP. This can be understood by considering the results shown in Figure 8.2, which shows the effect of boost pressure on the scavenging efficiency, residual gas fraction, and in-cylinder and exhaust Lambda values during the lean boost operations at 1000rpm. It can be seen that higher boost reduced the residual gas fraction and hence resulted in better scavenging process. But the improvement in the scavenging process was achieved at the expense of reduced trapping efficiency and higher air short-circuiting rates. As a result, the lambda measured in the exhaust increased from 1.08 to 1.7 whilst the lambda in the cylinder remained at slightly richer than 1 when the intake pressure was increased from 1.2 bar to 2.2 bar.

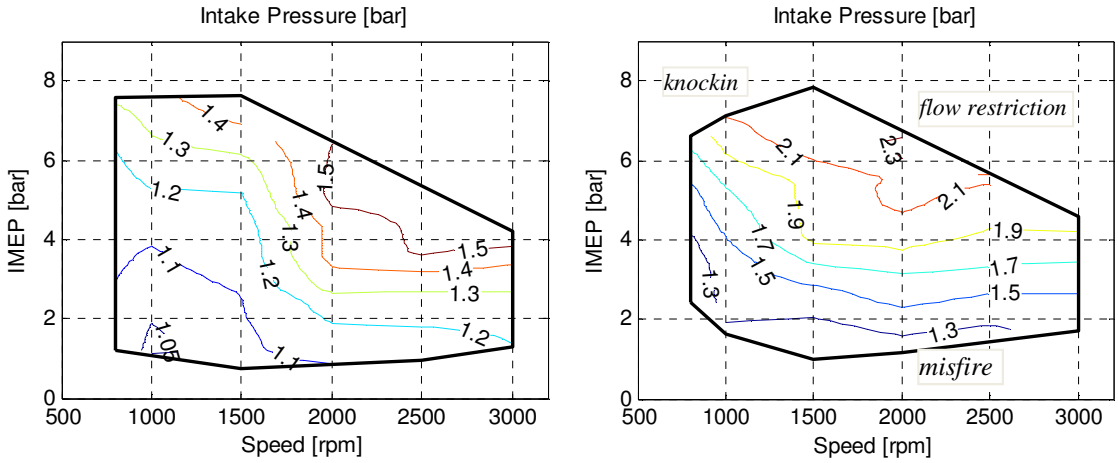

a) Exhaust lambda 1 **b) Lean boost**

Figure 8.1 CAI Operating Range and Intake Pressure Contours

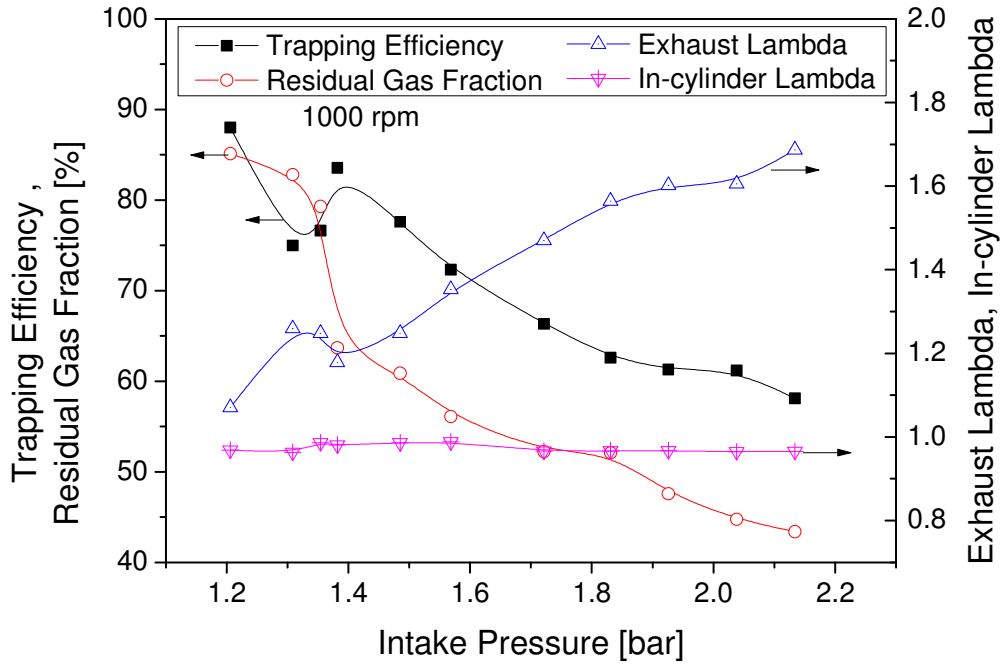

Figure 8.2 Effect of Intake Pressure on the Scavenging Process with Lean Boost at 1000rpm

Since the boost pressure was adjusted for best fuel conversion efficiency at each operating point, the in-cylinder lambda values were not directly controlled but determined by the boost pressure and the trapping efficiency. It can be seen in Figure 8.3 that the in-cylinder lambda values throughout the operating range were all close to one whilst the exhaust lambda value increased with load due to higher air short-circuiting

rates. In addition, it is noted that the best fuel conversion efficiency at the low speed and low load region was obtained with slightly fuel rich mixtures, which provided better ignitibility and faster combustion speed in order to maintain combustion stability and reduce the cycle to cycle variation. At higher load operations, combustion noise became the major issue due to earlier and faster heat release rate. In order to retard the combustion phase and reduce the combustion speed, the in-cylinder lambda was set slightly greater than 1 as a trade-off between the thermodynamic efficiency and combustion noise.

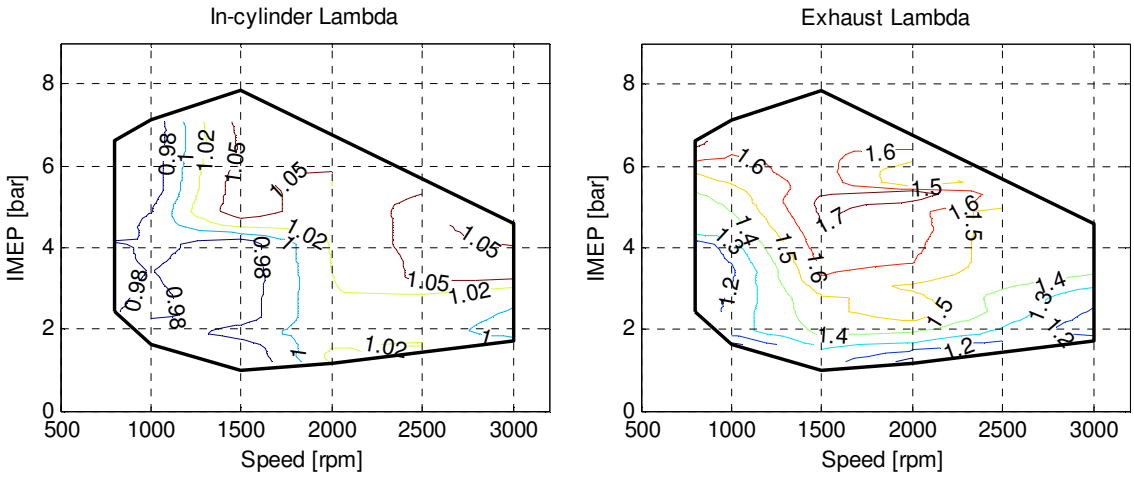

a) In-cylinder lambda **b) Exhaust lambda**

Figure 8.3 In-cylinder Lambda and Exhaust Lambda Values of Lean Boost Operations

8.3 The Effects of Valve Timing on Two-stroke Lean Boost CAI

The initial and boundary conditions of CAI combustion are determined by the gas exchange process and subsequent mixing process in the compression stroke in the two-stroke engine. Apart from pressure difference between engine inlet and exhaust ports, valve timings also strongly affect the gas exchange process. In order to understand the how the initial and boundary conditions affect CAI combustion, the effects of valve timing were investigated at three typical operating conditions: IMEP=2.2bar at low load boundary of CAI, IMEP=5.0bar at middle load condition of pure CAI, IMEP=7.8bar at high load boundary of spark-assisted CAI. The other engine operating parameters are given in Table 8.1. It can be seen in this table that the exhaust lambda increased with load due to the air short-circuiting issue explained previously. At high load, the valve timing

variable range is smaller than that at low load because valve timings have more impact on gas exchange process at higher intake pressure and the CAI combustion is more sensitive to lambda, where lowering lambda would cause knocking combustion and higher lambda would lead to misfire.

Table 8.1 Operating Parameters for Valve Timing Effect Tests

Speed	IMEP	Intake Pressure	Exhaust Lambda	Spark Timing	IVO	IVC	EVO	EVC
rpm	bar	bar		deg CA ATDC				
1500	2.2	1.2	0.96 ~ 1.16	N/A	157 ~ 171	-148	140	-176
			1.02 ~ 1.16		161	-154 ~ -143	140	-176
			0.99 ~ 1.14		161	-148	132 ~ 145	-176
			0.95 ~ 1.15		161	-148	140	-185 ~ -171
	5	1.4	1.17 ~ 1.24	N/A	150 ~ 161	-145	140	-172
			1.16 ~ 1.19		161	-154 ~ -132	140	-172
			1.17 ~ 1.28		161	-145	142 ~ 138	-172
			1.19 ~ 1.36		161	-145	140	-172 ~ -169
	7.8	1.8	1.48 ~ 1.51	-13	161 ~ 164	-136	140	-163
			1.50 ~ 1.54	-15	161	-136 ~ -131	140	-163
			1.47 ~ 1.60	-19 ~ -10	161	-136	144 ~ 138	-163
			1.51 ~ 1.70	-22 ~ -15	161	-136	140	-163 ~ -158

8.3.1 Effect of EVO

As the gas exchange process begins at the exhaust valve opening (EVO), the effect of EVO was firstly investigated. During the two-stroke operation, the exhaust valve opens towards the end of the expansion stroke before BDC. Therefore, the effective expansion ratio of the burnt gas in the cylinder is shorter than the engine geometric expansion ratio.

As shown in Figure 8.4a, the cylinder pressure started dropping when exhaust valves opened. The earlier the exhaust valves opened, the smaller the expansion work due to the pressure drop after EVO. Figure 8.4b shows the relationship between the effective expansion ratio (EER) and EVO, when EVO was varied from 132 deg ATDC to 145 deg ATDC.

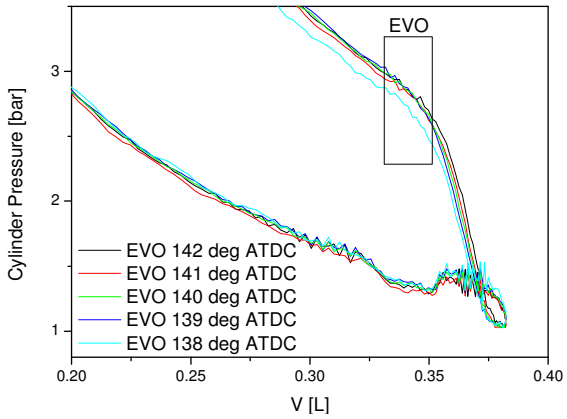

a) P-V Diagram

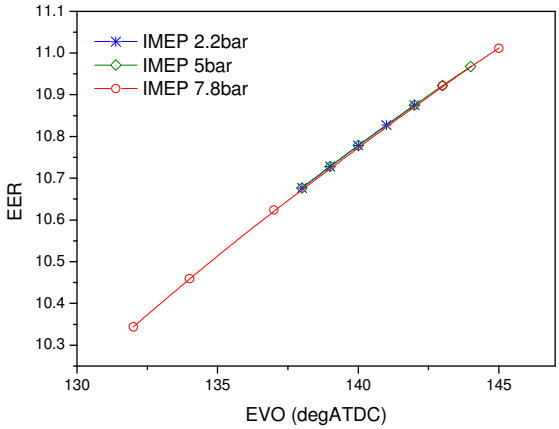

b) Effective Expansion Ratio

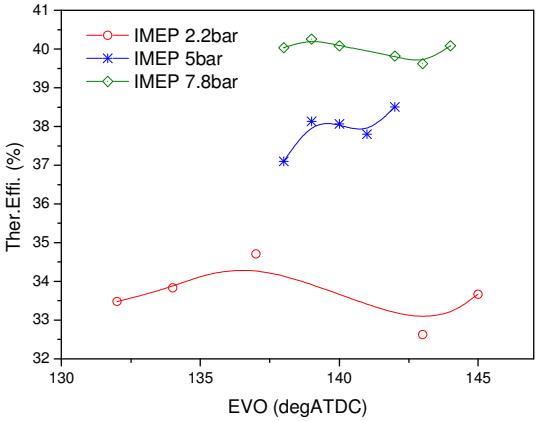

c) Thermodynamic Efficiency

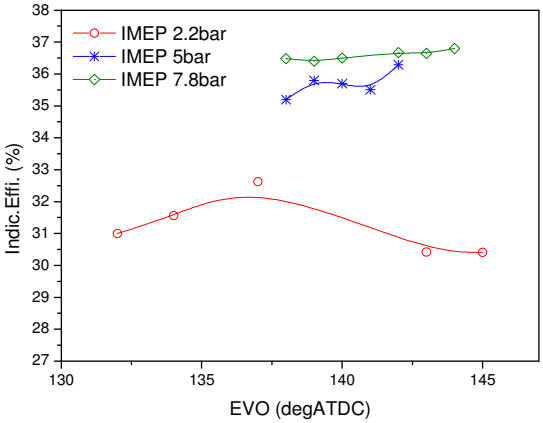

d) Indicated Efficiency

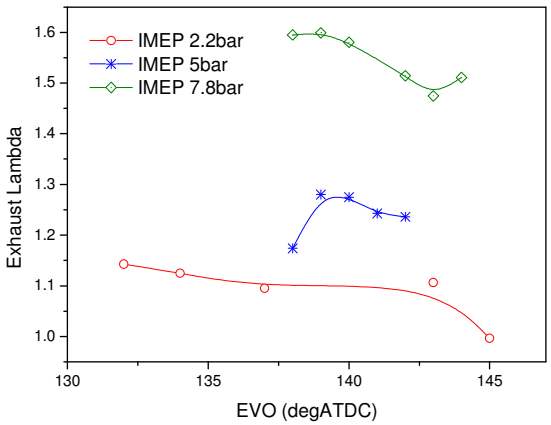

e) Exhaust Lambda

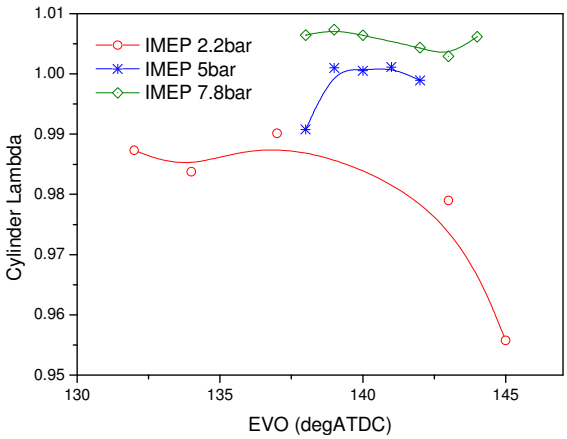

f) In-cylinder Lambda

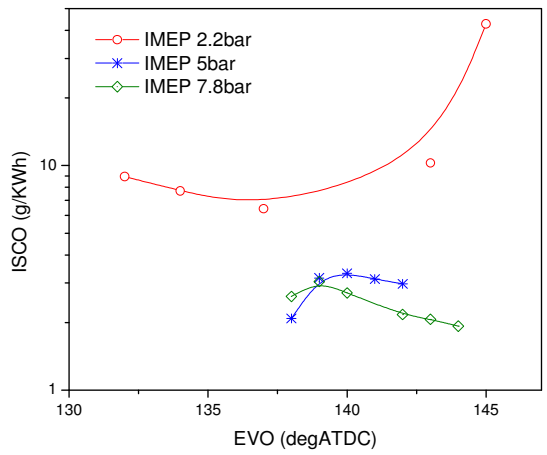

g) Indicated Specific CO emission

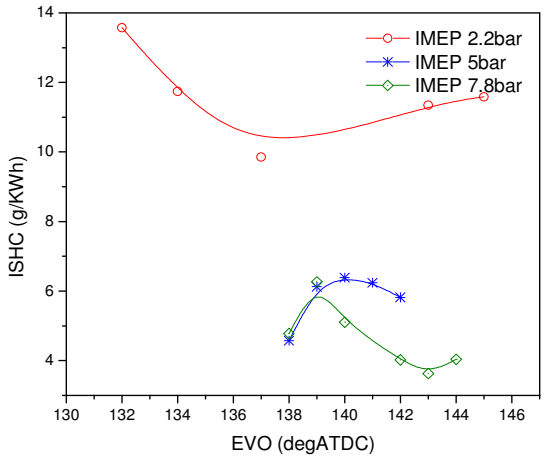

h) Indicated Specific HC emission

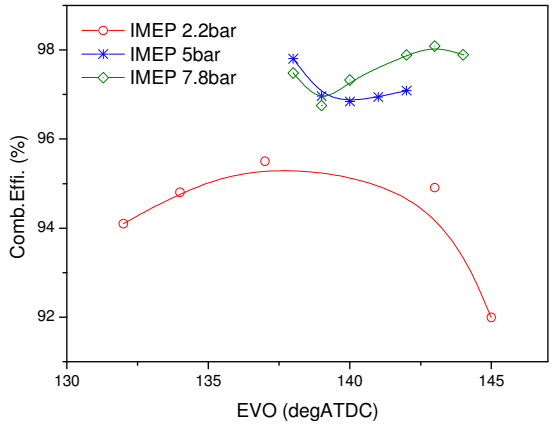

i) Combustion Efficiency

Figure 8.4 Effect of EVO at 1500rpm

In theory, the thermodynamic and engine indicated efficiency would be expected higher at higher EER. As shown in Figure 8.4c and 8.4d, both efficiencies varied little at the higher load of 7.8bar IMEP and they increased slightly at middle load of 5bar IMEP when the EVO was retarded. However, at the lower load of 2.2bar IMEP, the thermodynamic and indicated efficiencies rose initially with retarded EVO but started decreasing when the EVO was retarded beyond 138 deg CA ATDC. This is a result of richer mixture and incomplete combustion in the cylinder, as shown in Figure 8.4e and 8.4f. When EVO was retarded beyond 138 deg CA ATDC, the lambda reduced rapidly due to the too short exhaust valve opening duration which restricted intake air flow. As a result, the CO and HC emissions increased and the combustion efficiency was reduced as shown in Figures 8.4g, 8.4h and 8.4i, respectively.

8.3.2 Effect of IVO

In the two-stroke cycle, the scavenging process relies on the displacement of exhaust gas by the intake air once the intake valves are open. Therefore, the effect of intake valve opening on the gas exchange process was investigated.

The intake valve opening firstly affected the residual gas fraction, of which the measurement method was described in Chapter 4. As shown in Figure 8.5a, the residual gas fraction was reduced with more advanced intake valve open as the intake process became longer. In addition, it is noted that the slopes of the curve are different at the three conditions. At 2.2 bar IMEP when the boost pressure was lowest, a reduction in RGF by 3% was accomplished when the inlet valves was advanced by 15 degree CAs. At 7.8bar IMEP, the 3% reduction in RGF was achieved by opening the inlet valve 5 degree CAs earlier. At 5bar IMEP, the RGF rose rapidly when IVO was retarded beyond 160 deg ATDC, because the intake air flow was seriously restricted because of very short intake valve opening duration. As shown in Figure 8.5b, the IVO has stronger effect on air short-circuiting rate at low loads than high loads. If the gas exchange process in the two-stroke operation can be considered as a mixed scavenging process of fresh air mixing with burnt gas and fresh air displacing burnt gas, it can be seen that more fresh air is mixed with burnt gas at high load than low load because of the high flow rate at higher boosting pressure. The effect of IVO on air short-circuiting rates is reflected in the difference between lambda values in the cylinder and exhaust, as shown in Figure 8.5c &d.

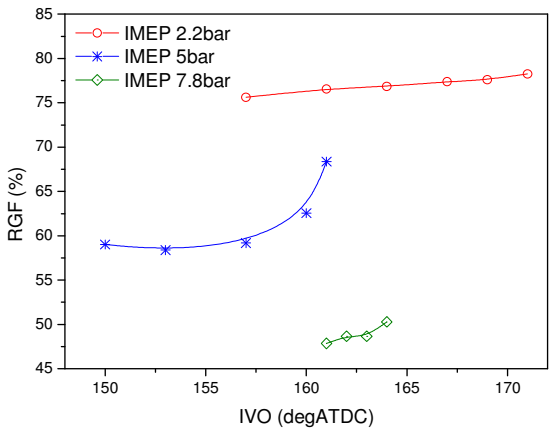

a) Residual Gas Fraction (RGF)

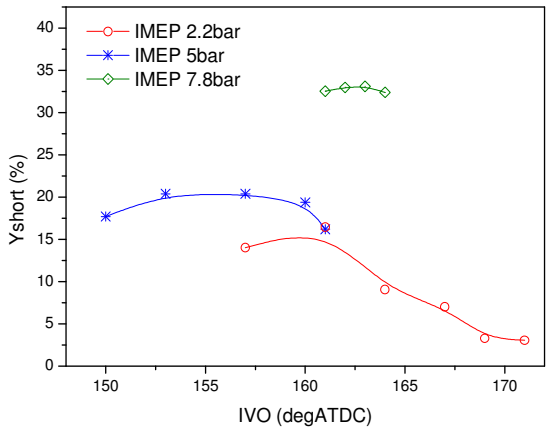

b) Air Short-circuiting Rate (Yshort)

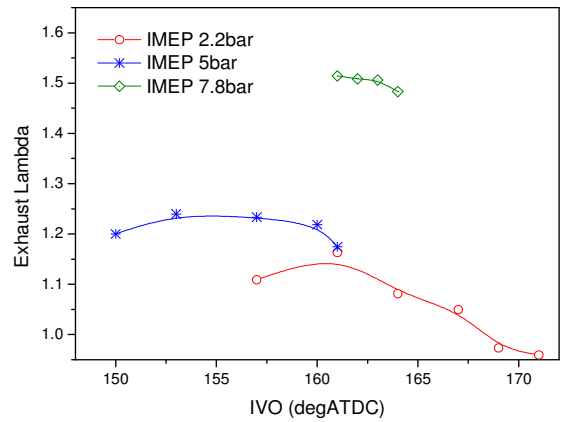

c) Exhaust Lambda

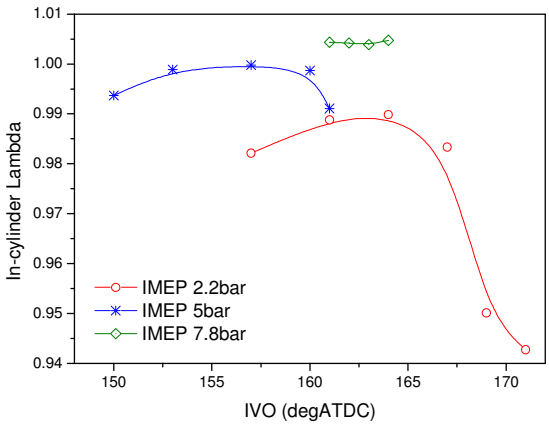

d) In-cylinder Lambda

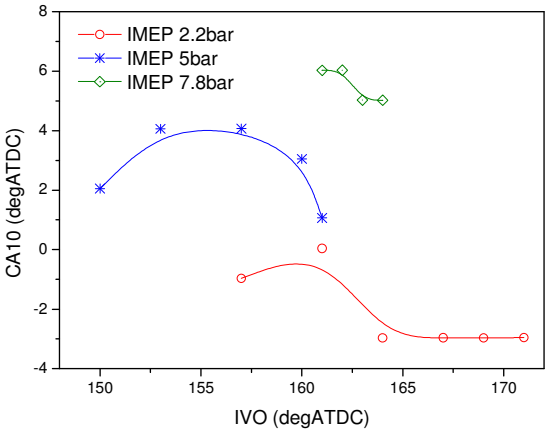

e) Crank Angle at 10% MFB (CA10)

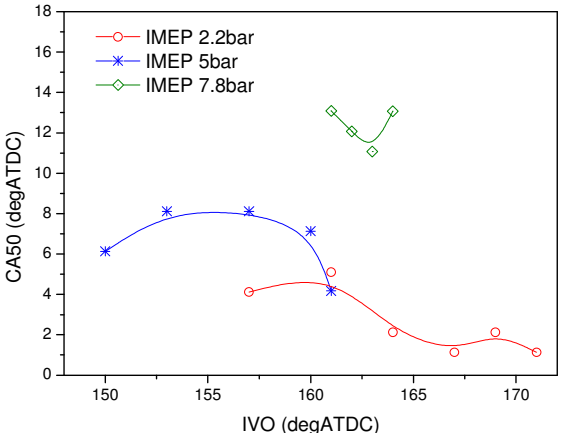

f) Crank Angle at 50% MFB (CA50)

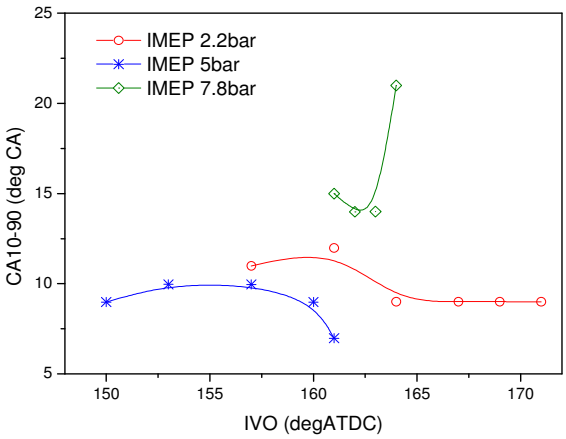

g) Crank Angle from 10% to 90% MFB (CA10-90)

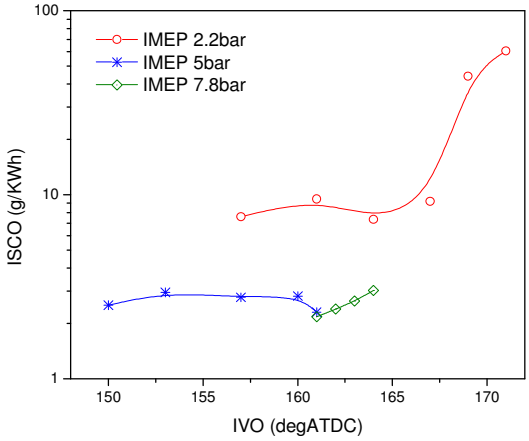

h) Indicated Specific CO (ISCO)

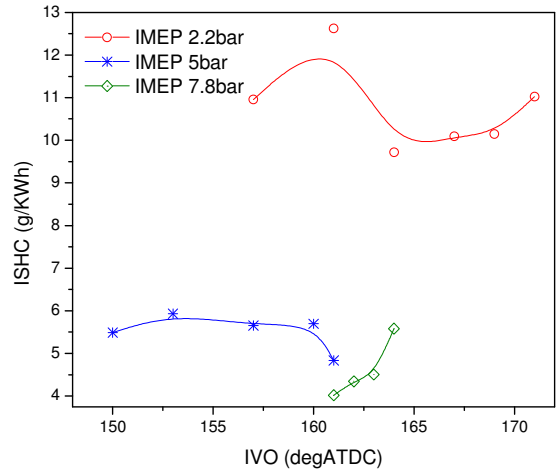

i) Indicated Specific HC (ISHC)

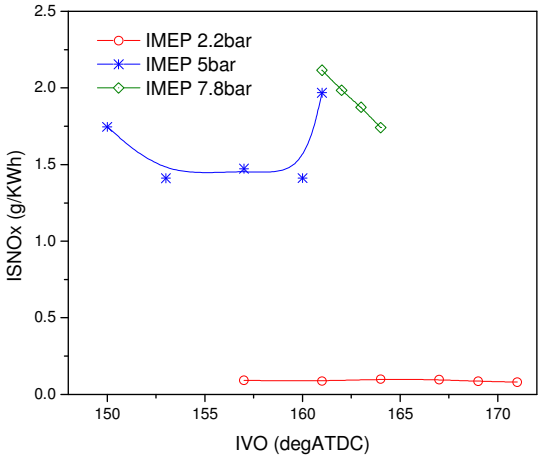

j) Indicated Specific NOx (ISNOx)

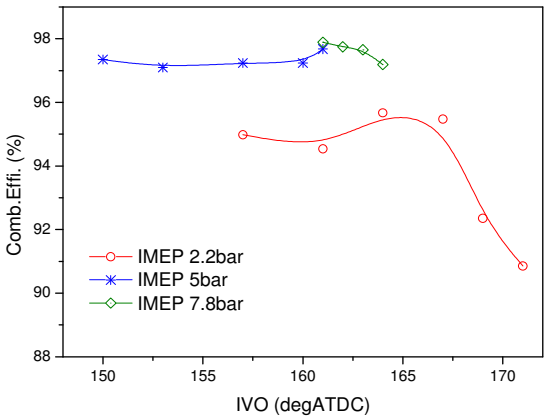

k) Combustion Efficiency

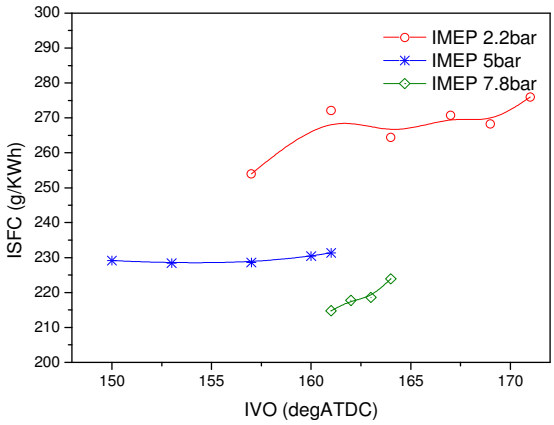

l) Indicated Specific Fuel Consumption

Figure 8.5 Effect of IVO at 1500rpm

As a result of the change in the air/fuel ratio and RGF in the cylinder, the start of combustion (CA10), the combustion phasing (CA50), and combustion duration were all affected by the IVO, as shown in Figure 8.5.e, 8.5f and 8.5g respectively. The start of auto ignition and combustion phase took place earlier at middle and low load conditions when the IO was advanced. At high load, as there was not enough residual gas to initiate CAI combustion, spark-assisted CAI combustion were implemented. The advance of CA10 was caused by advancing spark timing at higher RGF. At the highest RGF condition at 7.8bar IMEP, CA50 started retarding and CA10-90 became much longer, although its CA10 was advanced already, reflecting much deteriorated combustion process and probably flame quenching before the establishment of auto ignition temperature.

As shown in Figure 8.5h and 8.5k, at the lower load both CO emission and combustion inefficiency increased rapidly as the combustible mixture became fuel rich with the most advanced IVO. In addition, Figure 8.5h-j shows that at the higher load operation, both CO and HC emissions increased but NOx decreased as the IVO was advanced slightly, which could be caused by the lower charge temperature in the cylinder as more fresh air mixed with residual gas. At the middle load of 5 bar IMEP when CAI was stable, the effect of IVO was negligible other than at the two extreme IVOs.

8.3.3 Effect of EVC

Exhaust valve closure is also a critical control parameter for two-stroke scavenging process, as it determines how much residual gas is trapped in the cylinder. Thus, further experiments were carried out for a fixed EVO, IVO and IVC. As shown in Figure 8.6a and 8.6b, the residual gas fraction was reduced and air short-circuiting rate was increased with delayed EVC, because of longer exhaust valve opening duration. Compared with Figure 8.5a and 8.5b, the effect of EVC was greater than that of IVO because of the fact that most of air short-circuiting occurred in the last period of scavenging process. Delayed exhaust valve closure allowed more refresh air passing through the cylinder into the exhaust port without affecting the in-cylinder lambda, which was particularly noticeable at middle and high loads as shown in Figure 8.6c and 8.6d.

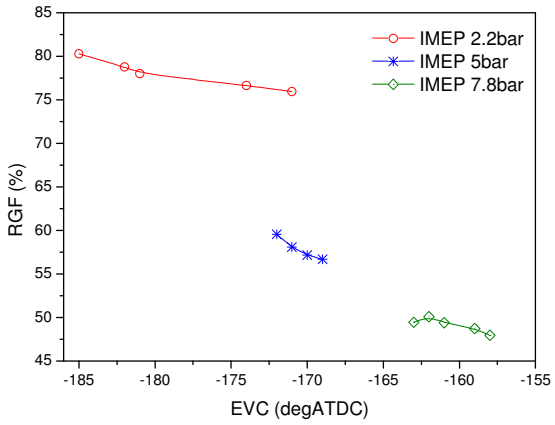

a) Residual Gas Fraction (RGF)

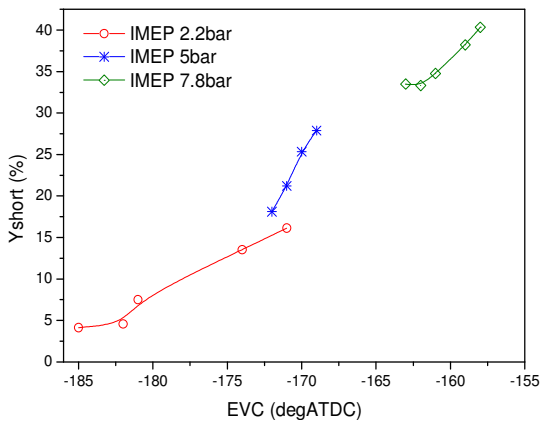

b) Air Short-circuiting Rate (Yshort)

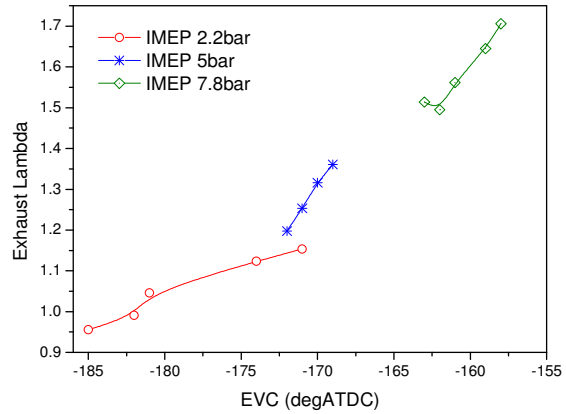

c) Exhaust Lambda

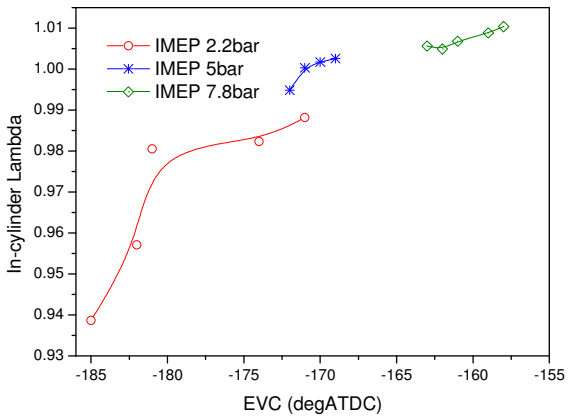

d) In-cylinder Lambda

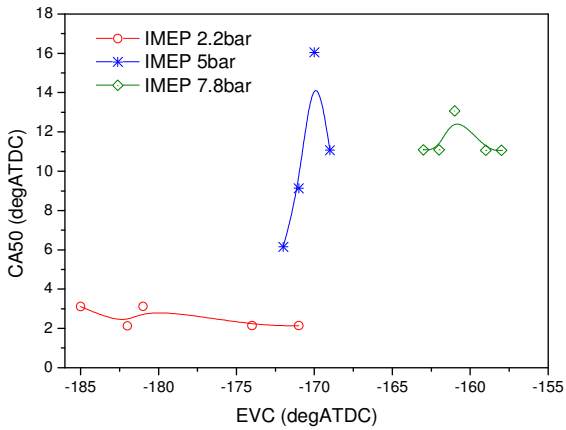

e) Crank Angle at 10% MFB (CA10)

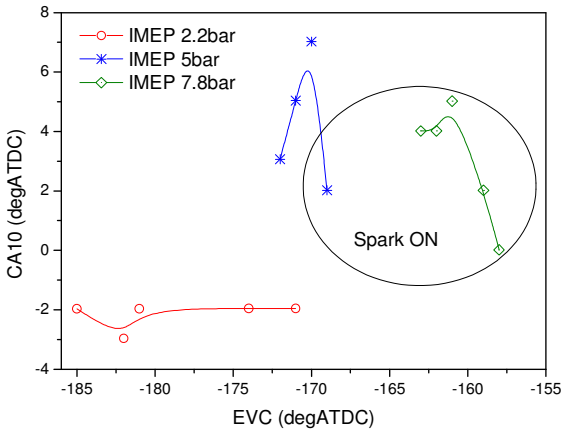

f) Crank Angle at 50% MFB (CA50)

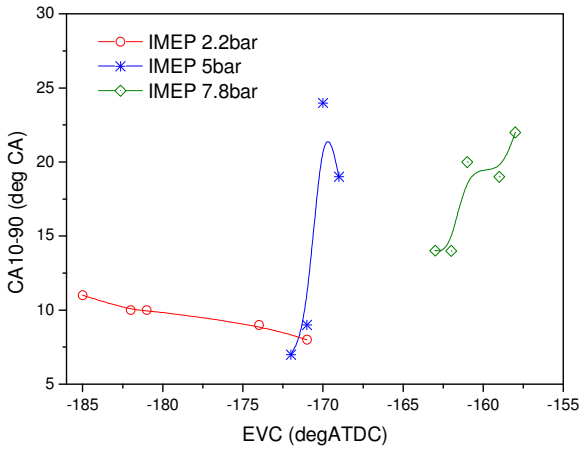

g) Crank Angle from 10% to 90% MFB (CA10-90)

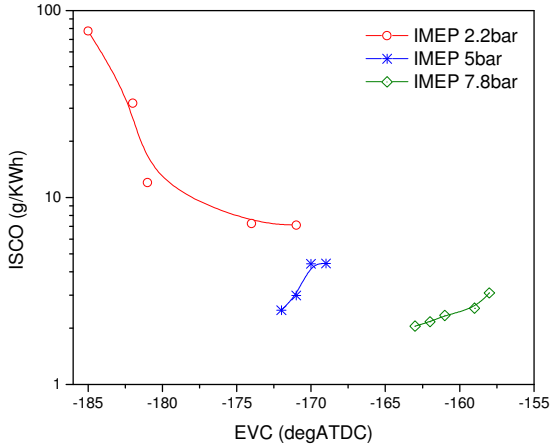

h) Indicated Specific CO (ISCO)

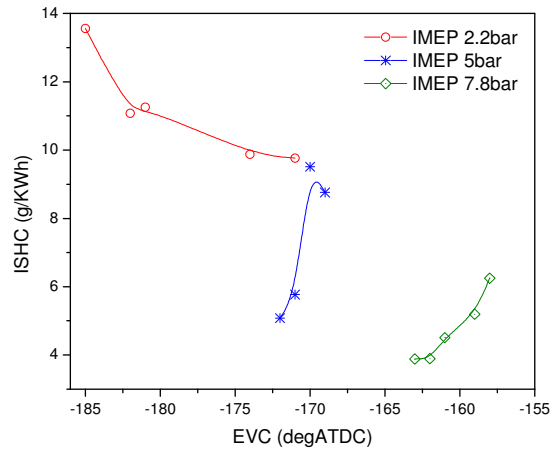

i) Indicated Specific HC (ISHC)

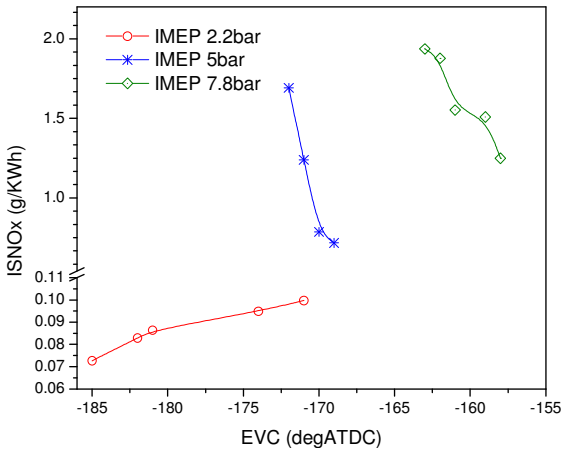

j) Indicated Specific NOx (ISNOx)

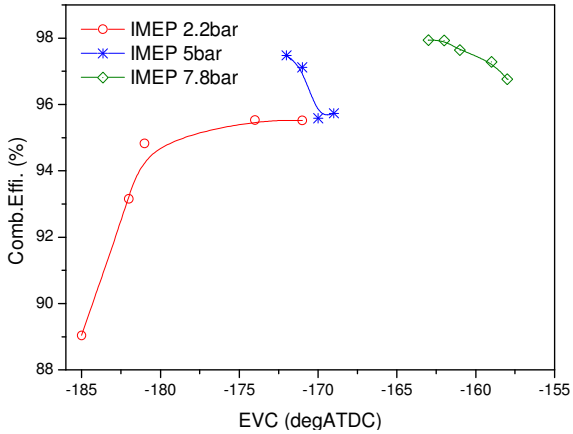

k) Combustion Efficiency

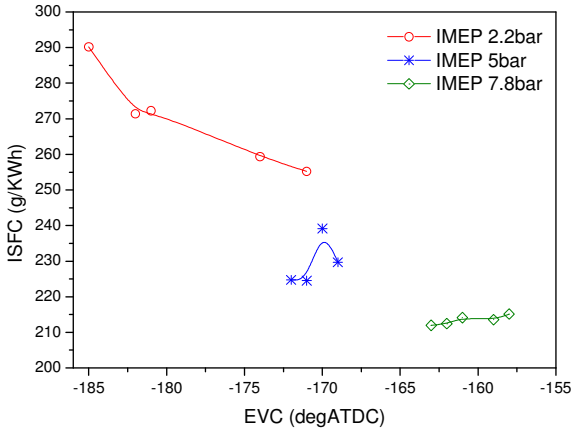

l) Indicated Specific Fuel Consumption

Figure 8.6 Effect of EVC at 1500rpm

As shown in Figure 8.6e to 8.6f, CA10 and CA50 were delayed with extended exhaust opening duration because of the higher air short-circuiting rate and associated cooling effect. In order to compensate for delayed combustion by intake air charge cooling at higher load operations, spark ignition was applied at an advanced timing. The emission results show that both CO and HC emissions were reduced with longer exhaust opening period at low loads when in-cylinder mixture became leaner. However, at middle and high loads, CO and HC emissions were higher at higher air short-circuiting rate conditions because of the lower in-cylinder temperature, which led to the significant reduction in NOx emissions, as shown in Figure 8.6j. As a result, combustion efficiency increased due to leaner mixture at low loads but decreased because of lower charge temperature at high load conditions, as shown in Figure 8.6k. As long as the in-cylinder lambda was not less than 1.0, the combustion efficiency remained higher than 95%.

Figure 7.3.3l shows that at low loads the fuel consumption was mainly determined by in-cylinder lambda. At middle and high loads, the exhaust valve should be closed earlier to minimize air short-circuiting and reduce fuel consumption.

8.3.4 Effect of IVC

The final valve timing examined was the intake valve closure while EVO, EVC and IVO were fixed. Figure 8.7a shows how the effective compression ratio (ECR) was reduced from 11.35 to 10.27 when IVC was retarded from -154 deg ATDC to -131 deg ATDC on this engine. As ECR directly affects the charge temperature history in the compression stroke, the combustion phase and combustion duration were altered. Fig.8.7b and 8.7c show that CA50 was retarded and CA10-90 extended with lower ECR. Lower ECR also made combustion less violent, as evidence by the maximum pressure rise rate in Figure 8.7d.

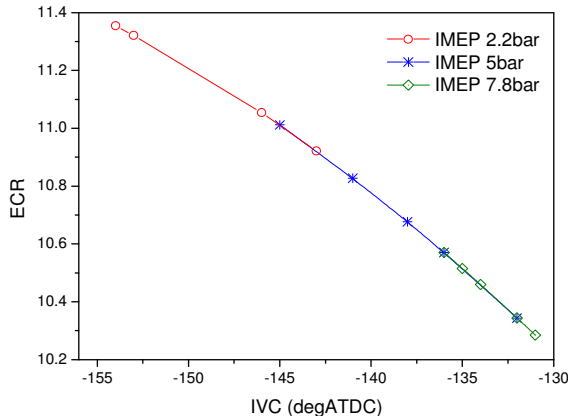

a) Effective compression ratio (ECR)

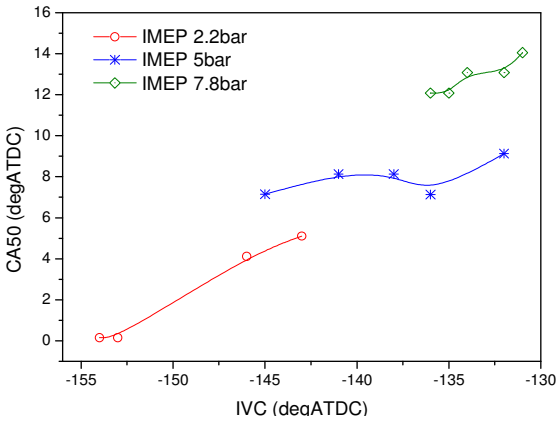

b) Crank Angle at 50% MFB (CA50)

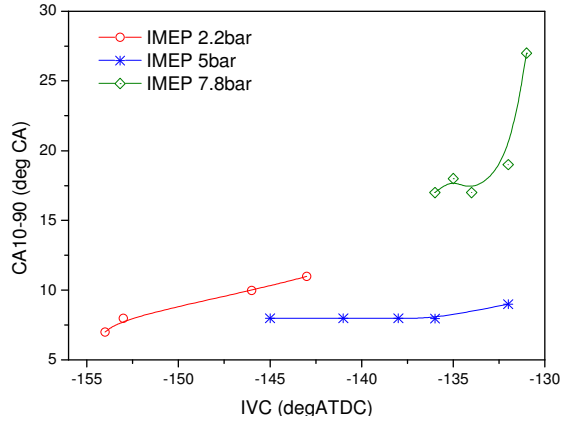

c) Crank Angle from 10% to 90% MFB (CA10-90)

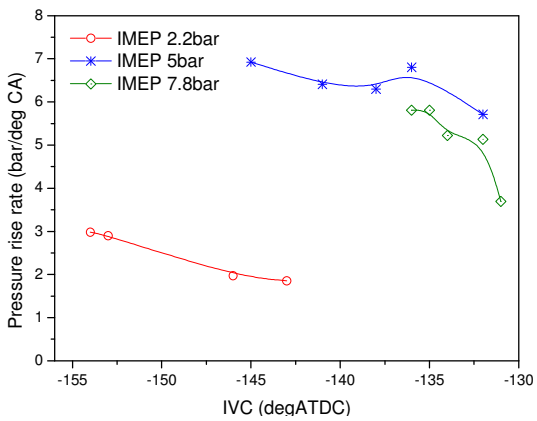

d) Pressure Rise Rate

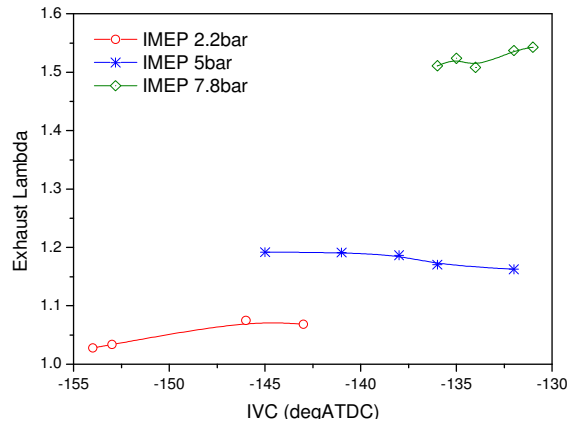

e) Exhaust Lambda

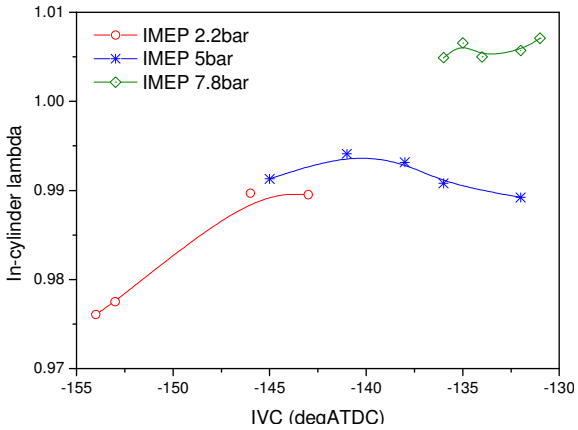

f) In-cylinder Lambda

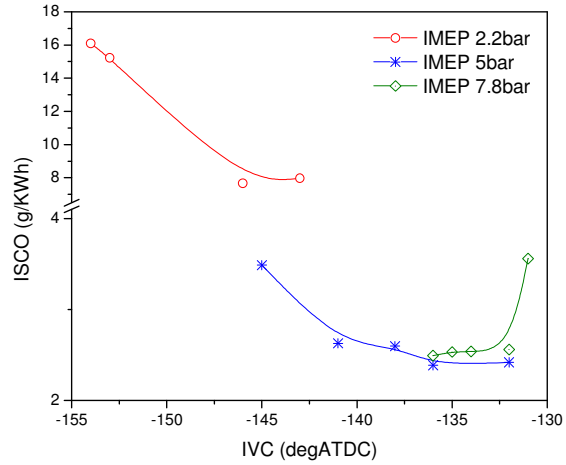

g) Indicated Specific CO (ISCO)

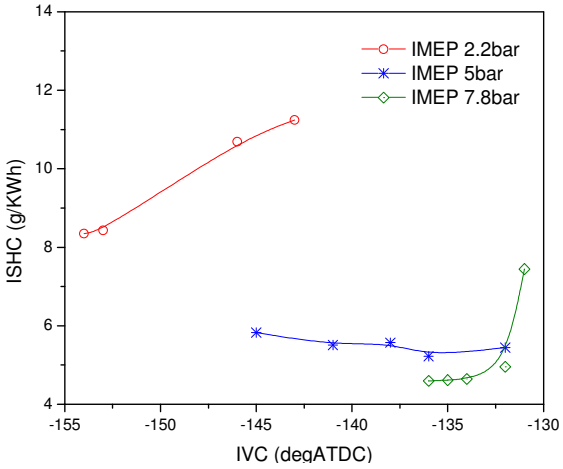

h) Indicated Specific HC (ISHC)

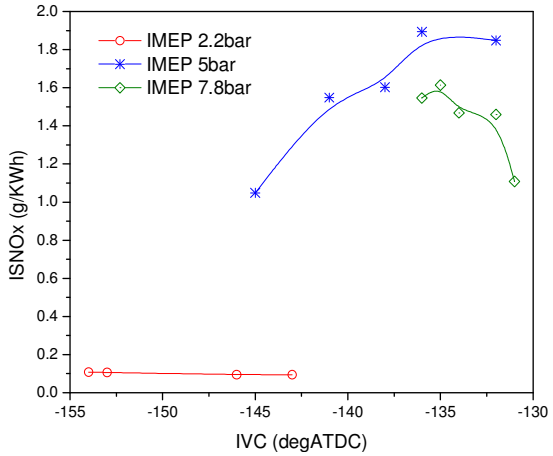

i) Indicated Specific NOx (ISNOx)

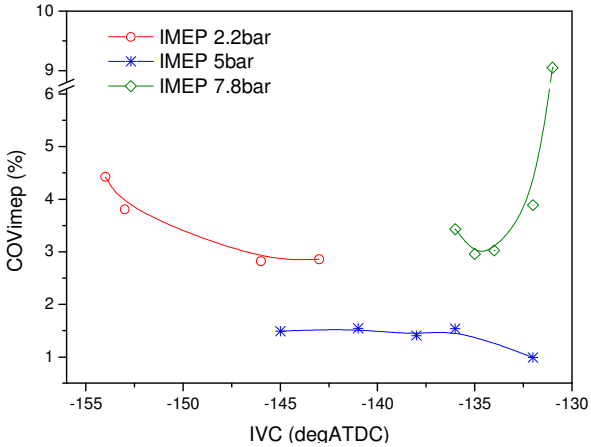

j) COVimep

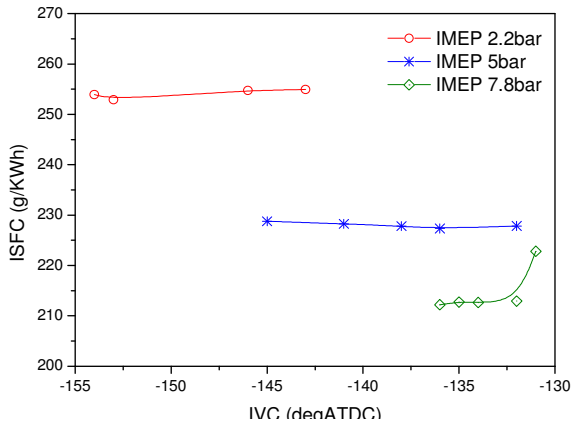

k) Indicated Specific Fuel Consumption (ISFC)

Figure 8.7 Effect of IVC at 1500rpm

The increase in exhaust and in-cylinder lambda at the lower load seen in Figure 8.7e and 8.7f indicated that additional air had been charged into and through the cylinder to the exhaust. This results in the reduction in ISCO emission shown in Figure 8.7g. The increase in ISHC emission shown in Figure 8.7h could be caused by the lower burned gas temperature due to the delayed combustion with late IVC.

At the middle load, too much delay in IVC caused the mixture to flow back into the intake port when the cylinder pressure was higher than the boosting pressure. Therefore, the in-cylinder lambda started to decrease as shown in Figure 8.7f.

In addition to reduce the rate of pressure rise and combustion noise at higher load, delayed IVC and hence lower ECR reduced the ISNOx emission. But further delay in IVC resulted in the combustion deteriorates and higher cycle-to-cycle variation, as shown in Figure 8.7j but IVC had little effect on ISFC. Therefore, the IVC could be used to control CAI combustion and emissions without negative impact on fuel consumption.

8.4 Fuel Consumption and Emissions

8.4.1 Heat Release Analysis of Lean Boost Two-stroke CAI Operation

During the engine experiments and subsequent heat release analysis, different combustion processes were detected as the engine load was changed. As shown in Figure 8.8, at 2.78 bar IMEP the heat release process was characterised with one peak and spark had no effect on the ignition and heat release process, indicating the occurrence of pure controlled autoignition combustion. As the load was increased to 5.49bar IMEP, the cylinder pressure and heat release curves exhibited a gradual and then a sudden rise, characteristics of the hybrid spark ignited and autoignition combustion. This is more apparent on the mass fraction burned curve. Similar hybrid combustion processes were also noted at the low load of 1 bar IMEP. The spark ignition during the hybrid combustion operation was found to be a useful means to control the combustion phasing. In the high load spark assisted CAI operation, retarded spark ignition was employed to minimise the rate of heat release. In the spark assisted CAI operation at idle, the spark timing was advanced before TDC to help stabilize the combustion process.

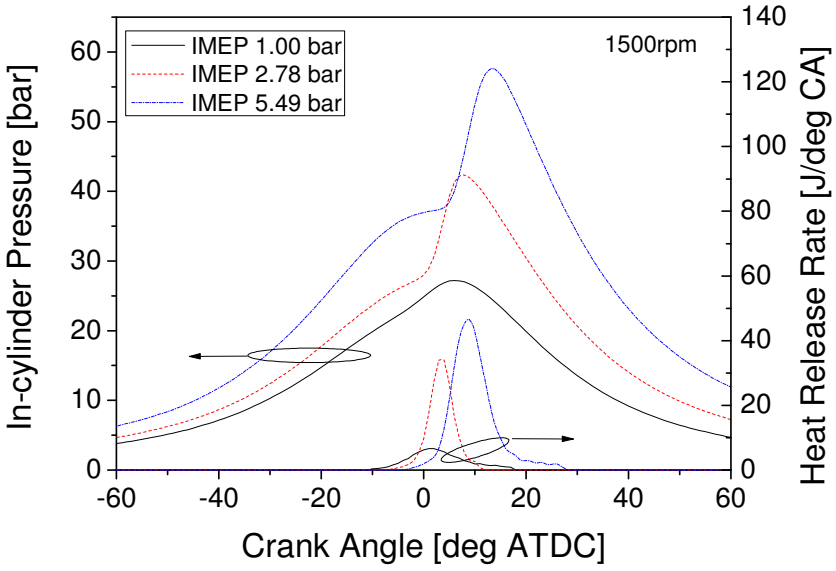

a) In-cylinder Pressure and Heat Release Rate

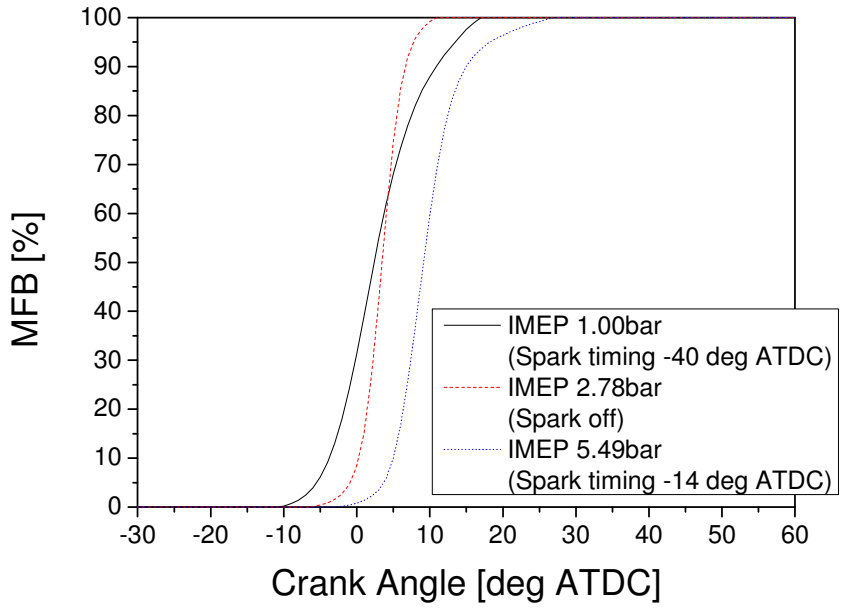

b) Mass Fraction Burned

Figure 8.8 In-cylinder Pressure and Heat Release Process of CAI Combustion at 1500rpm

As shown in Figure 8.9a, the combustion phase for the best fuel economy , defined by the value of CA50 (50% mass fraction burned), was in the range of 2 to 8 degrees CA ATDC in the lean boost two-stroke CAI operation. At low load operations, the combustion phase was more advanced and closer to TDC than that at high load, at which the spark assisted combustion took place and spark timing was retarded to reduce the rate of pressure rise below 5bar/CA, as illustrated by Figure 8.8b. Figure 8.9c shows that the combustion duration defined by the 10% to 90% mass fraction burned (CA10-CA90) was in the range of 8-14 degrees CA, much shorter than the spark ignited flame. As the load increased, the combustion duration was shortened as combustion took place at higher pressure and temperature but with less residual gases.

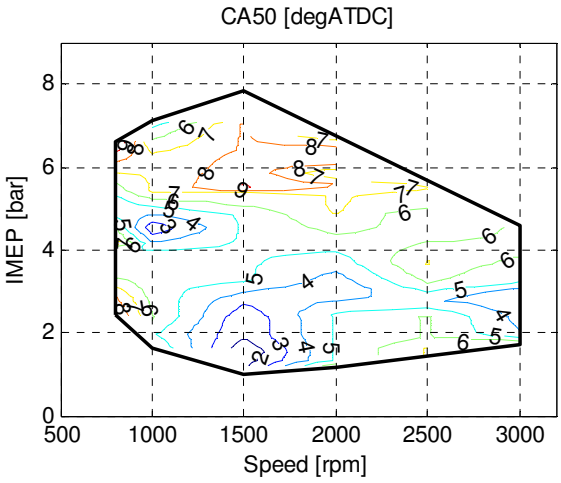

a) CA50

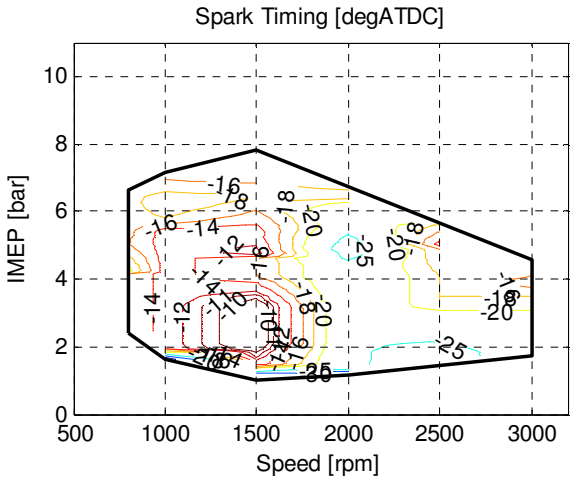

b) Spark Ignition Timings

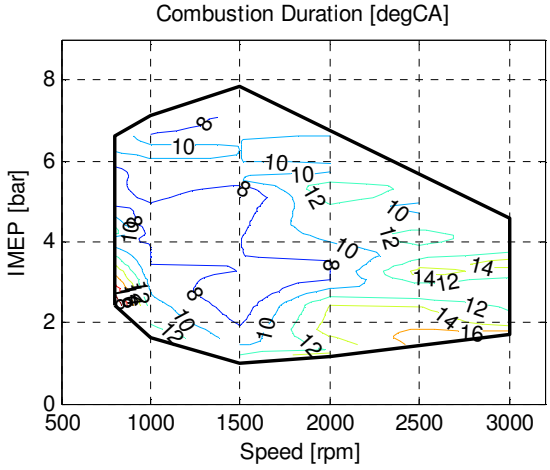

c) CA10-90

Figure 8.9 Combustion Phasing (CA50), Spark Timing and Combustion Duration (CA10-90) over the Operating Range

Figure 8.10 shows the Coefficient of Variation of IMEP over the CAI operating range. Under most of operating conditions, the COVimep was below 3%. The cycle variation became noticeably higher at the low load and high speed conditions as the residual gas fraction became higher and in-cylinder temperature lower, which hindered the autoignition process and slowed down the heat release reactions.

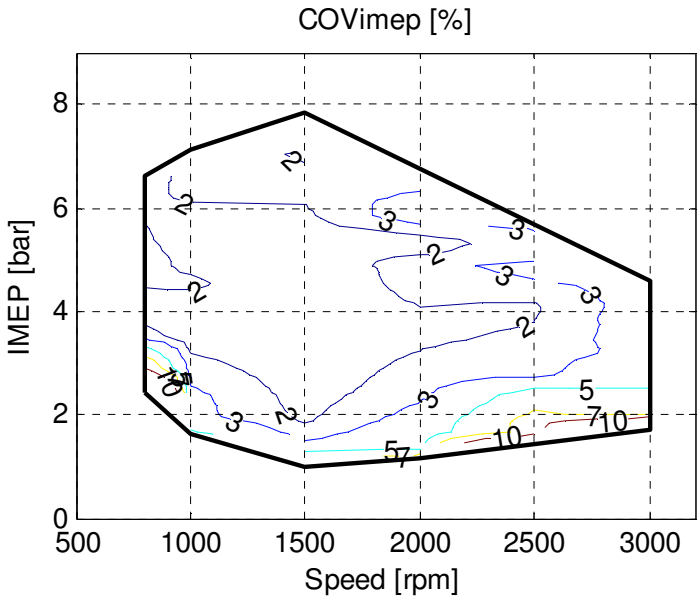

Figure 8.10 Coefficient of Variation (COV) of IMEP over the Lean Boost Two-stroke CAI Operating Range

8.4.2 Emissions of Lean Boost Two-stroke CAI Operation

In order to demonstrate the benefits by lean boost operations, CO and HC emissions from both exhaust lambda 1 and lean boosted operations are plotted in Figure 8.11 and Figure 8.12 respectively. It can be seen that the CO emission was reduced by 10 times and unburned HC emissions by 50% by lean boost because of the reduction in the in-cylinder air/fuel ratio and the removal of fuel rich combustion. At most of the operating conditions, CO and HC emissions were below 10g/KWh and decreased at higher engine load when more complete combustion took place at elevated combustion temperature. Near the low load boundary, CO and HC emissions increased rapidly due to much lower in-cylinder temperature and higher residual gas concentration.

As shown in Figure 8.13, NOx emissions were very low in most operating conditions. The relatively higher NOx emission near the knock limit was reduced by 80% by lean boost. This can be explained by the cooling effect of air short-circuiting. When fresh air flew into and out of the cylinder, it took heat away from the cylinder wall and in-cylinder charge. The cooling effect of air short-circuiting was reflected by the lower exhaust temperature measured at the exhaust port, as shown in Figure 8.14.

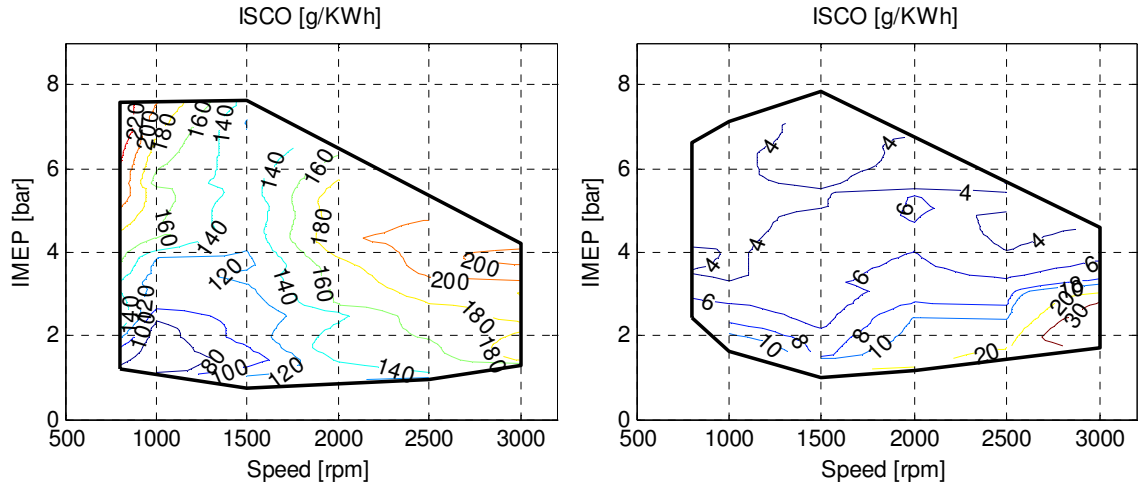

a) Exhaust lambda 1 b) Lean boost

Figure 8.11 Indicated Specific CO Emissions

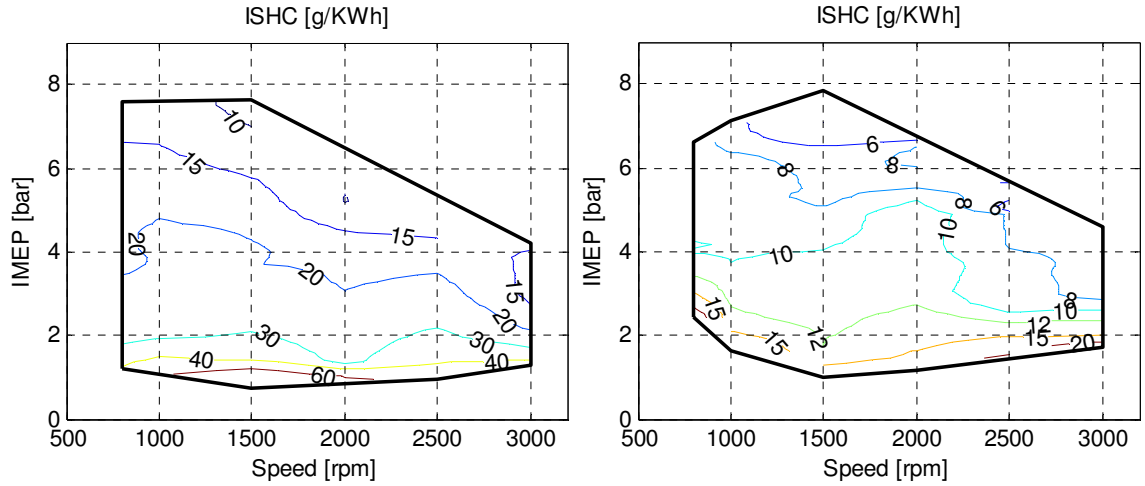

a) Exhaust lambda 1 b) Lean boost

Figure 8.12 Indicated Specific HC Emissions

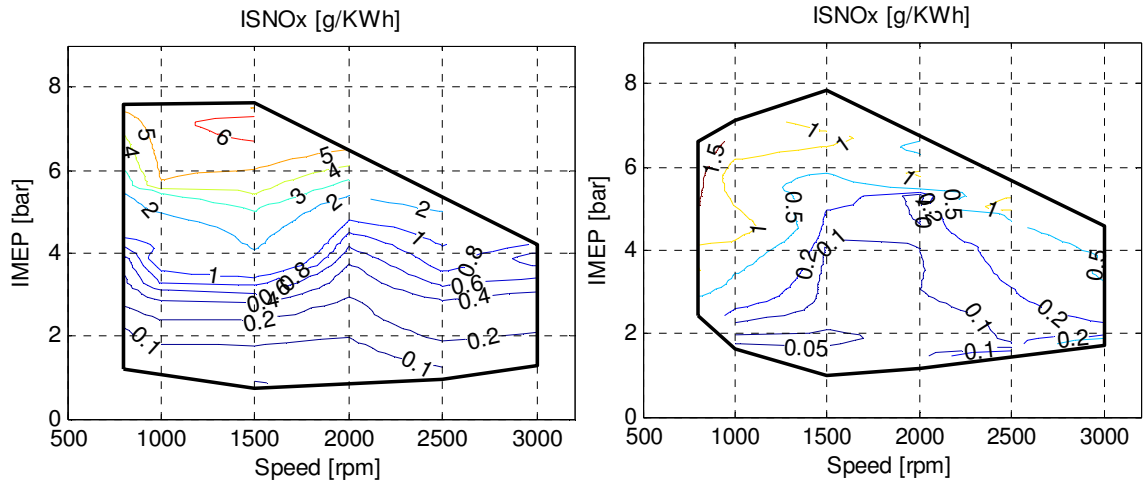

a) Exhaust lambda 1 b) Lean boost

Figure 8.13 NOx Emissions

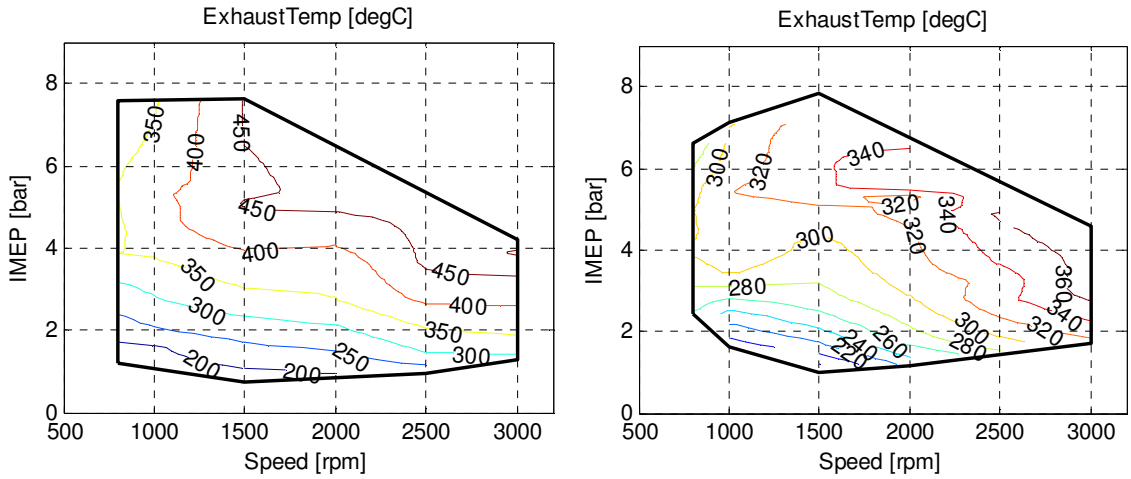

a) Exhaust lambda 1 b) Lean boost

Figure 8.14 Exhaust Temperatures

8.4.3 Combustion and Engine Efficiencies in the Lean Boost Two-stroke CAI Operation

As shown in Figure 8.15, the dramatic reduction in CO and unburned HC emissions by lean boost is accompanied with the significant improvement in combustion efficiencies throughout the CAI operational range. Near the low load boundary, in particular, the combustion efficiency was increased from 74% to 94%. The most complete combustion was seen at higher load conditions. As the load was reduced, the burned gas temperature was insufficient high to oxidise CO and unburned hydrocarbons. However, it is noted that there is still room for improvement in combustion efficiencies even at higher load range, which could be achieved by improved fuel injection equipment and combustion chamber design.

The consequence of the more complete combustion process of in-cylinder mixtures was large reductions in indicated specific fuel consumptions in the lean boost CAI operation. As it can be seen in Figure 8.16, the specific fuel consumption was reduced by more than 22% throughout the load and speed range. In addition, it is noted that the most dramatic reductions in ISFC were at the high load and low load limits. Furthermore, it can be seen that the most fuel efficient region was in the high load and high speed region where the combustion process was most complete and CO/HC emissions were the least.

Figure 8.17 shows the residual gas concentration values measured by a Cambustion fast CO2 analyser [96] in the operational range of the lean boost two-stroke CAI mode. Due to the response time limit of the analyser, the results were obtained up to 1500rpm. It is noted that the residual gas concentration varied between 40% at the high load limit to more than 80% at the low load limit.

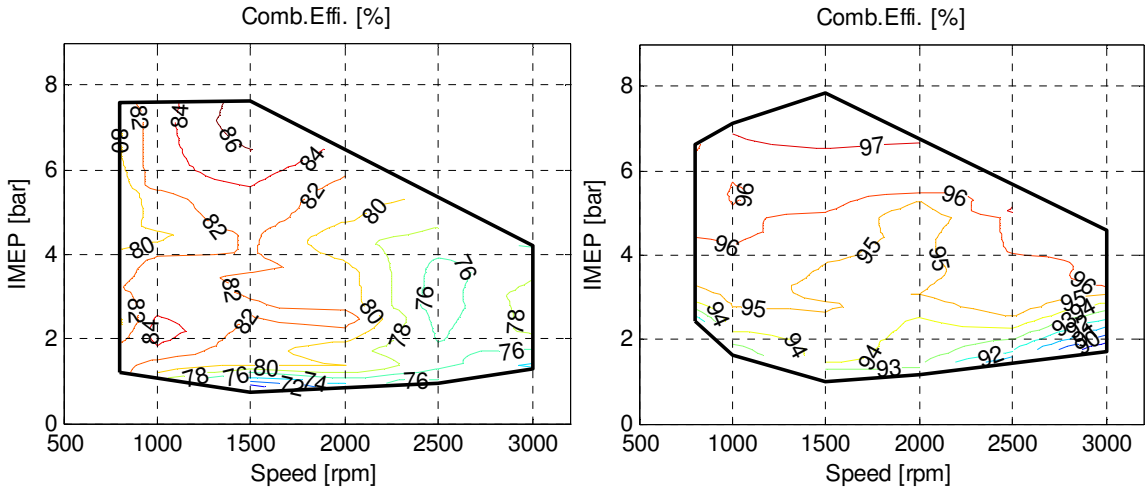

a) Exhaust Lambda 1 b) Lean Boost

Figure 8.15 Combustion Efficiencies

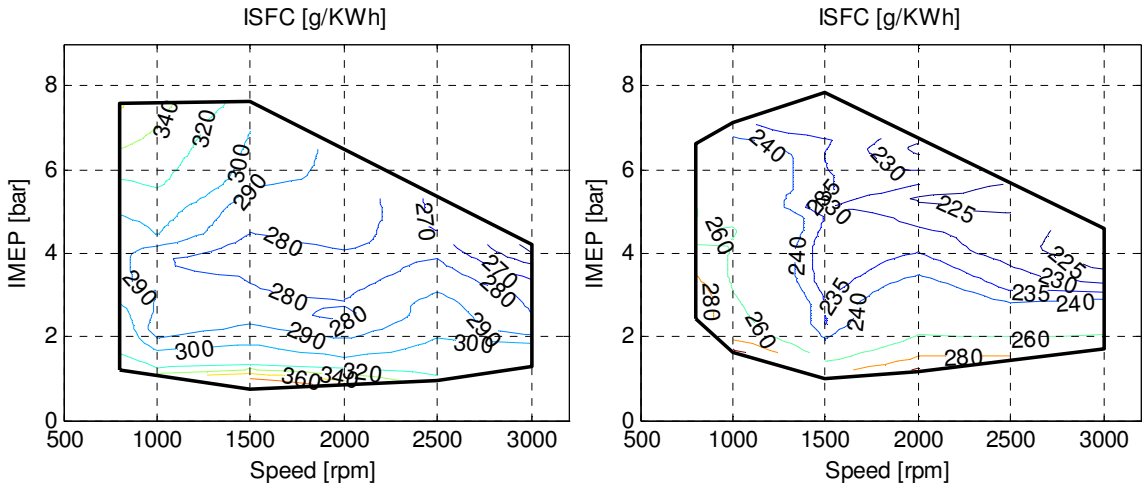

a) Exhaust Lambda 1 b) Lean Boost

Figure 8.16 Indicated Specific Fuel Consumptions

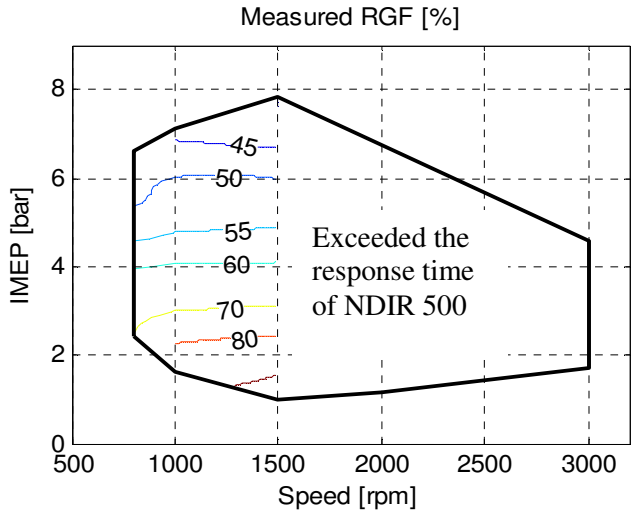

Figure 8.17 RGF Measured by Fast CO2 Analyser at Lean Boost Operation

8.5 Effect of Ethanol Content on Two-stroke Lean Boost CAI

In order to test the lean boost CAI compatibility and investigate the ethanol content effect on lean boost CAI, 15% ethanolled gasoline (E15) and 85% ethanolled gasoline (E85) were tested in two-stroke lean boost CAI operation with the same control strategy used for gasoline.

8.5.1 Operating Range

From previous results shown in Chapter 7.2, it can be seen the operating range of two-stroke CAI is mainly presented at three engine speeds, which are 800rpm (low speed limit), 1500rpm (low load and high load boundary) and 3000rpm (high speed limit). Therefore, the ethanolled gasoline tests were carried out at the three speeds with the same valve timing, injection timing and boosting pressure used for gasoline tests.

Figure 8.18 shows the operating range of two-stroke lean boost CAI when fuelling with gasoline, E15 and E85. As discussed previously, at high loads the operation is limited by violent combustion and too rapid heat release rate, which can be reflected by maximum cylinder pressure rise rate. In this study, the maximum cylinder pressure rise rate is limited at 5 bar/deg CA, no matter what fuel is used. As shown in Figure 8.19, the

pressure rise rate increases with engine load due to the increase in fuelling rate and higher cylinder temperature at higher loads. It also can be seen that with increasing ethanol content in the fuel, the maximum pressure rise rate reduced, in particular at middle and high load, because of the slower burning rate of ethanol, this will be discussed in Chapter 8.5.2. So with the same pressure rise rate limit, E15 and E85 can reach higher load conditions.

At low loads the operation is limited by misfire and unstable combustion, which can be reflected by cycle-to-cycle variation value, COVimep. As shown in Figure 8.20a, when IMEP falls below 2bar at 1500rpm, COVimep increases rapidly as combustion becomes unstable and misfire occurs in some cycles due to the large amount of trapped residual gases and too low combustion temperature. The COVimep of gasoline fuel is the lowest. When increasing the ethanol content in the fuel, the COVimep increases due to the slow combustion rate of ethanol and lower cylinder temperature caused by the higher vaporization latent heat value of ethanol. At lower speed, 800rpm, the increase in COVimep started below 4bar IMEP as shown in Figure 8.20b. Although the COVimep was limited at 5% throughout all the tests, the CAI combustion can reach lower load conditions at 1500rpm compared to that at 800rpm because of shorter time for heat transfer at higher speed. Therefore, adding the charge cooling effect of ethanol fuels, the low load operational range becomes narrower with higher ethanol content fuels. In addition, the reason of the increase in COVimep at high load conditions can be attributed to the effect of air short-circuiting on combustion process as air short-circuiting rate and its cycle-to-cycle variation are higher at high load conditions, as explained in Chapter 5.3.

As a result, the more ethanol is blended in the gasoline, the higher the upper load limit can be extended but at the expanse of the limited low load operations.

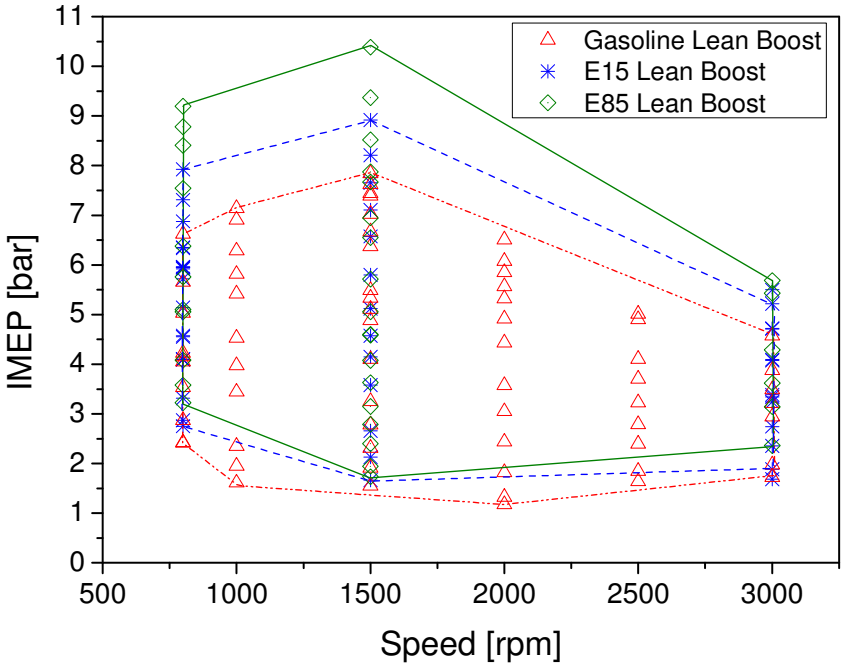

Figure 8.18 Operating Range of Two-stroke Lean Boost CAI with Gasoline, E15 and E85

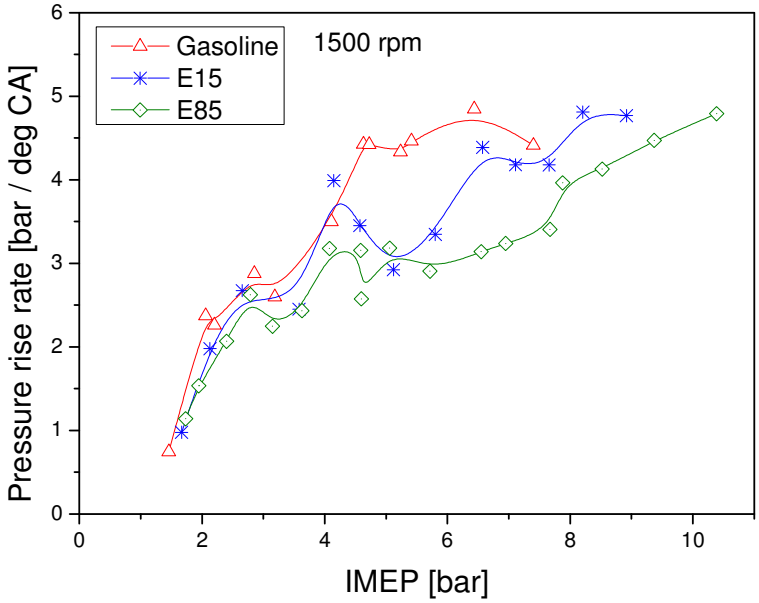

Figure 8.19 Maximum Pressure Rise Rate at 1500rpm

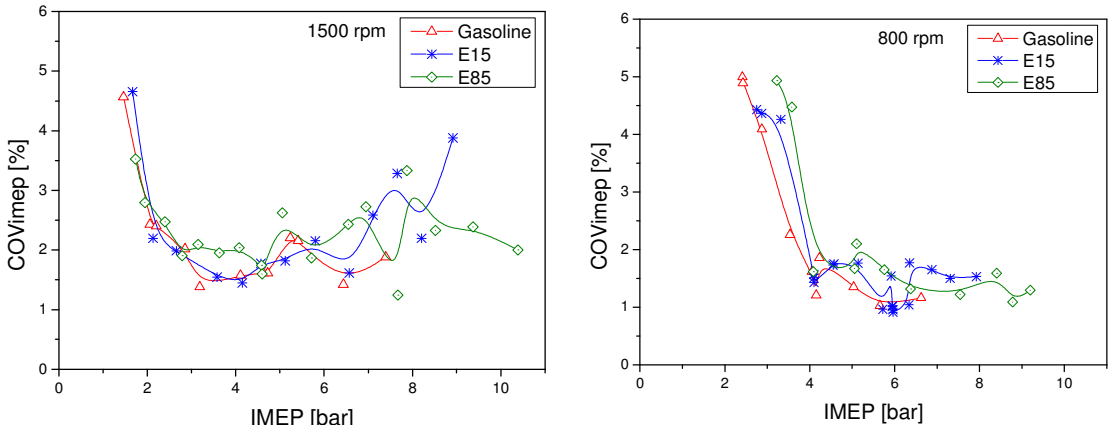

a) 1500rpm b) 800rpm

Figure 8.20 COVimep at 1500rpm and 800rpm

8.5.2 Combustion Process

In order to analyse the combustion process of gasoline, E15 and E85, the heat release rate and mass fraction burnt curve were calculated from cylinder pressure. Figure 8.21 shows the cylinder pressure and heat release rate of gasoline, E15 and E85 at a typical low load operating condition with pure CAI combustion. It can be seen that with the heating effect of residual gas, auto-ignition started nearly at same crack angle. However, with increased ethanol content, E85 burnt slower than E15 and gasoline. Therefore, the peak pressure of E85 is the lowest.

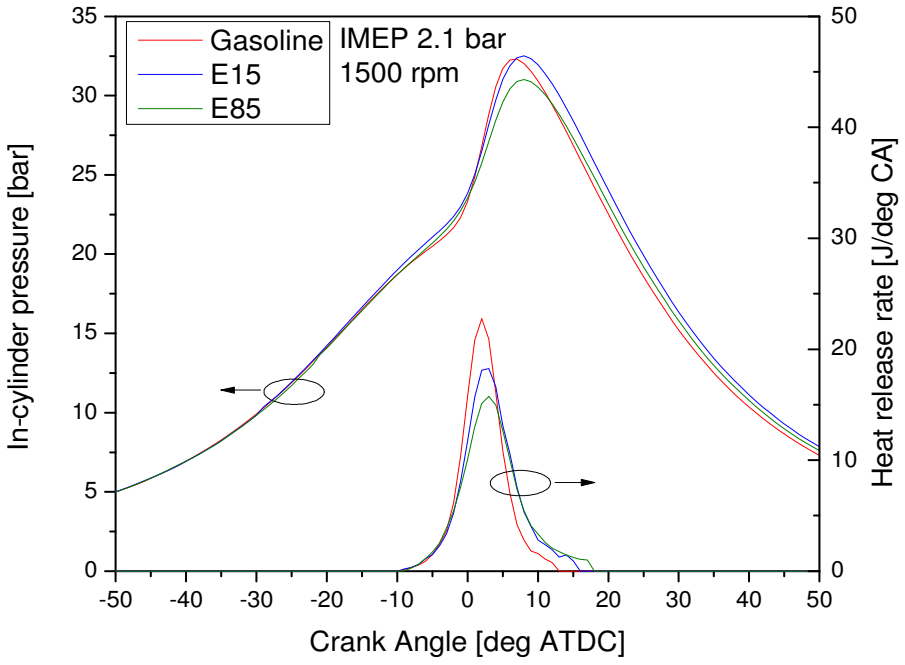

Figure 8.21 Cylinder Pressure and Heat Release Rate at 2.1bar IMEP and 1500rpm

As shown in Figure 8.22, at the higher load of 4.6bar IMEP, the heat release curve shape changed to one with a slow slope in the first part and a steep slope in the second part, separate by an apparent inflection at a certain crank angle. This two-stage heat release process is typical of the spark-assisted hybrid flame and autoignition combustion [97]. At middle to high load operation conditions, as more exhaust gases were scavenged by fresh air and residual gas fraction reduced to a certain value that residual gas could not provide enough heat to initiate auto-ignition, spark-assisted CAI had to be employed to stabilize combustion in the cylinder. The first part of heat release process is the slow flame propagation and the second part is the rapid auto-ignition at multipoint throughout combustion chamber with the aid of further compression from the burnt gas. On the other hand, the spark-assisted CAI operating mode allows auto-ignition timing to be controlled for CAI engines. In order to keep the optimum combustion phase in this study, the spark timing had to be advanced for E15 and E85 due to their slower burn rate. As shown in Figure 8.22, although the start of ignition had been advanced 2 deg CA for E15 and 5 deg CA for E85, their heat release process ended nearly at the same CA. Therefore, with increased ethanol content in the fuel, the spark timing needs to be advanced more to have the optimum combustion phase.

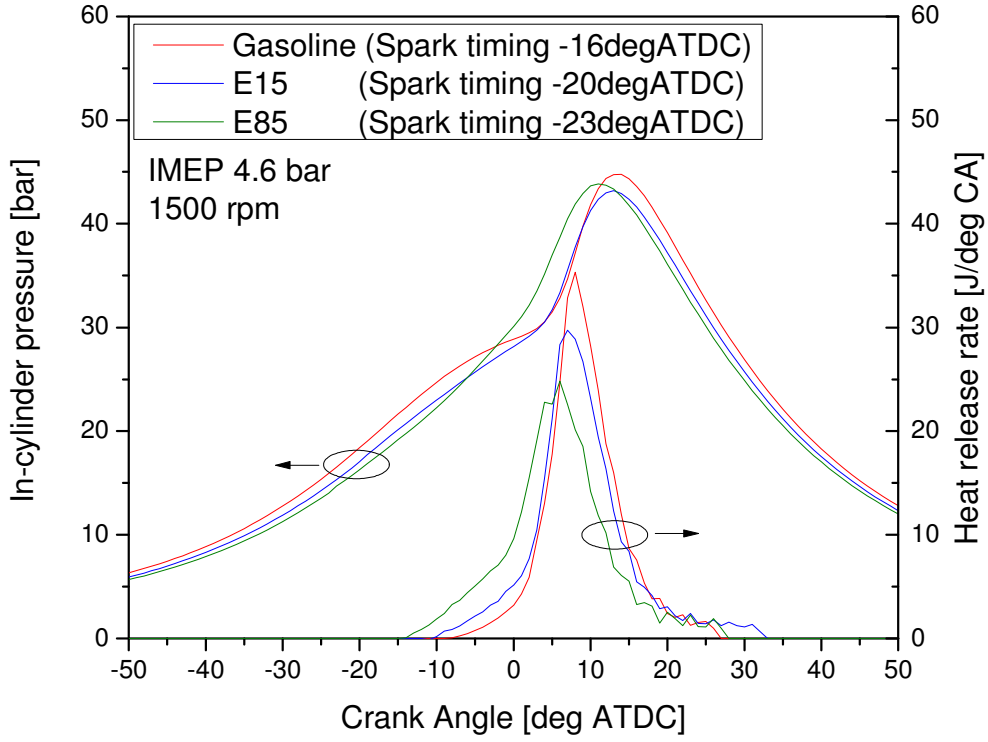

Figure 8.22 Cylinder Pressure and Heat Release Rate at 4.6bar IMEP and 1500rpm

When the engine load was increased further, the combustion process turned to be SI dominated due to the serious lack of the heat from residual gas and the cooling effect of larger amount of blow-through fresh air, as shown in Figure 8.23. In this case, the spark timing and combustion phase need to be further advanced for E15 and E85.

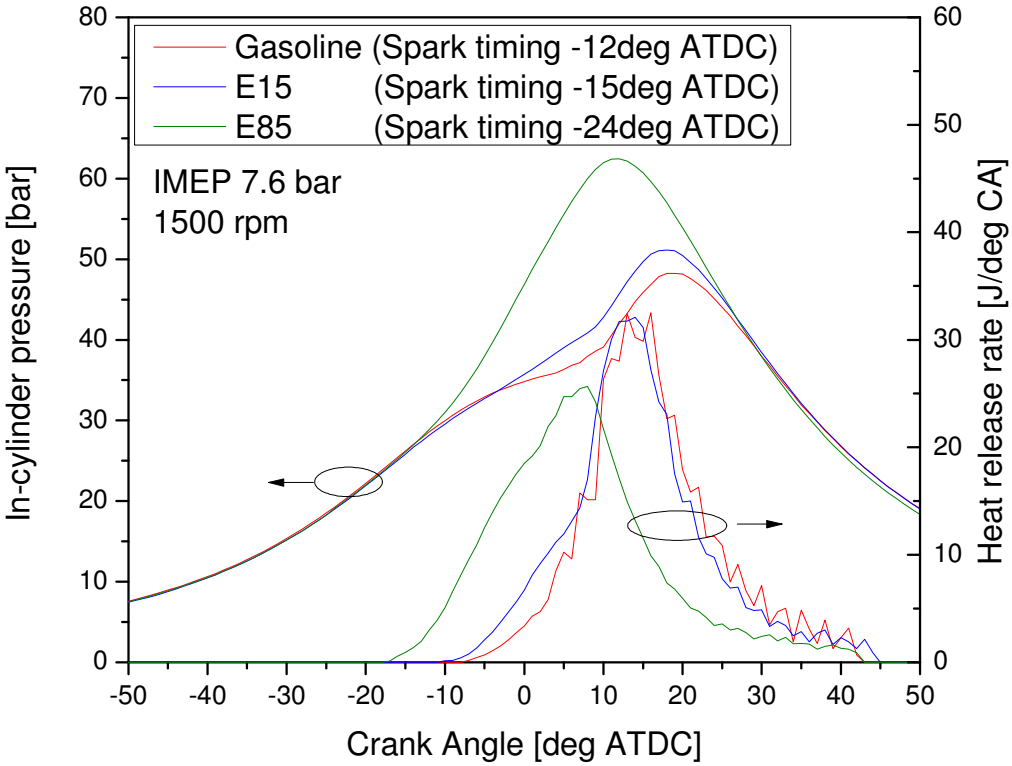

Figure 8.23 Cylinder Pressure and Heat Release Rate at 7.6bar IMEP and 1500rpm

Crank angle at 10% and 50% of mass fraction burnt, (CA10 and CA50), indicating Start of combustion and combustion phase respectively, are plotted against IMEP in Figure 8.24 and 8.25 at 1500rpm. The crank angle from 10% to 90% of mass fraction burnt, (CA10-90), indicating combustion duration is plotted in Figure 8.26. It can be seen that at low load conditions the start of combustion and combustion phase of gasoline, E15 and E85 were nearly at the same crank angle because there was a large amount of residual gas trapped in the cylinder which could provide enough heat to ignite the mixture in the cylinder. When engine load increases, the combustion phase of the three fuels has to be retarded to slower down combustion process and avoid too high pressure raise rate. Similarly, the start of combustion of gasoline was also retarded with increased load. And for E15 the start of combustion were remained roughly the same. But for E85

the start of combustion had to be advanced at middle and high load conditions, due to the slower burning rate of ethanol. As shown in Figure 8.26, even when the combustion phase of E15 and E85 was brought forward, their combustion duration was longer than that of gasoline. This also explains why pressure rise rate of E15 and E85 was lower than that of gasoline at the same load and how the engine could reach higher load operating conditions when fuelled with E15 and E85.

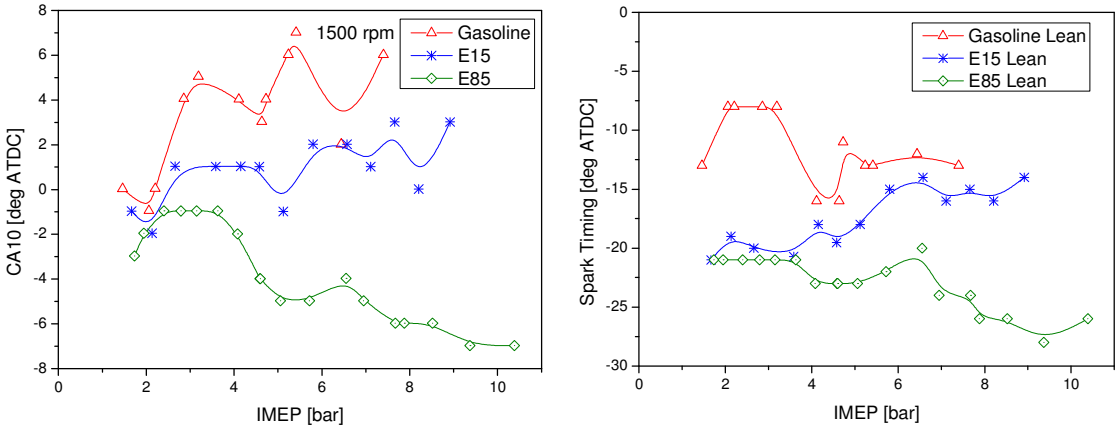

a) CA10 b) Spark Timing

Figure 8.24 CA10 (Start of Combustion) and Spark Timing

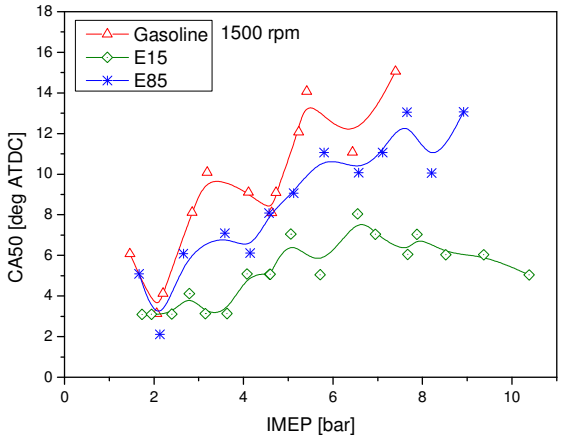

Figure 8.25 CA50

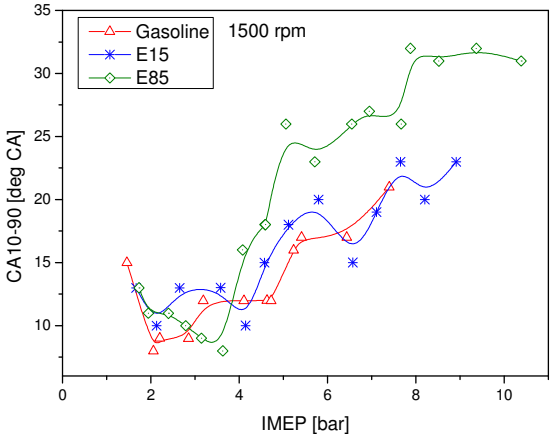

Figure 8.26 CA10-90

8.5.3 Emissions

As presented in Chapter 7.2, the ethanol content has strong effect on the improvement of CO, uHC and NOx emissions at exhaust lambda 1, when the in-cylinder lambda is lower than 1 due to the air short-circuiting and ethanol. When running in the lean boost mode, the advantage of ethanol blends fuels on emissions disappeared as there was enough oxygen participating in combustion in the cylinder, as shown in Figure 8.27, 8.28 and 8.29. In contrary, the E15 and E85 produced more CO emissions due to the lower combustion temperature caused by the higher vaporisation latent heat of ethanol, in particular at low load conditions, where combustion temperature was reaching lowest limit, as shown in Figure 8.27.

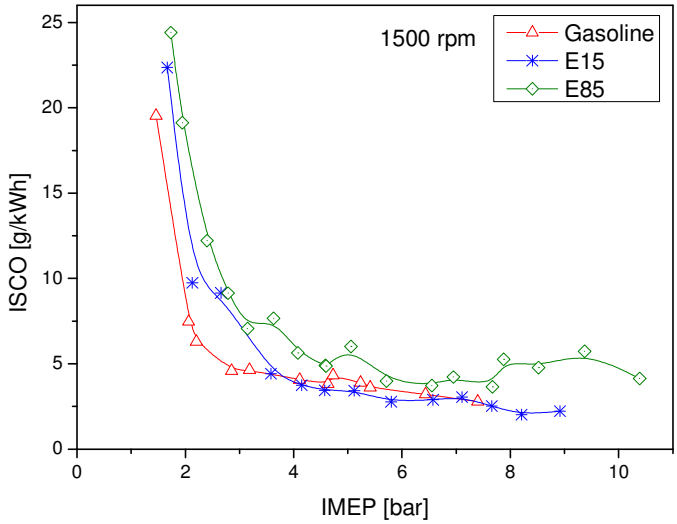

Figure 8.27 Indicated Specific CO Emissions

Figure 8.28 shows Indicated Specific HC (ISHC) emissions produced by gasoline, E15 and E85 at 1500rpm. It can be seen that there was little difference in ISHC emissions between the 3 fuels at low and middle loads. At high loads the E85 produced increasingly higher ISHC emissions, which is due to the wall wetting effect of injection, as the injection quantity of E85 is 1.5 times more than that of gasoline. The extra fuel impinges onto the piston and could not completely evaporate during compression stroke. When exhaust valve opened, the unburnt fuel went out into exhaust.

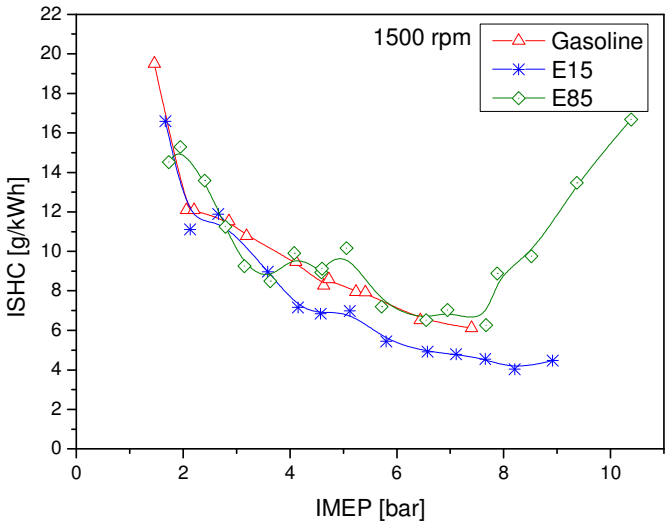

Figure 8.28 Indicated Specific HC Emissions

As shown in Figure 8.29, ISNOx emissions from the combustion of three fuels were similar because the NOx emission is mainly determined by combustion temperature. When load increased, more fuel was injected in the cylinder and the heat produced by combustion was almost the same for three fuels. Although ethanol could bring down the combustion temperature by its higher vaporisation latent heat and slower combustion speed, the combustion phase of E85 was advanced to achieve better fuel economy. As a result, ISNOx emission increased with engine load and E15 and E85 produced slightly higher NOx emissions at high loads compared to pure gasoline fuel.

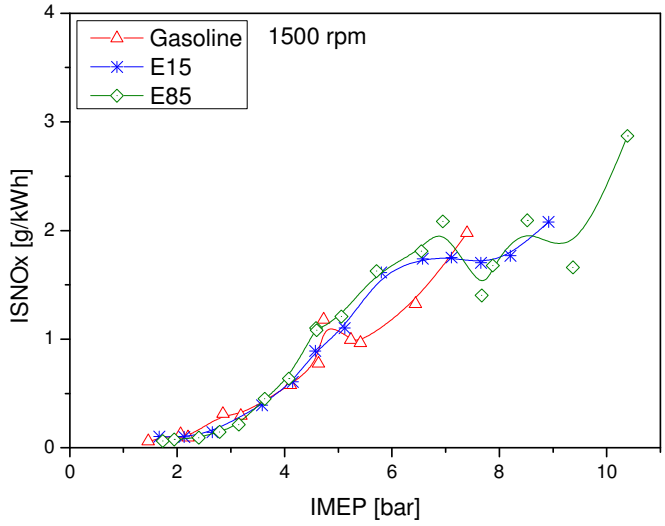

Figure 8.29 Indicated Specific NOx Emissions

8.5.4 Efficiencies

In order to compare the fuel economy and take into account of the different calorific values of gasoline and ethanol, combustion efficiency, thermodynamic efficiency and indicated fuel conversion efficiency are calculated and analysed for gasoline and its blends with ethanol, of which the formula were presented in Chapter 3.6.

The combustion efficiency is estimated from the CO and HC emissions in the exhaust gas and shown in Figure 8.30. It can be seen that by blending 15% ethanol in the gasoline, the combustion efficiency is improved by 1% at middle load and high load because of the improve oxidisation process. However, by adding 85% ethanol, the combustion efficiency dropped back to the same level as gasoline at low and middle load conditions, because of too low combustion temperature. At higher load operation, combustion efficiency of E85 dropped significantly due to the wall wetting of injection explained previously.

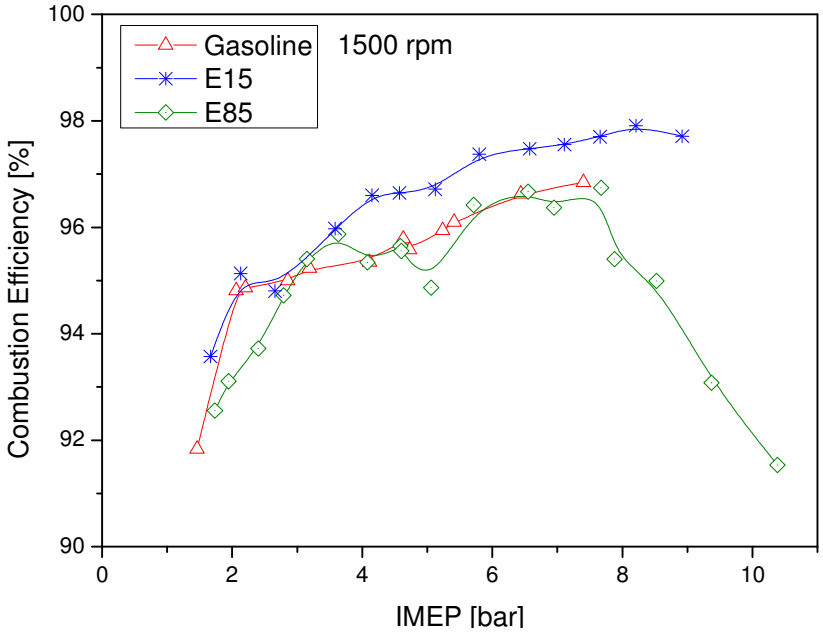

Figure 8.30 Combustion Efficiency

Figure 8.31 shows thermodynamic efficiency of three fuels at 1500rpm. It can be seen that at middle and high loads E15 and E85 have lower thermodynamic efficiency than gasoline, indicating their longer combustion.

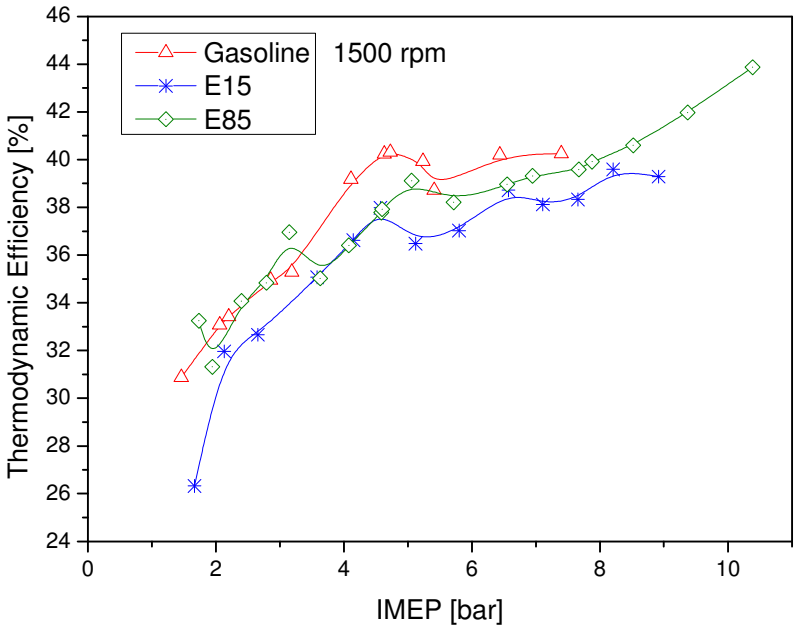

Figure 8.31 Thermodynamic Efficiency

As the product of combustion efficiency and thermodynamic efficiency, the indicated fuel conversion efficiency is shown in Figure 8.32. It can be seen that as long as the engine is not run with rich mixtures and the combustion phase is properly optimized, the E15 and E85 can reach the same efficiency as gasoline.

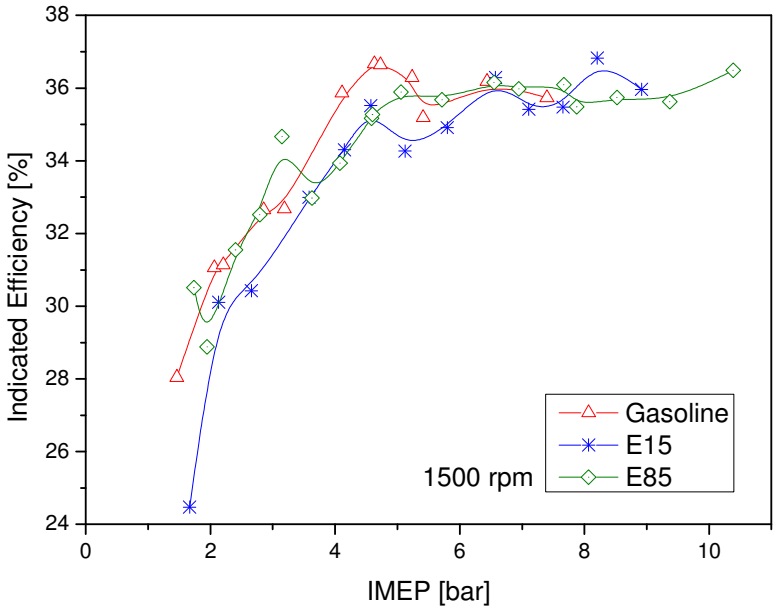

Figure 8.32 Indicated Efficiency

8.6 Summary

By means of fast in-cylinder and exhaust measurements, the air short-circuiting rate in the two-stroke cycle and its effect on in-cylinder mixture strength were quantified and analysed. It is shown that the engine was operating with a fuel rich mixture when the lambda value determined by an exhaust oxygen sensor was set to one because of the air short circuiting during the two-stroke cycle operation. This had led to engine experiments with increased intake air pressure in order to compensate for the air lost through the short-circuiting phenomenon. When the intake pressure was set to obtain the minimum indicated specific fuel consumption, it was found

1) Two-stroke CAI combustion in the single cylinder camless engine was limited by (i) knocking and rapid heat release rate at low speed high load operation, (ii) partial-burn and misfire at low load operation, (iii) the restricted opening period of the electro-hydraulic actuated intake valves at high load and higher engine speed.
2) Pure CAI combustion took place at the part load conditions whilst hybrid spark ignited and autoignition combustion occurred at low load and high load regions.
3) The in-cylinder air/fuel ratio was close to stoichiometric throughout the CAI operational range with lean boost. Slightly fuel rich mixture was required to obtain stable CAI combustion at the low load boundary.
4) The effect of valve timing on gas-exchange process and the subsequent combustion process were investigated. EVO mainly affects the thermodynamic efficiency through effective expansion ratio. IVC has strong effect on CAI combustion phase and duration through effective compression ratio. IVO and EVC are the main parameters affecting scavenging ratio, air short-circuting rate, residual gas fraction and cylinder lambda during gas exchange process.
5) The combustion phase (CA50) varied within a range of 2-8 degree CA ATDC and combustion duration (CA10-90) was 10-14 CAs.
6) CO emissions were reduced by 10 times and unburned HC emission by 50% by lean boost because of the removal of fuel rich combustion. In addition, lean boost

led to significant reduction in NOx emissions at high load due to the air charge cooling effect.

7) Combustion efficiencies were increased from 74% to above 94% by lean boost as the in-cylinder lambda was increased to 1.
8) The indicated fuel consumption throughout the CAI operational range was significantly improved by lean boost due to more complete combustion.
9) Ethanol burns slower than gasoline, so it can help extend high load operating range limited by too high pressure rise rate. However, the slower combustion rate leads to higher cycle-to-cycle variations and results in the loss of some low load operating conditions where COVimep is greater than 5%.
10) Spark-assisted CAI combustion as an additional approach to control auto-ignition timing and combustion phase of CAI was used at middle to high load operating conditions. By this approach the combustion phase needs to be advanced with increased ethanol content to improve the combustion speed of ethanol.
11) When lambda and combustion phase are properly optimized, the ethanol blended in gasoline fuels, like E15 an E85, exhibited similar indicated fuel conversion efficiency and CO, HC and NOx emissions to gasoline.

Chapter 9

Conclusions and Recommendation for Future Work

Chapter 9 Conclusions and Recommendation for Future Work

9.1 Conclusions

In this work, extensive engine experiments have been performed to determine the operational range of CAI combustion and the optimum boosting for minimum fuel consumption in a single cylinder gasoline direct injection camless engine operating in the two-stroke cycle. New measurement techniques have been developed and applied to the measurement of the air short-circuiting rate of the two-stroke cycle operation. In order to minimise the air short-circuiting rate, the intake and exhaust valve timings were adjusted. Lean boost was applied to the engine operation, which was found to extend the range of CAI combustion, resulting in higher combustion and thermal efficiencies, and significantly lower CO and HC emissions. By means of the cycle-resolved in-cylinder measurements and heat release analysis, the improvement in combustion and thermal efficiencies was attributed to the improved in-cylinder mixture, optimised autoignition and combustion phasing.

Two-stroke CAI combustion was studied at exhaust lambda 1. It is demonstrated that a wider range of CAI operation could be achieved at engine speeds from 800rpm to 3000rpm and with engine load from idle to 7.8bar IMEP, which is equivalent to 15.6 bar IMEP on the four-stroke operation. In the CAI operational range, the NOx emission was very low and the specific fuel consumption was also low. Due to the short-circuiting, the in-cylinder mixture was too rich for complete combustion when the exhaust lambda was controlled at 1.0 and hence higher CO and uHC emissions were observed.

The air short-circuiting rate was quantified and used to determine the in-cylinder relative air to fuel ratios from the lambda sensor readings. The combustion and emission results show that maximum combustion efficiency and lowest CO and uHC emissions occurred with a relatively lean overall in-cylinder mixture whilst the maximum CO_2 concentration was obtained with a stoichiometric in-cylinder mixture.

The effect of direct fuel injection timing on engine performance, combustion and emissions was investigated in 3 CAI operating modes. The charge cooling effect of direct fuel injection is most significant during the four-stroke NVO CAI operation. Its effect is

also noticeable in the two-stroke CAI operation but negligible in four-stroke exhaust rebreathing CAI operation. The injection timing has less effect on the start of combustion unless the fuel impingement is significant in the four-stroke NVO CAI and exhaust rebreathe CAI operation. In the two-stroke CAI operation, the injection timing significantly affects the combustion phase and duration due to the shortened mixing time from the fuel injection to ignition.

For further estimating two-stroke CAI operation, 7 operating modes were performed on the same engine, including either two-stroke or conventional four-stroke engine operations. It is found that the two-stroke CAI operation mode incurs the lowest fuel consumption at the part-load condition tested.

Gasoline and ethanol blends were tested in two-stroke CAI combustion mode at exhaust lambda 1. It was found a wide concentration range of ethanol in gasoline was suited over a wide range of speed and load. The presence of ethanol allowed CAI combustion to be extended to higher load conditions. In the case of E85 the maximum IMEP of 8.4bar was obtained at 800rpm. CO, uHC and NOx emissions are significantly reduced by injecting ethanol blended fuels. E85 has greater effect on the emission reduction than E15. Both combustion efficiency and thermodynamic efficiency are improved by the presence of ethanol because of the optimum combustion phasing and lower heat loss. E85 improved indicated fuel conversion efficiency by over 5% at 2000rpm.

The rich in-cylinder air fuel mixture with exhaust lambda 1 operation was corrected by using lean boost CAI operation on the two-stroke poppet valve engine. The in-cylinder air/fuel ratio was close to stoichiometric throughout the CAI operational range with lean boost. Slightly fuel rich mixture was required to obtain stable CAI combustion at the low load boundary.

The effect of valve timing on gas-exchange process and the subsequent combustion process were investigated in two-stroke lean boost CAI mode. EVO mainly affects the thermodynamic efficiency through effective expansion ratio. IVC has strong effect on CAI combustion phase and duration through effective compression ratio. IVO and EVC are the main parameters affecting scavenging ratio, air short-circuiting rate, residual gas fraction and cylinder lambda during gas exchange process. The combustion phase (CA50) varied within a range of 2-8 degree CA ATDC and combustion duration (CA10-90) was

10-14 CAs. Pure CAI combustion took place at the part load conditions whilst hybrid spark ignited and autoignition combustion occurred at low load and high load regions.

CO emissions were reduced by 10 times and unburned HC emission by 50% by lean boost because of the removal of fuel rich combustion. In addition, lean boost led to significant reduction in NOx emissions at high load due to the air charge cooling effect. Combustion efficiencies were increased from 74% to above 94% by lean boost as the in-cylinder lambda was increased to 1. The indicated fuel consumption throughout the CAI operational range was significantly improved by lean boost due to more complete combustion.

In lean boost CAI mode, ethanol still burns slower than gasoline, so the high load operating range limit was extended by the reduced pressure rise rate of burning ethanol. However, the slower combustion rate leads to higher cycle-to-cycle variations and results in the loss of some low load operating conditions where COVimep is greater than 5%. Spark-assisted CAI combustion as an additional approach to control auto-ignition timing and combustion phase of CAI was used at middle to high load operating conditions. By this approach the combustion phase needs to be advanced with increased ethanol content to improve the combustion speed of ethanol. When lambda and combustion phase are properly optimized, the ethanol blended in gasoline fuels, like E15 an E85, exhibited similar indicated fuel conversion efficiency and CO, HC and NOx emissions to gasoline.

9.2 Recommendations for Future Work

9.2.1 Combustion System Improvement

From the presented results, it can be seen the current combustion system is not optimised as evidenced by the low combustion efficiency. Further improvement in the two-stroke cycle engine performance and emissions can be achieved by optimisation of the piston top design and fuel injection system and injection strategy.

1) Higher injection pressure

The fuelling system is capable of running fuel pressure up to 150bar, but currently the injection pressure is 100bar. The high injection pressure will provide more fine fuel spray, which can lead to faster evaporation and form more homogeneous mixture before ignition.

2) Multiple injections

Multiple injections should be adopted in order to shorten fuel jet penetration and reduce wetting the piston top and cylinder wall. Also, the consequence of the multiple injections will be a good aid to control CAI ignition and combustion process. A piezo injector may be used to replace the current solenoid injector when very fast response of the injector is necessary.

3) Spray guided combustion system with centrally mounted injector

Ideally, a spray guided combustion system with a centrally mounted injector next to the spark plug would be able to minimize the wall impingement and to operate with stratified charge combustion, which could be employed to improve the combustion stability at low load.

9.2.2 Further Extension of CAI Operating Range by Miller Cycle

In recognition of the significant improvement on fuel economy and emissions with lean boost CAI operation, additional research could be done at high load limit by further retarding intake valve closure and rising boost pressure, commonly referred as Miller cycle. When boosting pressure increases, the higher charge density will lead to a high power output. In the meanwhile the retarded intake valve closure will lead to a lower effective compression ratio, which is also good for avoiding knocking at high load limit. This is a potential for further extending CAI operating range in two-stroke cycle.

References

1. "World Oil Outlook 2012", Organization of the Petroleum Exporting Countries (OPEC), 2012.
2. Environmental Protection Agency (EPA), USA, http://www.epa.gov/climatechange/basics/.
3. Global Comparison of Light-Duty Vehicle Fuel Economy/GHG Emissions Standards, The International Council on Clean Transportation, August 2011.
4. "Summary of Fuel Economy Performance", National Highway Traffic Safety Administration, USA.
5. "Pocket Guide", European Automobile Manufacturers' Association (ACEA).
6. "The Top Runner Program", Ministry of Economy, Trade and Industry (METI).
7. Dinsdale J., "Environmental Facts and Figures", Environment Agency, UK.
8. "EU Emission Standards for Passenger Cars", Dieselnet - Online information service on clean diesel engines and diesel emissions.
9. "Cars and Light-Duty Trucks—California", Emission Standards, US.
10. Johnson, T. V., Mobile emission control technologies in review, International Conference on 21st Century Emissions Control technology, IMechE Conference Transactions 2000-2, ISBN 1860583229, 2000.
11. Heywood J.B. and Sher Eran, The Two-stroke Cycle Engine: Its Development, Operation, and Design, Taylor and Francis, 1999.
12. Dedeoglu N., Model investigations on scavenging and mixture formation in the dual-fuel or gas engine, Sulzer Tech. Review, Vol 51, No 3, 1969.
13. Rizk W., Experimental studies of the mixing processes and flow configurations in two-cycle engine scavenging, Proc. IMechE, Vol172, 1958.
14. Ohigashi S. and Kashiwada Y., A study on the scavenging air flow through the scavenging ports, Bull. JSME, Vol 9, No36, 1966.
15. http://bikeadvice.in/supercharged-two-stroke-engine/
16. http://www.physics.byu.edu/faculty/rees/360/engine.jpg
17. Allen, J. and Law, D., "Production Electro-Hydraulic Variable Valve-Train for a New Generation of I.C. Engines," SAE Technical Paper 2002-01-1109, 2002, doi:10.4271/2002-01-1109.
18. Zhao, H.(ed.), Advanced direct injection combustion engine technologies and development,Volume 1: Gasoline and gas engines, Woodhead publishing, DOI 10.1533/9781845697327, 2010.

19. Blair G.P., Design and simulation of two-stroke engines, SAE Inc, 1996.
20. Stokes, J., Hundleby, G., Lake, T., and Christie, M., "Development Experience of a Poppet-Valved Two-Stroke Flagship Engine," SAE Technical Paper 920778, 1992, doi:10.4271/920778.
21. Sato, K., Ukawa, H., and Nakano, M., "A Two-Stroke Cycle Gasoline Engine with Poppet Valves in the Cylinder Head - Part II," SAE Technical Paper 920780, 1992, doi:10.4271/920780.
22. Osborne R. J., Stokes J., Lake T. H., Carden P. J., Mullineux J. D., Helle-Lorentzen R., Evans J. C., Heikal M. R., Zhu Y., Zhao H., Ma T., "Development of a Two-Stroke/Four-Stroke Switching Gasoline Engine –The 2/4SIGHT Concept", SAE Paper 2005-01-1137, ,2005.
23. Watson N.,Janota M. S., Turbocharging the Internal Combustion Engine, Wiley-Interscience publishing, ISBN:9780471870722, 1982.
24. BMW Mini Cooper S, Wikipedia website, http://en.wikipedia.org/wiki/BMW_MINI_COOPER. (Accessed April, 2014).
25. Fieweger, K. ; Paffrath, H. ; Schorn, N. , Drivability assessment of an HSDI Diesel engine with electrically assisted boosting systems, IMECH CONFERENCE TRANSACTIONS; 1; 283-296, Turbochargers and turbocharging International conference; 7th, Turbochargers and turbocharging. ISBN: 1860583830, 2002.
26. Kattwinkel, T., Weiss, R., and Boeschlin, J., "Mechatronic Solution for Electronic Turbocharger," SAE Technical Paper 2003-01-0712, 2003, doi:10.4271/2003-01-0712.
27. Shahed, S., "An Analysis of Assisted Turbocharging with Light Hybrid Powertrain," SAE Technical Paper 2006-01-0019, 2006, doi:10.4271/2006-01-0019.
28. Luttermann, C. and Mährle, W., "BMW High Precision Fuel Injectionin Conjunction with Twin-Turbo Technology: a Combination for Maximum Dynamic and High Fuel Efficiency," SAE Technical Paper 2007-01-1560, 2007, doi:10.4271/2007-01-1560.
29. Hopmann, U. and Algrain, M., "Diesel Engine Electric Turbo Compound Technology," SAE Technical Paper 2003-01-2294, 2003, doi:10.4271/2003-01-2294.
30. Arsie, I., Cricchio, A., Pianese, C., De Cesare, M., and Nesci, W., "A Comprehensive Powertrain Model to Evaluate the Benefits of Electric Turbo

Compound (ETC) in Reducing CO2 Emissions from Small Diesel Passenger Cars," SAE Technical Paper 2014-01-1650, 2014, doi:10.4271/2014-01-1650.

31. Zhao H. (ed.), HCCI and CAI engines for the Automotive Industry, Woodhead Publishing, Cambridge, 2007.
32. Gussak, L., Turkish, M., and Siegla, D., "High Chemical Activity of Incomplete Combustion Products and a Method of Prechamber Torch Ignition for Avalanche Activation of Combustion in Internal Combustion Engines," SAE Technical Paper 750890, 1975, doi:10.4271/750890.
33. Onishi, S., Jo, S., Shoda, K., Jo, P. et al., "Active Thermo-Atmosphere Combustion (ATAC) - A New Combustion Process for Internal Combustion Engines," SAE Technical Paper 790501, 1979, doi:10.4271/790501.
34. Noguchi, M., Tanaka, Y., Tanaka, T., and Takeuchi, Y., "A Study on Gasoline Engine Combustion by Observation of Intermediate Reactive Products during Combustion," SAE Technical Paper 790840, 1979, doi:10.4271/790840.
35. Najt, P. and Foster, D., "Compression-Ignited Homogeneous Charge Combustion," SAE Technical Paper 83, 1983, doi:10.4271/830264.
36. Thring, R., "Homogeneous-Charge Compression-Ignition (HCCI) Engines," SAE Technical Paper 892068, 1989, doi:10.4271/892068.
37. M. Stockinger,H. Schäpertöns,P.Kuhlmann, Versuchean einem gemischansugenden Verbrennungsmotor mit Selbstzündnung, MTZ, Motertechnisches Zeitschrift 53 (1992) pp 80-85, 1992.
38. Olsson, J., Tunestål, P., and Johansson, B., "Closed-Loop Control of an HCCI Engine," SAE Technical Paper 2001-01-1031, 2001, doi:10.4271/2001-01-1031.
39. Aaron Oakley, Hua Zhao and Nicos Ladommatos， Experimental Studies on Controlled Auto-ignition (CAI) Combustion of Gasoline in a 4-Stroke Engine， SAE 2001-01-1030, 2001
40. Aaron John Oakley， Experimental Investigations on Controlled Auto-Ignition Combustion in A Four-Stroke Gasoline Engine, PHD thesis, Department of Mechanical Engineering, Brunel University, UK, 2001.
41. Haraldsson, G., Tunestål, P., Johansson, B., and Hyvönen, J., "HCCI Combustion Phasing in a Multi Cylinder Engine Using Variable Compression Ratio," SAE Technical Paper 2002-01-2858, 2002, doi:10.4271/2002-01-2858.
42. Oakley, A., Zhao, H., Ladommatos, N., and Ma, T., "Dilution Effects on the Controlled Auto-Ignition (CAI) Combustion of Hydrocarbon and Alcohol Fuels," SAE Technical Paper 2001-01-3606, 2001, doi:10.4271/2001-01-3606.

43. Aroonsrisopon, T., Sohm, V., Werner, P., Foster, D. et al., "An Investigation Into the Effect of Fuel Composition on HCCI Combustion Characteristics," SAE Technical Paper 2002-01-2830, 2002, doi:10.4271/2002-01-2830.
44. Jeuland, N., Montagne, X., and Duret, P., "Engine and Fuel Related Issues of Gasoline CAI (Controlled Auto-Ignition) Combustion," SAE Technical Paper 2003-01-1856, 2003, doi:10.4271/2003-01-1856.
45. Cairns, A. and Blaxill, H., "The Effects of Combined Internal and External Exhaust Gas Recirculation on Gasoline Controlled Auto-Ignition," SAE Technical Paper 2005-01-0133, 2005, doi:10.4271/2005-01-0133.
46. Fuerhapter, A., Piock, W., and Fraidl, G., "CSI - Controlled Auto Ignition - the Best Solution for the Fuel Consumption - Versus Emission Trade-Off?," SAE Technical Paper 2003-01-0754, 2003, doi:10.4271/2003-01-0754.
47. Kaahaaina, N., Simon, A., Caton, P., and Edwards, C., "Use of Dynamic Valving to Achieve Residual-Affected Combustion," SAE Technical Paper 2001-01-0549, 2001, doi:10.4271/2001-01-0549.
48. Wolters, P., Salber, W., Geiger, J., Duesmann, M. et al., "Controlled Auto Ignition Combustion Process with an Electromechanical Valve Train," SAE Technical Paper 2003-01-0032, 2003, doi:10.4271/2003-01-0032.
49. Willand, J., Nieberding, R., Vent, G., and Enderle, C., "The Knocking Syndrome - Its Cure and Its Potential," SAE Technical Paper 982483, 1998, doi:10.4271/982483.
50. Kontarakis, G., Collings, N., and Ma, T., "Demonstration of HCCI Using a Single Cylinder Four-stroke SI Engine with Modified Valve Timing," SAE Technical Paper 2000-01-2870, 2000, doi:10.4271/2000-01-2870.
51. Zhao, H., Peng, Z., Williams, J., and Ladommatos, N., "Understanding the Effects of Recycled Burnt Gases on the Controlled Autoignition (CAI) Combustion in Four-Stroke Gasoline Engines," SAE Technical Paper 2001-01-3607, 2001, doi:10.4271/2001-01-3607.
52. Li, J., Zhao, H., Ladommatos, N., and Ma, T., "Research and Development of Controlled Auto-Ignition (CAI) Combustion in a 4-Stroke Multi-Cylinder Gasoline Engine," SAE Technical Paper 2001-01-3608, 2001, doi:10.4271/2001-01-3608.
53. Murase, E. and Hanada, K., "Control of the Start of HCCI Combustion by Pulsed Flame Jet," SAE Technical Paper 2002-01-2867, 2002, doi:10.4271/2002-01-2867.

54. Weinrotter, M., Wintner, E., Iskra, K., Neger, T. et al., "Optical Diagnostics of Laser-Induced and Spark Plug-Assisted HCCI Combustion," SAE Technical Paper 2005-01-0129, 2005, doi:10.4271/2005-01-0129.
55. Wolters, P., Salber, W., Geiger, J., Duesmann, M. et al., "Controlled Auto Ignition Combustion Process with an Electromechanical Valve Train," SAE Technical Paper 2003-01-0032, 2003, doi:10.4271/2003-01-0032.
56. Zhao F., Asmus T.W., Assanis D.N., Dec J.E., Eng J.A., Najt P.M., Homogeneous Charge Compression Ignition (HCCI) Engines, Key Research and Development Issues, SAE Publication PT-94, Soc. of Automotive Engineers, 2003.
57. U.S. Department of Energy, Energy Efficiency and Renewable Energy Office of Transportation Technologies, Homogeneous Charge Compression Ignition (HCCI) Technology- A Report to the U.S. Congress，April 2001.
58. Christensen, M. and Johansson, B., "Influence of Mixture Quality on Homogeneous Charge Compression Ignition," SAE Technical Paper 982454, 1998, doi:10.4271/982454.
59. Aceves, S., Martinez-Frias, J., Flowers, D., Smith, J. et al., "A Decoupled Model of Detailed Fluid Mechanics Followed by Detailed Chemical Kinetics for Prediction of Iso-Octane HCCI Combustion," SAE Technical Paper 2001-01-3612, 2001, doi:10.4271/2001-01-3612.
60. Stanglmaier, R. and Roberts, C., "Homogeneous Charge Compression Ignition (HCCI): Benefits, Compromises, and Future Engine Applications," SAE Technical Paper 1999-01-3682, 1999, doi:10.4271/1999-01-3682.
61. Yap, D., Megaritis, A., Wyszynski, M., and Xu, H., "Effect of inlet valve timing on boosted gasoline HCCI with residual gas trapping," SAE Technical Paper 2005-01-2136, 2005, doi:10.4271/2005-01-2136.
62. Milovanovic, N., Chen, R., and Turner, J., "Influence of the Variable Valve Timing Strategy on the Control of a Homogeneous Charge Compression (HCCI) Engine," SAE Technical Paper 2004-01-1899, 2004, doi:10.4271/2004-01-1899.
63. Morikawa, H. and Ishibashi, Y., "An Experimental Approach to the Controlled Auto-Ignition," SAE Technical Paper 2007-01-0173, 2007, doi:10.4271/2007-01-0173.
64. Ohyama, Y., "Simultaneous Control of Air/fuel Ratio and Intake, Exhaust Valve Timing for HCCI Operation," SAE Technical Paper 2003-01-1084, 2003, doi:10.4271/2003-01-1084.

65. Yelvington, P. and Green, W., "Prediction of the Knock Limit and Viable Operating Range for a Homogeneous-Charge Compression-Ignition (HCCI) Engine," SAE Technical Paper 2003-01-1092, 2003, doi:10.4271/2003-01-1092.
66. Duret, P., Ecomard, A., and Audinet, M., "A New Two-Stroke Engine with Compressed-Air Assisted Fuel Injection for High Efficiency low Emissions Applications," SAE Technical Paper 880176, 1988, doi:10.4271/880176.
67. Duret, P. ; Venturi, S. ; Carey, C. ; The IAPAC Fluid Dynamically Controlled Automotive Two-Stroke Combustion Process, in A new generation of two-stroke engines for the future? International seminar, 1993.
68. Duret, P. and Venturi, S., "Automotive Calibration of the IAPAC Fluid Dynamically Controlled Two-Stroke Combustion Process," SAE Technical Paper 960363, 1996, doi:10.4271/960363.
69. Ishibashi Y and Tsushima Y, 'A Trial for Stabilizing Combustion in Two-Stroke Engines at Part Throttle Operation', in Duret P, A New Generation of Two-Stroke Engines for the Future?, IFP International Seminar, Rueil-Malmaison, Editions Technip., 1993.
70. Iida, N., "Combustion Analysis of Methanol-Fueled Active Thermo-Atmosphere Combustion (ATAC) Engine Using a Spectroscopic Observation," SAE Technical Paper 940684, 1994, doi:10.4271/940684.
71. Takei, T., Iida, N., Study on autoignition and combustion completion of n-butane in a two-stroke homogeneous charge compression ignition (HCCI) engine, SAE paper 2002-32-1786, 2002.
72. Osborne, R., Li, G., Sapsford, S., Stokes, J. et al., "Evaluation of HCCI for Future Gasoline Powertrains," SAE Technical Paper 2003-01-0750, 2003, doi:10.4271/2003-01-0750.
73. Li, G., Bo, T., Chen, C., and Johns, R., "CFD Simulation of HCCI Combustion in a 2-Stroke DI Gasoline Engine," SAE Technical Paper 2003-01-1855, 2003, doi:10.4271/2003-01-1855.
74. Kim, K., Sakai, H., Kobayashi, T., and Nakano, M., "Performance of Two/Four Stroke Gasoline HCCI Engine with Electromagnetic Valve Train," SAE Technical Paper 2007-01-1868, 2007, doi:10.4271/2007-01-1868.
75. Li, Z., He, B., and Zhao, H., "The Influence of Intake Port and Pent-Roof Structures on Reversed Tumble Generation of a Poppet-Valved Two-Stroke Gasoline Engine," SAE Technical Paper 2014-01-1130, 2014, doi:10.4271/2014-01-1130.

76. Ikoma, T., Abe, S., Sonoda, Y., Suzuki, H. et al., "Development of V-6 3.5-liter Engine Adopting New Direct Injection System," SAE Technical Paper 2006-01-1259, 2006, doi:10.4271/2006-01-1259.
77. Zhao, H. and Ladommatos, N., Engine Combustion Instrumentation and Diagnostics, SAE Published, 2001, ISBN: 9780768040340 0768040345.
78. Heywood, J., Internal Combustion Engine Fundamentals, McGraw-Hill Mechanical Engineering published, 1988, ISBN-13: 978-0070286375.
79. Dedeoglu N., Model investigations on scavenging and mixture formation in the dual-fuel or gas engine, Sulzer Tech. Review, Vol 51, No 3, 1969.
80. Rizk W., Experimental studies of the mixing processes and flow configurations in two-cycle engine scavenging, Proc. IMechE, Vol172, 1958.
81. Ohigashi S. and Kashiwada Y., A study on the scavenging air flow through the scavenging ports, Bull. JSME, Vol 9, No36, 1966.
82. Phatak R.G., A new method of analysing two-stroke cycle engines, PhD thesis, Queen's University of Belfast, May 1980.
83. Blair G.P., Ashe M.C., The unsteady gas exchange characteristics of a two-cycle engine, SAE paper 760644, 1976.
84. Asanuma T., Yanigahara S., Gas sampling valve for measuring scavenging efficiency in high speed two-stroke engines, SAE Transactions, Vol 70, p.420, Paper T47, 1962.
85. Booy R.R., Evaluating scavenging efficiency of two-cycle gasoline engines, SAE paper 670029, 1967.
86. Jante A., Scavening and other problems of two-stroke spark-ignition engines, SAE paper 680468, 1968.
87. Blair G.P., Studying scavenge flow in a two-stroke cycle engine, SAE paper 750752, 1975.
88. Sammons H., A single-cycle test apparatus for studying loop-scavenging in a two-stroke engine, Proc. IMechE, Vol 160, 1949, p233.
89. Sweeney M.E.G., et al, Single cycle gas testing method for two-stroke engine scavenging, SAE paper 850178, 1985.
90. Blair G.P., Design and simulation of two-stroke engines, SAE Inc, 1996.
91. Heywood J.B. and Sher Eran, The Two-stroke Cycle Engine: Its Development, Operation, and Design, Taylor and Francis, 1999.
92. Andreae, M., Cheng, W., Kenney, T., and Yang, J., "On HCCI Engine Knock," SAE Technical Paper 2007-01-1858, 2007, doi:10.4271/2007-01-1858.

93. Yang C, Zhao H, Megaritis T., In-cylinder studies of CAI combustion with negative valve overlap and simultaneous chemiluminescence analysis, SAE technical paper 2009–01-1103; 2009. doi:10.4271/2009-01-1103.
94. Zhang Y, Zhao H, Xie H, Hou S, Yang C., Characterization and heat release model development of SI–CAI hybrid combustion and its application to a 4-stroke gasoline engine operating with highly diluted mixtures, In: 33rd International symposium of combustion, 3E07, Beijing (China): Tsinghua University; 2010.
95. Zhang Y,Zhao H., Measurement of short-circuiting and its effect on CAI or HCCI combustion in a two-stroke poppet valve engine. Proc Inst Mech Eng,Part D:J Automob Eng 2012. http://dx.doi.org/10.1177/095440701143425.
96. Zhang Y, Zhao H, Peckham M and Campbell B. Direct in-cylinder CO2 measurements of residual gas in a GDI engine for model validation and HCCI combustion development. SAE technical paper 2013-01-1654, 2013. DOI:10.4271/2013-01-1654.
97. Zhang, Y., Zhao, H., Xie, H., Hou, s. and Yang, C. (2010) Characterization and heat release model development of SI-CAI hybrid combustion and its application to a 4-stroke gasoline engine operating with highly diluted mixtures. In: 33rd International Symposium of Combustion, Beijing, China, 1st - 6th August, 2010.

Appendix A – Publications related to this study

1. Yan Zhang and Hua Zhao, Optimisation of boosting strategy for controlled auto-ignition combustion in a four-valve camless gasoline direct injection engine running in two-stroke cycle, International Journal of Engine Research, February, 2014, doi:10.1177/1468087413519991.
2. Yan Zhang and Hua Zhao, Investigation of combustion, performance and emission characteristics of 2-stroke and 4-stroke spark ignition and CAI/HCCI operations in a DI gasoline, Applied Energy, 130 (2014) 244–255.
3. Mohammed Moore Ojapah, Hua Zhao and Yan Zhang, Effects of Ethanol on Performance and Exhaust Emissions from a DI Spark Ignition Engine with Throttled and Unthrottled Operations, SAE Technical Paper 2014-01-1393, 2014.
4. Mohammed Moore Ojapah, Hua Zhao and Yan Zhang, Effects of Ethanol on Part-load Performance and Emissions Analysis of SI Combustion with EIVC and Throttled Operation and CAI Combustion, SAE Technical Paper 2014-01-1611, 2014.
5. Y Zhang and H Zhao, Lean boost CAI combustion in a two-stroke poppet valve GDI engine, Internal Combustion Engines: Performance, Fuel Economy and Emissions, ISBN: 978-1782421832, 2013.
6. Yan Zhang, Hua Zhao, Mohammed Ojapah and Alasdair Cairns, CAI combustion of gasoline and its mixture with ethanol in a 2-stroke poppet valve DI gasoline engine, Fuel, Vol. 109, 2013, Pages 661–668, http://dx.doi.org/10.1016/j.fuel.2013.03.002. EI: 20133716739597, SCI: WOS:000320651700083
7. Zhang, Y., Zhao, H., Peckham, M., and Campbell, B., "Direct In-cylinder CO2 Measurements of Residual Gas in a GDI Engine for Model Validation and HCCI Combustion Development," SAE Technical Paper 2013-01-1654, 2013, doi:10.4271/2013-01-1654.
8. Ojapah M, Zhang Y and Zhao H, Part-load Performance and Emissions Analysis of SI Combustion with EIVC and Throttled Operation and CAI Combustion, Internal Combustion Engines: Performance, Fuel Economy and Emissions, ISBN: 978-1782421832, 2013.
9. Ojapah, M., Zhang, Y., and Zhao, H., "Analysis of Gaseous and PM Emissions of 4-Stroke CAI/HCCI and SI Combustion in a DI Gasoline Engine," SAE Technical Paper 2013-01-1549, 2013, doi:10.4271/2013-01-1549.

10. Zhang, Y., Zhao, H., Ojapah, M., and Cairns, A., "Effects of Injection Timing on CAI Operation in a 2/4-Stroke Switchable GDI Engine," SAE Int. J. Engines 5(2):67-75, 2012, doi:10.4271/2011-01-1773. EI: 20121414931127.
11. Y. Zhang and H. Zhao, Measurement of short-circuiting and its effect on CAI or HCCI combustion in a two-stroke poppet valve engine, Proc Inst Mech Eng, Part D: J Automobile Engineering, vol. 226, No. 8, pp. 1110-1118,2012, http://dx.doi.org/10.1177/095440701143425.
12. Mohammed Ojapah, Yan Zhang, Hua Zhao, and Lionol Ganippa, Particulate matter emission from different combustion modes in a 2/4 stroke switchable direct injection gasoline engine, Internal Combustion Engines: Improving Performance, Fuel Economy and Emissions, Institution of Mechanical Engineers, ISBN: 978-0-85709-205-2, 2011.EI: 20123615398396